LNGS - ss 17 bis km 18,910 67100 Assergi (AQ) ITALY
tel. +39 0862 4371 - fax + 39 0862 437559
www.lngs.infn.it

ANNUAL REPORT 2011

ISBN - 978 - 88 - 907304 - 8 - 1

LNGS/EXP-01/12
September 2012

Annual Report 2011

Laboratori Nazionali del Gran Sasso

Codice ISBN
978-88-907304-8-1

Annual Report 2011

LNGS Director — Dr. Lucia Votano

Editor — Dr. Roberta Antolini

Technical Assistants — Dr. Adriano Di Giovanni
Mr. Marco Galeota

LNGS/EXP-01/12
September 2012

INFN

Laboratori Nazionali del Gran Sasso

Annual Report 2011

INFN Gran Sasso National Laboratory

Lucia Votano

INFN Gran Sasso National Laboratory (LNGS) is the largest underground laboratory in the world devoted to neutrino and astroparticle physics; it is a worldwide research facility for scientists working in this field of research, where particle physics, cosmology and astrophysics meet. It is unequalled anywhere else, as it offers the most advanced underground infrastructures in terms of dimensions, complexity and completeness.

Located between L'Aquila and Teramo, at about 120 kilometres from Rome, the underground structures are on one side of the 10-kilometre long highway tunnel which crosses the Gran Sasso massif (towards Rome); the underground complex consists of three huge experimental halls (each 100-metre long, 20-metre large and 18-metre high) and bypass tunnels, for a total volume of about 180.000 m^3 and a surface of 17.800 m^2. Access to experimental halls is horizontal and it is made easier by the highway tunnel. Halls are equipped with all technical and safety equipment and plants necessary for the experimental activities and to ensure proper working conditions for people involved.

The 1400 metre-rock thickness above the Laboratory represents a natural coverage that provides a cosmic ray flux reduction by one million times; moreover, the flux of neutrons in the underground halls is about thousand times less than on the surface due to the very small amount of uranium and thorium of the Dolomite calcareous rock of the mountain.

The permeability of cosmic radiation provided by the rock coverage together with the huge dimensions and the impressive basic infrastructure make the Laboratory unmatched in the detection of weak or rare signals which are relevant for astroparticle, sub nuclear and nuclear physics.

Outside, near the Assergi A24-highway tollgate, immersed in a National Park of exceptional environmental and naturalistic interest on the slopes of the Gran Sasso mountain chain, an area of more than 23 acres hosts laboratories and workshops (e.g. chemistry, electronics, mechanics, design), the Computing Centre, the Directorate and several other Offices. Currently LNGS staff consists of 82 people whereas more than 950 scientists from 29 different Countries take part in the experimental activities.

LNGS research activities range from neutrino physics to dark matter search, to nuclear astrophysics, and also to earth physics, biology and fundamental physics.

The study of the properties of neutrino is of prime interest in particle physics and one of the main research topics of the present scientific program of the Laboratory where various neutrino sources, both natural (the Sun, the stars and the Earth) and artificial (particle accelerators) are used. Despite the great success of the LHC experiments,

massive neutrinos still remain the only experimental evidence of phenomena beyond the SM of particle physics. Moreover new scenarios have now been opened by the recent measurements of a relative large value of θ_{13}.
Finally neutrinos from the cosmos are indeed very important messengers which transport fundamental information to our understanding of the stars functioning as energy sources, their evolution and what happens when they 'turn off'.
Besides, the study of the phenomenon of neutrinoless double beta decay could allow us to find out if the neutrino overlaps with its antiparticle, thus providing a very significant answer in understanding the evolution of the Universe.
Neutrino physics therefore offers a window to a new theory of elementary particles and to the comprehension of the evolution of the Universe.
LNGS activities range among various aspects of neutrino physics study.
The measurement of neutrino oscillations in the atmospheric sector and in appearance mode is the main goal of the CNGS (CERN Neutrino to Gran Sasso) program and of OPERA experiment, which aims to the detection of tau neutrinos in the artificial CNGS neutrino beam originally constituted by muon neutrinos only. In 2011 the data acquisition and analysis have been smoothly continued, with some improvements in the decay search strategy. Moreover a dedicated procedure was set up in order to make a systematic search for electron neutrinos.
ICARUS is the other experiment which is able to detect CNGS beam; it is an innovative apparatus consisting of a big mass (about 600 tons) of liquid argon, allowing 3D imaging of any interactions of charged particles inside its volume and associated with excellent spatial resolution and a good calorimetric reconstruction. The ICARUS T600 detector is smoothly running in HALL B since May 2010 with very high live time. In 2011 many progresses have been achieved in the optimization of analysis tools in terms of performance, calibrations and event reconstruction.
Such a massive liquid argon experiment running in an underground laboratory is, so far, the most important milestone for the LAr-TPC technology.
In September 2011 OPERA showed surprising results of the measurement of the velocity of neutrinos from the CERN CNGS beam over a baseline of about 730 km, making use of dedicated upgrades of the CNGS timing system and of a high precision geodesy campaign for the measurement of the neutrino baseline. The announcement of an early arrival time of CNGS muon neutrinos with respect to the one computed assuming the speed of light shook the scientific community. Later on a test of the 8.3 Km long optical fibre performed by OPERA, brought to the discovery of a faulty connection of an optical cable reducing the amount of light received by the optical/electrical converter of the Master Clock and thus increasing artificially the neutrino velocity by $\approx$ 74 ns. Following the OPERA announcement, all the big experiments at LNGS besides OPERA, BOREXINO, ICARUS and LVD set up a campaign to repeat the measurement with improved timing resolution, reduction of systematics, improved and redundant time stamp (White Rabbit System and Borexino new high precision GPS system) and an independent geodesy campaign. The measurements of all the experiments were consistent with no measurable deviation from the speed of light for neutrinos.

Borexino measures, in real-time, solar neutrinos interactions by means of a 300-ton sphere of scintillating liquid. This allows us to study the functioning of the Sun and at the same time neutrino properties. Thanks to the high stability of the detector Borexino showed the complete absence of any asymmetry in the study of the day-night effect of the 7Be signal. This result, combined with the other solar neutrino data, allows a rejection of the MSW-LOW solution of the neutrino oscillation based on solar data alone and without relying on the assumption of CPT symmetry in the neutrino sector. Thanks also to the development of a very effective procedure to identify and subtract the ^{11}C cosmogenic background based on threefold coincidences and the positronium formation study, Borexino is now able to explore the 1-2 MeV region with unprecedented sensitivity. This led to the first observation of solar neutrinos from the basic pep reaction and to publish the upper limit, the lowest ever published, for the CNO production in a star.

LVD experiment is continuously monitoring the Galaxy with its 1000-ton liquid scintillator, looking for collapsing stars. LVD is continuously taking data with a live time efficiency greater than 99%. This allows to monitor time variations in the environmental conditions during long periods including the seasonal modulation of the cosmic muon flux. A joint LVD-OPERA analysis using the horizontal cosmic muons crossing both detectors, allowed to unambiguously show that the instrumental bias on the OPERA data have affected the period used for the neutrino velocity measurement.

The study of neutrino properties through the research into a rare process called ‘neutrinoless double beta decay’ may give a direct indication to the value of its mass, ascertaining its nature of Majorana particle. At present LNGS hosts several experiments devoted to the search of neutrinoless double beta decay events.
GERDA experiment uses enriched Germanium crystals directly immersed into 60 m^3 of liquid argon, which is a first protection against cosmic radiation. A 10-metre diameter tank built all around the cryostat is a further protection and it acts as a veto Cerenkov for muons. In 2011, the commissioning of the experiment has been accomplished and the physics run started with the diodes of the former Heidelberg-Moscow and Igex experiments. The total mass is 17.6 kg. The background at $Q_{\beta\beta}$ is about 0.017 cts/(keV kg y) which is a factor of about 10 lower than the previous experiments. The study of background originating from ^{42}Ar was continued in the LArGe facility. Argon with a known ^{42}Ar activity was added and the behaviour of the (charged) progeny ^{42}K in electric fields has been studied. The preparations for the second phase have also started with the production of new detectors, conceptually new readout electronics and the liquid argon instrumentation.
CUORE experiment is the most recent and ambitious development of the ‘TeO2 bolometers’ technique, in which INFN has more than 20 year experience. CUORE will consist of a closed-packed array of 988 TeO2 crystals containing about 200 kilograms of ^{130}Te cooled at a temperature next to absolute zero. Significant steps

forward have been made in 2011 in many aspects of the construction of the experiment; the activities have been mainly concentrated on the construction of the cryogenic apparatus, the completion of the crystal test activity and the preparation of the first tower of the experiment CUORE-0 that has been the test bench for the assembly line including procedures, tools and materials.
COBRA aims to use CdZnTe (CZT) semiconductors as detectors operated at room temperature. Presently in R&D phase, the experiment consists of monolithic, calorimetric detectors in a coplanar grid design (CPG detectors), 1x1x1 cm3 in dimensions. Additionally, pixelated CZT detectors are under investigation. In 2011 the COBRA detector has been moved to a new location in the LNGS, adapted electronics have been installed and a complete new detector layer consisting of 16 new detectors was brought on line.
The LUCIFER experiment, presently in R&D phase, completes the outline of the research activities on neutrinoless double beta decay. It will consist of a closely packed array of tens of ZnSe scintillating bolometers, each equipped with a light detector. A growth procedure to guarantee a large yield, a very high radio-chemical purity and reproducibility has been developed. The LUCIFER approach, and the scintillating bolometer technique in general, could allow in principle to achieve an impressively low background [of the order of 10^{-4} cts/(kg keV y)].

Dark Matter search represents the second main topic of the Laboratory scientific program. As well known, experimental evidence shows the existence in the Universe of an amount of mass larger than the one that can be observed by telescopes: the so called dark matter. It is supposed to be five times bigger than the ordinary matter, which constitutes just only 5% of our Universe.
At LNGS, three experiments are presently in operation aiming to the hunting for dark matter candidates and their direct detection. One new experiment of larger mass, Xenon 1t, has been approved to be installed in Hall B and a new proposal, DarkSide-50, has been submitted for approval. These experiments, each one by means of different technologies, keep Gran Sasso Laboratory in the forefront of such studies.
DAMA/LIBRA experiment, made up of 250 kilograms of extremely radio-pure NaI(Tl) crystals, has been recording data since 2003. The analysis results corresponding to a total exposure of 1.17 ton x year confirm the annual modulation of low-energy single signals induced in the detector. Such modulation is identical to the one expected from the Dark Matter particle flux, regardless of any model. After the detector upgrade performed in the end of 2010, by replacing all the low background PMTs with new ones having higher quantum efficiency, since January 2011 the DAMA/LIBRA experiment is again in data taking. This can allow the lowering of the software energy threshold of the experiment and, hence, the improvement of its performance and sensitivity. During 2011 a detailed analysis of all the PMTs features and implications has been carried out.
Xenon100 is a two-phase liquid cryogenic detector and the apparatus contains 170 kilograms of Xenon, 65 kilograms of which constitute the active part while the remaining ones act as a shield.

In 2011 Xenon 100 published the results from 100.9 live days of data, acquired between January and June 2010. No evidence for dark matter was found. This leads to the most stringent limit on dark matter interactions today, excluding spin-independent elastic WIMP-nucleon scattering cross sections above 7.0×10^{45} cm^2 for a WIMP mass of 50 GeV/c^2 at 90% confidence level. Data taking continued over the year under improved conditions, since the maintenance works and ^{85}Kr purification campaign of 2010, in order to push the sensitivity further.
Meanwhile INFN has definitely approved the third stage of the Xenon program at LNGS: XENON1T, to be located in hall B at LNGS. Progress has also been made over the year on the design of the detector and on various topics and components of XENON1T.
CRESST experiment is based on the bolometer technique with $CaWO_4$ crystals cooled at 10 mK as well as on the simultaneous detection of scintillation light and the heat resulting by the interaction of a particle with the crystals. The latest run of CRESST ended in April 2011. Out of the 18 detector modules installed in the cryostat only 8 were used for the Dark Matter analysis. CRESST has submitted a paper with the analysis of data with a total exposure of 730 kg d. An excess of events has been found in the acceptance region where a WIMP signal would be expected. A new run with several detector improvements aiming at a reduction of the overall background is expected to start soon.
Cryogenic TPC employing a two-phases argon medium as active volume are a quite promising technique for WIMP detection. The Liquid Argon Technology for the search of dark matter particles has been pioneered at LNGS by WARP experiment, now it continues with DarkSide-50: a new proposal submitted for approval in 2011 to the LNGS Scientific Committee. DarkSide-50 aims to introduce innovative features in order to operate in a 'background-free' mode. The detector will be deployed, enclosed in its liquid scintillator neutron veto, in the Borexino Counting Test Facility in the hall C at LNGS.

Using the 400 kV accelerator, LUNA continued with its successful activity for the measurements of the cross section of thermonuclear reactions of astrophysical interest. In the course of the year 2011, the experimental activity has been focussed on the $^2H(\alpha,\gamma)^6Li$ and $^{17}O(p, \gamma)^{18}F$ reactions.
Moreover, the project of a new accelerator LUNA 3.5MV, with an experimental programme mainly devoted to the He burning reactions, has been approved by LNGS. A detailed project of the preparation of the "B node" of the interferometric area, assigned to the project, was accomplished, together with the design of the shielding against neutrons with respect to both the rest of the laboratory and the internal rock "walls" where water uptake points of the Teramo aqueduct are present.

The Laboratory hosts experiments aimed to study cosmogenic and primordial radionuclides in solid and fluid matrix inside LNGS, and a laser interferometer operating since 1994 and measuring permanent and transient strain episodes and monitoring slow earthquakes.

The LNGS is located in the Gran Sasso massif within Mesozoic carbonates, where the largest aquifer of central Italy is situated. The experiment ERMES studies cosmogenic and primordial radionuclides, including radon (222Rn), radiocarbon (14C) and tritium (3H), in solid and fluid matrix inside LNGS by means of HPGe gamma spectrometry, liquid scintillation and inductively coupled plasma-mass spectrometry. Uranium groundwater anomalies were observed by ERMES experiment during the preparation phases of the earthquake that hit L'Aquila o 6th April 2009, in the cataclastic rocks near the overthrust fault crossing the laboratory. The results suggest that U may be used as a potential strain indicator of geodynamic processes occurring before the seismic swarm and the main earthquake shock.

The Laboratory hosts also the PULEX experiment aiming at understanding if environmental radiation has a permanent influence on the biochemistry of living matter.

Finally the VIP experiment at LNGS aims to reduce by four orders of magnitude the limit on the probability of a possible violation of the Pauli exclusion principle for the electrons. VIP has already put a limit on the probability of PEP violation at the level of 4 x 10-29 (for electrons). In 2011 the collaboration proposed an upgrade of the setup in order to arrive in the range of 10^{-31}.

The activity of the theory group covers various aspects of astroparticle and particle physics, including astroparticle physics, compact stars, cosmology, large scale structures and dark matter, computer simulations of gauge theories, particle physics phenomenology. There is a long tradition of collaboration between the LNGS theory group and several experimental groups.

As a final remark I would like to underline the at present the Laboratory is at the climax of its activity with many experiments in different phases of their life, all at the forefront in astroparticle physics. LNGS owns a leadership in the mass experiments (order of Kton), with very high performances from the point of view of a low level of radioactivity.
This ensures the Laboratory, having a glorious past at its back, also a future as much bright ahead.

Assergi, october 2 2012

The Director of the Laboratory
Dr. Lucia Votano

Contents

View of the ICARUS experiment in the Hall B of LNGS.

THE BOREXINO EXPERIMENT

Borexino collaboration

G. Bellini[a], J. Benziger[c], D. Bick[v], G. Bonfini[b], D. Bravo[n], M. Buizza Avanzini[a], B. Caccianiga[a], L. Cadonati[t], F.P. Calaprice[d], C. Carraro[i], P. Cavalcante[b], A. Chavarria[d], A. Chepurnov[z], D. D'Angelo[h], S. Davini[i], A. Derbin[u], A. Etenko[s], K. Fomenko[m], D. Franco[a], C. Galbiati[d], S. Gazzana[b], C. Ghiano[b], M.G. Giammarchi[a], M. Goeger-Neff[h], A. Goretti[d], L. Grandi[d], E. Guardincerri[i], C. Hagner[v], S. Hardy[n], A. Ianni,[b], A.M. Ianni[d], D. Korablev[m], Y. Koshio[b], G. Korga[b], D. Kryn[o], M. Laubenstein[b], T. Lewke[h], E. Litvinovich[s], B. Loer[d], F. Lombardi[b], P. Lombardi[a], L. Ludhova[a], I. Machulin[s], S. Manecki[m], W. Maneschg[j], G. Manuzio[i], Q. Meindl[h], E. Meroni[a], L. Miramonti[a], M. Misiaszek[q], D. Montanari[b], P. Mosteiro[d], V. Muratova[u], L. Oberauer[h], M. Obolensky[o], F. Ortica[g], K. Otis[t], M. Pallavicini[i], L. Papp[b], L. Perasso[a], S. Perasso[i], A. Pocar[d], R.S. Raghavan[n], G. Ranucci[a], A. Razeto[b], A. Re[a], A. Romani[g], D. Rountree[n], A. Sabelnikov[s], R. Saldanha[d], C. Salvo[i], S. Schönert[j], H. Simgen[j], M. Skorokhvatov[s], O. Smirnov[m], A. Sotnikov[m], S. Sukhotin[s], Y. Suvorov[s], R. Tartaglia,[b], G. Testera[i], D. Vignaud[o], B. Vogelaar[n], F. von Feilitzsch[h], J. Winter[h], M. Wojcik[q], A. Wright[d], M. Wurm[h], J. Xu[d], O. Zaimidoroga[m], S. Zavatarelli[i], G. Zuzel[j]

[a]Dip. di Fisica dell'Università and Infn Milano - Italy
[b]Laboratori Nazionali del Gras Sasso, Assergi (Aq) - Italy
[c]Dept. of Chemical Engineering, Princeton University - NJ USA
[d]Dept. of Physics, Princeton University - NJ USA
[g]Dip. di Chimica dell'Università and Infn Perugia - Italy
[h]Dept. of Physics, Technische Universität München - Germany
[i]Dip. di Fisica dell'Università and Infn Genova - Italy
[j]Max Planck Inst. für Kernphysik, Heidelberg - Germany
[m]Joint Institute for Nuclear Research Dubna - Russia
[n]Dept. of Physics, Virginia Polytechnic Institute - VA USA
[o]Laboratoire de AstroParticule et Cosmologie, Paris - France
[q]Institute of Physics, Jagellonian University, Kracow - Poland
[s]RRC Kurchatov Institute, Moscow - Russia
[t]Dept. of Physics, University of Massachusetts, Amherst - MA USA
[u]St. Petersburg Nuclear Physics Institute, Gatchina, Russia
[v]Institut für Experimentalphysik, Universität Hamburg - Germany
[z]Institute of Nuclear Physics, Lomonosov State University, Moscow, Russia

Abstract

Borexino is a detector located in the Hall C of LNGS to study solar neutrino physics and other rare phenomena. The data taking started in May 2007 and led - among other things - to the first real time measurement of ^{7}Be solar neutrinos, the first experimental evidence of the matter/vacuum transition in solar neutrino oscillations,

the observation of geo-neutrinos and the first evidence for solar neutrinos from the pep reaction. We summarize here the status of the project and outline the perspectives for future measurements.

1 Introduction

Solar neutrino physics is a topic that originally started from the perspective of studying the basic working principle of the core of the Sun, nuclear fusion reactions producing energy and emitting neutrinos. The pioneer Davis experiment [1] was the first one to measure (with radiochemical methods) solar neutrinos as predicted by theoretical models and to detect a significant deficit with respect to the predicted flux. Additional experiments were performed starting from the end of the 80's, both in radiochemical mode [2, 3, 4] and in real-time mode [5, 6] while the most widely accepted model of the Sun evolved into what is now known as the Standard Solar Model [7] [8].

As a general statement, real-time experiments have been performed with large water Cerenkov detectors with an energy threshold of about 5 MeV, mainly due to natural radioactivity. This implies that only $\sim$0.001% of the total neutrino flux has been observed in real time prior to 2007.

The issue of directly measuring low energy solar neutrinos has been the subject of an intensive research study carried out in the frame of the Borexino development and starting from the very beginning of the 90's. Borexino [9] is a real time experiment to study sub-MeV solar neutrinos having as the main experimental goal the detection of the 0.862 MeV ^{7} Be solar neutrino line through the neutrino-electron elastic scattering reaction $\nu e \rightarrow \nu e$. The maximum energy of the recoiling electron is 664 KeV and the experimental design threshold is of 50 keV while the analysis threshold is 200 keV. The detection reaction is observed in a large mass (100 tons fiducial volume) of well shielded liquid scintillator.

The prediction of the ^{7}Be solar flux depends both on the Standard Solar Model and the value of the parameters of the LMA solution of neutrino oscillations [10] [11]. The Borexino experimental program makes it possible to directly test this prediction as well as opening up the unexplored territory of real time sub-MeV solar neutrino spectroscopy.

The main problem of an experiment with such a low energy threshold is the background coming from natural sources such as cosmic rays or radioactivity. This problem has been addressed by means of an intense R&D program focused on low radioactivity materials and purification techniques. This effort was complemented by a comparably thorough research in the field of detection and measurement of very low radioactivity levels [12]. As a part of this program, a prototype of the Borexino detector, called Counting Test Facility [13], was built and operated at LNGS to demonstrate very low radioactive contamination levels (10^{-16} g/g of U-238 equivalent or less [14]) in a ton scale scintillator detector. The CTF is currently being used as a low background facility for quality tests of the Borexino scintillator and future physics programs.

This research and development culminated into the construction, filling and operation of the full-scale Borexino detector. The experimental data taking in the final configuration began in May 2007.

2 The Borexino Detector

Borexino [15] is an unsegmented scintillation detector featuring 300 tonnes of well shielded liquid ultrapure scintillator viewed by 2200 photomultipliers (fig. 1). The detector core is a transparent spherical vessel (Nylon Sphere, 100μm thick), 8.5 m of diameter, filled with 300 tonnes of liquid scintillator and surrounded by 1000 tonnes of high-purity buffer liquid. The scintillator mixture is pseudocumene (PC) and PPO (1.5 g/l) as a fluor, while the buffer liquid consists of PC alone (with the addition of DMP as light quencher). The photomultipliers are supported by a Stainless Steel Sphere, which also separates the inner part of the detector from the external shielding, provided by 2400 tonnes of pure water (water buffer).An additional containment vessel (Nylon film Radon barrier) is interposed between the Scintillator Nylon Sphere and the photomultipliers, with the goal of reducing Radon diffusion towards the internal part of the detector.

The outer water shield is instrumented with 200 outward-pointing photomultipliers serving as a veto for penetrating muons, the only significant remaining cosmic ray background at the Gran Sasso depth (about 3700 meters of water equivalent). The innermost 2200 photomultipliers are divided into a set of 1800 photomultipliers equipped with light cones (so that they see light only from the Nylon Sphere region) and a set of 400 PMT's without light cones, sensitive to light originated in the whole Stainless Steel Sphere volume. This design greatly increases the capability of the system to identify muons crossing the PC buffer (and not the scintillator).

The Borexino design is based on the concept of a graded shield of progressively lower intrinsic radioactivity as one approaches the sensitive volume of the detector; this culminates in the use of 200 tonnes of the low background scintillator to shield the 100 tonnes innermost Fiducial Volume. In these conditions, the ultimate background will be dominated by the intrinsic contamination of the scintillator, while all backgrounds from the construction materials and external shieldings will be negligible.

Borexino also features several external systems conceived to purify the experimental fluids (water, nitrogen and scintillator) used by the experiment (see e.g. [16]).

3 Status of the project

The Borexino filling started in January 2007, with scintillator displacing the purified water from inside the detector volumes. The detector was completed and the data taking started in May 2007.

The radiopurity of the detector has been found in general to be better than the specifications. In particular, among the best radioactivity levels found during the data taking:

1. C-14 contamination of the scintillator was found to be at $\sim 2 \times 10^{-18}$ $^{14}\mathrm{C}/^{12}\mathrm{C}$.
2. The general level of Th-232 contamination - as measured by means of $^{212}Bi/^{212}Po$ delayed coincidences was found to be at $\sim 4.6 \times 10^{-18}$ g/g.
3. The U-238 family contamination - assessed by studying the $^{214}Bi/^{214}Po$ delayed coincidence rate, was measured to be $\sim 1.7 \times 10^{-17}$ g/g.

4. Kr-85 contamination, of considerable importance due to the spectral shape similar to the one of the signal searched for was found (by means of the ^{85m}Rb decay and the related β/γ tagging) to be at the level of 30 counts/day in the 100 tons fiducial volume.

This level of radiopurity, together with the use of mild cuts and the α/β discrimination technique has allowed - among other things - the first real-time detection of the Be-7 solar signal [17] [18], the first observation of the B-8 spectrum with a 3 MeV threshold [19] and the observation of geoneutrinos at LNGS [20].

During 2010 Borexino has completed an intense campaign of calibration. Sources such as Co-57, Ce-139,Hg-203, Sr-85, Mn-54, Zn-65, Co-60 and K-40 were used for gamma calibration, while C-14, Bi-214 and Po214 activities were used to understand the response of the detector to β's and α's. Finally, an AmBe source was used for neutrons. These studies allowed a significant reduction of the systematic error on the determination of the Fiducial Mass and on the determination of the energy scale and made it possible to tune several parameters of the Monte Carlo simulation codes, such as the light yield and the quenching factor. External sources were deployed in several positions the detector.

At the same time, purification campaigns have been conducted (water extraction and nitrogen stripping) that have significantly reduced two of the most important backgrounds, Kr-85 and Bi-210.

A series of physics results were obtained in 2011.

First of all, limits were publichsed about solar and other antineutrino sources [21]; this work took advantage from the methodology developed for the geoneutrino analysis [20].

Secondly, the improved understanding of the detector characteristics due to the calibration campaigns made it possible to significantly refine the Be-7 analysis. The new result [22] features an accuracy better than 5%.

The stability of the detector allowed also to study the day-night effect of the Be-7 signal, thereby allowing to completely exclude the LOW solution of the neutrino oscillation based on solar data alone [23].

Finally, the low background of the detector, the refined analysis on threefold coincidences [24] and the positronium formation study [25] made it possible to explore the 1-2 MeV region with unprecedented sensitivity. This led to the first observation of solar neutrinos from the basic pep reaction [26]. In addition, the best limit for the CNO production in a star has been established.

In this way, Borexino has completed direct detection of Be-7, pep and B-8 solar neutrino components thereby providing complete evidence of the transition from MSW and vacuum oscillation of the LMA solution of the Solar Neutrino Problem (fig. 2).

4 Future perspectives

Additional physics topics are under study or considered for future investigation, depending on the background conditions and on the refinement of the ongoing analysis:

1. Measuring the CNO solar neutrinos.

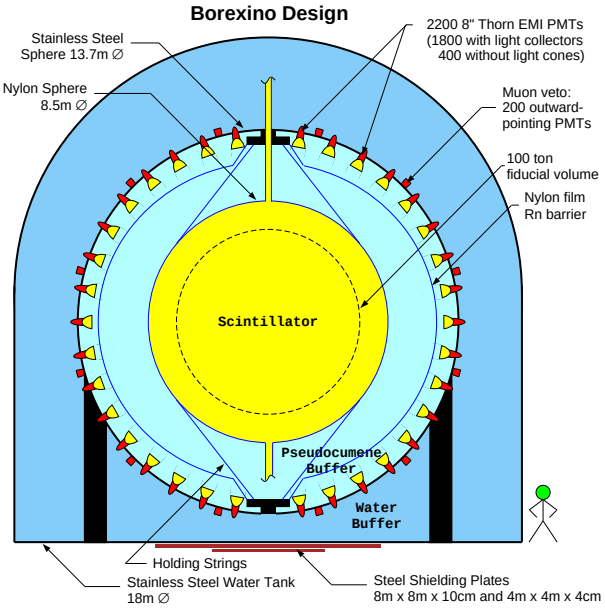

Figure 1: Schematic view of the Borexino detector.

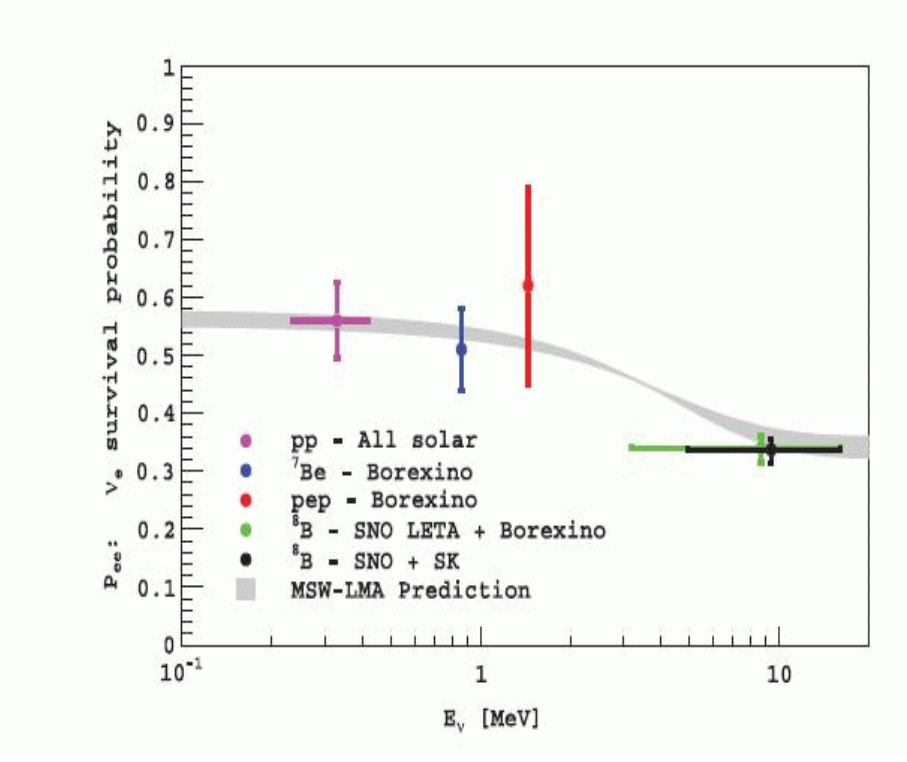

Figure 2: Electron neutrino survival probability as a function of energy. The results from Borexino alone are shown (Be-7,pep,B-8), together with the SNO results for B-8 and the result of all solar experiments for pp.

2. Watch for neutrino bursts from Supernovae events: Borexino is part of the international SNEWS program for early detection of Supernovae with neutrinos.

3. Short baseline oscillation tests with Cr-51 neutrino (or ^{144}Ce-^{144}Pr antineutrino) sources. This topic is of particular interest in view of the present controversial experimental scenario, encompassing the recently highlighted reactor and Gallium anomalies as well as the long standing LSND puzzle confirmed by the new Miniboone antineutrino data. The emerging picture of an oscillation paradigm comprising 3 active plus 2 sterile neutrinos, the latter with masses at eV scale, could verified with a source test in Borexino for a significant portion of the parameter space, through the search of the oscillation pattern that at the considered L/E values should develop clearly throughout the detector.

4. Measuring the neutrino velocity by exploiting the CNGS neutrino beam.

5 List of articles published in year 2011

1. G. Bellini et al., *Study of solar and other unknown anti-neutrino fluxes with Borexino at LNGS.* Phys. Lett. B, 696 (2011) 191.

2. G. Bellini et al., *Precision Measurement of the ^{7}Be Solar Neutrino Interaction Rate in Borexino.* Phys. Rev. Lett., 107 (2011) 141302.

3. G. Bellini et al., *Muon and cosmogenic neutron detection in Borexino.* Journal of Instrumentation, doi:10.1088/1748-0221/6/05/P05005.

References

[1] R. Davis, Nobel Prize Lecture 2002.

[2] W. Hampel et al., Phys. Lett. B 447 (1999) 127.

[3] J.N. Abdurashitov et al., Phys. Rev. Lett. 83 (1999) 4686.

[4] M. Altmann et al., Phys. Lett. B 616 (2005) 174.

[5] S. Fukuda et al., Phys. Rev. Lett. 86 (2001) 5651; Phys. Lett. B 539 (2002) 179.

[6] Q.R. Ahmad et al., Phys. Rev. Lett. 87 (2001) 071301.

[7] J.N. Bahcall and M.H. Pinsonneault, Phys. Rev. Lett. 92 (2004) 121301.

[8] A. Serenelli et al., Astr. J. Lett., 705 (2009) L123.

[9] G. Alimonti et al., Astroparticle Physics 16 (2002) 205.

[10] J.N. Bahcall et al., JHEP 0408 (2004) 016.

[11] G.L. Fogli et al., Progr. Nucl. Phys., 57 (2006) 742.

[12] C. Arpesella et al., Astroparticle Physics 18 (2002) 1.

[13] G. Alimonti et al., Nucl. Instr. & Methods A406 (1998) 411.

[14] G. Alimonti et al., Astroparticle Physics 8 (1998) 141.

[15] G. Alimonti et al., Nucl. Instr. & Methods, A600 (2009) 568.

[16] G. Alimonti et al., Nucl. Instr. & Methods, A609 (2009) 58.

[17] C. Arpesella et al., Phys. Lett. B 658 (2008) 101.

[18] C. Arpesella et al., Phys. Rev. Lett. 101 (2008) 091302.

[19] G. Bellini et al., Phys. Rev. D 82 (2010) 033006.

[20] G. Bellini et al., Phys. Lett. B 687 (2010) 299.

[21] G. Bellini et al., Phys. Lett. B, 696 (2011) 191.

[22] G. Bellini et al., Phys. Rev. Lett. 107 (2011) 141302.

[23] G. Bellini et al., Phys. Lett. B 707 (2012) 22.

[24] G. Bellini et al., Journal of Instrumentation, doi:10.1088/1748-0221/6/05/P05005.

[25] D. Franco, G. Consolati and D. Trezzi, Phys. Rev. C 83 (2011) 015504.

[26] G. Bellini et al., Phys. Rev. Lett. 108 (2012) 051302.

COBRA Annual Report 2011

G. Anton[a], M. Bergmann[a], J. Durst[a], M. Filipenko[a], T. Gleixner[a], T. Michel[a],
B. Biskup[b], V. Bocarov[b], P. Cermak[b], J. M. Jose[b], I. Stekl[b],
O. Civitarese[c],
C. Disch[d], A. Fauler[d]. M. Fiederle[d],
M. Bellicke[e], A. Garson[e], Q. Guo[e], H. Krawczynski[e], V.K. Lee[e], J. Martin[e],
M. Fritts[f], D. Gehre[f], T. Göpfert[f], B. Janutta[f], M. Janutta[f], O. Reinecke[f],
A. Sörensen[f], T. Wester[f], K. Zuber[f,*]
C. Gößling[g], M. Homann[g], T. Köttig[g], D. Münstermann[g], T. Neddermann[g], S. Rajek[g],
O. Schulz[g], J. Tebrügge[g], T. Quante[g],
J. Ebert[h], C. Hagner[h], N. Heidrich[h], S. Kietzmann[h], C. Oldorf[h], J. Timm[h], B. Wonsak[h],
M. Junker[i], F. Simkovic[j], J. Suhonen[k],

[a] *Universität Erlangen–Nürnberg* – Germany
[b] *Technical University of Prague* – Czech Republic
[c] *University of La Plata* – Argentina
[d] *Freiburg Materials Research Center* – Germany
[e] *Washington University in St. Louis* – USA
[f] *Technische Universität Dresden* – Germany
[g] *Technische Universität Dortmund* – Germany
[h] *Universität Hamburg* – Germany
[i] *Laboratori Nazionali del Gran Sasso* – Italy
[j] *University of Bratislava* – Slovakia
[k] *University of Jyvaskyla* – Finnland
(* Spokesperson)

Abstract

The aim of the COBRA-Experiment (**C**admium Zinc Telluride **0**-Neutrino Double-**B**eta **R**esearch **A**pparatus) is to prove the existence of neutrinoless double beta decay ($0\nu\beta\beta$-decay) and to measure its half life.

Therefore a detector array made of Cadmium-Zinc-Telluride detectors (CZT) is operated in the LNGS in Italy. This prototype is used to investigate the experimental issues of operating CZT detectors in low background mode and identify potential background components, whilst additional studies are proceeding in surface laboratories. The experiment currently consists of monolithic, calorimetric detectors in a coplanar grid design (CPG detectors). These detectors are 1x1x1 cm^3 and will be operated in a 4x4x4 detector array.

Additionally, pixelated CZT detectors are under investigation to check their properties to distinguish the different background contributions. Based on pattern recognition in combination with energy resolved measurements it could be possible to directly image the $0\nu\beta\beta$-decay by particle identification.

1 Activities at the LNGS

In 2011 the complete COBRA experiment has been moved to a new location in the LNGS, adapted electronics have been installed and a complete new detector layer consisting of 16 new detectors was brought on line.

1.1 Moving the COBRA experiment

Due to the progress in the research activities, the COBRA collaboration requested a larger laboratory space in the LNGS Underground facility. This request was kindly fulfilled with the reassignment of the former Heidelberg-Moscow hut to the COBRA collaboration. Moving of the office, laboratory equipment and the whole experimental setup was done in spring 2011. Within this move a general overhaul of the experiment has been performed and a lot of minor and major revisions have been installed.

The relocation and the extended laboratory space offered the opportunity to redesign and improve the complete shielding of the experimental setup as well as the readout and operational electronics. The neutron shielding, which houses an electromagnetic shield and a shield against environmental radioactivity (lead castle), was rebuilt to allow a better utilization of the space inside and to give better access. The electromagnetic shielding has been replaced by a new one made of galvanized steel sheets with adapted EMI-compatible seals as substitutes for the formerly used, less efficient copper EMI-cage. To suppress the background induced by the radioactive noble gas radon, the setup is now sealed with a gas tight barrier foil and is continuously flushed with dry nitrogen gas since the recommissioning.

1.2 Installation of new electronics

The operational electronics, the data acquisition system (DAQ) and the read-out electronics have been completely renewed within the last year. The large number of fast analog-digital converters required to instrument the COBRA experiment recently became available due to the decommissioning of the Amanda Experiment, offering a sudden chance to acquire a sufficient number of such fast devices.

The exchange of the peak sensing ADCs with the FADCs began in 2010 and was finalized in 2011 during the installation of the new detector layer. Hence, now it is possible to record the pulse shape of each event completely instead of recording just its energy, which offers great advantages for the offline data analysis. A schematic drawing is shown in Figure 1.

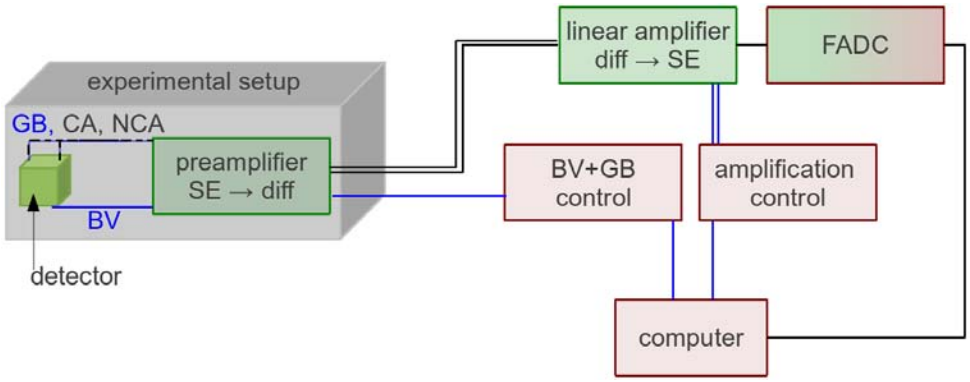

Figure 1: Data acquisition chain and read-out electronics

The detectors and preamplifiers are placed within the experimental setup (gray cuboid). The black signal lines are connected to the linear amplifier and fast analog to digital converters (FADC). Here the signals are digitized, indicated by a change from green to red. The bias voltage (BV), grid bias (GB) and amplification are controlled remotely and can be adjusted via network connection, indicated by the blue lines. The old DAQ-system was very susceptible to electromagnetic interferences; much of the signal transmission is now done via differential signaling. This enables the transmission of sensitive signals very robust over long distances. The differential signaling is symbolized with two lines close to each other. The use of this new DAQ- system enhanced the energy resolution to 1.9 %FWHM at 662 keV in laboratory test measurements [1]. This unique technique of signal analysis offers the possibility to separate background disturbances from valid physics events and allows access to important physical quantities (e.g. depth reconstruction) in addition to the energy deposition.

1.3 Commissioning of an improved shielding for the experiment

In addition to the new electronics it was necessary to overhaul the electromagnetic shielding of the experimental setup. Therefore a complete new EMI-Box (Electro Magnetic Interference) has been designed and manufactured at the Technical University of Dortmund. The new design adopts the use of galvanized steel plates (instead of the copper plates used so far) in order to improve the absorption of the magnetic component of EM radiation. Furthermore, now a copper granule bath is used for the cable feedthrough to handle the increasing number of cables needed for the installation of the next detector layers (Figure 2).

The construction of the neutron shielding has been adapted to the new lab layout and takes advantage of the possibility to use the gantry crane in the COBRA hut. This has greatly improved the access to the experimental setup, as the polyethylene plates have a weight of 140 kg (Figure 3). Furthermore the innermost lead bricks have been replaced by ultra low activity lead with an activity of less than 3 Bq/kg (Figures 4 and 5). That assures a reduced background due to decay products of the Uranium and Thorium decay chains in the ultimate vicinity of the copper nest and the detector layers. The additional installed radon tight foil reduces the

Figure 2: Optimized cable feedthrough, constructed as copper granule bath.

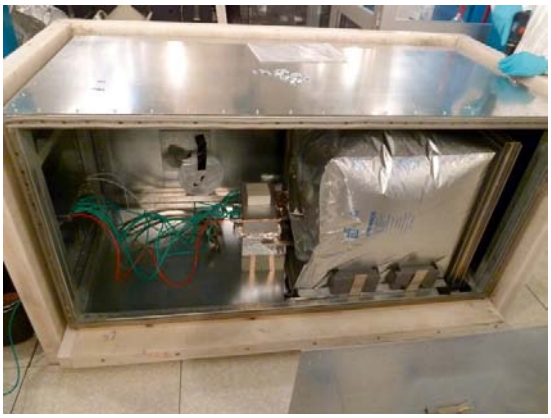

Figure 3: Opened setup with radon tight foil, EMI shield and neutron shield

diffusion of radioactive noble gases into the setup. Therefore the gas shield is inflated and continuously flushed with nitrogen (Figure 3).

Figure 4: Nearly finished lead castle with HV-, capton-signal cable and N_2 pipes

Figure 5: Cu-Nest surrounded with ULA lead and installed detector layer

1.4 Assembly of the new detector layer

In september 2011 sixteen new detectors were assembled into a complete new layer. These detectors previously had been carefully examined at the TU Dresden (see 2.2). The larger lab space enabled us to install a detector assembly facility under cleanroom conditions in the immediate vicinity of the experiment. This reduces the risk of crystal damage and radioactive pollution of relevant nearby detector components. Immediate on-site repairs and replacements are now possible and a constant upgrade of the experiment is feasible. The goal is to install 16 new detectors every 6 months until the NEST is completed.

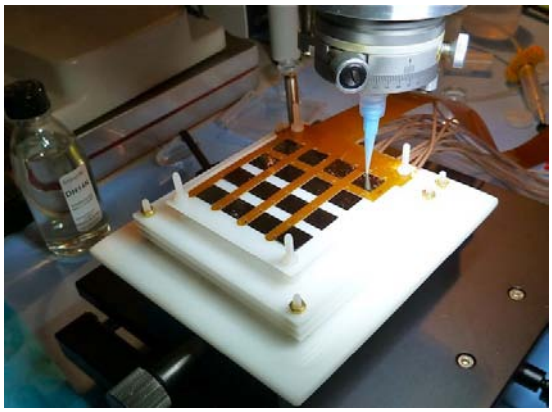

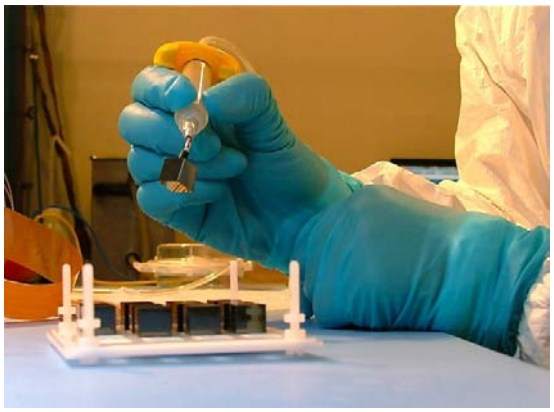

Figure 6: Newly installed detector assembly station in the COBRA hut at the LNGS. Since 2011 layers can be completely assembled and connected at the Underground-Lab.

2 CPG activities

2.1 Background recognition and reduction with PSA

The huge effort of the replacement of the peak sensing data acquisition (DAQ) system with pulse shape analysis readout (PSA) offers much more information for the offline data analysis. Even though much work had to be done to restructure the data processing chain according to the needs of the pulse shape data analysis, the benefits and potential of this readout system are already clearly perceptible. The recording of the whole signal shape does not only allow for a clear distinction between physics and artificial events (electronic noise for example), but also e.g. for the distinction between multiple interactions and single interactions within the detector, called single-site and multi-site events, respectively. Multi-site events can be induced by gamma particles that first interact incoherently, depositing only a part of their energy, and are then scattered again or fully absorbed. More than one particle that interact in a short time frame in the detector can also produce multi site events. For example ^{114}Cd, produced by neutron capture of ^{113}Cd, can de-excite with the emission of several gamma particles with a sum energy of up to 8 MeV. As this can cause a background as they are able to mimic the energy deposition of a double beta event, the distinction between multi- and single site events can contribute to the background reduction. Together with the special coplanar grid design of the detectors and the pulse shape readout also the interaction depth of an event within the detector can be determined [2]. If the interaction depth is plotted versus the energy, the different sorts of particles can be identified by means of energy and where the energy deposition happened. Using this method, it should be possible to reduce the background significantly, as for example the cathode below the detector attracts background from the surroundings due to the applied high voltage. With this technique an important background source could be determined and can now be vetoed with a fiducial cut on the cathode of the detectors (Figure 7).

The events at the cathode of the CPG detector are very likely caused by the decay of radon and its daughter products. As the cathode of the detector is set to negative potential it attracts positively charged particles from α-decays. Those particle stick to the surface and decay further producing those events. The identification of this background shows on the one hand the value of the additional information and on the other hand the low level of background achieved as the small number of events deriving from the contaminants was a significant part of the remaining background in the region of the expected signal (Figure 8).

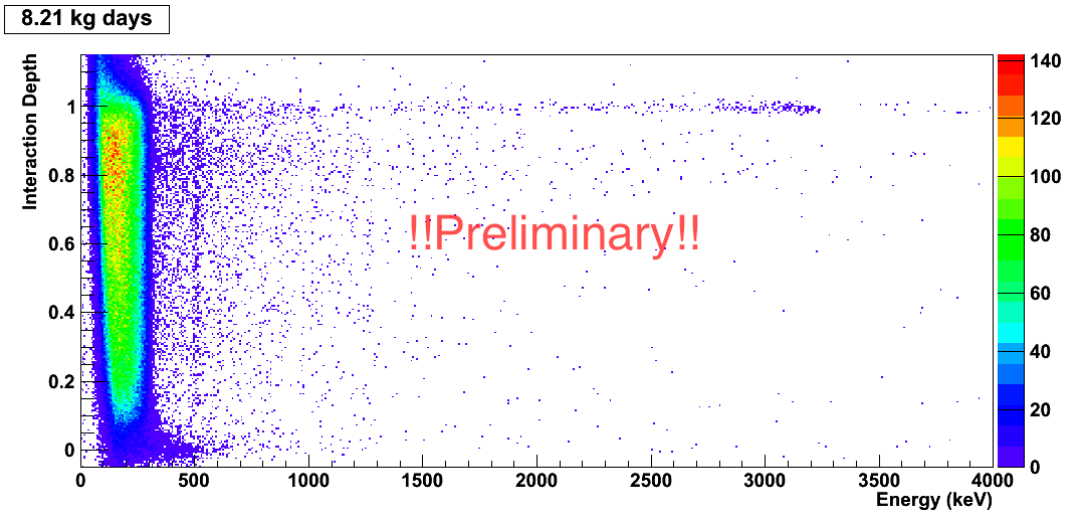

Figure 7: Distribution of the events from 8.21 kg·days in an interaction depth versus energy plot. The cathode is located at z=1. The enhanced number of high energy events at the cathode is likely caused by the α-decay of radon and its daughter products but can be removed by adapted Z-cuts. The prominent area below 300 keV is mainly caused by the β-decay of ^{113}Cd.

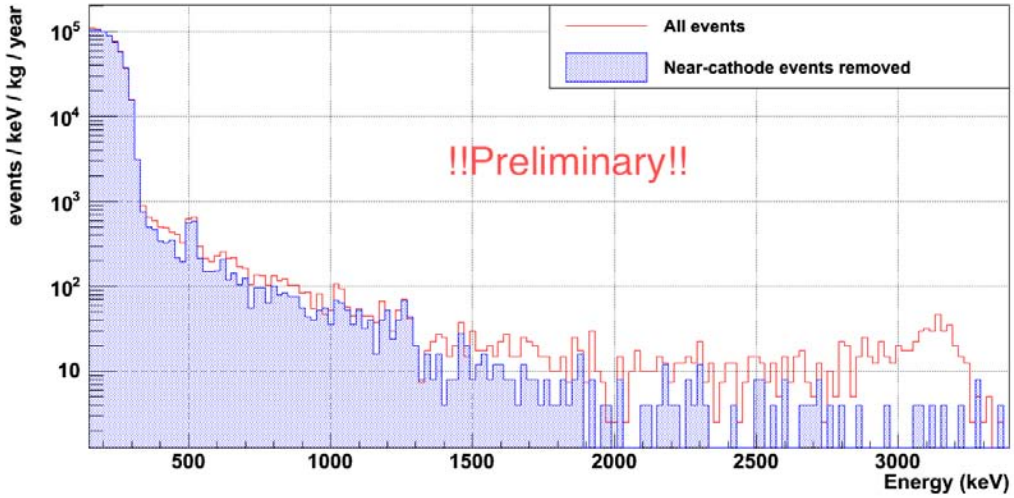

Figure 8: The full spectrum of all recorded events. The fiducial volume cut removes the events that occur in the vicinity of the cathode. The result is a clean spectrum at the ROI around 2.8 MeV.

The possibilities of the new data acquisition system and readout electronics were demonstrated in laboratory test measurements. A detector was irradiated with α-, β- and γ-radiation to 5 sides. When short ranged α- or β-radiation is pointed directly to the anodes, an interesting effect occurs: These particles only penetrate the margin of the detector, i.e. the area of the anodes, the cathode is irrelevant. As a consequence, the pulse shapes of these events are highly symmetric, and the reconstructed energy seems to be distorted with values up to two times the real energy deposition. With this mechanism it is possible that (background) events can increase their energy spuriously into COBRAs ROI. This effect is important to background reduction in

particular, as these events can be recognized due to their pulse shapes and their reconstructed interaction depth. This seems to be the most promising option for the COBRA experiment in near future to reach the aimed background level.

2.2 Detector characterization at TUD

For the COBRA experiment an energy resolution below 1% in the ROI at around 2.8 MeV is required to achieve the needed sensitivity. Hence, one of the key points to improve the overall performance of the experiment is to carefully examine the best operational conditions for each detector. The complete detector characterization of the CPG detectors for the COBRA experiment is performed at the Technical University Dresden (TUD). Therefore two test setups have been designed and manufactured and are currently in operation at the TUD.

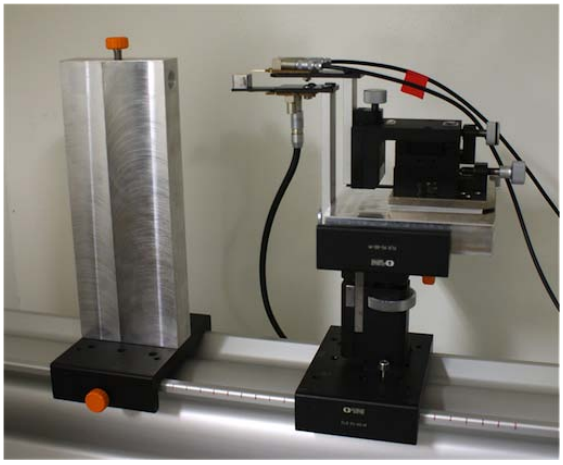

Figure 9: Test rig for determination of energy resolution, GB and HV

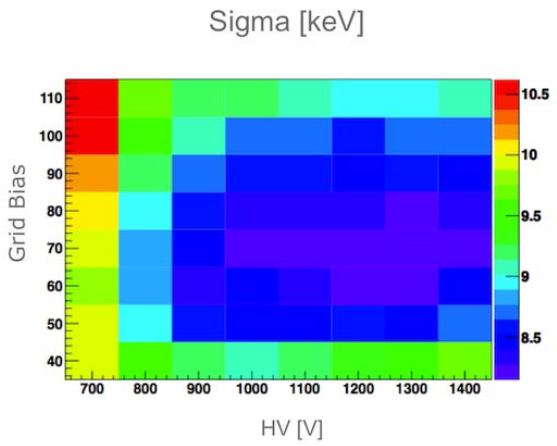

Figure 10: 3D-plot of FWHM for ^{137}Cs (662 keV) over GB and HV

The first setup was built to determine the best working conditions for the Grid Bias (GB) and High Voltage (HV) supply for each detector (Figure 9). For this analysis the full parameter space is automatically scanned, and the spectral response is recorded and evaluated. The result is a 3D plot that allows to select the optimal working point for every specific detector (Figure 10). Besides this analysis it is also possible to measure the global full energy efficiency (FEE) and charge collection efficiency (CCE) of the detector by using a radioactive ^{137}Cs source with a well known activity. This is done by irradiating the whole detector with this point-like source, analyzing the events in the full energy peak of the spectrum and comparing them to the expectations from Monte-Carlo simulations.

The second setup is used to determine the local charge collection efficiency of the detectors. It is well known that the homogeneity of the CZT material strongly depends on the growth conditions and the purity of the feed material used. As the detectors are from different batches and, hence, from different crystal ingots, an inspection of the material is mandatory to group the detectors into different quality bins. The effect of the incomplete charge collection shows up in a broadened energy spectrum and leads to a decreased detector performance. The integral analysis of the detector does not reveal any local disturbances. To analyze these highly localized effects a spatially resolved measurement is necessary. Therefore a test rig with two orthogonal stepper motors with μm precision has been built (Figure 12) carrying a lead collimator. The

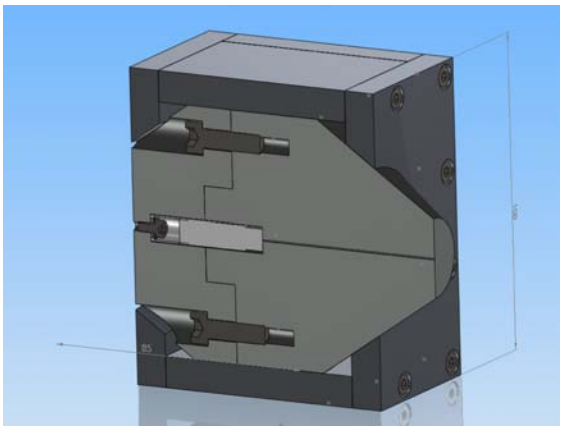

Figure 11: Schematic drawing of the lead collimator used for the 2D-mapping

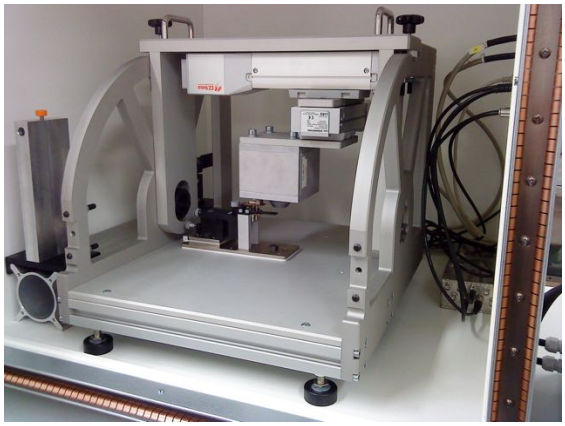

Figure 12: Fully automated test rig for 2D-mapping of the detectors with highly collimated γ-rays

collimator contains a 100 MBq ^{137}Cs source. The diameter of the collimator channel is 0.5 mm (Figure 11).

The resulting beam is used to irradiate a 0.8 mm^2 spot on the detector. This allows to determine the CCE and FEE with spatial resolution of less than 1 mm. Figure 13 shows the results for one detector which has been scanned on 4 sides (anode side is in the center of the cube-grid). The color scale depicts the shift of the local photopeak centroid versus the global one. Blue areas are less efficient, while the red areas represent an improved performance compared to the integral performance of the crystal. These results are useful for corrections and further investigations via pulse shape analysis.

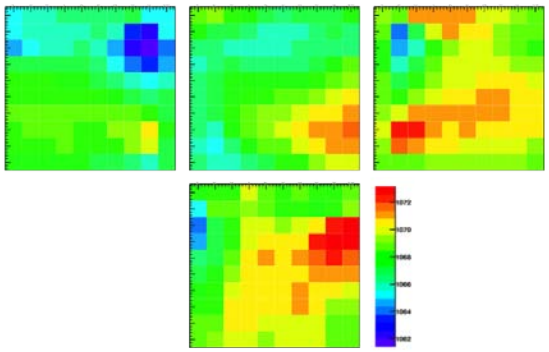

Figure 13: 2d-CCE scan of one detector, colors indicating the centroid shift of the full energy peak

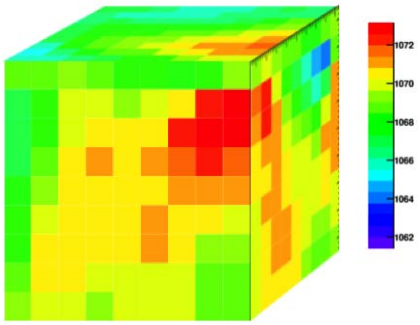

Figure 14: The semi-3d distribution of areas with different efficiencies folded around a cube

Both methods have been applied to all 16 deployed detectors and the measurements continue for those still to come, in order to maintain consistency and gain good knowledge of the performances of all 64 detectors to be installed.

2.3 Activities of the Freiburg Materialforschungszentrum (FMF)

The originally purchased CZT detectors were covered with red lacquer as a passivation layer to protect the material against humidity and surface contamination. It turned out, that the radioactive inventory of this passivation disturbs the measurements immensely. This is mainly caused by the α-decay of thorium and uranium and their daughter products present in the lacquer. As a substitution for the red lacquer Parylene is the material of choice.
At the FMF a Parylene deposition tool was installed and put into operation. The deposition process was improved during the last year, when it was discovered that (unwanted) pinholes could be created in the coating, effectively removing any protection by the Parylene passivation. This was found during humidity tests with several CPG detectors. Surface leakage current increased with humidity and caused severe detector performance degradation. Changed parameters during the coating process removed the pinholes, as well as improving adhesive properties of the Parylene coating. This improved coating process is now available for the passivation of the originally red passivated 1x1x1 cm^3 detectors for the COBRA experiment.

3 Pixelated detector activities

3.1 Development of sub-mm pixel detectors at WUSTL

The group at Washington University in Saint Louis (WUSTL) has focused on the development of sub-mm pixel detectors. The primary efforts can be broken into two separate initiatives, which follow a similar procedure. The programs involve a collaborating institution which provides an ASIC chip to be bonded to a WUSTL-fabricated CZT detector. In each case, the detector is deposited with a highly customized pixel pattern which allows rapid-prototyping and optimization of the best pixel and steering grid dimensions for the ASIC/detector system. This is made possible by the facilities operating at the WUSTL CZT Detector Development Laboratory, which include photolithographic equipment and an electron-beam vaporization chamber in a class-100 cleanroom environment. It is this flexibility in detector development which has fostered collaboration between the WUSTL group and these outside institutions.
The first initiative is in collaboration with the University of Illinois in Champagne-Urbana. The UIUC group has developed an ASIC chip manufactured by the Finnish company, Ajat. The ASIC has 2048 channels set at a 350 μm pitch. While Ajat has provided a propriety data acquisition system, WUSTL engineers have developed their own readout board (Figure 15) for which greater performance and prototyping flexibility is expected. Detectors have been fabricated for the project at both 350 μm and 700 μm. The 700 μm detector - shown in Figure 16 - is an example of the rapid-prototyping pixel patterns which the WUSTL group specializes in fabricating. On a single crystal, pixels with different gap widths can be tested in addition to pixels with and without a steering grid. Even the width of the steering grid varies. These detectors are currently in testing at UIUC with the WUSTL-developed data acquisition system.

The second initiative is a collaboration with Black Forest Engineering, LLC. They have acquired an ASIC chip of Berkley design and wish to test it using a WUSTL-fabricated detector. Their implementation makes use of 608 channels at 600 μm pitch. WUSTL provided two detectors matching BFE's specifications. Both employ the same pattern with three pixel widths, where one of the widths is deposited with and without a steering grid. In the first detector, all contacts are formed by a single deposition of indium. In the second, the steering grid is isolated from the CZT surface by a layer of gold which forms a blocking contact. The detectors are currently being tested in BFE labs.

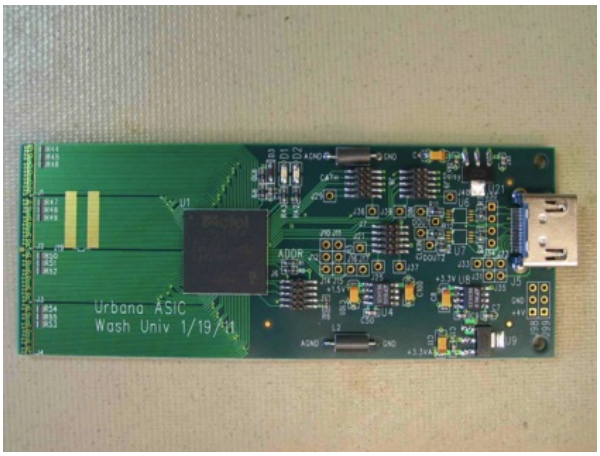

Figure 15: Custom data acquisition board developed by WUSTL for readout of the 350 μm and 700 μm detectors supported by the 2048-channel UIUC/Ajat ASIC.

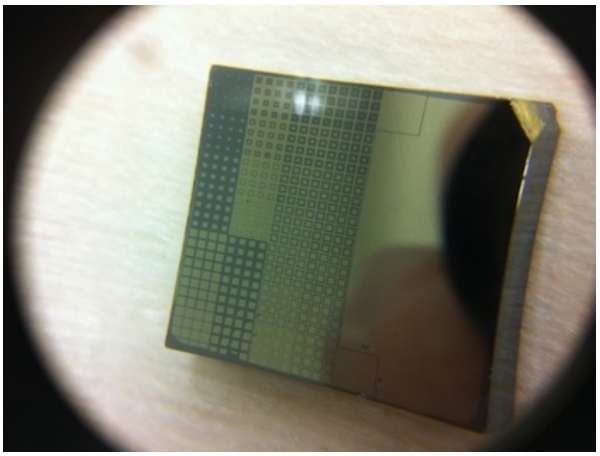

Figure 16: 700 μm-pitch detector fabricated at WUSTL which employs multiple pixel widths and steering grids for rapid prototyping.

3.2 Reconstruction of particle tracks at ECAP

The main advantage of the fine pixel pitch detector is that the track of an event in the sensor can be used to identify the particles involved. While the identification of alpha particles and muons is quite easy due to their characteristic signature, the discrimination of single electrons and double beta events is challenging (Figure 17, energy color coded in keV). One approach is to define several features that can be calculated from a track and evaluate them with a classification software. We mostly used an artificial neural network [3] and a random decision forest [4]. The software can be used to calculate one value (cv) for each track, which corresponds to the probability of an event being a one electron or a double beta event. Then the events can be classified by choosing a value k and classifying all events with $cv > k$ as double beta events, and $cv \leq k$ as single electrons.

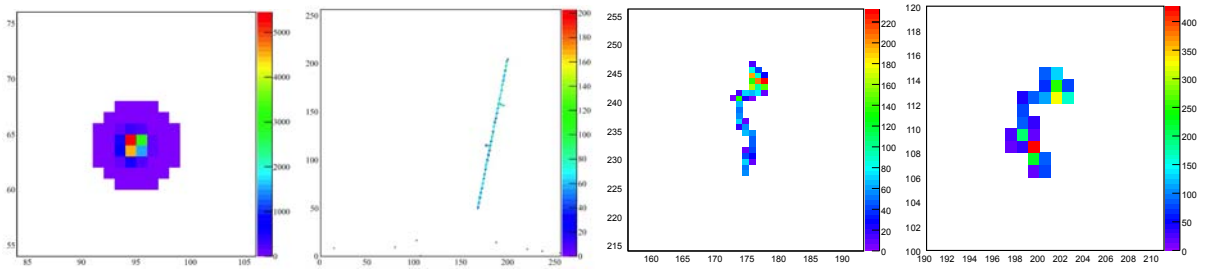

Figure 17: From left to right: signature of an alpha particle (Si sensor, 55 μm pixel pitch), track of a muon (Si sensor, 55 μm pixel pitch), track of a single electron (CdTe sensor, 110 μm pixel pitch, simulated) track of a double beta event (CdTe sensor, 110 μm pixel pitch, simulated, color indicates deposited energy)

A simulations is used to train the software and to calculate the efficiency of the discrimi-

nation. The information about the efficiency of the classification can be used to calculate the increase in sensitivity for a real experiment, depending on the background. For a background with alpha particles and muons, the increase would be much higher since they can be discriminated very easily.

3.2.1 Experimental results of Timepix operation

For the experiments we calibrated and used a CdTe-Timepix detector with 110 μm pixelsize [5]. The disadvantage of this method is that the calibration can be performed only up to 122.06 keV but according to our simulations energy depositions up to 800 keV per pixel are not unlikely for $0\nu\beta\beta$–events. We investigated the reliability of the calibration on extrapolation (i.e. for photopeaks at about 300 keV) and obtained that the calibration mistakes increase with the energy. We recorded data of background radiation in a lead shielding which mainly contained tracks of α-particles and muons. Both signatures could be identified very efficiently by the algorithms that we implemented and applied to the data. The characteristic signature of the α-particles is a round shaped cluster with a size of about 25 - 30 pixels and a high energy deposition in the center (Figure 18 A). The signature of muons are straight lines with a very similar energy deposition in all pixels (Figure 18 B). A reduced Hough-Transformation can be applied to obtain a reliable identification of this pattern.

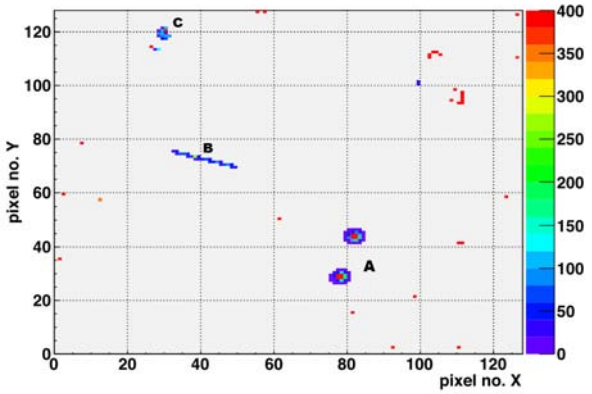

Figure 18: The pixel matrix of a measured frame. The color denotes the energy deposition in keV. There are two α-particles (A), a muon (B) and an electron (C) pictured.

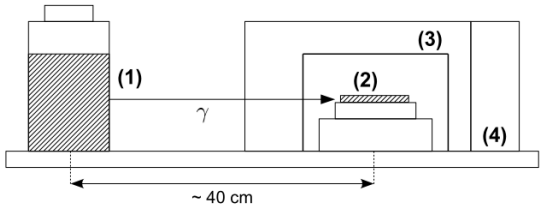

Figure 19: A scheme of the experimental setup for the ^{232}Th measurement. (1) The ^{232}Th source, (2) the sensor layer, (3) the cardboard and (4) the lead wall.

Concerning the tracking of electrons we performed an experiment with a ^{232}Th source. The decay chain of ^{232}Th contains ^{208}Tl which emits 2.615 MeV photons with an energy close to the COBRA ROI. The aim of this experiment was to verify the predictions of the simulations and evaluate the event classification quality of the ANNs with experimental data. A scheme of the setup is shown in Figure 19. About 400 g of ^{232}Th (Fig.19 (1)) with an activity of about 14.3 MBq is placed in front of the detector (Fig.19 (2)) which is taped to a lead block and shielded by cardboard (Fig.19 (3)) from low energy photons. The sensor of the detector is parallel to the table surface. Most likely, these photons will either induce pair-production or be Compton-scattered within the sensor layer. As the detector is charge-blind, electron-positron pairs starting at the same point will give a pattern which is very close to the pattern of a $0\nu\beta\beta$

event and, therefore, can be used as a dummy for a test on our method of pattern recognition. Effective background from single electrons is provided by the Compton-scattering.

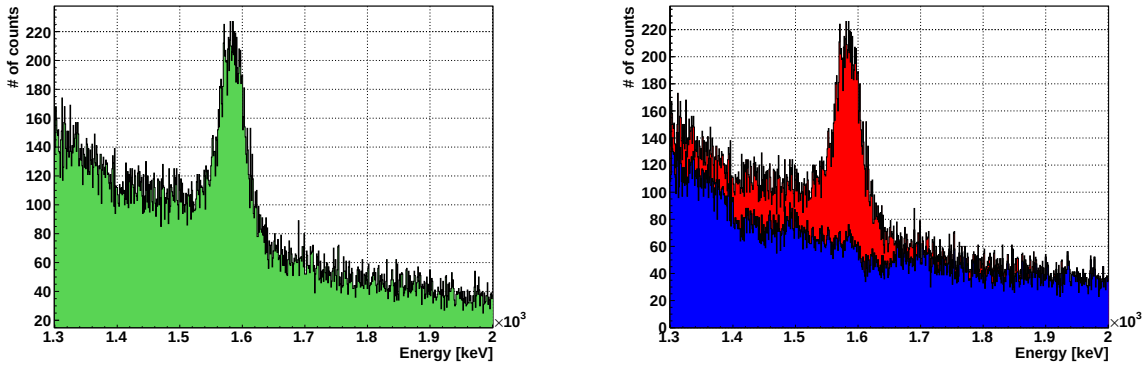

Figure 20: The electron spectrum in the ROI (a) before and (b) after event classification by the ANNs.

The spectrum in the ROI is presented in Figure 20 (a). The prominent peak is due to the pair-production events and the large flat spectrum is the expected Compton-spectrum. The width of the peak (FWHM) is 5.17 % which is about a factor of 4 worse than predicted by the simulation. We think that the main reason for this discrepancy is the calibration error on extrapolation and the energy resolution could significantly be improved by a better calibration up to 400 keV. If the ANNs are applied to the data (Figure 20 (b)) and classification mistakes which were evaluated with simulated data are taken into account, the peak (red) can be separated from the Compton-spectrum (blue). For pair-production events which are below the peak energy probably at least one of the particles escaped the sensor layer and therefore only a part of the full kinetic energy was deposited in the sensor.

3.3 Pixel detector activities in IEAP, Prague

Background measurements were divided into two steps: 1) measurements produced by pixel detectors themselves, which estimate the influence of external and internal background signals, 2) measurements of different constituent materials of the detector setup by HPGe spectrometer, to determine the intrinsic background. The CdTe-Timepix detector was installed inside the passive shielding of the current COBRA prototype in LNGS. Two sets of data, one with Nitrogen (N_2) flushing for 45 days and another without N_2 flushing for 11 days were collected for analysis. Also 13 days of measurement in surface laboratory (IEAP, Prague) was collected for comparison. Surface measurement was performed without N_2 flushing and inside 5 cm of lead shielding.

Readout electronics, noise and detector material quality are other concerns for such rare decay measurements. Some pixels in the detector show noisy behavior, counting unrealistic values (mainly single-pixel events but sometimes also multi-pixel events). This behavior influences the measurements considerably. This effect is prominent in CdTe detectors due to the material quality. During the equalization [11] of the detector, the noise level in each pixel is identified. A measurement mask (left side Figure 21) is generated from pixels for which the noise level is too high. This mask is used during further measurement. But all the noisy pixels may not be identified yet, or new pixels may become noisy during measurement. From the long term measurement data collected, pixels with excessive activity can be identified. A noisy pixel mask (Figure 21, right side) is generated from such pixels and these pixels are removed from further

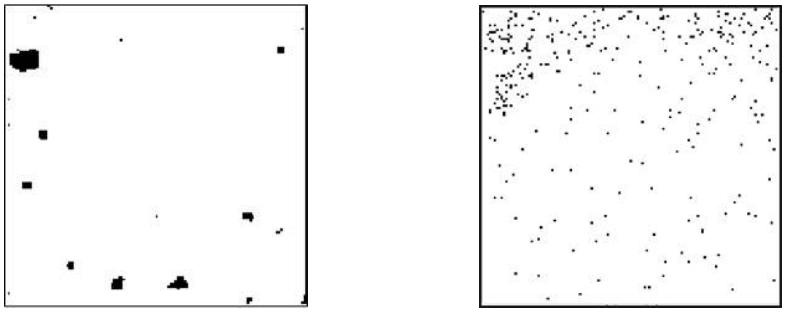

Figure 21: Example of measurement mask (left) and noisy pixel mask (right) generated for the CdTe detector. Measurement mask is generated during equalization, before measurements; and noisy pixel mask is generated after measurements, analyzing the data.

processing. After applying all the masking, the clean data set is generated, suppressing the influence of noisy pixels.

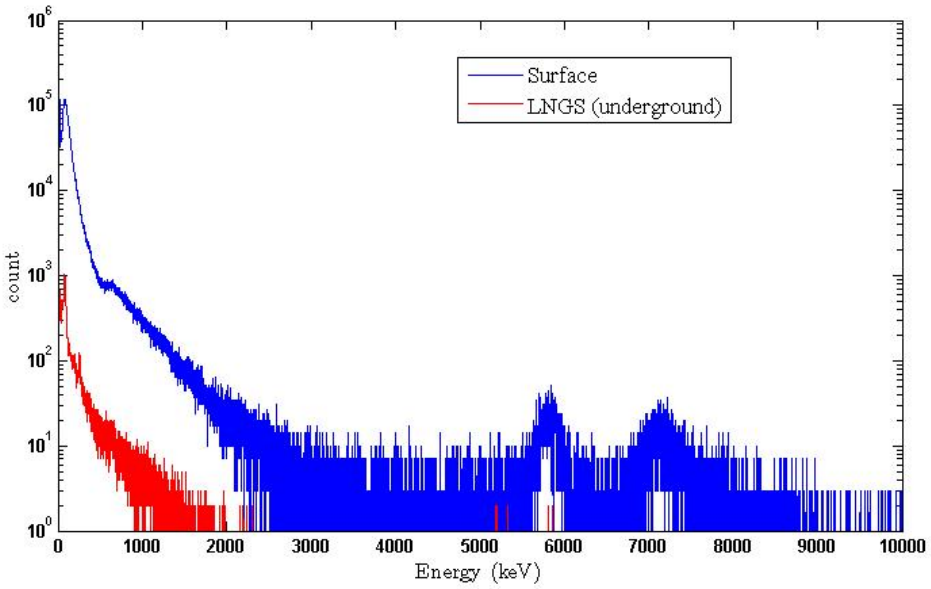

Figure 22: Comparison of spectra measured at surface (without N_2 flushing) and LNGS (with N_2 flushing). Spectra are normalized to 45 days of measurement. A background suppression by a factor of >100 in the ROI was observed.

Table 1 shows the results of analysis for all sets of experimental data (surface, LNGS with and without N_2 flushing). The results [12] show high suppression of alphas and electrons between surface and underground (factor 137 and 104 for electrons and alphas respectively). Data also confirm the influence of N_2 flushing on Rn suppression by a factor of 11. The number of detected electrons in the region of interest (2.5-3 MeV) for underground data is negligible. Criteria used for the classification were cluster size, linearity, and roundness of the clusters [14]. Alpha particle interactions generally create round clusters, and electrons generate curly tracks. Figure 22 compares the full spectrum from underground data (with N_2 flushing) with full spectrum from surface data (without N_2 flushing). All the materials of pixel the detector setup (detector,

Data set	Alphas		Electrons	
	Total	ROI	Total	ROI
LNGS, with N_2 flushing	3.9±0.5	<0.05	20.0±1.1	$0.02^{+0.08}_{-0.02}$
LNGS, without N_2 flushing	43.5 ±3.3	<0.22	22.1±2.3	$0.09^{+0.31}_{-0.08}$
Surface (IEAP), without N_2 flushing	406.0±9.2	$0.15^{+0.30}_{-0.12}$	2740.0±23.9	37.00±2.78

Table 1: Results of background measurements, surface vs. LNGS. All numbers are normalized to one day of measurement, with 90 % confidence level. Number of electrons in the ROI is negligible in underground data. The region of interest is taken in the range (2.5-3) MeV.

Timepix ASIC, PCB, etc.) were measured for intrinsic background, at low the background setup in LSM Modane laboratory (HPGe planar detector, 150 cm^2, range 20 keV-1.5 MeV). The results showed that the printed circuit board (PCB) material on which readout chip and detector were mounted has significant contribution to background [13]. Therefore, different PCB materials were collected and measured at the same low background setup. Pure Teflon based PCB material CuFlon [15] has very low background contamination, and it seems to be very favorable. Also flexible PCB materials have lower background contamination.

4 List of Publications

1. *Status and Perspectives of the COBRA-Experiment* - D. Muenstermann on behalf of the COBRA collaboration (PoS(EPS-HEP2011)434)

2. *Timepix background studies for double beta decay experiments* - J.M. Jose, P. Cermak, I. Stekl, J. Cermak, M. Fiederle, A. Fauler, Yu.A. Shitov, E.N. Rukhadze, N.I. Rukhadze, V.B. Brudanin, K. Zuber, P. Loaiza (JINST 6 C11030)

3. *Application of Hybrid Pixel Detectors for Searches of Rare Decays* - J. Durst, Gisela Anton, Michael Böhnel, Thomas Gleixner, Ferdinand Lück, Thilo Michel, Maria Schwenke, Kai Zuber (Nuclear Physics B (Proc. Suppl.) 215 (2011) 275277)

4. *Exploration of Pixelated detectors for double beta decay searches within the COBRA experiment* - M.Schwenke, K.Zuber, B.Janutta, Z.He, F.Zeng, G.Anton, T.Michel, J.Durstc, F.Lück, T.Gleixner, C.Gössling, O.Schulz, T.Köttig, H.Krawczynski, J.Martin, I.Stekl , P.Cermak (Nuclear Instruments and Methods in Physics Research A 650 (2011) 7378)

5. *Background capabilities of pixel detectors for double beta decay measurements* - P. Cermak, I. Stekl, V. Bocarov, J. M. Jose, J. Jakubek, S. Pospisil, M. Fiederle, A. Fauler, K. Zuber, P. Loaiza, Y. Shitov (Nuclear Instruments and Methods in Physics Research A 633 (2011) S210S211)

References

[1] O. Schulz *Exploration of new Data Acquisition and Background Reduction Techniques for the COBRA Experiment*, Technische Universität Dortmund, 2011.

[2] Z. He, G.F. Knoll, D.K. Wehe, R. Rojeski, C.H. Mastrangelo, M. Hammig, C. Barrett, and A. Uritani, *1-D position sensitive single carrier semiconductor detectors.* Nuclear Instruments and Methods in Physics Research A, 380:228231, 1996.

[3] Steffen Nissen *Implementation of a Fast Artificial Neural Network Library (fann)*, Department of Computer Science, October 2003, University of Copenhagen (DIKU)

[4] Stefan Geielsöder *Classification of events for the ANTARES neutrino detector*, Department Informatik, July 2011, Friedrich-Alexander-Universität Erlangen-Nürnberg

[5] J. Jakubek et al., Nuclear Instruments and Methods A **591** (2008), pp. 155-158

[6] M. Filipenko, Master Thesis, *Experimental Investigation of Pixelated Semiconductor Photodetectors with CdTe Sensor Material for the Search for the Neutrinoless Double Beta Decay* (2011), Erlangen Centre for Astroparticle Physics (ECAP)

[7] M. Dambacher, *Digital Spectroscopic System Based on Large Volume Stacked Coplanar Grid (Cd,Zn)Te detectors*, IEEE 2011 Proceedings

[8] C. Disch, *Digital Spectroscopic System Based on Large Volume Stacked Coplanar Grid (Cd,Zn)Te Detectors*, TNS 2012 (to be published)

[9] C. Disch, *Coincidence Measurements with Stacked (Cd,Zn)Te Coplanar Grid Detectors*, IEEE 2010 Proceedings

[10] C. Disch, *Coincidence Measurements and long-term Stability Analysis with Stacked (Cd,Zn)Te Coplanar Grid Detectors* IEEE 2011 Proceedings

[11] X. Llopart et al., *Timepix, a 65k programmable pixel readout chip for arrival time, energy and/or photon counting measurements*, *Nucl. Inst. Meth.* **A581** (2007) pp. 485-494.

[12] J. M. Jose et al., *Timepix background studies for double beta decay experiments*, 2011 JINST 6 C11030 .

[13] P. Cermak et al., *Use of silicon pixel detectors in double electron capture experiments*, 2011 JINST 6 C01057 .

[14] Jan Jakubek, Carlos Granja, Oliver Jäkel, Maria Martisikova and Stanislav Pospíšil, *Detection and Track Visualization of Primary and Secondary Radiation in Hadron Therapy Beams with the Pixel Detector Timepix*, IEEE NSS/MIC Knoxville Conf. Record (2011).

[15] http://www.polyflon.com/microw.htm (verified Feb. 2012)

The CRESST Dark Matter Search

G. Angloher [a], M. Bauer [e], I. Bavykina [a], C. Bucci [d], A. Brown [b], C. Ciemniak [c], F. von Feilitzsch [c], D. Hauff [a], P. Huff [a], S. Henry [b], S. Ingleby [b], C. Isaila [c], J. Jochum [e], M. Kiefer [a], M. Kimmerle [e], H. Kraus [b], J.C. Lanfranchi [c], F. Petricca [a], S. Pfister [c], W. Potzel [c], F. Pröbst [a], F. Reindl[a], S. Roth [c], K. Rottler [e], C. Sailer[e], K. Schäffner[a], S. Scholl [e], J. Schmaler [a], W. Seidel [a, +], M. von Sivers[c], C. Strandhagen [e], L. Stodolsky [a], R. Strauss[c], A. Tanzke[a], I. Usherov[e], S. Wawoczny[c], M. Willers[c], A. Zöller[c]

[a] *MPI für Physik, Föhringer Ring 6, 80805 Munich, Germany*
[b] *University of Oxford, Department of Physics, Oxford OX1 3RH, U.K.*
[c] *Technische Universität München, Physik Department, D-85747 Garching, Germany*
[d] *Laboratori Nazionali del Gran Sasso, I-67010 Assergi, Italy*
[e] *Eberhard-Karls-Universität Tübingen, D-72076 Tübingen, Germany*
[+] *Spokesperson E-mail address: seidel@mppmu.mpg.de*
[*] *present address: University of Warwick, Coventry CV4 7AL, U.K.*

Abstract

The aim of CRESST (**C**ryogenic **R**are **E**vent **S**earch with **S**uperconducting **T**hermometers) is to search for particle Dark Matter and to contribute to the elucidation of its nature. The experiment is located at the 'Laboratori Nazionali del Gran Sasso' (LNGS), Italy, and it uses low background cryogenic detectors with superconducting phase transition thermometers for the direct detection of WIMP-nucleus scattering events.

1 Dark Matter

There is strong evidence for the existence of dark matter on all astronomical scales, ranging from dwarf galaxies, through spiral galaxies like our own, to large-scale structures. The history of the universe is difficult to reconstruct without dark matter, be it Big Bang Nucleosynthesis or structure formation.

Despite this persuasive indirect evidence for its existence, the direct detection of dark matter remains one of the outstanding experimental challenges of present-day physics and cosmology.

A plausible candidate for the dark matter is the Weakly Interacting Massive Particle (WIMP) and it is possible that it can be detected by laboratory experiments, particularly using cryogenic methods, which are well adapted to the small energy deposit anticipated. Supersymmetry provides a well-motivated WIMP candidate in the form of the Lightest Supersymmetric Particle. WIMPs are expected to be gravitationally bound in a roughly isothermal halo around the visible part of our galaxy with a density of about $0.3\,\mathrm{GeV/cm^3}$ at the position of the Earth.

Interaction with ordinary matter is expected via elastic scattering on nuclei. This elastic scattering can occur via coherent ("spin-independent") and spin-dependent interactions. For the coherent case, a factor A^2 is expected in the cross-section, favouring heavy nuclei.

Conventional methods for direct detection rely on the ionisation or scintillation caused by the recoiling nucleus. This leads to certain limitations connected with the low ionisation or scintillation efficiency of the slow recoil nuclei. The cryogenic detectors developed for CRESST measure the deposited energy calorimetrically, independent of the type of interaction, and allow for the detection of much smaller recoil energies. When such a calorimetric measurement of the deposited energy is combined with a measurement of scintillation light, an extremely efficient discrimination of the nuclear recoil signals from radioactive background signals can be obtained. These type of detectors are being used in the present phase CRESST-II.

2 Detection Principle

The low-temperature calorimeters consist of a target crystal with an extremely sensitive superconducting phase transition thermometer on its surface. A weak thermal coupling to a heat bath restores again the equilibrium

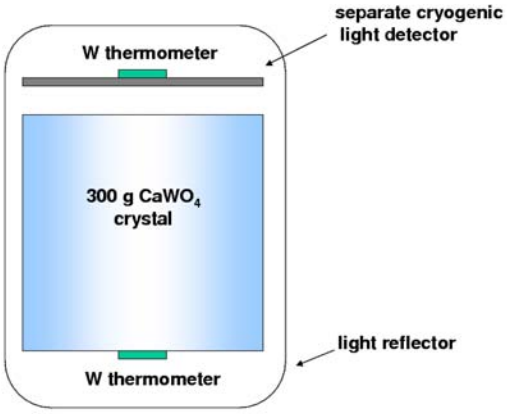

Figure 1: Schematic representation of the detector for simultaneous phonon and light measurement. It consists of two separate cryogenic detectors enclosed in a highly reflective housing, read out by tungsten superconducting phase-transition thermometers. This concept, developed by scientists of the institute, is used in CRESST-II. It allows a very efficient discrimination of the searched nuclear recoil signals from the dominant radioactive β- and γ-backgrounds.

temperature after an interaction. The thermometer is made of a tungsten film evaporated onto the target crystal. Its temperature is stabilised within the transition from the superconducting to the normal conducting state, which occurs at temperatures of about 10 mK. A typical width of the transition is about 1 mK. A small temperature rise e.g. from a WIMP–nucleus scattering event (typically some μK), leads to an increase of resistance, which is measured with a SQUID (**S**uperconducting **Qu**antum **I**nterference **D**evice). For the first phase of CRESST, which ended in 2001, 262 g sapphire detectors had been developed at MPI. These detectors provided an excellent energy resolution of 133 eV at 6 keV and a very low energy threshold of 600 eV.

In the second phase, CRESST-II, we are using 300 g scintillating $CaWO_4$ target crystals. The scintillating crystal is equipped with a superconducting tungsten phase-transition thermometer for the detection of the phonons created by a particle interaction in the scintillating crystal. A small fraction of $\sim$ 1% of the deposited energy is emitted as scintillation light, which is measured with a separate cryogenic detector, optimised for light detection. Fig. 1 shows a scheme of this composite detector.

Starting with a proof-of-principle experiment in 1998, the technique of

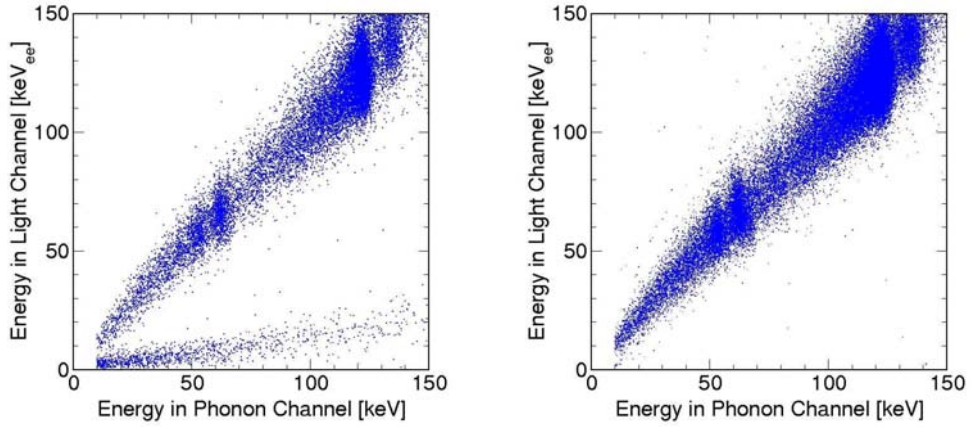

Figure 2: Coincident detection of phonons and scintillation light with a $CaWO_4$ detector. Left: The upper band of events is due to irradiation of the $CaWO_4$ crystal with electrons and gammas, whereas the lower band with lower light yield, is from nuclear recoils caused by a neutron source. Right: Removing the neutron source confirms that there is no leakage of ionising events into the nuclear recoil region.

simultaneous measurement of phonons and scintillation light has been developed at the Max-Planck-Institute. The important advantage of this technique is that it offers an extremely efficient suppression of the radioactive background down to very low recoil energies of about 10 keV. While the phonon signal measures the deposited energy, the amplitude of the corresponding light signal depends on the type of interaction. Nuclear recoils, such as WIMP or neutron scattering events, emit substantially less scintillation light than fully ionising interactions, e.g. γ or β interactions, do. As the overwhelming part of the background consists of β and γ interactions, this phonon/light technique provides a very effective method of background suppression. Fig. 2 illustrates this detection method.

Compared with the alternative approach of simultaneous measurement of phonons and charge in a semiconductor crystal, which is applied in the experiments CDMS-II and Edelweiss-II, the method developed for CRESST-II has the important advantage that it does not suffer from dead layers at the surface. A reduced charge collection for ionising events occurring close to the surface in semiconducting crystals may lead to a false identification of low energetic γ's and β's as nuclear recoils. The result in Fig. 2, which was obtained with a gamma and beta source, confirms that the suppression also works for low-energy electrons impinging onto the crystal surface.

3 The CRESST Setup in Gran Sasso

The central part of the CRESST installation at Gran Sasso is the cryostat. The low temperature which is generated in the mixing chamber of the dilution refrigerator is transferred into the radio-pure cold box, via a 1.5 m long cold finger. The cold finger is protected by thermal radiation shields, all fabricated of low-background copper. The detectors are mounted inside the cold box at the end of the cold finger. Two internal cold shields consisting of low-level lead are attached to the mixing chamber and to a thermal radiation shield at liquid N_2 temperature, respectively, in order to block any line-of-sight from the non-radio-pure parts of the dilution refrigerator to the detectors inside the cold box. The design completely avoids potentially contaminated cryogenic liquids inside the cold box.

An extensive passive shielding of low-background copper and lead surrounds the cold box and serves to shield radioactivity from the surrounding rock. The entire shielding is enclosed inside a gas-tight radon box that is

flushed with boil of N_2 gas and maintained at a small overpressure. Special care was taken to minimise above-ground exposure of the construction materials of the cold box and the shielding to cosmic rays, in order to avoid activation.

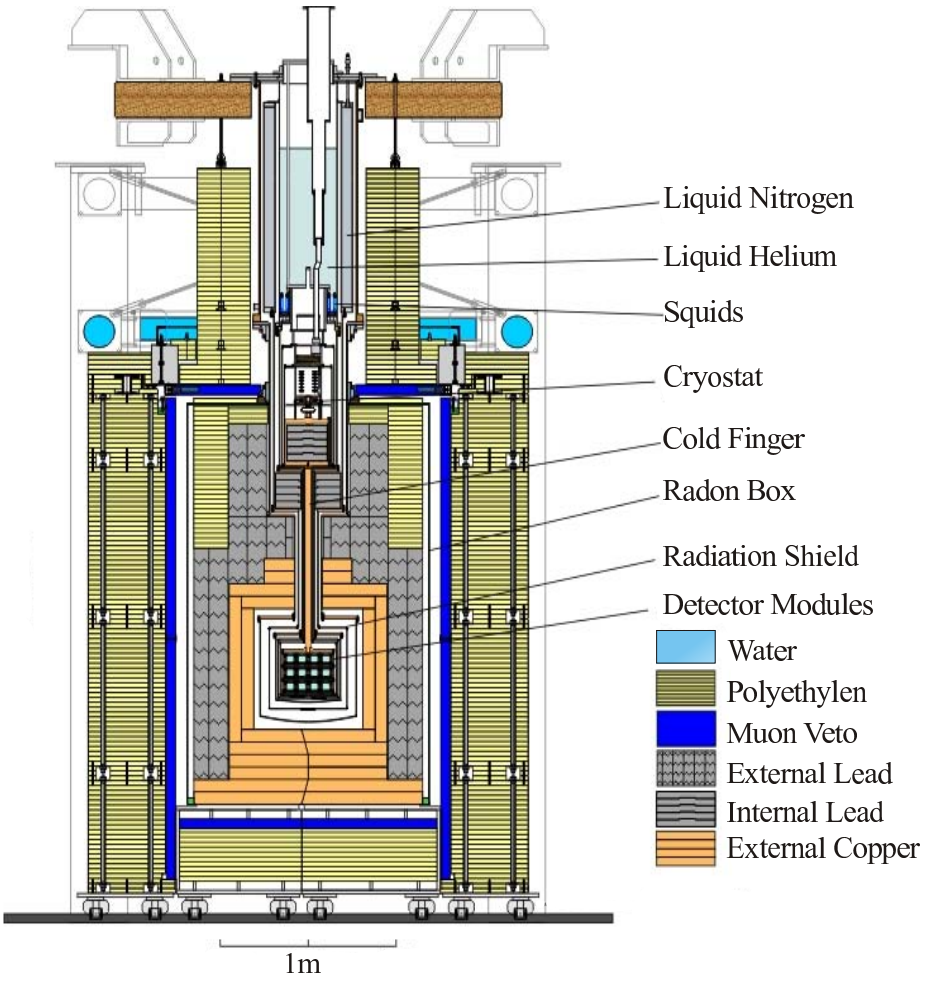

Figure 3: Dilution refrigerator and low-background cold box with its shielding upgraded for CRESST-II. The gas-tight radon box enclosing the Cu (shown in gray) and Pb (blue) shielding is completely covered by a plastic scintillator μ-veto (pink) and 40 cm of polyethylene (red).

4 2009/2010/2011 Data Taking

The latest run of CRESST took place between June 2009 and April 2011. It included a neutron test and γ-calibrations with ^{57}Co and ^{232}Th sources. Out of the 18 detector modules installed in the cryostat only 8 were used for the Dark Matter analysis. One was excluded due to its unusually poor energy resolution and an additional one was excluded being equipped with a test $ZnWO_4$ crystal. The remaining ones mainly had difficulties in cooling the light detectors and could therefore not provide the full information needed for Dark Matter analysis, but still were used to tag coincident events with signals in more than one detector module.The validity of events which are considered for analysis is ured with few basic quality cuts applied to the raw data [1]. The data set discussed here was collected by eight detector modules, between July 2009 and March 2011, corresponding to a total net exposure after cuts of 730 kg days.

4.1 Acceptance region

As any of the nuclei in $CaWO_4$ can be the relevant target for WIMP scattering depending on the mass of a possible WIMP, the acceptance region is chosen such that it extends between the upper boundary of the oxygen band and the lower boundary of the tungsten band and that implicitly includes the calcium band. Since, as a result of the incoming WIMP velocities and nuclear form factors, no significant WIMP signal is expected at energies above 40 keV, the accepted recoil energies are limited by this value. The lower energy bound, in each detector module, is chosen such that the expected e/γ-leakage into the acceptance region is one event in the whole data set of that module. Due to the different resolutions (width of the bands) and levels of e/γ-background in the crystals, this value is different for each module.
A typical acceptance region is shown in orange in Figure 4 which presents in the light yield-energy plane the data set collected with one detector module (Ch51). The calculated bands for α's, oxygen recoils, and tungsten recoils shown in the figure are determined as described in [1].
With this definition of the acceptance region we find 67 accepted events in the sum over the eight detector modules used for Dark Matter analysis.

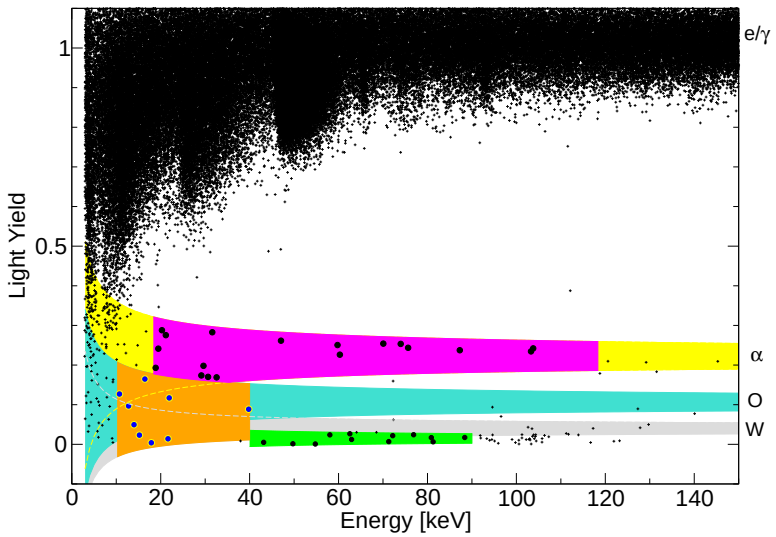

Figure 4: The data of one detector module (Ch51), shown in the light yield vs. recoil energy plane. The large population around a light yield of 1 is due to e/γ-background events. The shaded areas indicate the bands, where alpha (yellow), oxygen (turquoise), and tungsten (grey) recoil events are expected. Additionally highlighted is the acceptance region of this detector (orange) and the reference regions in the α-band (magenta) and in the ^{206}Pb-recoils band (green).

5 Background in the acceptance region

In Figure 4, next to the dominant e/γ-background, which is observed around a light yield of 1, we identify other background sources which could contribute events into the acceptance region. The scope of the analysis is to estimate the contribution of each of the identified backgrounds and to investigate a possible excess above the expectation. This is done using a maximum likelihood analysis which is thoroughly discussed in [1]. Here only its final results will be presented together with a qualitative discussion of the backgrounds in order to clarify the basic arguments and assumptions used in the analysis.

5.1 Alpha Background

In the data (see Figure 4 as an example) we observe low-energy α's with energies down to few keV. We understand these events to be due to α particles

which have lost most of their energy before reaching the target crystals (for details on the housing of the detector modules see [1]). The presence of these events in our data is a consequence of the contamination with α emitters of the non-scintillating clamps holding the crystals. These events are present in all detectors, though the rates vary among modules.
Since the acceptance region has some overlap with the α-band, low energy α-events may be misidentified, leading to a certain number of background events in the acceptance region. In order to estimate this background contribution we select a reference region of the alpha band (highlighted in magenta in Figure 4) which is free of overlap with any other band. For this reference region we use an energy range of 100 keV whose low-energy bound is chosen in each detector module such that the expected e/γ-leakage is 0.1 event in the whole reference region of that module [1]. For each module we estimate in the reference region the energy spectrum dN_α/dE of the low-energy α-events. Using this spectrum we calculate for each individual module the ratio of α-events expected in the reference region and of α-events expected in the acceptance region. This ratio is then used to estimate the expected α-events in the whole acceptance region from the number of events observed in the reference region.

5.2 Lead Recoil Background

In Figure 4 we also identify an event population in and below the tungsten band around 100 keV. This population is caused by the lead nuclei from the α-decays of ^{210}Po present on the surface of the holding clamps and is present, though with different intensities, in all detector modules.
The event distribution of the ^{206}Pb recoils peaks at the full recoil energy of 103 keV but it exhibits a decreasing low-energy tail which, in some detectors, reaches the energy range of interest for Dark Matter. Since this lead-recoil band and the acceptance region overlap considerably, a leakage of some ^{206}Pb events into the acceptance region cannot be excluded.
For an estimate of this background, we follow a similar strategy as for the α background. We define a reference region for each detector module which contains predominantly ^{206}Pb recoils. As a reference region, we choose the low-energy tail of the distribution ($\leq$90 keV) at energies above the acceptance region ($\geq$40 keV), where a possible WIMP signal cannot contribute. An example is highlighted in green in Figure 4. In this region we model the spectral energy density dN_{Pb}/dE of the ^{206}Pb events and then extrapolate

the fit function into the energy range of the acceptance region to estimate the number of ^{206}Pb events expected there [1].

5.3 Neutron Background

Neutron scatterings, which mainly induce oxygen recoils in the energy range of interest, could -if neutrons are present- also contribute to events observed in the acceptance region. Differently from WIMPs, neutrons can cause coincident events in more than one detector module and this characteristic feature was exploited to estimate the contribution of neutrons to the background. Two classes of neutron production mechanisms are identified as possibly relevant sources of background:

1. neutrons emitted by radioactive processes inside the neutron shielding (for a detailed description of the CRESST-II setup see [2, 3]);

2. neutrons produced by muons in the lead or copper shielding where the muon is missed by the veto.

For each of the two production mechanisms we used a corresponding calibration to infer the characteristic ratio between singles and coincident scatterings and to estimate from the observed coincidences the expected number of single neutron events [1].

6 Likelihood Analysis Results

The maximum likelihood fit, described in detail in [1], is based on a parameterized model of the background sources discussed in Section 5 and of a possible signal. The final results are summarized in Table 1. The total likelihood function has two maxima in the parameter space. M1 is the global maximum, but M2 is only slightly disfavored with respect to M1. The background contributions are very similar for M1 and M2 and in both cases the largest contribution is assigned to a possible WIMP signal. The possibility of two different solutions for the WIMP mass is a consequence of the different nuclei present in our target material. The given shape of the observed energy spectrum can be explained by two sets of WIMP parameters. In the case of M1, the WIMPs are heavy enough for the recoils of tungsten nuclei to appear in the energy range of the acceptance region and the possible signal is composed of 69 % of recoils on tungsten, 25 % on calcium and 7 % on oxygen.

Table 1: Results of the maximum likelihood fit. The expected contributions from the considered backgrounds and from a possible WIMP signal are listed for the two solutions together with the corresponding WIMP masses and interaction cross sections. The small statistical error given for the e/γ-background reflects the large number of observed events in the e/γ-band. The other listed errors correspond to a 1σ confidence interval.

	M1	M2
e/γ-events	8.00 ± 0.05	8.00 ± 0.05
α-events	$11.5\,^{+2.6}_{-2.3}$	$11.2\,^{+2.5}_{-2.3}$
neutron events	$7.5\,^{+6.3}_{-5.5}$	$9.7\,^{+6.1}_{-5.1}$
Pb recoils	$14.8\,^{+5.3}_{-5.2}$	$18.7\,^{+4.9}_{-4.7}$
signal events	$29.4\,^{+8.5}_{-7.7}$	$24.2\,^{+8.1}_{-7.2}$
m_χ [GeV]	25.3	11.6
σ_{WN} [pb]	$1.6 \cdot 10^{-6}$	$3.7 \cdot 10^{-5}$

In the case of M2 tungsten recoils appear below the low-energy bound of the acceptance region. The observed signal constitutes of 52 % oxygen and 48 % calcium recoils.
Figure 5 illustrates the fit result, showing an energy spectrum of all accepted events together with the expected contributions of backgrounds and a possible WIMP signal.

The leakage of e/γ-events is the only contribution whose energy spectrum resembles that of a possible WIMP signal. A severe underestimation of this contribution could therefore explain the energy spectrum of the observed excess. However, in addition to the energy spectrum, we have to take into account the information coming from the distribution in the light-yield parameter. Figure 6 shows the corresponding light-yield spectrum of the accepted events (grey) and of all events in the energy range of the acceptance region (brown), together with the expectations from all considered background sources, as inferred from the likelihood fit. The leakage of events from the e/γ-band is naturally expected to be close to the band itself. For this reason the light-yield distribution of the e/γ contribution is expected to rise towards high light yields. However, Figure 6 clearly shows that the distribution of the total accepted events does not allow a relevant increase of the e/γ contribution.

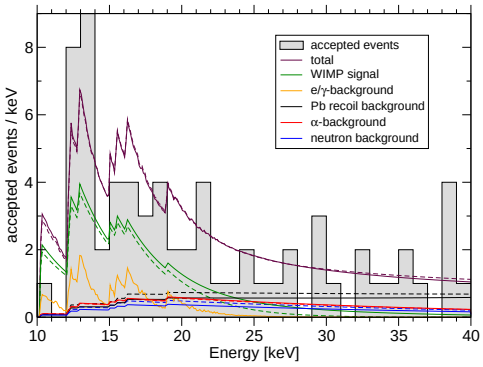

Figure 5: Energy spectrum of the accepted events from all detector modules, together with the expected contributions from the considered backgrounds and a possible WIMP signal, as inferred from the likelihood fit. The solid and dashed lines correspond to the fit results for M1 and M2, respectively.

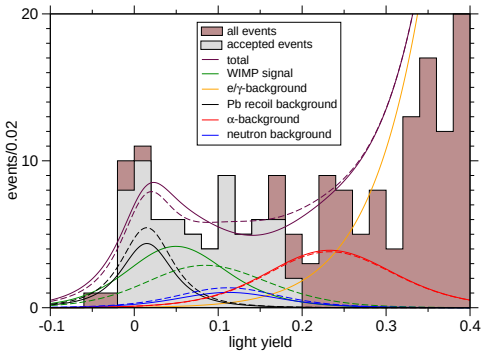

Figure 6: Light-yield distribution of all events in the energy range of the acceptance region (brown) and of the accepted events (grey). The expected contributions of background and of a possible WIMP signal from the likelihood fit are calculated for the fixed yield range of the plot. Outside the (energy dependent) yield boundaries of the acceptance region they are extrapolations of the fit. The solid and dashed lines correspond to the parameter values in M1 and M2, respectively.

The statistical significance at which we can reject the background-only hypothesis, determined with the likelihood ratio test, is 4.7σ for M1 and 4.2σ for M2, meaning that the backgrounds which have been considered are alone insufficient to explain the data. The properties of the additional source of events indicated by the result could be satisfied by Dark Matter particles, in the form of coherently scattering WIMPs. The background contributions are nonetheless still relatively high, therefore a reduction of the overall background rate is necessary to reduce the uncertainties in the modeling of it and to clarify the observation.
Despite the fact that we have an unfavorable situation in terms of background, it is still interesting to study the WIMP parameter space compatible

with our observations. Figure 7 shows the location of the two likelihood maxima in the $(m_\chi, \sigma_{\mathrm{WN}})$-plane, together with the 1σ and 2σ confidence regions. The latest result is consistent with the data of an earlier CRESST run [2]

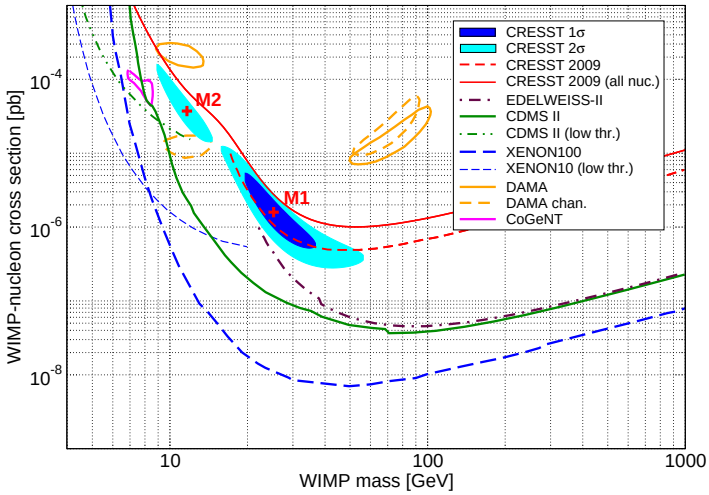

Figure 7: The WIMP parameter space compatible with the latest CRESST results. The CRESST contours have been calculated with respect to the global likelihood maximum M1. In addition the exclusion limits from CDMS-II [4], XENON100 [5], and EDELWEISS-II [6] are shown as well as the 90% confidence regions favored by CoGeNT [7] and DAMA/LIBRA [8]. For comparison we also show the CRESST limit obtained in an earlier run [2] in 2009 and the results of the reanalysis of the same run which takes into account all three nuclei in the target material.

where only tungsten nuclei were considered as a possible target for WIMP scatterings and the 1σ region of M1 is slightly disfavored. The same data of [2] have been reanalyzed considering all three nuclear recoil bands like it is done in the analysis of the present data [1] to increase the sensitivity for light WIMPs. The resulting exclusion limit, which is above the 2σ regions of [1], is shown in Figure 7. A similar analysis was presented in [9] where, however, the acceptance region was restricted to the tungsten band as in [2] accepting, as a consequence, only a fraction of the oxygen and calcium recoils.
The parameters derived from our observation are in tension with the limits published by other experiments [4, 5, 6]. Furthermore, the parameter regions compatible with the observation of DAMA/LIBRA (regions taken from [8]) and CoGeNT [7] are located outside the 2σ CRESST region.

7 Future Developments

At present, a new physics run is in preparation and several improvements aimed at a reduction of the overall background level are being implemented. The most important one addresses modifications of the clamps holding the target crystals aiming at the reduction of the α and ^{206}Pb-recoil backgrounds. Another modification addresses the neutron background and foresees the installation of an additional layer of polyethylene shielding inside the vacuum can of the cryostat. This additional layer which will complement the present polyethylene shielding which is located outside the lead and copper shielding.

References

[1] Godehard Angloher et al. 2011.

[2] Godehard Angloher et al. Commissioning run of the CRESST-II dark matter search. *Astropart. Phys.*, 31:270, 2009.

[3] G. Angloher et al. Limits on WIMP dark matter using scintillating $CaWO_4$ cryogenic detectors with active background suppression. *Astropart.Phys.*, 23:325, 2005.

[4] Z. Ahmed et al. Dark matter search results from the CDMS II experiment. *Science*, 327:1619, 2010.

[5] E. Aprile et al. Dark matter results from 100 live days of xenon100 data. 107:131302, 2011.

[6] E. Armengaud et al. Final results of the edelweiss-ii wimp search using a 4-kg array of cryogenic germanium detectors with interleaved electrodes. *Phys. Lett. B*, 702:329, 2011.

[7] C. E. Aalseth et al. Search for an annual modulation in a p-type point contact germanium dark matter detector. *Phys. Rev. Lett.*, 107:141301, 2011.

[8] Christopher Savage et al. Compatibility of DAMA/LIBRA dark matter detection with other searches. *JCAP*, 0904:010, 2009.

[9] Andrew Brown et al. 2011.

CUORE
2011 LNGS Report

F. Alessandria[1], E. Andreotti[2, 3, *], R. Ardito[4], C. Arnaboldi[5], F. T. Avignone III[6], O. Azzolini[7], M. Balata[8], I. Bandac[6], T. I. Banks[8, 9, 10], G. Bari[11], A. Bau[3], J. Beeman[12], F. Bellini[13, 14], A. Bersani[15], M. Biassoni[3, 5], T. Bloxham[10], C. Brofferio[3, 5], A. Bryant[9, 10], A. Bucchery[14], C. Bucci[8], C. Bulfon[14], X. Z. Cai[16], L. Canonica[15, 17], S. Capelli[3, 5], M. Capodiferro[14], L. Carbone[3], L. Cardani[13, 14], M. Carrettoni[3, 5], N. Casali[13, 14], G. Ceruti[3], A. Chiarini[11], N. Chott[6], M. Clemenza[3, 5], A. Corsi[8], C. Cosmelli[13, 14], O. Cremonesi[3], C. Crescentini[11], R. J. Creswick[6], I. Dafinei[14], A. Dally[18], V. Datskov[3], A. De Biasi[7], M. P. Decowski[9, 10, †], M. M. Deninno[11], A. de Waard[19], S. Di Domizio[15, 17], L. Ejzak[18], R. Faccini[13, 14], D. Q. Fang[16], H. A. Farach[6], E. Ferri[3, 5], F. Ferroni[13, 14], S. Finelli[11], E. Fiorini[3], L. Foggetta[2, 3, ‡], M. A. Franceschi[20], S. J. Freedman[9, 10], G. Frossati[19], B. K. Fujikawa[10], R. Gaigher[3], A. Giachero[3], L. Gironi[3, 5], A. Giuliani[21], J. Goett[8], P. Gorla[22], C. Gotti[3, 5], C. Guandalini[11], E. Guardincerri[8, 10, §], M. Guerzoni[11], T. D. Gutierrez[23], E. E. Haller[12, 24], K. Han[10], K. M. Heeger[18], H. Z. Huang[25], M. Iannone[14], K. Ichimura[10], R. Kadel[26], K. Kazkaz[27], G. Keppel[7], L. Kogler[9, 10], Yu. G. Kolomensky[9, 26], D. Lenz[18], Y. L. Li[16], C. Ligi[20], X. Liu[25], E. Longo[13, 14], Y. G. Ma [16], C. Maiano[3, 5], G. Maier[4], M. Maino[3, 5], C. Mancini[13, 14], C. Martinez[6], R. H. Maruyama[18], R. Mazza[3], R. Michinelli[11], N. Moggi[11], S. Morganti[14], T. Napolitano[20], S. Newman[6, 8], S. Nisi[8], C. Nones[2, 3, **], E. B. Norman[27, 28], A. Nucciotti[3, 5], F. Orio[14], D. Orlandi[8], J. Ouellet[9, 10], M. Pallavicini[15, 17], V. Palmieri[7], G. Pancaldi[11], A. Passerini[3], L. Pattavina[3], M. Pavan[3, 5], M. Pedretti[27], A. Pelosi[14], M. Perego[3], G. Pessina[3], S. Pirro[3], E. Previtali[3], V. Rampazzo[7], F. Rimondi[11, 29, ††], B. Romualdi[8], C. Rosenfeld [6], A. Rotilio[8], C. Rusconi[3], S. Sangiorgio[27], D. Schaeffer[3, 5], N. D. Scielzo[27], M. Sisti[3, 5], A. R. Smith[30], F. Stivanello[7], L. Taffarello[31], E. Tatananni[8], G. Terenziani[7], W. D. Tian[16], C. Tomei[14], S. Trentalange[25], G. Ventura[32, 33], M. Vignati[13, 14], B. Wang[27, 28], H. W. Wang[16], C. A. Whitten Jr.[25, ††], T. Wise[18], A. Woodcraft[34], L. Zanotti[3, 5], C. Zarra[8], B. X. Zhu[25], S. Zucchelli[11, 29],

(The CUORE Collaboration)

[1]INFN - Sezione di Milano, Milano I-20133 - Italy
[2]Dipartimento di Fisica e Matematica, Università dell'Insubria, Como I-22100 - Italy
[3]INFN - Sezione di Milano Bicocca, Milano I-20126 - Italy
[4]Dipartimento di Ingegneria Strutturale, Politecnico di Milano, Milano I-20133 - Italy
[5]Dipartimento di Fisica, Università di Milano-Bicocca, Milano I-20126 - Italy
[6]Department of Physics and Astronomy, University of South Carolina, Columbia, SC 29208 - USA
[7]INFN - Laboratori Nazionali di Legnaro, Legnaro (Padova) I-35020 - Italy
[8]INFN - Laboratori Nazionali del Gran Sasso, Assergi (L'Aquila) I-67010 - Italy
[9]Department of Physics, University of California, Berkeley, CA 94720 - USA
[10]Nuclear Science Division, Lawrence Berkeley National Laboratory, Berkeley, CA 94720 - USA
[11]INFN - Sezione di Bologna, Bologna I-40127 - Italy
[12]Materials Science Division, Lawrence Berkeley National Laboratory, Berkeley, CA 94720 - USA
[13]Dipartimento di Fisica, Sapienza Università di Roma, Roma I-00185 - Italy
[14]INFN - Sezione di Roma, Roma I-00185 - Italy

[15]INFN - Sezione di Genova, Genova I-16146 - Italy
[16]Shanghai Institute of Applied Physics (Chinese Academy of Sciences), Shanghai 201800 - China
[17]Dipartimento di Fisica, Università di Genova, Genova I-16146 - Italy
[18]Department of Physics, University of Wisconsin, Madison, WI 53706 - USA
[19]Kamerlingh Onnes Laboratorium, Leiden University, 2300 RA Leiden - The Netherlands
[20]INFN - Laboratori Nazionali di Frascati, Frascati (Roma) I-00044 - Italy
[21]Centre de Spectrométrie Nucléaire et de Spectrométrie de Masse, 91405 Orsay Campus - France
[22]INFN - Sezione di Roma Tor Vergata, Roma I-00133 - Italy
[23]Physics Department, California Polytechnic State University, San Luis Obispo, CA 93407 - USA
[24]Department of Materials Science and Engineering, University of California, Berkeley, CA 94720 - USA
[25]Department of Physics and Astronomy, University of California, Los Angeles, CA 90095 - USA
[26]Physics Division, Lawrence Berkeley National Laboratory, Berkeley, CA 94720 - USA
[27]Lawrence Livermore National Laboratory, Livermore, CA 94550 - USA
[28]Department of Nuclear Engineering, University of California, Berkeley, CA 94720 - USA
[29]Dipartimento di Fisica, Università di Bologna, Bologna I-40127 - Italy
[30]EH&S Division, Lawrence Berkeley National Laboratory, Berkeley, CA 94720 - USA
[31]INFN - Sezione di Padova, Padova I-35131 - Italy
[32]Dipartimento di Fisica, Università di Firenze, Firenze I-50125 - Italy
[33]INFN - Sezione di Firenze, Firenze I-50125 - Italy
[34]SUPA, Institute for Astronomy, University of Edinburgh, Blackford Hill, Edinburgh EH9 3HJ - UK
[*]Presently at: Joint Research Center, Institute for Reference Materials and Measurements, 2440 Geel - Belgium
[†]Presently at: Nikhef, 1098 XG Amsterdam - The Netherlands
[‡]Presently at: Laboratoire de l'Accélérateur Linéaire, Centre Scientifique d'Orsay, 91898 Orsay - France
[§]Presently at: Los Alamos National Laboratory, Los Alamos, NM 87545 - USA
[**]Presently at: CEA / Saclay, 91191 Gif-sur-Yvette - France
[††]Deceased

Abstract

We report on activities carried out in 2011 for the CUORE neutrinoless double beta decay experiment.

1 CUORE experiment: 2010 activities and present status

The Cryogenic Underground Observatory for Rare Events (CUORE) [1] is an upcoming cryogenic bolometer experiment designed to search for $\beta\beta(0\nu)$ in the isotope ^{130}Te. The CUORE detector will consist of a close-packed array of 988 TeO_2 crystals containing ~ 200 kg of ^{130}Te and cooled inside a large cryostat to 10 mK. At this low temperature the crystals function as highly sensitive calorimeters, converting the relatively small energies deposited inside them by particles into measurable rises in temperature. The expected signature of $\beta\beta(0\nu)$ in ^{130}Te is a peak in the measured energy spectrum at 2527 keV, the Q-value for the transition $^{130}\text{Te} \rightarrow^{130}\text{Xe} + 2\beta^-$. The goal of CUORE is to reduce the background level below 10^{-2} counts/keV/kg/y in this region of interest (ROI) and to make a high-precision measurement of the spectrum in a narrow energy window around the Q-value of the decay. If successful, the experiment will be sensitive to an effective Majorana neutrino mass of the order of 50 meV, better than any previous experiment. While the primary focus of the experiment is to search for $\beta\beta(0\nu)$, other rare-event studies will also be possible, such as searches for dark matter particles and axions.

The current best limit on $\beta\beta(0\nu)$ in ^{130}Te, $\tau_{1/2}^{\beta\beta(0\nu)} > 2.8 \times 10^{24}$ y (90% C.L.), comes from CUORE's predecessor, the Cuoricino experiment [2]. The Cuoricino detector was comprised of a tower of 62 TeO_2 crystal bolometers containing 11 kg of ^{130}Te and operated in a cryostat at the underground Laboratori Nazionali del Gran Sasso (LNGS), Italy, from 2003–2008. CUORE is essentially a scaled-up version of Cuoricino that exploits the experience and results gained from its predecessor while aiming at an improvement in sensitivity by roughly two orders of magnitude. The CUORE bolometers will be arranged in a cylindrical matrix of 19 towers, each tower containing 13 planes of four crystals supported inside a copper frame. The experiment will be located in Hall "A" of Laboratori Nazionali del Gran Sasso (LNGS) where the rock overburden provides 3650 m.w.e. of shielding against cosmic rays, while the cryostat has numerous internal and external lead shields to block natural environmental radiation.

The experiment is now in the construction phase.

A fully dedicated hut, located in the southern wing of the Hall "A" have been contructed to host the CUORE experimental setup together with all the needed accessories. Most of the CUORE infrastructure will be located inside the Hut, including the Clean room and the Counting room. In particular, the hut will host the CUORE cryostat which will be hanging (from a supporting platform located at the second floor) into the CUORE clean room at the first floor of the Hut. The Hut frame, walls, stairwells, floors and conventional untilities and the clean room on the middle floor are now ready. The main detector support, which is mechanically separated from the Hut has also been installed. This includes the concrete foundation (installed on the top of a series of elastomers) and column supports for the detector, the main support plate (MSP) that rests on the columns, the "Y" frame and its "negative" spring constant supports designed for vibration isolation of the detector from external sources and a set of three hoists to lift the cryogenic vessels or shields and their flanges.

Most of the details regarding the CUORE project and the construction of its apparatus

have been disussed in the CUORE LNGS Annual Reports of the last few years. Here we simply give an update of the year 2011 activities that have been mainly concentrated on the construction of the cryogenic apparatus (Section 1.1), the completion of the crystal test activity (Section 1.2) and the preparation of a single-tower experiment CUORE-0 (Section 1.3) that have been the test bench for the assembly line – with its procedures, tools and materials – projected for the construction of the 19 CUORE towers.

1.1 Cryogenics

The technical specifications for the CUORE experiment –namely, the total detector mass, the working temperature, and the background level – place very stringent requirements on the refrigerator, suspension system, the radiopurity of materials, and the reliability of the cryogenic system. The CUORE cryogenic apparatus (Figure 1) is separated into different sections having specific goals:

- Cooling system: A ^{3}He/^{4}He dilution refrigerator (including its control system), the ^{3}He circulation system, and the pumping and compressor system.
- Cryostat: 2 separated vacuum chambers with six closed (shields) vessels at decreasing temperatures: 300 K, 40 K, 4 K, 600 mK, 50 mK, and 10 mK.
- Cold lead shield: 4π solid-angle lead shielding of the detector.
- Detector suspension system: A mechanical decoupling to minimize vibrations in the few Hz-few kHz frequency band.
- Calibration system: A system allowing insertion of gamma-calibration sources in between the detector towers.

1.1.1 Cryostat

The CUORE cryostat is described in detail in the 2007 LNGS Annual Report, so here we merely summarize its present status. The cryostat's design and construction drawings underwent significant revision following the comprehensive seismic analysis of the CUORE setup in 2009. Consultants from Dipartimento di Ingegneria Strutturale of Politecnico di Milano reviewed the project and proposed actions to improve the safety of the structure. In particular, for what concerns the cryostat, the design of the internal tie rods was improved and stoppers between the vessels were introduced to limit their displacement. The 40 K, 4 K and Still tie rods are designed to be loaded each with about 0.33, 0.66 and 3.2 tons, respectively, and to resist without damage only to more frequent and weaker earthquakes with Peak Ground Acceleration (PGA) of about 0.08 g (intensity V on the Modified Mercalli scale, expected once in 35 years). The construction schedule has been updated accordingly. The vessels and their top plates are being produced by Simic (Camerana, Cuneo, Italia). Presently, the 300 K, 40 K and 4 K cryostat plates have been completed and the corresponding vessels are being e-beam welded by Pro-Beam (Burg, Germany). The production of all other cryostat components, such as

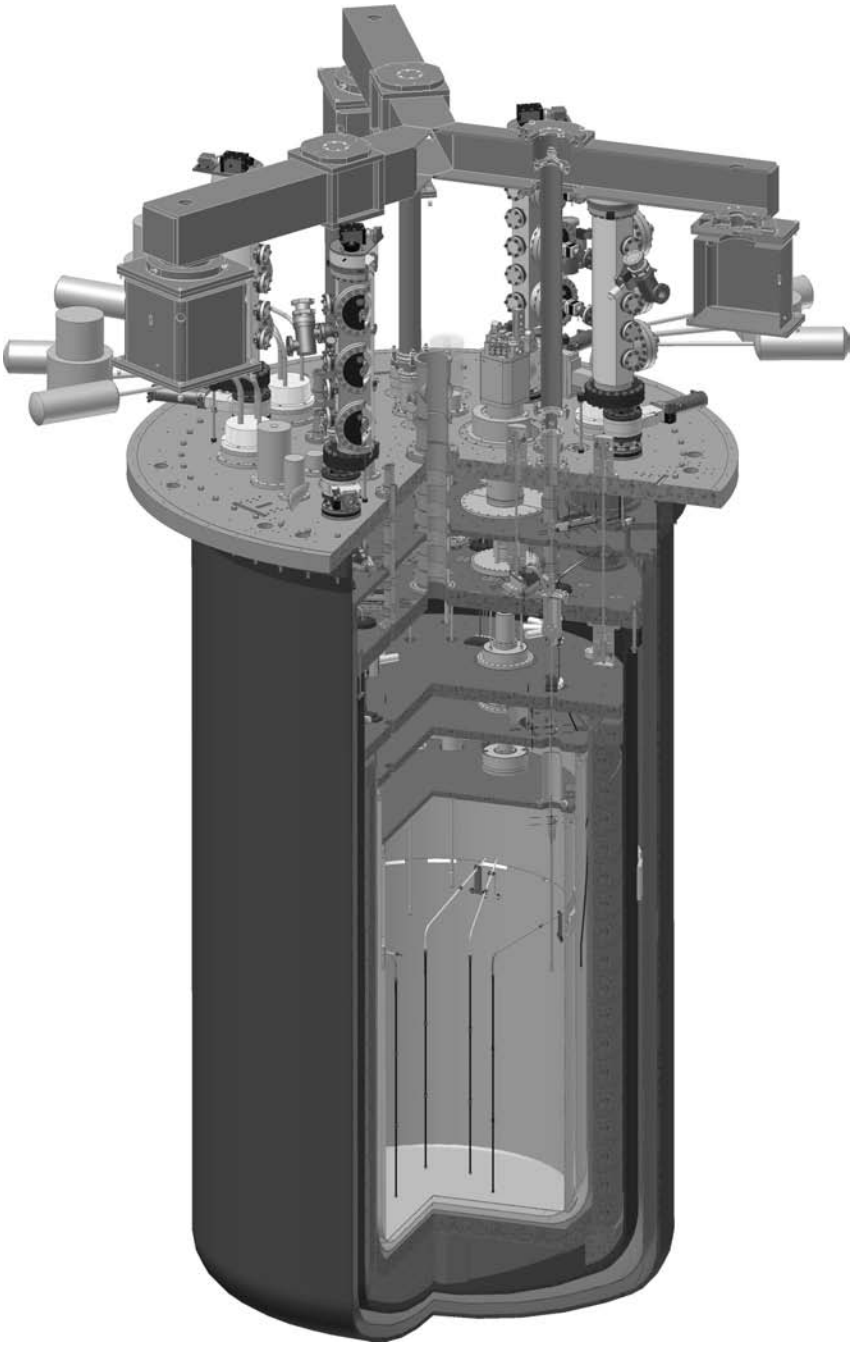

Figure 1: CUORE cryostat.

the 316LN stainless tie rods, the IVC access ports and the thermal links, is in progress as well. The design of the inner cryostat parts is complete and the construction of the inner shields will start soon after the outer vessels will be successfully tested at 77 K by Simic. The full commissioning at LNGS of the three outer chambers is expected by April 2012. Presently at LNGS the MSP, with the integrated hoist system for lifting the cryostat plates and vessels, is already in place. All tools necessary for the test are being prepared, in particular a high-vacuum system and a computer system for controlling the cooldown process have been developed and successfully tested in the Milano-Bicocca laboratory. Progress has also been made on the copper thermal links for the tie rods and the pulse tubes. High-thermal-conductance copper has been procured and characterized in the Milano-Bicocca laboratory, and assembly procedures have been developed. The design of multilayer insulation for the cryostat has been completed and the blankets have been procured. Laboratory tests have been made on the 4 K indium-sealed flanges and the low-pressure safety valves. The progress on production of the cryostat's vacuum chambers and their connecting systems suggests a likely start of the integration process in Spring 2012. The first step will be to assemble the 300 K, 40 K and 4 K vessels with one detector calibration box, the upper suspension components, one upper wire insert, and two pulse tubes. The system will be cooled to 4 K and the functionality of the various subsystems will be tested. Integration of the dilution unit will follow shortly.

1.1.2 Cooling System DU

The cooling power to operate the CUORE detectors at temperatures in the 10 mK range, is provided by a custom cryogen-free high-power ^{3}He/^{4}He Dilution Unit (DU) developed by Leiden Cryogenics (Leiden, The Netherlands). The DU includes a Joule-Thompson condensing stage specially designed for high circulation rates and fitted with two spring loaded variable flow impedances. Thanks to two magnetically levitated turbo pumps (about 1850 l/s each), the ^{3}He Gas Handling System (GHS) can provide a ^{3}He flow rate up to about 6 μmoles/s. In order to prevent excessive thermal loading of the 4 K cryostat stage at high circulating rates, the incoming ^{3}He gas is pre-cooled thanks to tubes soldered on the PT bodies. The minimum cooling power specifications on the MC are 5 μW at 12 mK and 1.5 mW at 120 mK during continuous operation in a test cryostat. Presently the DU with its GHS is being characterized and optimized at Leiden Cryogenics in a standard test cryostat with two PTs. Preliminary runs showed a base temperature as low as 5.3 mK (with no external load) and a cooling power of about 3 mW at about 120 mK. Leiden Cryogenics is also developing a system (Fast Cooling System or FCS) for a quick pre-cooling of the IVC and of the whole experimental mass from room temperature to less than 30 K. The FCS will consists of an external vessel with heat exchangers, three Gifford-McMahon cryo-coolers (each with a cooling power of about 600 W at 77 K), a helium blower and double-walled pipes. Helium gas, progressively cooled in the external vessel, will be circulated and routed to three location at the bottom of the cryostat IVC. A preliminary estimate for the pre-cooling time of the complete cryogenic system by means of the FCS with the help of the five PTs gives less than 4 days to reach 4 K.

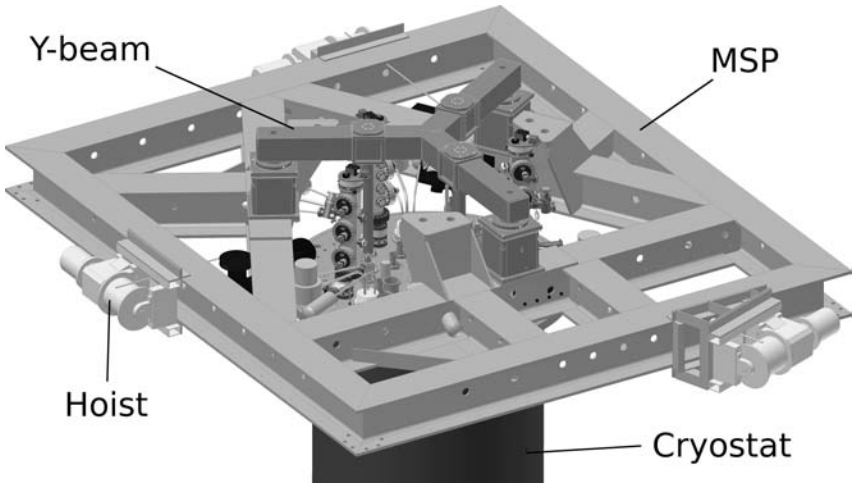

Figure 2: CUORE cryostat.

1.1.3 Detector and shield suspension system

The detector suspension has been designed to minimize the transmission of mechanical vibrations due to both seismic noise and the operation of cryo-coolers and pumps. The suspension is a two-stage low-frequency isolator in the vertical direction, while in the horizontal direction the structure is a pendulum with a natural frequency of about 0.4 Hz. A second suspension system, designed in a similar way as the one for the detector, is foreseen for the top lead disk. Both suspensions must provide a load path while minimizing the heat input and the vibration transmission. The detector suspension is made by several parts: three Minus-K springs and the Y-beam positioned on top of them are already mounted in the CUORE Hut on top of the MSP (Figure 2). The detector will be suspended to the Y-beam through three composite rods. The system formed by the Minus-K springs and the rest of the detector will behave like a spring-mass system with a cut-off frequency of 0.5 Hz. For the inner top lead shield assembly a similar suspension scheme has been designed: the lead suspension will be hung to the 300 K top plate and not to the Y-beam to guarantee the best mechanical decoupling of the detector from the cryostat assembly. Both suspensions have been designed and the detector suspension parts have been built and pre-assembled, preliminary vibrational mode measurements on the Y-beam structure and a satisfactory first test in air of the Minus-K springs with a dummy load have been performed.

1.2 Crystal production and testing

The CUORE detector will consist of 988 $5 \times 5 \times 5$ cm^3 TeO_2 crystals purchased from the Shanghai Institute of Ceramics, Chinese Academy of Sciences (SICCAS). Crystal production has been ongoing since 2009 at a dedicated clean room facility in Jiading, China, and batches of finished crystals are shipped to LNGS every 1–2 months, traveling by sea to limit cosmogenic activation. As of January 2012, 832 crystals (out of a total order of 1060) have been delivered to LNGS, where they are stored in nitrogen-fluxed cabinets in

CUORE's underground Parts Storage Area (PSA). The remaining complement of crystals will be delivered in 2012.

It is essential to the success of the experiment that the CUORE crystals possess exceptionally low levels of radioactive contamination. As such, the contracts with SICCAS specify very stringent radiopurity requirements, primarily regarding the bulk contamination levels of ^{238}U and ^{232}Th. In order to verify that contaminations are within contract limits (and also to check overall performance), approximately 4% of the delivered crystals are tested as cryogenic bolometers in so-called CUORE Crystal Validation Runs (CCVRs). In a CCVR, four crystals are randomly selected from the most recent shipments, assembled into a detector module, and cooled to 10 mK inside the CUORE R&D cryostat in Hall "C"at LNGS. Each CCVR typically lasts for $\sim$ 1 month, which is the time needed to acquire sufficient statistics to verify that the crystals meet contract specifications. Eight CCVRs have been performed to date—three of them in 2011—and we intend to perform three more in 2012. All of the tested crystals have met or exceeded the specifications for bulk radioactivity and dimensional tolerances, and based on this experience we expect all crystals to meet the requirements for CUORE.

The CCVR measurements of crystal bulk and surface contaminations also serve as critical inputs to simulations of the expected backgrounds in CUORE. In early 2011 we began a comprehensive reanalysis of data from CCVRs 1–5 to systematically study the radioactive contamination in those detectors. Making very conservative assumptions, we concluded that background contributions to CUORE from crystal bulk and surface contaminations will be 1.1×10^{-4} counts/keV/kg/y and 5.5×10^{-3} counts/keV/kg/y, respectively, in the neutrinoless double beta decay region of interest [3]. The data for this study will be doubled when the CCVR program concludes in 2012, and we expect to produce more accurate estimates for the crystal-generated backgrounds in CUORE soon after.

It is worth noting that the CCVRs have the added benefit of providing valuable experience to the younger members of the collaboration, as postdocs and graduate students are largely responsible for building the detectors and analyzing the data. Detector construction is a time-intensive, two-week process that offers the opportunity to become familiar with the details of bolometric devices, while the data analysis for each CCVR is a relatively short-time-scale project that enables analyzers to become acquainted with both basic bolometer physics and the CUORE software framework. For the data analysis we have instituted a training system whereby an individual first apprentices as the "rookie" analyzer on a CCVR before becoming the "expert" analyzer on the subsequent CCVR. In this way the CCVR program serves as a useful training ground for CUORE-0 and CUORE.

1.3 CUORE-0

The CUORE collaboration plans to operate a single CUORE-like tower in the former Cuoricino cryostat, starting in early 2012. This configuration, named CUORE-0, will validate the assembly procedure and the readiness of the background reduction measures, and it will also serve as a sensitive $\beta\beta0\nu$ experiment in its own right.

CUORE-0 will consist of 52 CUORE crystals mounted in CUORE-style frames as

a single tower with a total TeO_2 mass of 39 kg. It will be assembled from detector components manufactured, cleaned, and stored following the same stringent protocols defined for CUORE; its construction will also be performed following the no-contact procedures developed for CUORE detector assembly. The preparation of CUORE-0 will allow the collaboration to confirm the efficacy and feasibility of the CUORE production and assemby procedures, and it will also provide a forum in which to refine the necessary expertise for the construction of the final CUORE detector.

In addition, CUORE-0 represents an opportunity to evaluate the bolometric performance of a CUORE-like detector apparatus in a familiar cryostat, and it will be the first large-scale empirical test of the extensive background-reduction measures undertaken by the collaboration following the Cuoricino experience.

An analysis of the background sources responsible for the flat background in the ROI in Cuoricino has been performed on a partial set of statistics [4], following the technique and the model developed for the MiDBD experiment [5]. The result of this analysis was the identification of three main contributions: $30 \pm 10\%$ of the measured flat background in the ROI is due to multi-Compton events due to the 2615 keV gamma ray from the decay chain of ^{232}Th from the contamination of the cryostat shields; $10 \pm 5\%$ is due to surface contamination of the TeO_2 crystals with ^{238}U and ^{232}Th (primarily degraded alphas from these chains); and $50 \pm 20\%$ is ascribed to similar surface contamination of inert materials surrounding the crystals, most likely copper.

On the basis of this result, the R&D for CUORE has aggressively pursued methods to reduce the surface contamination of both the copper and the crystals. The required surface contamination levels are extremely low, on the order of 1–10 nBq/cm^2, nearly undetectable with any standard technique used in surface analysis. In most cases, only bolometric detectors are sufficiently sensitive; at this time, our understanding of these contaminations comes only from the statistics-limited data sets collected by small test detectors constructed from CUORE materials (see Ref. [3] for the contract requirements on and measurements of the contamination levels of the crystals). Based on these limited-statistics measurements, it has been established that the surface-treatment techniques chosen for the CUORE copper and crystals are both capable of reducing the surface contaminations by at least a factor of 2 as compared with those observed in Cuoricino. There is a good chance that the reduction factors are in fact much higher, but this cannot be confirmed at present due to the limited statistics of our measurements. Only CUORE-0 will ultimately be able to measure the true level of radiopurity achieved with the chosen surface treatments.

CUORE-0 will thus serve as a test bench for CUORE, not only with respect to the production and construction procedures but also with respect to anticipated physics performance.

Although the exact background rate that will be seen in CUORE-0 will not be known until CUORE-0 begins taking data, we can offer some simple scaling arguments to establish that we can expect CUORE-0 to be a sensitive $\beta\beta0\nu$ experiment in its own right during the approximately two years for which it will operate prior to the start of CUORE. Because the single-tower geometry of CUORE-0 is similar to that of Cuoricino, the contamination reduction factors reported above for the copper and crystals scale almost directly to the background we expect to observe in the ROI. The total amount of cop-

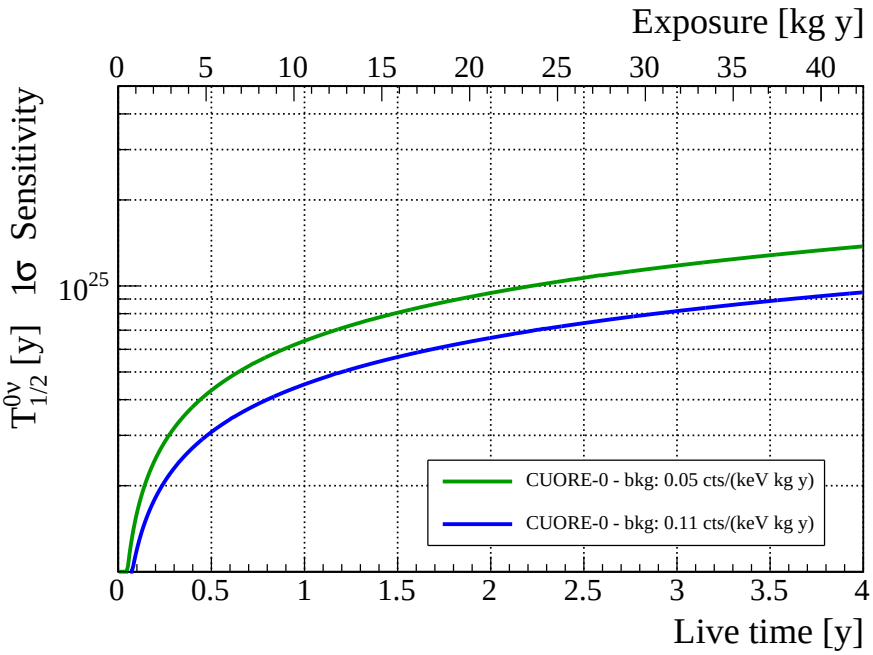

Figure 3: CUORE-0 sensitivity at 1σ for two different values of the background rate in the region of interest, 0.05 counts/keV/kg/y (solid line) and 0.11 counts/keV/kg/y (dotted line), representing the range into which the CUORE-0 background is expected to fall.

per facing the crystals will be only slightly reduced with respect to Cuoricino, but its surface will be treated with the new procedure studied for CUORE. CUORE-0 will be assembled in the Cuoricino cryostat, so the gamma background from contamination in the cryostat shields will remain approximately the same as in Cuoricino. We consider that the irreducible background for CUORE-0 comes from the 2615 keV ^{208}Tl line due to ^{232}Th contaminations in the cryostat, in the case that all other background sources (i.e., surface contaminations) have been rendered negligible; this would imply a lower limit of ~ 0.05 cts/(keV kg y) on the expected background in CUORE-0. Similarly, an upper limit of 0.11 cts/(keV kg y) follows from scaling the Cuoricino background in the conservative case of a factor of 2 improvement in crystal and copper contamination.

A plot of the expected 1σ sensitivity (comparable to a 68% C.L. sensitivity) of CUORE-0 as a function of live time in these two bounding cases is shown in Fig. 3. The anticipated total live time of CUORE-0 is approximately two years; the 1σ sensitivity for this live time is between 6.6×10^{24} y (at the 0.11 counts/keV/kg/y background level) and 9.4×10^{24} y (at the 0.05 counts/keV/kg/y background level).

1.3.1 CUORE-0 Crystal Instrumentation

The new gluing system for the sensor-to-crystal connection of the CUORE and CUORE-0 detector has been commissioned during summer 2011 inside the new CUORE clean room. Three are the main goals of the new system:

- to obtain a reliable and reproducible sensor-to-absorber thermal and mechanical connection, a crucial detector parameter that drives the bolometric performances.

- to avoid problems of crystal surfaces recontamination. For this reason all the operations are performed inside a nitrogen fluxed glove box and all the used material have been carefully selected by the radioactivity point of view.

- to have a fast procedure allowing a high rate of instrumented crystals.

More details about the system components and the procedures are described in previous CUORE LNGS Annual Reports.

At the beginning of September 2011, after a careful cleaning of all the system parts, the gluing system parameters have been tuned. Starting from middle of September the instrumentation of the CUORE-0 crystals have been realized. It took about 10 days to process all them and the maximum production rate has been 10 crystals per day. For each crystal instrumentation, the temperature and humidity values, as well as the time durations of the various operations, have been collected and recorded in a dedicated database. The database contains also all the pictures of the glue spots on the sensors. At the end of each gluing series, all the instrumented crystals have been located on a PTFE holder and stored under vacuum inside a Reber box. The boxes have been closed inside nitrogen filled bags and located in the PSA nitrogen fluxed cabinets.

In view of CUORE some improvements of the system have been planned. In particular, during the CUORE-0 crystal instrumentation, a temperature drift of the system have been observed. This temperature instability seems correlated with the glue spots diameter variation. For this reason the implementation of a temperature stabilization system for the glove box has been planned.

The improvement of the system is foreseen to end in May 2012. June will be dedicated to the training of operators that will use the CUORE gluing system. In July the instrumentation of the crystals for 4 towers of CUORE should start.

1.3.2 CUORE-0 Tower Assembly

CUORE-0 preparation represents the first test of the CUORE Tower Assembly Line (CTAL), described in detail in the previous CUORE LNGS Annual Reports. CTAL construction, installation in the CUORE clean room and subsequent commissioning ended in Summer 2011.

CUORE-0 assembly started in October 2011. Despite the general results, the assembly line performs well and satisfies all its requirements. In particular CTAL equipment can be conveniently arranged not only to build a CUORE tower, but also to perform unexpected operations, measurements and a complete reverse engineering of each step. All the assembly line procedures demonstrated to be safe and to ensure the protection of all the detector pieces from the outside. The zero contact request is hence completely fulfilled. CTAL proved to be ready for the construction of CUORE-0 and CUORE.

CTAL precision tools allowed us to discover problems never observed before. In particular, the tower was assembled and afterwards dismounted because of unexpected copper softness and machining defects found in the copper frames. The operation was repeated several times, using different pieces coming from different batches, revealing problems both in the production and cleaning chain.

Figure 4: Pictures of ten instrumented CUORE-0 crystals. The crystals are in the crystal storage area inside the gluing glove box and they are waiting to be stored in the Reber boxes.

Copper frames production procedures have been modified so that new pieces are now in specifics. Copper cleaning is presently being corrected in order to ensure better mechanical properties. Final tests are foreseen at the beginning of March 2012. The final cleaning procedures will be defined within March 2012 testing the assembly of a full tower structure (no crystals) with the new copper components. The construction of CUORE-0 will than follow. As stated before the CTAL tools and procedures have been proven to be effective and reliable hence, as soon as the CUORE-0 construction is over, the procedure to hire and train the CUORE construction team will start. For training purpose an ad hoc clean tower mockup will be produced. The training course is planned to start during summer to have the first 4 CUORE towers assembled in October 2012.

2 Publications in 2011

1. M. Carrettoni and M. Vignati, J. Instr. 6 (2011) 08007.
2. C. Arnaboldi *et al.*, CUORICINO-Collaboration, Astroparticle Physics 34 (2011) 822.
3. C. Arnaboldi *et al.*, CUORICINO-Collaboration, Astroparticle Physics 34 (2011) 643.
4. L. Foggetta *et al.*, Astroparticle Phys. 34 (2011) 809.
5. S. Di Domizio, F. Orio and M. Vignati, J. Inst. 6 (2011) 02007.

References

[1] C. Arnaboldi *et al.*, Astropart. Phys. **20**(2003) 91.
C. Arnaboldi *et al.*, Nucl. Instr. Meth. A **518** (2004) 775.
R. Ardito *et al.*, CUORE: A cryogenic underground observatory for rare events, arXiv hep-ex/0501010 (2005).

[2] C. Arnaboldi *et al.*, Phys. Rev. Lett. **95** (2005) 14501.
E. Andreotti, *et al.*, Astropart. Ph. 34 **34** (2011) 822.

[3] F. Alessandria *et al.*, accepted for publication on Astropart. Phys., arXiv:1108.4757.

[4] C. Arnaboldi *et al.*, Phys. Rev. C **78** (2008) 035502.

[5] C. Bucci *et al.*, Eur. Phys. J A **41** (2009) 155.

DAMA

Collaboration:

P. Belli[a], R. Bernabei[a,@], A. Bussolotti[a,*], S. d'Angelo[a], A. Di Marco[a], F. Montecchia[a], A. d'Angelo[b], F. Cappella[b], A. Incicchitti[b], A. Mattei[b,*], R. Cerulli[c], V. Caracciolo[c], C.J. Dai[d], H.L. He[d], H.H. Kuang[d], X.H. Ma[d], X.D. Sheng[d], R.G. Wang[d], Z.P. Ye[d,e]

in some detector developments, by-product results and small scale experiments: A.S. Barabash[r], R.S. Boiko[g], V.B. Brudanin[h], D.M. Chernyak[g], F.A. Danevich[g], M.L. di Vacri[c] A.E. Dossovitskiy[k], A.M. Dubovik [n] E.N. Galashov[l], B.V. Grinyov[n] V.V. Kobychev[g], S.I. Konovalov[r] G.P. Kovtun[m], B.N. Kropivyansky[g], V.M. Kudovbenko-Mokina[g], M. Laubenstein[c], A.L. Mikhlin[k], L.L. Nagornaya[n], P.G. Nagornyi[j], S.S. Nagorny[g], A.S. Nikolaiko[g], S. Nisi[c], D.V. Poda[c,g], R.B. Podvujanyuk[g], O.G. Polischuk-Shkulkova[g], A.P. Shcherban[m], V.N. Shlegel[l], D.A. Solopikhin[m], Yu.G. Stenin[l], J. Suhonen[o], A.V. Tolmachev[q], V.I. Tretyak[g], I.A. Tupitsyna[n], V.I. Umatov[r], Ya.V. Vasiliev[l], V.D. Virich[m], Yu. Ya. Vostretsov[n], I.M. Vyshnevskyi[g], R.P. Yavetskiy[q], S.S. Yurchenko[g]

in some studies on $\beta^+\beta^+$, EC/β^+, EC/EC decay modes (under the joint Indo-Italian DST-MAE project and inter-universities agreement): P.K. Raina[p], A.K. Singh[p], P.K. Rath[p], S. Ghorui[p]

[a]Dip. Fisica, Univ. Roma "Tor Vergata" and INFN-Roma Tor Vergata, Roma, Italy.
[b]Dip. Fisica, Univ. Roma "La Sapienza" and INFN-Roma, 00185 Roma, Italy.
[c]Laboratorio Nazionale del Gran Sasso, INFN, 67010 Assergi (Aq), Italy.
[d]IHEP, Chinese Academy, P.O. Box 918/3, Beijing 100039, China.
[e]Physics Dept, Jing Gangshan University 343009, Jiangxi, China.
[f]Russian Chemistry-Technological University of D.I.Mendeleev, Moscow, Russia.
[g]Institute for Nuclear Research, MSP 03680, Kiev, Ukraine.
[h]Joint Institute for Nuclear Research, 141980 Dubna, Russia.
[i]Department of Applied Physics, Curtin University, GPO, Box U1987 Perth, Australia.
[j]Kiev National Taras Shevchenko University, MSP 01033 Kiev, Ukraine.
[k]Joint stock company NeoChem, 117647 Moscow, Russia.
[l]Nikolaev Institute of Inorganic Chemistry, 630090 Novosibirsk, Russia.
[m]National Science Center Kharkiv Institute of Physics and Technology, Kharkiv, Ukraine.
[n]Institute for Scintillation Materials, 61001 Kharkiv, Ukraine.
[o]Dep. of Physics, University of Jyvaskyla, P.O. Box 35, FIN-40351, Jyvaskyla, Finland
[p]Indian Institute of Technology, Kharagpur, India.
[q]Institute for Single Crystals, 61001 Kharkiv, Ukraine
[r]Institute of Theoretical and Experimental Physics, 117259 Moscow, Russia

[@] Spokesperson; [*] technical staff.

Abstract

Due to the very peculiar features of its apparata DAMA works as an observatory for rare processes located deep underground at the Gran Sasso National Laboratory of the I.N.F.N. (LNGS). It develops and uses low background scintillators. During 2011 the main experimental set-ups in operation have been: i) the second generation DAMA/LIBRA set-up (sensitive mass: $\simeq$ 250 kg highly radiopure NaI(Tl)), furtherly upgraded during 2010; ii) the DAMA/LXe set-up (sensitive mass: $\simeq$ 6.5 kg liquid Kr-free Xenon enriched either in ^{129}Xe or in ^{136}Xe); iii) the DAMA/R&D set-up (a facility dedicated to test prototypes and to perform small scale experiments, mainly investigating double beta decay modes in various isotopes); iv) the DAMA/Ge set-up (mainly dedicated to sample measurements and to specific measurements on rare processes). A small location (named DAMA/CRYS) is in preparation for prototype tests and detectors' qualification. In the following the main DAMA activities during 2011 are summarised.

1 DAMA/LIBRA

DAMA/LIBRA (Large sodium Iodide Bulk for Rare processes) is a unique apparatus for its sensitive mass, target material, intrinsic radio-purity, methodological approach and all the controls performed on the experimental parameters (c.f.r. [1, 2, 3, 4] and in the 2011 publication list). It is the successor of DAMA/NaI[5, 6, 7, 8, 9, 10, 11, 12, 13], with a higher exposed mass, higher duty cycle and increased sensitivity. Its granularity (25 detectors in a matrix 5×5) is an interesting feature to study Dark Matter (DM) and for background identification. The apparatus has also the unique feature (as well as DAMA/NaI) that gamma calibrations are regularly performed down to the energy threshold in the same conditions as the production runs, without any contact with the environment and without switching-off the electronics. The high light yield and other response features have allowed working in a safe and reliable way down to 2 keV; in incoming years this software energy threshold will be lowered thanks to the use of the new PMTs, installed at end of 2010, and of other optimisations.

Among the scientific goals of this set-up we mention: i) investigation with high sensitivity of a DM particle component in the galactic halo by the model independent approach known as DM annual modulation signature with high precision determination of the modulation parameters; ii) corollary investigations on the nature of the candidate and on the many possible astrophysical, nuclear and particle physics scenarios that require very high exposure, in particular considering the potentiality offered by the reaching of a lower energy threshold; iii) investigations on other possible model dependent and/or model independent approaches to study DM particles and second order effects; iv) study of exotic scenarios (as SIMPS, neutral nuclearities, Q-balls, etc.); v) improved search for processes of Pauli exclusion principle violation in ^{23}Na and ^{127}I; vi) search for processes of electric charge conservation violation (CNC), as the electron decay into invisible channels and in the $e^- \to \nu_e + \gamma$ channel, excitations of nuclear levels of ^{23}Na and ^{127}I after CNC electronic capture, etc.; vii) search for possible nucleon, di-nucleon and tri-nucleon decay

into invisible channels in ^{23}Na and ^{127}I; viii) search for solar axions by Primakoff effect in NaI(Tl); ix) search for nuclear rare decays in ^{23}Na, ^{127}I and Tl isotopes (superdense states, cluster decay, etc.); x) etc..

The most of such investigations require dedicated data taking and high exposure to reach competitive sensitivities.

The main goal of DAMA/LIBRA is the investigation of the Dark Matter particles in the galactic halo by exploiting the DM model independent annual modulation signature[14, 15]. In fact, as a consequence of its annual revolution around the Sun, which is moving in the Galaxy travelling with respect to the Local Standard of Rest towards the star Vega near the constellation of Hercules, the Earth should be crossed by a larger flux of Dark Matter particles around $\sim$ 2 June (when the Earth orbital velocity is summed to the one of the solar system with respect to the Galaxy) and by a smaller one around $\sim$ 2 December (when the two velocities are subtracted). Thus, this signature has a different origin and peculiarities than the seasons on the Earth and than those effects correlated with seasons (consider e.g. the expected value of the phase as well as the other requirements listed below).

Thus, the contribution of the signal to the counting rate in the k–th energy interval can be written as: $S_k = S_{0,k} + S_{m,k} \cos \omega(t - t_0)$, where: i) $S_{0,k}$ is the constant part of the signal; ii) $S_{m,k}$ is the modulation amplitude; iii) $\omega = \frac{2\pi}{T}$ with period T; iv) t_0 is the phase.

The DM annual modulation signature is very distinctive since it requires the simultaneous satisfaction of all the following peculiarities: the rate must contain a component modulated according to a cosine function (1) with one year period (2) and a phase that peaks roughly around $\simeq 2^{nd}$ June (3); this modulation must only be found in a well-defined low energy range, where DM particle induced events can be present (4); it must apply only to those events in which just one detector of many actually "fires" (*single-hit events*), since the DM particle multi-interaction probability is negligible (5); the modulation amplitude in the region of maximal sensitivity must be $\lesssim$7% for usually adopted halo distributions (6), but it can be larger in case of some possible scenarios. Only systematic effects or side reactions able to fulfil these requirements and to account for the whole observed modulation amplitude could mimic this signature; thus, no other effect investigated so far in the field of rare processes offers a so stringent and unambiguous signature.

At present status of technology the DM annual modulation is the only model independent signature available in direct dark matter investigation that can be effectively exploited.

So far the results on the first six annual cycles have been released; a peculiar annual modulation of the single-hit events in the (2—6) keV energy region satisfying all the many requests of the DM annual modulation signature has been confirmed(see Fig.1) The total exposure by the former DAMA/NaI and present DAMA/LIBRA is 1.17 ton $\times$ yr. In particular, as required by the DM annual modulation signature: (1) the single-hit events show a clear cosine-like modulation as expected for the DM signal; (2) the measured period is equal to (0.999$\pm$0.002) yr, a value well compatible with the 1 yr period expected for the DM signal; (3) the measured phase (146 $\pm$7) days is well compatible with about 152.5 days, as expected for the DM signal; (4) the modulation is present only in the low energy (2—6) keV interval and not in other higher energy regions, consistently with

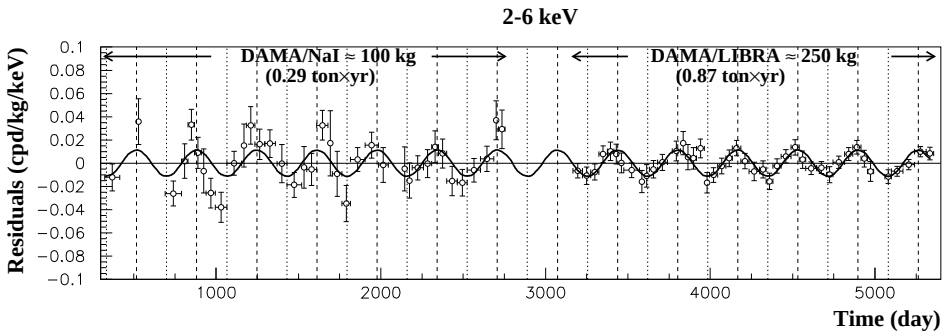

Figure 1: Experimental model-independent residual rate of the *single-hit* scintillation events, measured by DAMA/NaI over seven and by DAMA/LIBRA over six annual cycles in the (2 – 6) keV energy interval as a function of the time [9, 10, 2, 3]. The zero of the time scale is January 1^{st} of the first year of data taking of the former DAMA/NaI experiment. The experimental points present the errors as vertical bars and the associated time bin width as horizontal bars. The superimposed curve is the cosinusoidal function behavior $A\cos\omega(t-t_0)$ with a period $T=\frac{2\pi}{\omega}=1$ yr, with a phase $t_0=152.5$ day (June 2^{nd}) and with modulation amplitude, A, equal to the central value obtained by best fit over the whole data: cumulative exposure is 1.17 ton × yr. The dashed vertical lines correspond to the maximum expected for the DM signal (June 2^{nd}), while the dotted vertical lines correspond to the minimum. When all the three parameters are kept free, one gets from the data: $A=(0.0116\pm0.0013)$ cpd/kg/keV, $T=(0.999\pm0.002)$ yr and $t_0=(146\pm7)$ day, values well in agreement with expectations for DM signal.

expectation for the DM signal; (5) the modulation is present only in the single-hit events, while it is absent in the multiple-hit ones as expected for the DM signal; (6) the measured modulation amplitude in NaI(Tl) of the single-hit events in the (2—6) keV energy interval is: (0.0116±0.0013) cpd/kg/keV (8.9σ C.L.). No systematics or side processes able to simultaneously satisfy all the many peculiarities f the signature and to account for the whole measured modulation amplitude is available[8, 10, 2, 3].

Firstly, it is worth noting that DAMA has a model independent result due to the exploitation of a DM signature with specific peculiarities. No other experiment exists, whose result can be directly compared in a model independent way with those by DAMA/NaI and DAMA/LIBRA. In particular, results obtained with different target materials and/or different approaches cannot be directly compared among them even when considering the same kind of candidate and of coupling, although apparently all the presentations generally refer to cross section on nucleon. Anyhow, as regards possible model dependent hints by indirect experiments at present they are not in conflict with the DAMA results as well as – as mentioned above – some recent possible hints from direct experiments, in particular CoGeNT and CRESST. Therefore, claims for contradictions made by experiments insensitive to the DM annual modulation signature (because of marginal exposure, of the application of many data subtraction procedures, etc.) using different target materials and approaches, having well different sensitivities to various DM candidate and interactions, etc. have by the fact no impact even in the single arbitrary scenario they usually consider without – in addition – accounting for the existing experimental and theoretical uncertainties, using often crude approximation in the calculation, and optimistic estimates

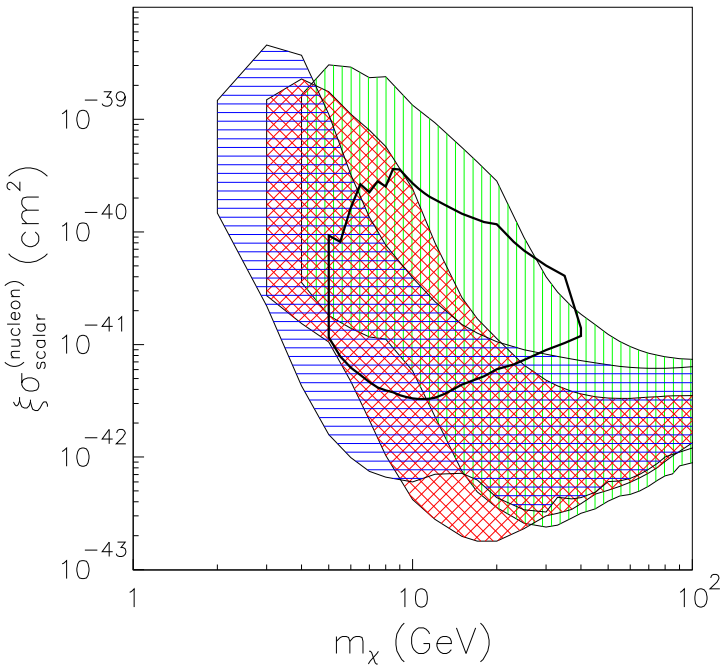

Figure 2: Regions in the $\xi\sigma_{\rm scalar}^{\rm (nucleon)}$ vs m_χ plane allowed by DAMA experiments in three considered instances for the Na and I quenching factors, including all the velocity distribution functions considered in ref. [16] and the same uncertainties as in refs. [9, 10] for a Dark Matter candidate with coherent interaction with nuclei (that is, some WIMP with pure SI coupling). The three (colored) hatched regions denote the regions allowed by the DAMA model independent annual-modulation results in the case of such a candidate and in 3 different instances: i) without including the channeling effect [(green) vertically-hatched region], ii) by including the channeling effect according to ref. [17] [(blue) horizontally-hatched region)], and iii) without the channeling effect but using the energy-dependent Na and I quenching factors as established by the procedure given in ref. [18] [(red) cross-hatched region]. They represent the domain where the likelihood-function values differ more than 7.5σ from the null hypothesis (absence of modulation). It is worth noting that, depending on other possible uncertainties not included here, the channeled (blue) horizontally-hatched region could span the domain between the present channeled region and the unchanneled one. The allowed region obtained for the CoGeNT experiment, including the same astrophysical models as in refs. [9, 10] and assuming for simplicity a fixed value for the Ge quenching factor and a Helm form factor with fixed parameters, is also reported and denoted by a (black) thick solid line. This region is meant to include configurations whose likelihood-function values differ more than 1.64σ from the null hypothesis (absence of modulation). This corresponds roughly to 90% CL far from zero signal. See the recent paper in the 2011 publication list, where also the expectations for the neutralino in the effective MSSM are shown.

for their experimental/theoretical parameters and the worst/arbitrary for the others, etc. Moreover, (see for example recent literature) some critical points exist in those activi-

ties, claiming for exclusion, on important experimental aspects (energy threshold, energy scale, UV light lost/absorption, non-uniformity of detector's response, multiple selection procedures, related efficiencies, stabilities, etc..)

The approaches based on many selections and handling procedures to "reject" the electromagnetic component of the counting rate are insensitive to various DM scenarios and cannot offer any signature also for the particular candidates, they would look for. In fact, even under the assumption of an "ideal" electromagnetic component rejection, e.g. the neutrons and the internal end-range α's induce signals indistinguishable from recoils which cannot be estimated and subtracted in any reliable manner at the needed (and sometime claimed) precision. In addition, part or all the signal can have electromagnetic nature; see in literature. Moreover, in a safe investigation of the DM annual modulation signature those data handling cannot be applied e.g. because of their – always – statistical nature which would affect the reliability of an annual modulation analysis and restrict the sensitivity to many kinds of candidates. On the other hand, as pointed out already in the 80's, the exploitation of the DM annual modulation signature acts itself as an effective background rejection.

Finally, they generally quote some of the implications of the DAMA model independent result in incorrect, partial and non updated way, as done elsewhere also in this book of activities reports. Thus, claims for contradiction have no scientific basis.

The obtained DAMA model independent evidence is compatible with a wide set of scenarios regarding the nature of the DM candidate and related astrophysical, nuclear and particle Physics. For examples some given scenarios and parameters are discussed e.g. in Refs. [6, 9, 10, 11] and in Appendix A of Ref. [2]. Further large literature is available on the topics [19]; other possibilities are open and we just recall the recent paper (see the 2011 publication list) where allowed regions are given for DM candidates interacting by elastic scattering on nuclei including some of the existing uncertainties; comparison with theoretical expectations for neutralino candidate and with the recent possible positive hint by CoGeNT[20] are also discussed there (see Fig. 2). Comparison with possible positive hint by CRESST[21] is discussed in ref. [22].

In conclusion, it is also worth noting that DAMA/LIBRA is still in the DM field the set-up having the highest intrinsic radiopurity, the largest exposed sensitive mass, the largest collected exposure, the deepest controlled running condition and stability, and the only one with highly sensitive ULB (Ultra-Low Background) NaI(Tl).

The exposure of another year (acquired before the upgrade of 2010) is available.

1.1 Works after the second upgrade at the end of 2010

A first upgrade of the DAMA/LIBRA set-up was performed in September 2008.

A further and more important upgrade was performed in the end of 2010 (see Fig. 3). In fact, all the low background PMTs have been replaced with new ones having higher quantum efficiency, realized with a special dedicated development by HAMAMATSU co..

This can allow the lowering of the software energy threshold of the experiment and, hence, the improvement of its performance and sensitivity also for deeper corollary information on the nature of the DM candidate particle(s) and on the various related astrophysical, nuclear and particle Physics scenarios.

Since January 2011 the DAMA/LIBRA experiment is again in data taking in the new configuration.

Figure 3: Replacement of the PMTs in DAMA/LIBRA during the upgrade of 2010. All procedures involving detectors, photomultipliers (PMTs), etc. have been carried out in HP (High Purity) Nitrogen atmosphere.

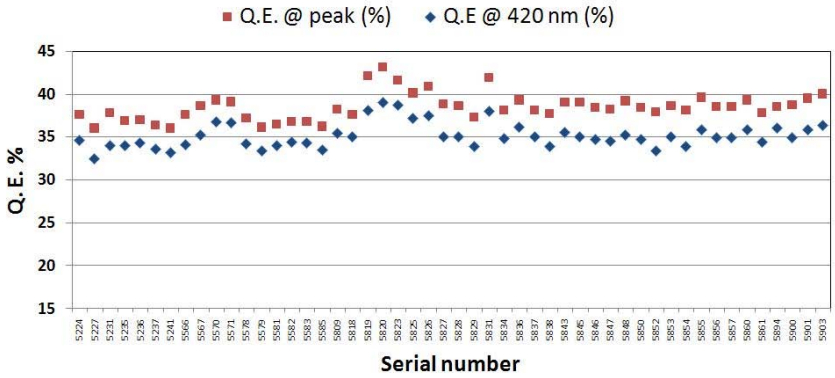

Figure 4: The Q.E. at peak and at 420 nm of each one of the 50 high Q.E. PMTs, installed in DAMA/LIBRA. The averages (RMS) are 38.5% (1.6%) and 35.1% (1.4%), respectively; the RMS show that the Q.E. spread in the PMTs production is well limited.

We remind that up to October 2010 low background PMTs, developed by EMI-Electron Tubes with dedicated R&D, were used; those PMTs had Q.E. 30% at λ=380 nm. The light yield and other response features allowed a software energy threshold of 2 keV in the data analysis.

During 2011 a detailed analysis of all the PMTs features and implications has been carried out and a dedicated paper has been prepared where all the details can be found; see in the 2011 publication list, accepted in 2012 for publication on J. of Instrum..

Just as example in Fig. 4 we show the values of the Q.E. of the new 50 HAMAMATSU PMTs installed in DAMA/LIBRA both at peak and the the λ of the NaI(Tl) scintillation light.

Moreover, during 2011 the design, the prototypes achievement and the tests on new-concept preamplifiers and on some particular trigger modules have been carried out. The reached performances allowed the funding of all the needed modules, which will be installed in DAMA/LIBRA at end 2012.

1.2 Conclusions and perspectives

The model independent positive evidence for the presence of DM particles in the galactic halo is now supported at 8.9σ C.L. (on a cumulative exposure of 1.17 ton$\times$yr i.e. 13 annual cycles of DAMA/NaI and DAMA/LIBRA). An update of corollary analyses in some of the many possible scenarios for DM candidates, interactions, halo models, nuclear/atomic properties, etc. is in progress as well as analyses/data taking to investigate other rare processes. Various preliminary analyses on possible CNC processes have been carried out and presented at conferences, and a detailed paper on a search for charge non-conserving processes in ^{127}I by coincidence technique has been completed. It has been accepted for publication on EPJC in 2012 and, thus, it will be described in the next activity report. In the future DAMA/LIBRA will also continue its study on several other rare processes [4] as also the former DAMA/NaI apparatus did [12].

The last upgrade in fall 2010 was successfully concluded, while further improvements are planned. The plans foresee, after the performed technical characterisation of the PMTs and the optimisation phase, many annual cycles of data taking needed to achieve all the goals of the experiment. Other DM features, second order effects, and several other rare processes will be investigated with high sensitivity.

The strictly quality control allows DAMA/LIBRA to be still the highest radiopure set-up in the field with the largest exposed sensitive mass, the full control of running conditions, the largest duty-cycle and an exposure orders of magnitude larger than any other activity in the field.

We remind that a 1 ton set-up made of highly radiopure NaI(Tl) was proposed in 1996 to INFN-CSN2, and the funded R&D II and III and DAMA/LIBRA were considered as an intermediate steps. We have already reminded some steps about it in previous reports. As mentioned there the final design is based now on the fulfilment of three additional replica of the present DAMA/LIBRA set-up, solution that offers many technical and scientific advantages; thus, the technical design is completely known, since DAMA/LIBRA is operative. As already mentioned some activities are carried out in the light of overcoming the present problems regarding the supplying and purifications of high quality NaI and, mainly, TlI powders and the creation of updated protocols.

2 DAMA/LXe

We further remind that we pointed out since 1990[23] the possible interest in using the liquid Xenon as target-detector material for particle Dark Matter investigations. Since the end of 80's (former Xelidon experiment of the INFN) we have realised several liquid Xenon (LXe) prototype detectors. In 1996 we pointed out to the INFN-CSN2 the intrinsic problems of this detector medium for large scale experiments dedicated to DM investi-

gation and agreed to pursue the activity by exploiting Kr-free enriched Xenon gases in limited volume. The set-up presently running (having a Cu inner vessel filled by $\simeq$ 6.5 kg ($\simeq$2 l - of liquid Xenon) can work either with Kr-free Xenon enriched in ^{129}Xe at 99.5% or Kr-free Xenon enriched in ^{136}Xe at 68.8%[24, 25, 26]. Many competing results were achieved on several rare processes[27, 24, 25, 28, 26, 29]. It is worth noting that the mass exposed when using the Xenon enriched in ^{129}Xe correspond for spin-dependent coupled particles to expose 24.5 kg of natural Xenon, while the exposed mass when using the Xenon enriched in ^{136}Xe correspond for spin-independent coupled particles to an exposed mass of 50.4 kg of natural Xenon.

After the forbiddeness of using cryogenic liquids in the LNGS underground laboratories, the set-up took data just few months until December 2004; then, it has been put in standby waiting for the restarting of the LNGS cooling water plant and of the local water refrigeration system. We profited from this period to perform several upgrades of the apparatus. Finally, thanks to a new chiller system and to the restoring of the use of water plants deep underground, the DAMA/LXe set-up restarted the data taking in December 2007, continuously during 2008 up to January 2009; after maintenance the data taking has been restarted at fall 2009 and data taking periods have been carried out during 2010. In the period of interest here a first stop of the data taking was made at beginning of 2011. Then the data taking has been restarted for few months needed to substitute the old compressor. The installation and tests deep underground have been completed in September 2011 and the restart of the data taking was performed at end 2011, with the detector still filled with Kr-free Xenon enriched in ^{136}Xe and focusing on the high energy region. Various data analyses are in progress and some works are in preparations.

3 DAMA/R&D

The DAMA/R&D installation is a low-background set-up used for measurements on low background prototypes and relatively small scale experiments (often in collaboration with INR-Kiev as foreseen in the agreements)[30]. The measurements mainly investigate 2β decay modes in various isotopes; both the active and the passive source techniques have been exploited as well as sometimes the coincidence technique with particular attention to $2\beta^+$ processes. It is worth to note that a gap of several orders of magnitude between theory and experiment is usual situation in $2\beta^+$ investigations for which the achieved sensitivity does not exceed the level of $T_{1/2} \simeq 10^{21}$ yr. It should be stressed that the searches for $2\beta^+$ processes are interesting not so much for the neutrino mass, but rather to study the contribution of right-handed currents in weak interaction. Studies of the neutrinoless double electron capture (2ϵ) and electron capture with positron emission ($\epsilon\beta^+$) decays could help to understand a contribution of the right- handed admixtures in weak interaction to the neutrinoless $2\beta^-$ decay [31].

Even more important motivation to search for double electron capture appears from a possibility of a resonant process thanks to energy degeneracy between initial and final state of mother and daughter nuclei. Such a resonant process could occur if the energy of transition ($Q_{2\beta}$) minus two energies of bounded electrons on K or/and L atomic shells of daughter nucleus is near to the energy of an excited level (E_{exc}) of a daughter isotope.

Therefore developments of experimental technique to search for 2ϵ, $\epsilon\beta^+$, and $2\beta^+$ processes are strongly required.

Finally, investigations on various kinds of new scintillators and preliminary works for the future measurements are also in progress.

Some of the 2011 results and works are shortly summarised in the following.

3.1 Search for 2β processes in zinc and tungsten with $ZnWO_4$ crystal scintillators

In recent years we have made measurements with $ZnWO_4$ crystal scintillators to investigate double beta decay of Zn and W isotopes [32]. In order to perform new improved measurements in future the radioactive contamination of various $ZnWO_4$ crystal scintillators has been investigated deep underground in the low background DAMA/R&D set-up with a total exposure of 3197 kg $\times$ h (see 2011 publication list). In particular, the creation of more radiopure $ZnWO_4$ crystals could be expected e.g. by applying vacuum distillation and filtering to obtain high purity zinc, and by zone melting for additional purification of the tungsten.

Zinc tungstate ($ZnWO_4$) scintillators contain four potentially 2β active isotopes: ^{64}Zn, ^{70}Zn, ^{180}W and ^{186}W. It is worthwhile mentioning that ^{64}Zn and ^{186}W have comparatively large natural abundance that allows us to apply $ZnWO_4$ detectors without high cost enriched isotopes. Moreover, the $2\nu2\beta^-$ decay of ^{186}W is expected to be strongly suppressed which could provide favourable conditions to search for neutrinoless $2\beta^-$ decays, including processes with emission of majoron(s) which have broad energy spectra, somewhat similar to that of the two-neutrino mode. The ^{180}W isotope is also an interesting 2β nuclide because in the case of the capture of two electrons from the K shell (E_K = 65.4 keV), the decay energy is rather small (13 $\pm$4) keV. Such a coincidence could give a resonant enhancement of the 0ν double electron capture to the corresponding level of the daughter nucleus.

In 2011 the final results on double beta decay modes in Zn and W isotopes with four $ZnWO_4$ crystal scintillators (0.1— 0.7 kg) have been derived (see 2011 publication list). The total exposure of the low background measurements was 0.529 kg $\times$ yr.

Two crystals (117 g and 699 g) were produced by the Czochralski method in the Institute for Scintillation Materials (Kharkiv, Ukraine). After 2130 h of low-background measurements, the crystal of 699 g was re-crystallised with the aim to study the effect of the re-crystallisation on the radioactive contamination of the material. The third $ZnWO_4$ crystal (141 g, the sample had a slightly irregular shape) was obtained by the re- crystallisation process and used in further measurements. The fourth $ZnWO_4$ crystal scintillator (239 g) was produced in the Nikolaev Institute of Inorganic Chemistry (Novosibirsk, Russia) by the low-thermal gradient Czochralski technique.

The energy spectrum accumulated over 4305 h with the 239 g $ZnWO_4$ crystal scintillator in the low background set-up is shown in Fig. 5. Previous limits on the $T_{1/2}$ of the $\beta\beta$ decay modes of ^{64}Zn, ^{70}Zn, ^{180}W and ^{186}W have been improved up to 2 orders of magnitude in some cases have been established at the level of 10^{18} — 10^{21} yr (the $0\nu2\epsilon$ capture in ^{180}W is of particular interest due to the possibility of the resonant process). It is worth noting that up to now only 5 nuclides (^{40}Ca, ^{78}Kr, ^{112}Sn, ^{120}Te and ^{106}Cd) of 34

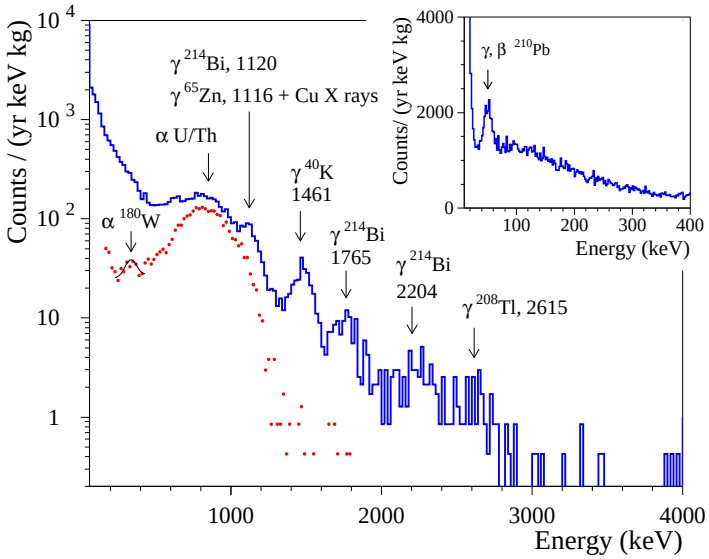

Figure 5: The energy spectrum accumulated with the $ZnWO_4$ crystal scintillator ⌀41 × 27 mm in the low background DAMA/R&D set-up over 4305 h. The energy spectrum of α events selected by the pulse-shape discrimination is drawn by points. Fit of the α peak of ^{180}W by Gaussian function (solid line) is shown. (Inset) The energy spectrum of γ and β events selected by the pulse-shape discrimination technique from the data measured over 2798 h with the same crystal scintillator in the set-up with lower energy threshold and with additional quartz light-guides. Energies of γ lines are in keV.

candidates for 2ϵ, $\epsilon\beta^+$, $2\beta^+$ have been studied with similar sensitivity in direct experiments. In particular: a) a previous possible positive indication on the $(2\nu+0\nu)\epsilon\beta^+$ decay mode of ^{64}Zn with $T_{1/2} = (1.1\pm 0.9) \times 10^{19}$ yr, suggested in ref.[33] is not confirmed; b) the rare α decay of ^{180}W with $T_{1/2} = (1.3^{+0.6}_{-0.5}) \times 10^{18}$ yr has been observed and a new limit on the $T_{1/2}$ of the α transition of ^{183}W to the $\frac{1}{2}^-$ 375 keV metastable level of the ^{179}Hf has been derived as: $T_{1/2} \geq 6.7 \times 10^{20}$ yr; c) the limit on the $0\nu2\beta^-$ of the ^{186}W has been derived to be 1.0×10^{21} yr with respect to a theoretical expectation of 6.4×10^{24} yr in case $< m_\nu > =1$ eV.

New developments of this kind of radiopure scintillators are in preparation to improve thanks to even higher radiopurity and much larger exposure the experimental sensitivities.

3.2 Search for 2β processes in ^{106}Cd with enriched $^{106}CdWO_4$ crystal scintillators.

The isotope ^{106}Cd is one of the most promising objects for $2\beta^+$ decay because: 1) of its natural isotopic abundance $(1.25 \pm 0.06)\%$ and of the possibility to achieve samples enriched up to 100%; 2) of its rather large $Q_{2\beta}$= (2770±7) keV and of the possibility to study all the various $2\beta^+$, $\epsilon\beta^+$ and 2ϵ decay modes (also see Sect. 4); 3) the favourable theoretical estimates of the half-lives. Thus, with the $CdWO_4$ crystal scintillator (215 g) enriched in ^{106}Cd to 66%, described in details in a previous paper[34], a high sensitivity experiment to search for $2\beta^+$ processes in ^{106}Cd has been carried out and the paper is

in preparation (see Fig. 6). Preliminary results with partial exposures were presented at

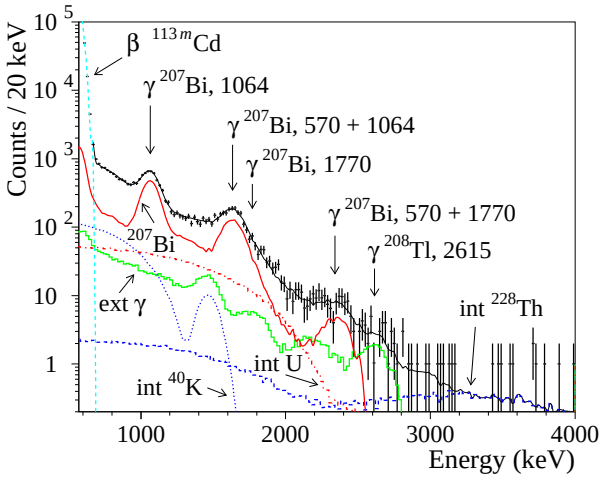

Figure 6: The energy spectrum of the $\beta(\gamma)$ events (6590 h) in the set-up with the $^{106}CdWO_4$ crystal scintillator (points) together with the background model (black continuous line). The main components of the background are: the β spectrum of the internal ^{113m}Cd, the distributions of ^{40}K, ^{228}Th, ^{238}U, ^{207}Bi (deposited on the crystal surface), and the contribution from the external γ quanta from PMTs and copper box ("ext γ").

conferences (see 2011 publication list). This search for the double β processes in ^{106}Cd was realised in 6590 h of data taking; new improved half-life limits on the double beta processes in ^{106}Cd have been established at the level of 10^{19} - 10^{21} yr; in particular, $T_{1/2}$ $(2\nu\epsilon\beta^+)$ $\geq 2.1 \times 10^{20}$ yr, $T_{1/2}$ $(2\nu2\beta^+)) \geq 4.3 \times 10^{20}$ yr, and $T_{1/2}$ $(0\nu2\epsilon) \geq 1.0 \times 10^{21}$ yr. The resonant neutrinoless double electron capture to the 2718 keV and the 2741 keV excited levels of ^{106}Pd is restricted to $T_{1/2}(0\nu2K) \geq 4.3 \times 10^{20}$ yr, $T_{1/2}$ $(0\nu KL_1) \geq 9.5 \times 10^{20}$ yr and $T_{1/2}$ $(0\nu KL_3) \geq 4.3 \times 10^{20}$ yr, respectively (all limits at 90% C.L.). A possible resonant enhancement of the $0\nu2\epsilon$ processes has been estimated in the framework of the QRPA approach. The radioactive contamination of the $^{106}CdWO_4$ crystal scintillator has also been reported. At present developments for a new more sensitive data taking in a different set up is in preparation.

3.3 Low background detector with enriched $^{116}CdWO_4$ crystal scintillators to search for double β decay of ^{116}Cd

The ^{116}Cd isotope is one of the best candidates for the neutrinoless $2\beta^-$ decay because of: 1) its natural isotopic abundance is comparatively high (7.49%) and of the possibility to achieve samples enriched up to 100%; 2) its rather large $Q_{2\beta}$ value (2805 keV); 3) the favourable theoretical estimates of the half-lives and nuclear matrix elements.

A cadmium tungstate crystal boule enriched in ^{116}Cd to 82% with mass of 1868 g was grown by the low-thermal-gradient Czochralski technique (see Fig. 7 left). This is the second boule never produced of $^{116}CdWO_4$. The isotopic composition of cadmium and the trace contamination of the crystal boule were estimated by High Resolution Inductively Coupled Plasma Mass-Spectrometry.

Thus, two $CdWO_4$ crystal scintillators (586 g and 589 g, see Fig. 7 right) have been realised from the boule and their features investigated; the technical paper is now published (see 2011 publication list). The crystal scintillators produced from the boule were

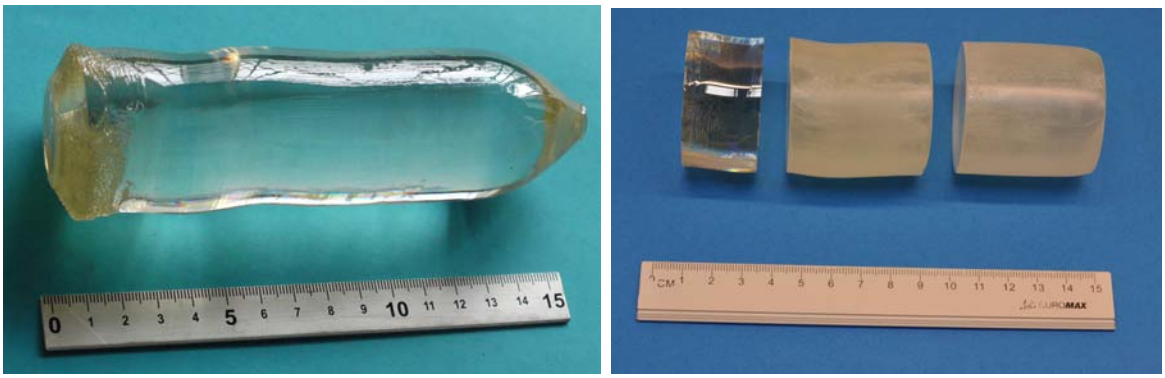

Figure 7: (Color online) Left: Boule of enriched $^{116}CdWO_4$ crystal. The conic part of the boule is the beginning of the crystal growth. Right: Crystal samples cut from the boule: $\approx \oslash 45 \times 46.7$ mm, 586.2 g, No. 1 (right); $\approx \oslash 45 \times 46.1$ mm, 589.3 g, No. 2 (middle); $\approx \oslash 45.7 \times 25.1$ mm, 325.6 g, No. 3 (left).

subjected to characterisation that included measurements of transmittance and energy resolution. Moreover, all other detectors, light guides and PMTs needed in the detector system for a high sensitive measurement of the double beta decay modes in ^{116}Cd have been built, brought underground, assembled and tested in laboratory. The detector was running over 1727 h deep underground at the Gran Sasso National Laboratories of the INFN, which allowed to estimate the radioactive contamination of the enriched crystal scintillators.

At beginning of 2011 the detectors system has been installed in DAMA/R&D and the 3 yr data taking is started. In the period of interest here, a short stop has been realised in order to perform annealing procedures of the enriched crystals to improve their performances, then the measurements have been then restarted. At end of the data taking in DAMA/R&D (several years from now), the $2\nu2\beta$ transitions of ^{116}Cd to the excited states of ^{116}Sn is planned to be investigated at level of sensitivity $T_{1/2} = 10^{22}$ yr expected by the theoretical predictions by installing the enriched scintillator in the the low-background 4 HPGe detectors facility.

3.4 Search for 2β decay of cerium isotopes with $CeCl_3$ scintillator

Cerium offers three double beta decaying isotopes: ^{136}Ce, ^{138}Ce and ^{142}Ce and the recent development of new scintillating materials containing Ce also allows the exploitation of the efficient "source=detector" approach. In particular, the ^{136}Ce is a very interesting isotope since the high energy release allows the $2\beta^+$ decay mode, which is energetically possible only for 6 candidate-nuclei. Moreover, some resonant neutrinoless 2ε captures in ^{136}Ce to the excited states of the ^{136}Ba are also energetically allowed.

Double beta processes in ^{136}Ce, ^{138}Ce and ^{142}Ce have been searched for by exploiting the active source approach with the help of a 6.9 g $CeCl_3$ crystal as a scintillator at LNGS for the first time(see 2011 publication list). The total measurement time is 1638 h; even such a small exposure has allowed the achievement of some improved half-life limits on 2β decay processes in these isotopes at the level of 10^{16}—10^{18} yr. In particular (90% C.L.): $T^{0\nu\epsilon\beta^+}_{1/2}$ (^{136}Ce) $\geq 8.8 \times 10^{16}$ yr, $T^{2\nu\epsilon\beta^+}_{1/2}$ (^{136}Ce) $\geq 2.4 \times 10^{16}$ yr, $T^{2\nu2K}_{1/2}$ (^{136}Ce) $\geq 3.2 \times 10^{16}$ yr, $T^{2\nu2K}_{1/2}$ (^{138}Ce) $\geq 4.4 \times 10^{16}$ yr and $T^{2\nu2\beta^-}_{1/2}$ (^{142}Ce) $\geq 1.4 \times 10^{18}$ yr. This supports the interest in realising larger mass and longer exposure deep underground with new $CeCl_3$ crystal scintillators exploiting the active source technique. A further relevant topic is the future preliminary selection of all the materials and of the growing/handling procedures as well as the development of chemical/physical purification techniques in order to improve the radiopurity of the crystal and housing materials.

It should also be stressed the advantage of much better energy resolution of $CeCl_3$ crystal scintillator (FWHM 5% at 662 keV γ line of ^{137}Cs) in comparison with e.g. CeF_3 crystal scintillators ($\simeq$18% at the same energy).

Further improvements in sensitivity can be reached by using enriched ^{136}Ce, increasing the detection efficiency by using larger $CeCl_3$ detector, and developing $CeCl_3$ scintillators with lower level of radioactive contamination. An experiment involving $\simeq$100 kg of crystals enriched in ^{136}Ce to 20% (5×10^{25} nuclei of ^{136}Ce) could reach over 5 years of measurements the half-life sensitivity $T_{1/2} \simeq 10^{25}$ yr (supposing zero background).

4 Measurements with DAMA/Ge and LNGS Ge facility

Various R&D developments to improve low background set-ups and scintillators are carried out. Thus, measurements on samples are performed by means of the DAMA low background Ge detector, specially realised with a low Z window; it is operative deep underground in the low background facility of the LNGS. Some selected materials are in addition measured with high sensitivity ICP-MS and mass spectrometers.

In particular, the main data takings/results during year 2011 are summarised in the following.

- Preliminary results of new measurements with LiF(W) have been presented at Conference; a paper was in preparation during 2011.
- After the chemical/physical purification procedures of the about 1 kg of Ru, new measurements have been started in order to investigate the 2β processes of ^{96}Ru and ^{104}Ru with higher sensitivity.
- 3.16 kg of Nd_2O_3 have been further purified and together with about 1.5 kg of metallic Nd are at LNGS ready to test a result that declared the observation of the $2\nu2\beta$ decay of the ^{150}Nd to the first excited level 0^+_1 of ^{150}Sm.
- The first experimental investigation of the 2ϵ and $\epsilon\beta^+$ of ^{184}Os is in progress by using a sample of ultra-pure osmium.

- The preparation for a more sensitive measurement with the $^{106}CdWO_4$ crystal scintillator inside the 4π low-background HPGe detectors facility has been planned. In particular a special light guide for the $^{106}CdWO_4$ in this configuration has been built; it is made of $PbWO_4$ from archeological Pb. Such a set-up configuration will be effective to investigate 2ν mode of $\epsilon\beta^+$ and $2\beta^+$ decays, and also 2ϵ transitions of ^{106}Cd to excited states of ^{106}Pd, at the level of sensitivity of the theoretical predictions: $T_{1/2} = 10^{20}$ - 10^{22} yr. Moreover, the development of a $^{106}CdWO_4$ crystal scintillator depleted in $^{113/113m}$Cd isotopes is also foreseen in future.

The future measurements on all other topics for incoming years are in preparation. In the following just the results of the measurements published in 2011 are summarised.

4.1 First study on feasibility for double β decay search with dysprosium

The first experimental search for the 2β decay modes of ^{156}Dy and ^{158}Dy has been realised and the related paper published (see 2011 publication list). In fact, after 2512 h of data taking with a 322 g sample of dysprosium oxide (see Fig. 8) limits on double beta processes

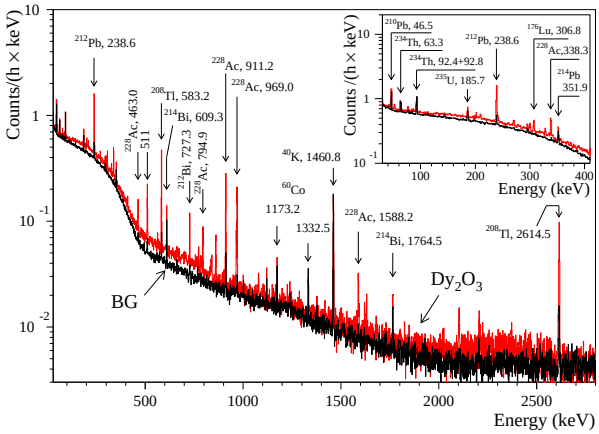

Figure 8: Energy spectra accumulated with dysprosium sample over 2512 h (Dy_2O_3) and without sample over 6110 h (BG) by ultra-low background HP Ge γ spectrometer. (Inset) Low energy part of the spectra. Energy of γ lines are in keV.

in ^{156}Dy and ^{158}Dy have been established on the level of $T_{1/2} \geq 10^{14} - 10^{16}$ yr. Possible resonant double electron captures in ^{156}Dy and ^{158}Dy have been restricted on a similar level. The sensitivity of the experiment can be advanced in future to the level of $T_{1/2} \simeq 10^{23} - 10^{24}$ yr by using enriched ^{156}Dy and ^{158}Dy isotopes deeply purified from radioactive elements, and increasing the exposure and detection efficiency by application of multi-crystal HP Ge detectors. As a by-product of the present experiment we have measured the radioactive contamination of the Dy_2O_3 sample and set limits on the α decay of dysprosium isotopes to the excited levels of daughter nuclei as $T_{1/2} \geq 10^{15} - 10^{17}$ yr. We have found that the Dy_2O_3 sample contains on the level of several mBq/kg ^{176}Lu, ^{235}U and ^{226}Ra; the activities of ^{228}Ra and ^{228}Th are $\simeq 0.18$ and $\simeq 0.16$ Bq/kg, respectively. The results of the γ spectrometry are consistent with the data of the ICP-MS analysis

for radionuclides. The contamination of the dysprosium sample can be explained by the production of lanthanides from monazite, an ore with high concentration of uranium and thorium. Presence of radioactive ^{176}Lu can be due to the similar chemical properties of lutetium and dysprosium, which provides some difficulties in chemical separation of the elements.

4.2 First observation of α decay of ^{190}Pt to the first excited level (E_{exc} = 137.2 keV) of ^{186}Os

The α decays of naturally occurring platinum isotopes, which are accompanied by the emission of γ quanta, have been searched for deep underground at LNGS (see 2011 publication list). A sample of Pt with a mass of 42.5 g and a natural isotopic composition

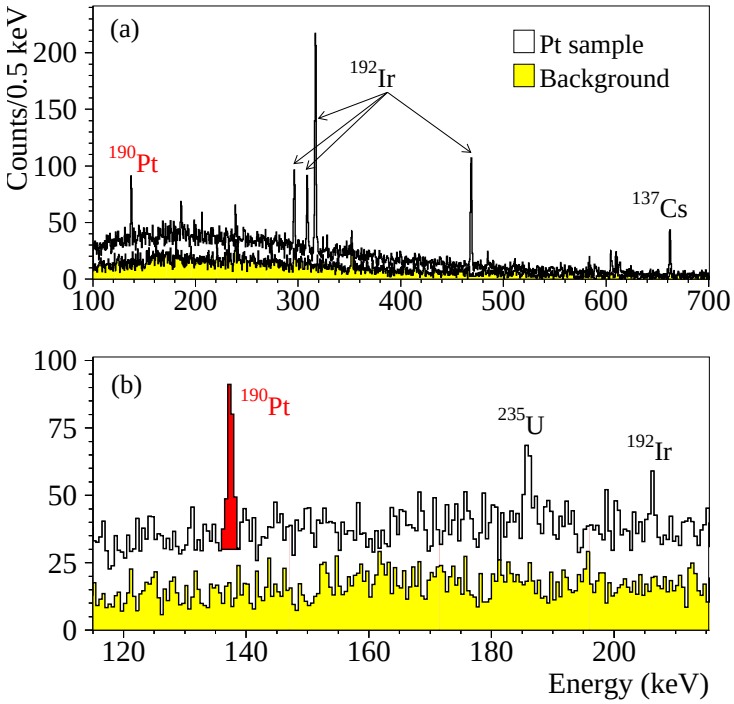

Figure 9: Energy spectrum of the Pt sample with mass of 42.5 g measured during 1815 h in the 100 – 700 keV energy interval (a), and in more detail around the 137 keV region (b). The background spectrum (measured during 1046 h but normalised here to 1815 h) is also shown (filled histogram). Peak at 137 keV after α decay ^{190}Pt $\rightarrow$ ^{186}Os(2_1^+) is clearly visible in the Pt spectrum being absent in the background.

has been measured with a low background HP Ge detector (468 cm^3) during 1815 h. The α decay of ^{190}Pt to the first excited level of ^{186}Os ($J^\pi = 2^+$, E_{exc} = 137.2 keV) has been observed for the first time (see Fig. 9), by the observation of the γ line at energy (137.1$\pm$ 0.1) keV at the 8σ significance level while it is absent in the background spectrum of the detector. In addition to the ^{190}Pt decay, the γ quanta can be emitted in the α decays of other Pt isotopes: (1) when the excited levels of the daughter Os nuclei are populated; (2) when the daughter Os nuclei are unstable and further decay with emission of some γ rays, as in the case of ^{195}Pt and ^{198}Pt. We also determined $T_{1/2}$ limits for such decays

(to our knowledge, for the first time). We did not find alternative processes that could mimic this effect. The half-life was determined as $T_{1/2} = 2.6^{+0.4}_{-0.3}$(stat.) $\pm$ 0.6(syst.) $\times$ 10^{14} yr. This value is in agreement with theoretical calculations and has stimulated a deep interest in literature(see e.g. ref.[35]).

In addition, the $T_{1/2}$ limits for the α decays with population of the lowest excited levels of Os nuclei (for ^{192}Pt, ^{194}Pt, ^{196}Pt) and for transition to the ground states of Os nuclei (for ^{195}Pt, ^{198}Pt) were determined at the level of $T_{1/2} \simeq 10^{16}$ – 10^{20} yr. These limits have been set for the first time or they are better than those known from earlier experiments. The α decay of ^{190}Pt to the second excited level of ^{186}Os ($J^{\pi} = 4^{+}$, E_{exc} = 434.1 keV) could be detected in a higher sensitivity experiment with platinum enriched in ^{190}Pt to $\simeq$10%. This task is under study. However, because its natural abundance is extremely low (δ = 0.014%), this is a very expensive task with the current technologies.

4.3 First search for double β decay of platinum by ultra-low background HP Ge γ spectrometry

The ^{190}Pt is a potentially $\epsilon\beta^{+}$ active nuclide, and could present a resonant enhancement of the neutrinoless double electron capture in result of the energy degeneracy. In 2011 the paper on the results obtained in the preliminary measurements with a Pt sample of 42.5 g mass (see Fig. 10) during 1815 h has been published (see 2011 publication list). Improved limits on various decay modes in ^{190}Pt have been established on the level of 10^{14}

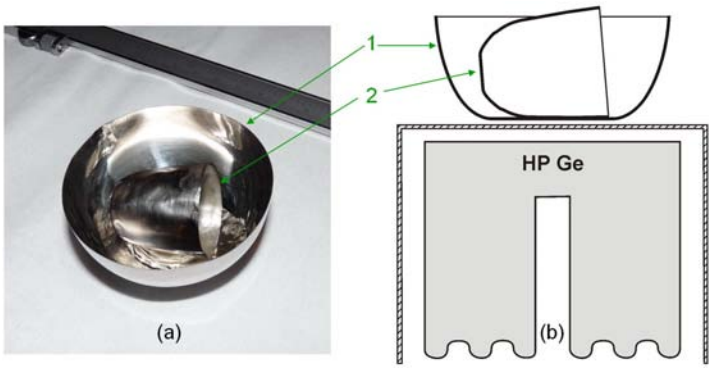

Figure 10: (a) Photo of the Pt sample and (b) simplified scheme of the measurements with the HP Ge detector. The bigger Pt cup and smaller Pt crucible are labeled as 1 and 2, respectively.

- 10^{16} yr, 3 to 4 orders of magnitude higher than those known previously. In particular the first experimental limit on the possible resonant $0\nu2\epsilon$ process in ^{190}Pt was restricted on the level of 2.9 $\times$ 10^{16} yr at 90% C.L.. In addition, $T_{1/2}$ limit on on $2\beta^{-}$ transition of ^{198}Pt ($2\nu + 0\nu$) to the 411.8 keV excited level of ^{198}Hg, has been set at the first time: $T_{1/2}$ $> 3.5 \times 10^{18}$ y. The measurements allowed us to estimate the radioactive contamination of the used platinum sample. In particular, we have detected 7 mBq/kg of ^{137}Cs and 40 mBq/kg of ^{192}Ir in this platinum sample. The contamination of ^{60}Co, ^{226}Ra, ^{228}Ra and

^{228}Th does not exceed the level of a few mBq/kg, while the activities of ^{40}K, ^{235}U, ^{238}U are less than a few tens mBq/kg (we assume a broken equilibrium in U/Th chains).

To improve the sensitivity to the 2β decay processes searched for, new measurements using $\simeq$ 0.2 kg sample of platinum in a different optimised installation are foreseen. Further improvements can be achieved by increasing the detection efficiency and the exposition, and obviously by using enriched ^{190}Pt isotope. Specially developed multi-crystal HP Ge detectors could also be applied to reach a sensitivity to double β processes in ^{190}Pt on the level of 10^{22} - 10^{24} yr. This would be particularly interesting also because of the possibility of a resonant double electron capture in ^{190}Pt having such isotope the largest Z value (the nuclear parameter which greatly favours the process) among the nuclei where a resonant double-electron capture could occur.

5 Conclusions

The positive model independent evidence for the presence of DM particles in the galactic halo is now supported at 8.9σ C.L. (on a cumulative exposure of 1.17 ton$\times$yr i.e. 13 annual cycles of DAMA/NaI and DAMA/LIBRA) and is compatible with a wide set of scenarios regarding the nature of the DM candidate and related astrophysical, nuclear and particle Physics. An update of corollary analyses in some of the many possible scenarios for DM candidates, interactions, halo models, nuclear/atomic properties, etc. is in progress as well as analyses/data taking to investigate other rare processes.

The last upgrade in fall 2010 was successfully concluded, while further improvements are planned. Another year of statistics (acquired with the set-up configuration of the other published six annual cycles) will be released soon. The strictly quality control allows DAMA/LIBRA to be still the highest radiopure set-up in the field with the largest exposed sensitive mass, the full control of running conditions, the largest duty-cycle and an exposure orders of magnitude larger than any other activity in the field.

In 2011 all the DAMA/set-ups have regularly been in data taking and various kinds of measurements are in progress and planned for the future.

6 List of Publications during 2011

1. R. Bernabei, P.Belli, F.Cappella, R.Cerulli, C.J.Dai, A. d'Angelo, H.L.He, A. Incicchitti, H.H.Kuang, X.H.Ma, F.Montecchia, F.Nozzoli, D.Prosperi, X.D. Sheng, R.G.Wang, Z.P.Ye, DAMA/LIBRA results, in the volume in the volume "Particle Physics in the Year of Astronomy", World Scientific pub. (2011), 207.

2. R. Bernabei, P.Belli, F.Montecchia, F.Nozzoli, F.Cappella, A. d.Angelo, A. Incicchitti, R.Cerulli, C.J.Dai, H.L.He, H.H.Kuang, X.H.Ma, D.Prosperi, X.D. Sheng, R.G.Wang, Z.P.Ye, Searching for processes violating tha Pauli exclusion Principle in Na and I with DAMA/LIBRA, in the volume in the volume "Particle Physics in the Year of Astronomy", World Scientific pub. (2011), 216.

3. P. Belli, R. Bernabei, R. S. Boiko, V. B. Brudanin, F. Cappella, V. Caracciolo, R. Cerulli, D. M. Chernyak, F. A. Danevich, S. d'Angelo, A. E. Dossovitskiy, E.

N. Galashov, A. Incicchitti, V. V. Kobychev, S. S. Nagorny, F. Nozzoli, B. N. Kropivyansky, V. M. Kudovbenko, A. L. Mikhlin, A. S. Nikolaiko, D. V. Poda, R. B. Podviyanuk, O. G. Polischuk, D. Prosperi, V. N. Shlegel, Yu. G. Stenin, J. Suhonen, V. I. Tretyak, Ya. V. Vasiliev, First results of the experiment to search for2β decay of ^{106}Cd with the help of $^{106}CdWO_4$ crystal scintillators, Nucl. Phys. and Atom. En. 12 (2011) 124.

4. R. Bernabei, P. Belli, F. Cappella, R. Cerulli, C.J. Dai, A. d.Angelo, H.L. He, A. Incicchitti, X.H. Ma, F. Montecchia, F. Nozzoli, D. Prosperi, X.D. Sheng, Z.P. Ye, R.G. Wang, Particle Dark Matter in the galactic halo: recent results from DAMA/LIBRA, Nucl. Phys. B (Proc. Suppl.) 212-213 (2011) 307.

5. R. Bernabei, P.Belli, F.Cappella, R.Cerulli, C.J.Dai, A. d.Angelo, H.L.He, A. Incicchitti, H.H.Kuang, X.H.Ma, F.Montecchia, F.Nozzoli, D.Prosperi, X.D. Sheng, R.G.Wang, Z.P.Ye, Signals from the dark Universe: new results from DAMA/LIBRA, in the volume Physics Beyond The Standard Models of Particles, Cosmology and Astrophysics, World Scientific pub. (2011), 511.

6. R. Bernabei, P. Belli, F. Cappella, R. Cerulli, A. d'Angelo, C.J. Dai, H.L. He, A. Incicchitti, H.H. Kuang, X.H. Ma, F. Montecchia, F. Nozzoli, D. Prosperi, X.D. Sheng, Z.P. Ye, R.G. Wang, Direct detection of dark matter particles, Nucl. Instr. & Meth. A630 (2011) 279.

7. R. Bernabei, P.Belli, F.Cappella, R.Cerulli, C.J.Dai, A. d.Angelo, H.L.He, A. Incicchitti, X.H.Ma, F.Montecchia, F.Nozzoli, D.Prosperi, X.D. Sheng, R.G.Wang, Z.P.Ye, Results on Dark Matter by DAMA/LIBRA at Gran Sasso, Nucl. Phys. and Atom. Energy 12 (2011) 40.

8. P. Belli, R. Bernabei, F. Cappella, R. Cerulli, F. A. Danevich, A.M. Dubovik, S. d'Angelo, E. N. Galashov, B.V. Grinyov, A. Incicchitti, V. V. Kobychev, M. Laubenstein, L.L. Nagornaya, F. Nozzoli, D. V. Poda, R. B. Podviyanuk, O. G. Polischuk, D. Prosperi, V. N. Shlegel, V. I. Tretyak, I.A. Tupitsyna, Ya. V. Vasiliev, Yu.Ya. Vostretsov, Radioactive contamination of $ZnWO_4$ crystal scintillators, Nucl. Instr. & Meth. A 626 (2011) 31

9. R. Bernabei, P.Belli, F.Montecchia, F.Nozzoli, F.Cappella, A. d.Angelo, A. Incicchitti, D.Prosperi, R.Cerulli, C.J.Dai, H.L.He, X.H.Ma, X.D. Sheng, R.G.Wang, Z.P.Ye, Particle Dark Matter in the galactic halo: recent results from DAMA/LIBRA, Can. J. Phys. 89 (2011) 11

10. P Belli, R Bernabei, F Cappella, R Cerulli, F A Danevich, A d'Angelo, A Di Marco, A Incicchitti, F Nozzoli and V I Tretyak Search for 2β decay of cerium isotopes with $CeCl_3$ scintillator, J. Phys. G: Nucl. Part. Phys. 38 (2011) 015103.

11. R. Bernabei, P. Belli, F. Cappella, R. Cerulli, C.J. Dai, A. d.Angelo, H.L. He, A. Incicchitti, X.H. Ma, F. Montecchia, F. Nozzoli, D. Prosperi, X.D. Sheng, R.G. Wang, Z.P. Ye, Particle Dark Matter in the galactic halo, Prog. Part. Nucl. Phys. 66 (2011) 169.

12. P. Belli, R. Bernabei, F. Cappella, R. Cerulli, F.A. Danevich, A. Incicchitti, M. Laubenstein, S.S. Nagorny, S. Nisi, O.G. Polischuk, V.I. Tretyak, First observation of α decay of ^{190}Pt to the first excited level (E_{exc} = 137.2 keV) of ^{186}Os, Phys. Rev. C 83 (2011) 034603

13. R. Bernabei, P. Belli, A. Di Marco, F. Montecchia, F. Cappella, A. d'Angelo, A. Incicchitti, D. Prosperi, R. Cerulli, C. J. Dai, H. L. He, X. M. Ma, X. D. Sheng, R. G. Wang, Z. P. Ye, Recent results from DAMA/LIBRA and perspectives, to appear in the Proceed. of MEDEX11, Praga, June 2011.

14. A. Barabash, P. Belli, R. Bernabei, R.S. Boiko, V.B. Brudanin, F. Cappella, V. Caracciolo, R. Cerulli, D.M. Chernyak, F.A. Danevich, S. d'Angelo, A. Di Marco, M.L. Di Vacri, A.E. Dossovitskiy, E.N. Galashov, B.V. Grinyov, A. Incicchitti, V.V. Kobychev, S.I. Konovalov, G.P. Kovtun, B.N. Kropivyansky, V.M. Kudovbenko, M. Laubenstein, A.L. Mikhlin, L.L. Nagornaya, S.S. Nagorny, P.G. Nagornyi, S. Nisi, D.V. Poda, R.B. Podviyanuk, D. Prosperi, O.G. Polischuk, A.P. Shcherban, V.N. Shlegel, D.A. Solopikhin, Y.G. Stenin, J. Suhonen, A.V. Tolmachev, V.I. Tretyak, V.I. Umatov, Y.V. Vasiliev, V.D. Virich, I.M. Vyshnevskyi, R.P. Yavetskiy, S.S. Yurchenko, Double beta experiments with the help of scintillation and HPGe detectors at Gran Sasso, to appear in the Proceed. of MEDEX11, Praga, June 2011.

15. P. Belli, R. Bernabei, F. Cappella, R. Cerulli, F.A. Danevich, S. d'Angelo, M.L. Di Vacri, A. Incicchitti, M. Laubenstein, S.S. Nagorny, S. Nisi, A.V. Tolmachev, V.I. Tretyak, R.P. Yavetskiy First search for 2β decay of dysprosium, Nucl.Phys. A 859 (2011) 126-139.

16. P. Belli, R. Bernabei, F. Cappella, R. Cerulli, F.A. Danevich, A. Di Marco, A. Incicchitti, M. Laubenstein, S.S. Nagorny, S. Nisi, O.G. Polischuk, V.I. Tretyak, First search for double beta decay of platinum by ultra-low background HP Ge spectrometry, Eur. Phys. J. A 47 (2011) 91.

17. P. Belli, R. Bernabei, A. Bottino, F. Cappella, R. Cerulli, N. Fornengo, S. Scopel, Observations of annual modulation in direct detection of relic particles and light neutralinos Phys. Rev. D 84 (2011) 055014.

18. A.S. Barabash, P. Belli, R. Bernabei, R.S. Boiko, F. Cappella, V. Caracciolo, D.M. Chernyak, R. Cerulli, F.A. Danevich, M.L. Di Vacri, A.E. Dossovitskiy, E.N. Galashov, A. Incicchitti, V.V. Kobychev, S.I. Konovalov, G.P. Kovtun, V.M. Kudovbenko, M. Laubenstein, A.L. Mikhlin, S. Nisi, D.V. Poda, R.B. Podviyanuk, O.G. Polischuk, A.P. Shcherban, V.N. Shlegel, D.A. Solopikhin, Yu.G. Stenin, V.I. Tretyak, V.I. Umatov, Ya.V. Vasiliev, V.D. Virich, Low background detector with enriched $^{116}CdWO_4$ crystal scintillators to search for double beta decay of ^{116}Cd, J. of Instr. 6 (2011) P08011.

19. P. Belli, R. Bernabei, F. Cappella, R. Cerulli, F.A. Danevich, S. d'Angelo, A. Incicchitti, V.V. Kobychev, D.V. Poda, V.I. Tretyak, Final results of experiment to search for 2β processes in zinc and tungsten with the help of radiopure $ZnWO_4$ crystal scintillators, J. Phys. G: Nucl. Part. Phys. 38 (2011), 115107

20. R. Bernabei, P. Belli, F. Cappella, R. Cerulli, C.J. Dai, A. d.Angelo, A. Di Marco, H.L. He, A. Incicchitti, X.H. Ma, F. Montecchia, D. Prosperi, X.D. Sheng, R.G. Wang, Z.P. Ye, "DAMA/LIBRA at Gran Sasso", in the volume New Trends in High Enegy Physics, P.N. Bogolyubov and L.L. Jenkovszky Eds, Bolgolyubov Institute for theoretical Physics, National Academy of Sciences of Ukraine (2011), 3-13.

21. R. Bernabei, P. Belli, A. Di Marco, F. Montecchia, F. Cappella, A. d.Angelo, A. Incicchitti, V. Caracciolo, R. Cerulli, C.J. Dai, H.L. He, X.H. Ma, X.D. Sheng, R.G. Wang, Z.P. Ye, "Particle Dark Matter in the galactic halo: results and perspectives", to appear in the Proceed. of the 3rd Galileo- Xu Guangqi meeting, 11-15 October 2011, Beijing (China).

22. R. Bernabei, P. Belli, A. Bussolotti, F. Cappella, V. Caracciolo, M. Casalboni, R. Cerulli, C.J. Dai, A. d'Angelo, A. Di Marco, H.L. He, A. Incicchitti, H.H. Kuang, M. Laubenstein, X.H. Ma, A. Mattei, F. Montecchia, C. Palazzesi, P. Prosposito, X.D. Sheng, R.G. Wang, Z.P. Ye, "Performances of the new high quantum efficiency PMTs in DAMA/LIBRA" in publication on J. of Instr.

References

[1] R. Bernabei et al., Nucl. Instr. & Meth. A 592 (2008) 297.

[2] R. Bernabei et al., Eur. Phys. J. C 56 (2008) 333.

[3] R. Bernabei et al., Eur. Phys. J. C 67 (2010) 39.

[4] R. Bernabei et al., Eur. Phys. J. C 62 (2009) 327.

[5] P. Belli, R. Bernabei, C. Bacci, A. Incicchitti, R. Marcovaldi, D. Prosperi, DAMA proposal to INFN Scientific Committee II, April 24^{th} 1990.

[6] R. Bernabei et al., Phys. Lett. B 389 (1996) 757; R. Bernabei et al., Phys. Lett. B 424 (1998) 195; R. Bernabei et al., Phys. Lett. B 450 (1999) 448; P. Belli et al., Phys. Rev. D 61 (2000) 023512; R. Bernabei et al., Phys. Lett. B 480 (2000) 23; R. Bernabei et al., Phys. Lett. B 509 (2001) 197; R. Bernabei et al., Eur. Phys. J. C 23 (2002) 61; P. Belli et al., Phys. Rev. D 66 (2002) 043503.

[7] R. Bernabei et al., Il Nuovo Cim. A 112 (1999) 545.

[8] R. Bernabei et al., Eur. Phys. J. C18 (2000) 283.

[9] R. Bernabei el al., La Rivista del Nuovo Cimento 26 n.1 (2003) 1-73.

[10] R. Bernabei et al., Int. J. Mod. Phys. D 13 (2004) 2127.

[11] R. Bernabei et al., Int. J. Mod. Phys. A 21 (2006) 1445; R. Bernabei et al., Eur. Phys. J. C. 47 (2006) 263; R. Bernabei et al., Int. J. Mod. Phys. A 22 (2007) 3155; R. Bernabei et al., Eur. Phys. J. C 53 (2008) 205; R. Bernabei et al., Phys. Rev. D 77 (2008) 023506; R. Bernabei et al., Mod. Phys. Lett. A 23 (2008) 2125.

[12] R. Bernabei et al., Phys. Lett. B408 (1997) 439; P. Belli et al., Phys. Lett. B460 (1999) 236; R. Bernabei et al., Phys. Rev. Lett. 83 (1999) 4918; P. Belli et al., Phys. Rev. C60 (1999) 065501; R. Bernabei et al., Il Nuovo Cimento A112 (1999) 1541; R. Bernabei et al., Phys. Lett. B 515 (2001) 6; F. Cappella et al., Eur. Phys. J.-direct

C14 (2002) 1; R. Bernabei et al., Eur. Phys. J. A 23 (2005) 7; R. Bernabei et al., Eur. Phys. J. A 24 (2005) 51; R. Bernabei et al., Astrop. Phys. 4 (1995) 45.

[13] R. Bernabei, in the volume *The identification of Dark Matter*, World Sc. Pub. (1997) 574; R. Bernabei et al., Phys. Lett. B 424 (1998) 195; R. Bernabei et al., Phys. Lett. B 450 (1999) 448; P. Belli et al., Phys. Rev. D 61 (2000) 023512; R. Bernabei et al., Eur. Phys. J. C 18 (2000) 283; R. Bernabei et al., Phys. Lett. B 509 (2001) 197; R. Bernabei et al., Eur. Phys. J. C 23 (2002) 61; P. Belli et al., Phys. Rev. D 66 (2002) 043503; R. Bernabei et al., Int. J. Mod. Phys. A 22 (2007) 3155-3168.

[14] K.A. Drukier et al., Phys. Rev. D 33 (1986) 3495.

[15] K. Freese et al., Phys. Rev. D 37 (1988) 3388.

[16] P. Belli et al., Phys. Rev. D 66 (2002) 043503.

[17] R. Bernabei et al., Eur. Phys. J. C 53 (2008) 205.

[18] V.I. Tretyak, Astropart. Phys. 33 (2010) 40 (arXiv:0911.3041v1 [nucl-ex]).

[19] Bottino A et al 2010 *Phys. Rev.* D **81** 107302; Fornengo N et al 2011 *Phys. Rev.* D **83** 15001; Fitzpatrick A L et al 2010 `arXiv:1003.0014`; Hooper D et al 2010 `arXiv:1007.1005v2`; Cerdeno D G and Seto 0 2009 *JCAP* **0908** 032; Cerdeno D G, Munoz C and Seto 0 2009 *Phys. Rev.* D **79** 023510; Cerdeno D G et al 2007 *JCAP* **0706** 008; Gunion J F et al 2009 `arXiv:1009.2555`; Belikov A V et al 2010 `arXiv:1009.0549`; Arina C and Fornengo N 2007 *JHEP* **11** 029; Belanger G et al `arXiv:1105.4878`; Chang S et al 2009 `Phys. Rev.` D **79** 043513; Chang S et al 2010 `arXiv:1007.2688`; Foot R 2010 `arXiv:1001.0096`, `arXiv:1106.2688`, *Phys. Rev.* D **82** 095001; Mambrini Y 2011 *JCAP* **1107** 009, *JCAP* 2010 **1009** 022; Bai Y and Fox P J 2009 *JHEP* **0911** 052; Alwall J et al 2010 `arXiv:1002.3366`; Khlopov M. Yu et al `arXiv:1003.1144`; Andreas S et al 2010 *Phys. Rev.* D **82** 043522; Boucenna M S, Profumo S 2011 `arXiv:1106.3368` Graham P W et al 2010 `Phys. Rev.` D **82** 063512; Batell B, Pospelov M and Ritz A 2009 `Phys. Rev.` D **79** 115019; Del Nobile E et al 2011 `Phys. Rev.` D **84** 027301; Kopp J et al 2010 *JCAP* **1002** 014; Barger V et al 2010 `Phys. Rev.` D **82** 035019; Chang S et al 2010 *JCAP* **1008** 018; Feng J L et al 2011 *Phys. Lett.* B **703** 124 Frandsen M T et al 2011 `Phys. Rev.` D **84** 041301; Kim Y G and Shin S 2009 *JHEP* **0905** 036; Shin S 2010 `arXiv:1011.6377`; Buckley M R 2011 `arXiv:1106.3583` Fornengo N et al 2011 `arXiv:1108.4661` Gondolo P et al 2011 `arXiv:1106.0885` Kuflik E et al 2010 `arXiv:1003.0682`; Arina C et al 2011 `arXiv:1105.5121`; Buckley M R et al `1011.1499`

[20] C.E. Aalseth et al., 2010 `arXiv:1002.4703; 2011 arXiv:1106.0650`

[21] G. Angloher et al., `arXiv:1109.0702`.

[22] A. Bottino et al., `arXiv:1112.5666`

[23] P. Belli et al., Il Nuovo Cim. 103A (1990) 767.

[24] P. Belli et al., Phys. Lett. B 387 (1996) 222 and Phys. Lett. B 389 (1996) 783 (erratum); R. Bernabei et al., New J. Phys. 2 (2000) 15.1; Eur. Phys. J.-direct C11 (2001) 1; Phys. Lett. B 436 (1998) 379; R. Bernabei et al., in the volume "Beyond the Desert 2003", Springer (2003) 365.

[25] R. Bernabei et al., Nucl. Instr. & Meth. A482 (2002) 728.

[26] R. Bernabei et al., Phys. Lett. B 546 (2002) 23; F. Cappella, PhD Thesis, Università di Roma "Tor Vergata", 2005.

[27] P. Belli et al., Il Nuovo Cim. C 19 (1996) 537; Astrop. Phys. 5 (1996) 217.

[28] R. Bernabei et al., Phys. Lett. B 527 (2002) 182.

[29] P. Belli et al., Phys. Rev. D 61 (2000) 117301; Phys. Lett. B 465 (1999) 315; R. Bernabei et al., Phys. Lett. B 493 (2000) 12; Eur. Phys. J. A 27 s01 (2006) 35.

[30] R. Bernabei et al., Astropart. Phys. 7 (1997) 73; R. Bernabei et al., Il Nuovo Cim. A 110 (1997) 189; P. Belli et al., Nucl. Phys. B 563 (1999) 97; R. Bernabei et al., Nucl. Phys. A 705 (2002) 29; P. Belli et al., Nucl. Instr. Meth. A 498 (2003) 352; R. Cerulli et al., Nucl. Instr. Meth. A 525 (2004) 535; R. Bernabei et al., Nucl. Instr. Meth. A 555 (2005) 270; R. Bernabei et al., Ukr. J. Phys. 51 (2006) 1037; P. Belli et al., Nucl. Phys. A 789 (2007) 15; P. Belli et al., Phys. Rev. C 76 (2007) 064603; P. Belli et al., Eur. Phys. J. A 36 (2008) 167; P. Belli et al., J. Phys. G 38 (2011) 015103; P. Belli et al., Nucl. Instr. Meth. A 626 (2011) 31.

[31] M. Hirsch et al., Z. Phys. A 347 (1994) 151.

[32] P. Belli et al., Nucl. Phys. A 826 (2009) 256; P. Belli et al., Phys. Lett. B 658 (2008) 193.

[33] I. Bikit et al., Appl. Radiat. Isot. 46 (1995) 455.

[34] P. Belli et al., Nucl. Instr. Meth. A 615 (2010) 301.

[35] O. A. P. Tavares and E. L. Medeiros, Phys. Scr. 84 (2011) 045202 and Dongdong Ni and Zhongzhou Ren, Phys. Rev. C84 (2011) 037301.

The GERDA experiment

M. Agostini [n], M. Allardt [c], E. Andreotti [e], A.M. Bakalyarov [l], M. Balata [a], I. Barabanov [j], L. Baudis [s], C. Bauer [f], N. Becerici-Schmidt [m], E. Bellotti [g,h], S. Belogurov [k,j], S.T. Belyaev [l], G. Benato [s], A. Bettini [o,p], L. Bezrukov [j], T. Bode [n], V. Brudanin [d], R. Brugnera [o,p], D. Budjas [n], A. Caldwell [m], C. Cattadori [h], A. Chernogorov [k], F. Cossavella [m], E.V. Demidova [k], A. Denisov [j], A. Domula [c], V. Egorov [d], R. Falkenstein [r], A. Ferella [s], N. Fiuza de Barros [c], K. Freund [r], F. Froborg [s], N. Frodyma [b], A. Gangapshev [j,f], A. Garfagnini [o,p], S. Gazzana [f,a], P. Grabmayr [r], V. Gurentsov [j], K.N. Gusev [l,d], W. Hampel [f], A. Hegai [r], M. Heisel [f], S. Hemmer [o,p], G. Heusser [f], W. Hofmann [f], M. Hult [e], L.V. Inzhechik [j], L. Ioanucci [a], J. Janicsko [n], J. Jochum [r], M. Junker [a], S. Kianovsky [j], I.V. Kirpichnikov [k], A. Kirsch [f], A. Klimenko [d,j], K.T. Knoepfle [f], O. Kochetov [d], V.N. Kornoukhov [k,j], V. Kusminov [j], M. Laubenstein [a], A. Lazzaro [n], V.I. Lebedev [l], B. Lehnert [c], M. Lindner [f], X. Liu [q], A. Lubashevskiy [f], B. Lubsandorzhiev [j], A.A. Machado [f], B. Majorovits [m], W. Maneschg [f], G. Marissens [e], A. Michel [m], I. Nemchenok [d], S. Nisi [a], C. O'Shaughnessy [m], L. Pandola [a], K. Pelczar [b], A. Pullia [i], M. Reissfelder [f], S. Riboldi [i], C. Sada [o,p], C. Schmitt [r], B. Scholz [c], J. Schreiner [f], O. Schulz [m], B. Schwingenheuer [f], S. Schönert [n], H. Seitz [m], M. Shirchenko [l,d], H. Simgen [f], A. Smolnikov [f], L. Stanco [p], F. Stelzer [m], H. Strecker [f], M. Tarka [s], C.A. Ur [p], A.A. Vasenko [k], O. Volynets [m], K. von Sturm [r], V. Wagner [f], M. Walter [s], A. Wegmann [f], M. Wojcik [b], E. Yanovich [j], P. Zavarise [a], S.V. Zhukov [l], D. Zinatulina [d], K. Zuber [c], and G. Zuzel [b].

[a]) INFN Laboratori Nazionali del Gran Sasso, LNGS, Assergi, Italy

[b]) Institute of Physics, Jagellonian University, Cracow, Poland

[c]) Institut für Kern- und Teilchenphysik, Technische Universität Dresden, Dresden, Germany

[d]) Joint Institute for Nuclear Research, Dubna, Russia

[e]) Institute for Reference Materials and Measurements, Geel, Belgium

[f]) Max Planck Institut für Kernphysik, Heidelberg, Germany

[g]) Dipartimento di Fisica, Università Milano Bicocca, Milano, Italy

[h]) INFN Milano Bicocca, Milano, Italy

[i]) Dipartimento di Fisica, Università degli Studi di Milano e INFN Milano, Milano, Italy

[j]) Institute for Nuclear Research of the Russian Academy of Sciences, Moscow, Russia

[k]) Institute for Theoretical and Experimental Physics, Moscow, Russia

[l]) Russian Research Center Kurchatov Institute, Moscow, Russia

[m]) Max-Planck-Institut für Physik, München, Germany

[n]) Physik Department E15, Technische Universität München, Germany

[o]) Dipartimento di Fisica dell'Università di Padova, Padova, Italy

[p]) INFN Padova, Padova, Italy
[q]) Shanghai Jiaotong University, Shanghai, China
[r]) Physikalisches Institut, Eberhard Karls Universität Tübingen, Tübingen, Germany
[s]) Physik Institut der Universität Zürich, Zürich, Switzerland

Spokesperson: S. Schönert (*Stefan.Schoenert@ph.tum.de*)
Deputy Spokesperson: C. Cattadori (*Carla.Cattadori@lngs.infn.it*)
Technical Coordinator: K.T. Knoepfle (*Karl-Tasso.Knoepfle@mpi-hd.mpg.de*)
Analysis Coordinator: L. Pandola (*Luciano.Pandola@lngs.infn.it*)
Phase II Coordinator: B. Majorovits (*bela@mppmu.mpg.de*)
URL: `http://www.mpi-hd.mpg.de/GERDA/`

Abstract

The GERmanium Detector Array (GERDA) experiment searches for neutrinoless double beta decay ($0\nu\beta\beta$) of the isotope ^{76}Ge. In 2011, the commissioning of the experiment finished and data taking started with the diodes of the former Heidelberg-Moscow and IGEX experiments. These are made from material isotopically enriched to about 86% in ^{76}Ge. The total mass is 17.6 kg. The background at $Q_{\beta\beta}$ is about 0.017 cts/(keV·kg·y) which is a factor of about 10 lower than for the previous experiments.
The study of background originating from ^{42}Ar was continued in the LARGE facility. Argon with a known ^{42}Ar activity was added and the behavior of the (charged) progeny ^{42}K in electric fields has been studied.
The preparations for the second phase have started. These include the production of new detectors, conceptually new readout electronics and the liquid argon instrumentation.

1 Introduction

The GERmanium Detector Array (GERDA) [1] searches for neutrinoless double beta decay ($0\nu\beta\beta$) of the germanium isotope ^{76}Ge. Its observation would establish that lepton number is violated and that the neutrino is its own antiparticle.

GERDA uses a novel shielding concept (Fig. 1): bare Ge diodes are operated in a 65 m^3 cryostat filled with liquid argon (LAr) which acts as coolant for the detectors and as shield against the radioactivity of the cryostat and the underground environment. The shielding is supplemented by a 3 m thick water buffer. The diodes are both source and detector for $0\nu\beta\beta$ decay. Since no neutrino is emitted, the signal is a line at the Q-value of the decay ($Q_{\beta\beta} = 2039$ keV). The water is instrumented with photo-multipliers tubes (PMTs) to detect the Cherenkov light of muons passing through the water tank. On top is a clean room for diode handling and at its center a lock for transferring the detectors to the argon atmosphere. Next to the water tank is the GERDA building which houses the cryogenic infrastructure and the electronics for data taking.

In summer 2010 the construction of the experiment was completed and the commissioning started with three detectors of natural isotope composition. An unexpected high background was found and the most prominent identified source originated from ^{42}Ar. Several different configurations were tried to learn about the background sources at $Q_{\beta\beta}$ (section 2). Commissioning concluded in autumn 2011 and since November 2011 Phase I data taking started with detectors of the former Heidelberg-Moscow and IGEX experiment made from germanium with 86% enrichment in ^{76}Ge. The current status is discussed in section 3.

The R&D facility LArGe is a 1 m^3 copper cryostat filled with liquid argon which is instrumented with photo-multiplier tubes to detect scintillation light simultaneously to signals from a germanium detector. The LAr instrumentation is an active veto for background rejection. In 2011 this facility has been used to study the ^{42}Ar background in more detail. Argon spiked with a known activity was introduced and the rate of 1525 keV γ-rays from the decay of ^{42}K (the progeny of ^{42}Ar) was measured under different conditions (section 5).

While GERDA Phase I has started, a second phase with an even lower background of 10^{-3} cts/(keV·kg·y) and with new detectors and new front-end electronics is under preparation. The detectors are planar diodes with a small readout contact. They offer superior pulse shape discrimination against many sources of backgrounds. Its production has started in 2011. Together with the LAr instrumentation the background goal should be reached (section 6).

Further detailed information is available in the biannual progress reports to the LNGS scientific committee [2].

2 GERDA commissioning

The commissioning started in June 2010 with a string of three low-background detectors made from germanium with natural isotope composition. These diodes had been operated before in the Genius Test Facility (GTF) and were modified by Canberra in the same way as the "enriched detectors", i.e. the diodes made from material enriched to 86% in ^{76}Ge.

In spring 2011 the lock for transferring the detectors into the cryostat was expanded to accommodate up to 4 strings of 3 detectors each. In summer the first string of enriched detectors was added to the existing string of natural detectors. This allowed to compare the backgrounds between the two strings and to search for differences between enriched and natural detectors.

The entire list of runs of the different configurations is shown in table 1. Some of the commissioning results have been reported already in last year's annual report. Here we will summarize the main points from all runs until fall 2011.

- The most prominent feature of all background spectra since the beginning of the commissioning is a line at 1525 keV originating from the β decay of ^{42}K ($T_{1/2} = 12$ h), the progeny of ^{42}Ar ($T_{1/2} = 33$ y, $Q = 599$ keV). Since the Q value of the ^{42}K decay is 3.5 MeV, β particles can contribute to the background at $Q_{\beta\beta}$ if the decay occurs at a detector surface.

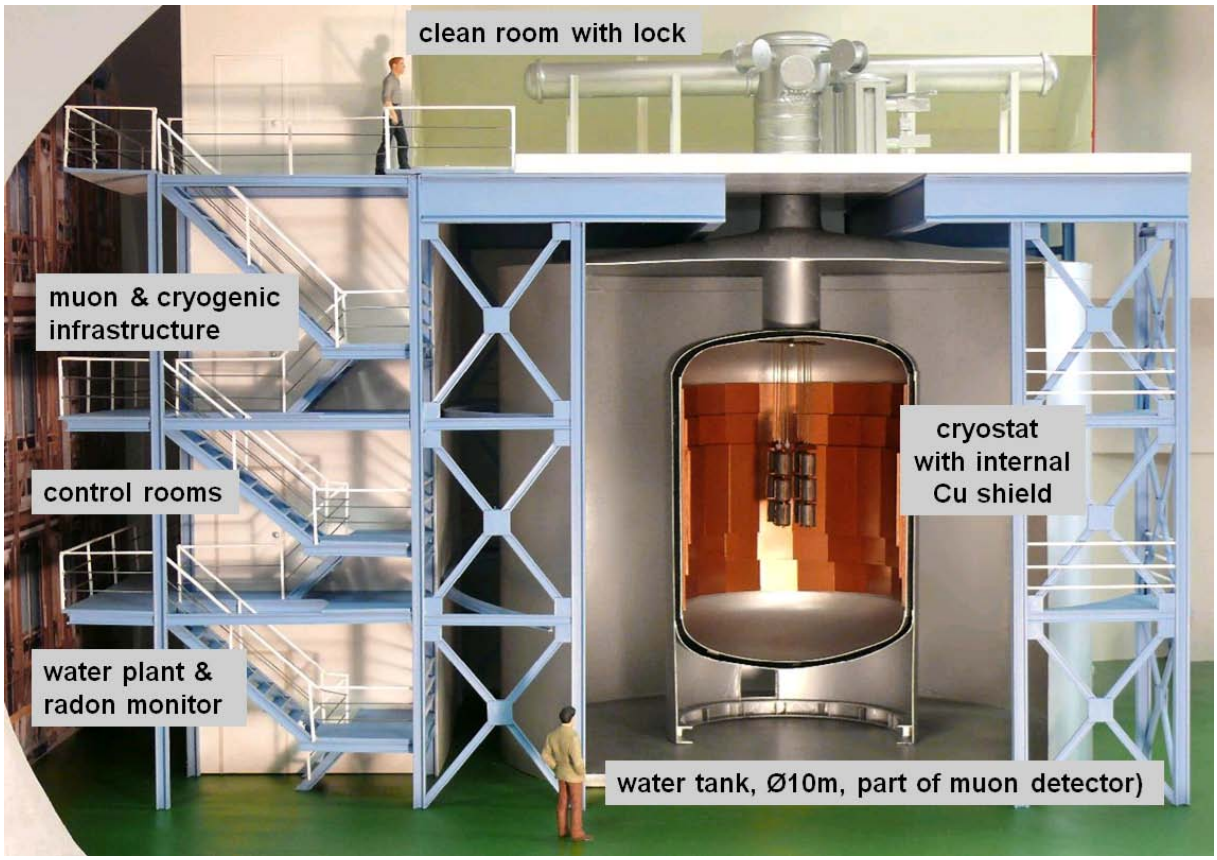

Figure 1: Model of the GERDA experiment.

- Potassium from ^{42}Ar decay is initially positively charged. Hence these ions drift in the electric fields surrounding the bare detectors[1] until they get neutralized. This neutralization time could be estimated as 20 minutes using electric field and ion drift calculations together with simulations for the detection efficiency of the 1525 keV gamma as a function of the distance between the decay and the detector.

- The count rate at 1525 keV and $Q_{\beta\beta}$ could be reduced by a factor of $\approx$3 if the string of three detectors is surrounded by a copper foil (called "mini-shroud", MS). This can be seen by comparing runs 1-3 with 4, 6 and 7. There is a second copper foil called "shroud" (S) at a larger diameter of 760 mm which surrounds the detector array. S and MS can be biased independently, i.e. the drifting of ^{42}K ions can be studied (run 5). The MS minimizes the LAr volume with electric field lines originating from the detector biasing and at the same time strongly reduces LAr convection effects. The numbers suggest that the background for runs 1-3 is dominated by ^{42}K surface events.

- To understand what fraction of the background at $Q_{\beta\beta}$ after the installation of the

[1]Positive high voltage is applied to the outer contact of the coaxial detectors and the inner contact is at ground potential and read out with a charge sensitive amplifier.

MS is due to surface ^{42}K decays, several configurations have been tested. These include encapsulation of detectors with PTFE or copper (runs 10 and 11) and reversing the operating voltage[2] (run 12) to strongly reduce electric fields lines surrounding the detectors. For all these configurations the background at $Q_{\beta\beta}$ did not change significantly. This suggests that surface events are not a dominant contribution for these runs.

- Other gamma lines from the natural decay chains have a low count rate. Therefore the origin of the background at $Q_{\beta\beta}$ is not easily quantified.

- The enriched detectors have on average a lower background than the natural detectors (runs 15, 18 and 22). This suggests that intrinsic contamination like ^{60}Co are present in the GTF detectors.

- The background at $Q_{\beta\beta}$ could be exclusively due to ^{208}Tl if the source is far away and strong enough. With the observed number of events in the 2615 keV peak (runs 10-12) and a Compton-to-peak ratio of a 2 m distant source (about 0.011/keV), such a condition could be met. This can be tested by changing the axial position of the detector string in the cryostat. In run 20 one detector string was lifted by 1.2 m. While the count rate at 2615 keV was considerably higher, the level was not high enough to explain the background at the nominal position.

- The count rate at 1525 keV was lowest when all cables on high voltage are shielded and the MS hermetically closed, i.e. when ion drifting is reduced to a minimum. For the Phase I data taking special care was taken to achieve this.

3 Phase I data taking

In autumn 2011 all eight enriched detectors with a total mass of 17.6 kg together with 3 GTF detectors were installed and physics data taking started. Fig. 2 shows the three strings of the enriched detectors and one GTF diode. A calibration taken on December 19^{th} is shown in Fig. 3. Resolutions (FWHM) are typically between 4.5 and 5.5 keV at 2.6 MeV which translates to 4-5 keV at $Q_{\beta\beta}$. The performance of RG3 deteriorated with time due to high leakage current and the operating voltage had to be reduced continuously. Consequently RG3 can not be used for physics analysis. The same problem occurred later with the ANG1 detector and the total mass of the used enriched detectors is therefore reduced to 14.6 kg. The mass of the 3 GTF detectors is 7.6 kg.

Fig. 4 shows the background spectra of the enriched and the GTF detectors. Note that a 40 keV window around $Q_{\beta\beta}$ is empty. The data in this "blinded" window will only be processed once the analysis is finished in order to avoid any bias in applying selection cuts.

Other peaks visible are at 1460 keV from ^{40}K (13 counts/(kg·y)), at 1764 keV from ^{214}Bi (3.8 counts/(kg·y)) and at 2615 keV from ^{208}Tl (2.4 counts/(kg·y)). The count

[2]Negative HV is applied to the inner contact and the outer contact is read out. A copper disk is added next to the inner contact to close the field lines.

Table 1: Run list from GERDA commissioning. "MS" and "S" are abbreviations for mini-shroud and shroud, respectively. "ENR" and "GTF" stand for strings with enriched and GTF detectors, respectively. Uncertainties on the background index at $Q_{\beta\beta}$ are omitted for readability. They can be extracted by calculating the observed number of events as "index·exposure·400 keV".

run	detectors	exposure [kg·y]	configuration	bkg. index [cts/(keV·kg·y)]
1	3×GTF	0.34	no MS, S floating	0.20
2	3×GTF	0.12	no MS, S -400 V	0.10
3	3×GTF	0.14	no MS, S -400 V	0.22
sum		0.60	no MS	0.18
4	3×GTF	0.37	MS=0 V, S=-400 V	0.067
5	3×GTF	0.19	MS=-200 V, S=+500 V attract pos. ions to diodes	0.066
6	3×GTF	0.26	MS & S at 0 V,	0.029
7	2×GTF	0.23	MS=-200 V, S=-400 V, repel pos. ions	0.055
sum 4,6,7		0.86		0.052
8	2×GTF,BEGe	0.16	MS=0 V, S=-400 V, no μ veto	0.29
9	2×GTF,BEGe	0.04	MS=0 V, S=-400 V	0.40
sum		0.20		0.31
10	3×GTF	0.56	MS=0 V, S=-400 V, 2 det. encapsulated, 1 det. reverse bias	0.067
11	3×GTF	0.46	MS & S at 0 V, 2 det. encapsulated, 1 det. reverse bias	0.055
sum		1.02		0.061
12	3×GTF	0.56	MS=0 V, S=-400 V, all det. reverse bias	0.062
13	3×GTF	0.51	no MS, S=-400 V, all det. reverse bias	0.27
14	3×ENR	0.13	MS=0 V, S=0 V, string position 50 cm higher	0.12
15	3×ENR	0.29	As run 14, normal str. position	0.051
16	3×ENR/3×GTF	0.16/0.19	MS=0 V, S=0 V, ENR 50 cm higher	0.015/0.27
17	3×ENR/3×GTF	0.11/0.12	as run 16, MS of ENR 3000 V	0.069/0.44
18	3×ENR/3×GTF	0.11/0.13	as run 16, ENR & GTF normal pos.	0.045/0.078
20	3×ENR/3×GTF	0.12/0.14	ENR 120 cm higher, GTF at nominal pos., MS & S at 0 V	1.5/0.089
21	3×ENR/3×GTF	0.25/0.28	ENR 60 cm higher. GTF at nominal pos., MS & S at 0 V	0.15/0.044
22	3×ENR/3×GTF	0.29/0.33	ENR and GTF at nominal pos., MS & S at 0 V	0.035/0.076

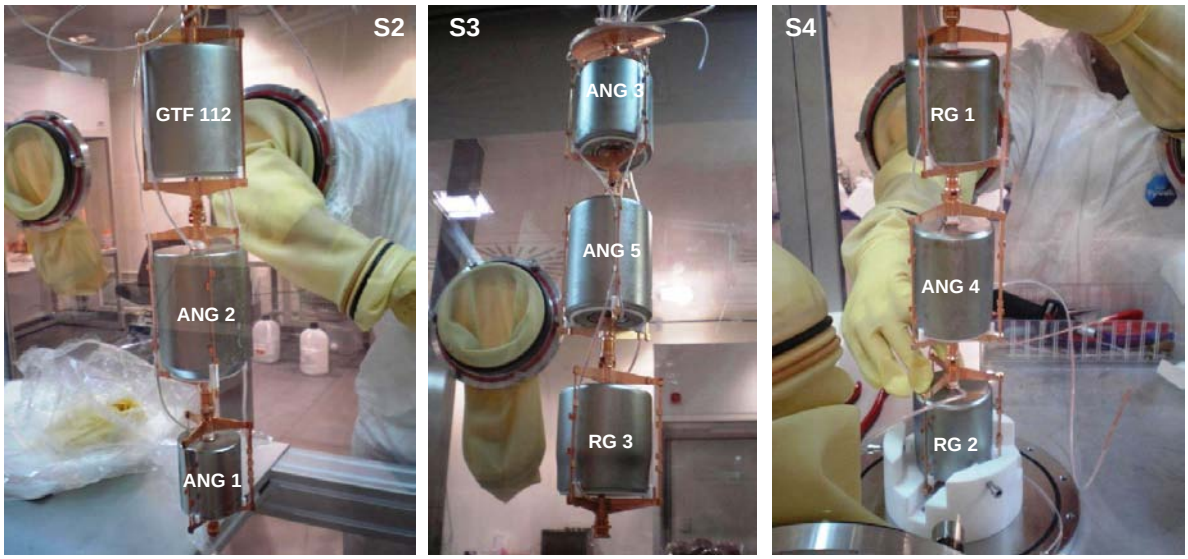

Figure 2: Three strings with the enriched detectors and one GTF detector.

rate in a ±200 keV window around $Q_{\beta\beta}$ is $(0.017^{+0.009}_{-0.005})$ cts/(keV·kg·y) for the enriched detectors and $(0.051^{+0.011}_{-0.009})$ cts/(keV·kg·y) for the natural detectors. These are the rates after applying an anti-coincidence cut among the detectors and an anti-coincidence cut with the muon veto. No pulse shape information is used at the moment. Since some events in this window are from well-known γ lines in the interval (like at 2204 keV from ^{214}Bi) the true background at $Q_{\beta\beta}$ is lower, i.e. close to the design goal of 0.01 cts/(keV·kg·y) for Phase I. The background rate for Heidelberg-Moscow was about 0.13 cts/(keV·kg·y) for the entire statistics of 71.7 kg·y or 0.16 cts/(keV·kg·y) if the average in the energy interval 2-2.1 MeV is taken [3] (similar to our determination). The line count rates were 16.4 counts/(kg·y) at 2615 keV and 30.6 counts/(kg·y) at 1764 keV [4]. The GERDA background at $Q_{\beta\beta}$ is about a factor of 10 lower for the enriched detectors. The higher rate in the GTF detectors is similar to the numbers observed in the previous commissioning runs.

Fig. 5 shows the spectrum for the enriched detectors below 1700 keV (square points). Below 400 keV the main contribution is from ^{39}Ar β decay (green curve) with an activity of 1.01 Bq/kg [5]. Above 600 keV $2\nu\beta\beta$ decays of ^{76}Ge (red curve) dominate. Here we take an active volume of 85% [6] and a half life of $T^{2\nu\beta\beta}_{1/2} = 1.74 \cdot 10^{21}$ years [7]. The blue curve shows the contribution from the 1525 keV line from ^{42}K decays normalized to the observed line count and assuming a homogeneous distribution in the liquid argon. The magenta line displays the expected contribution from ^{40}K decays occurring close to the detectors normalized to the observed line count rate. The black line is the sum of all contributions which fits quite well to the data (square points). It should be emphasized that the green and red curves are not a fit but absolute predictions based on previous measurements.

The spectrum above 1550 keV and hence the background at $Q_{\beta\beta}$ is less well understood at the moment. The observed 1764 keV and 2615 keV lines clearly show the presence of

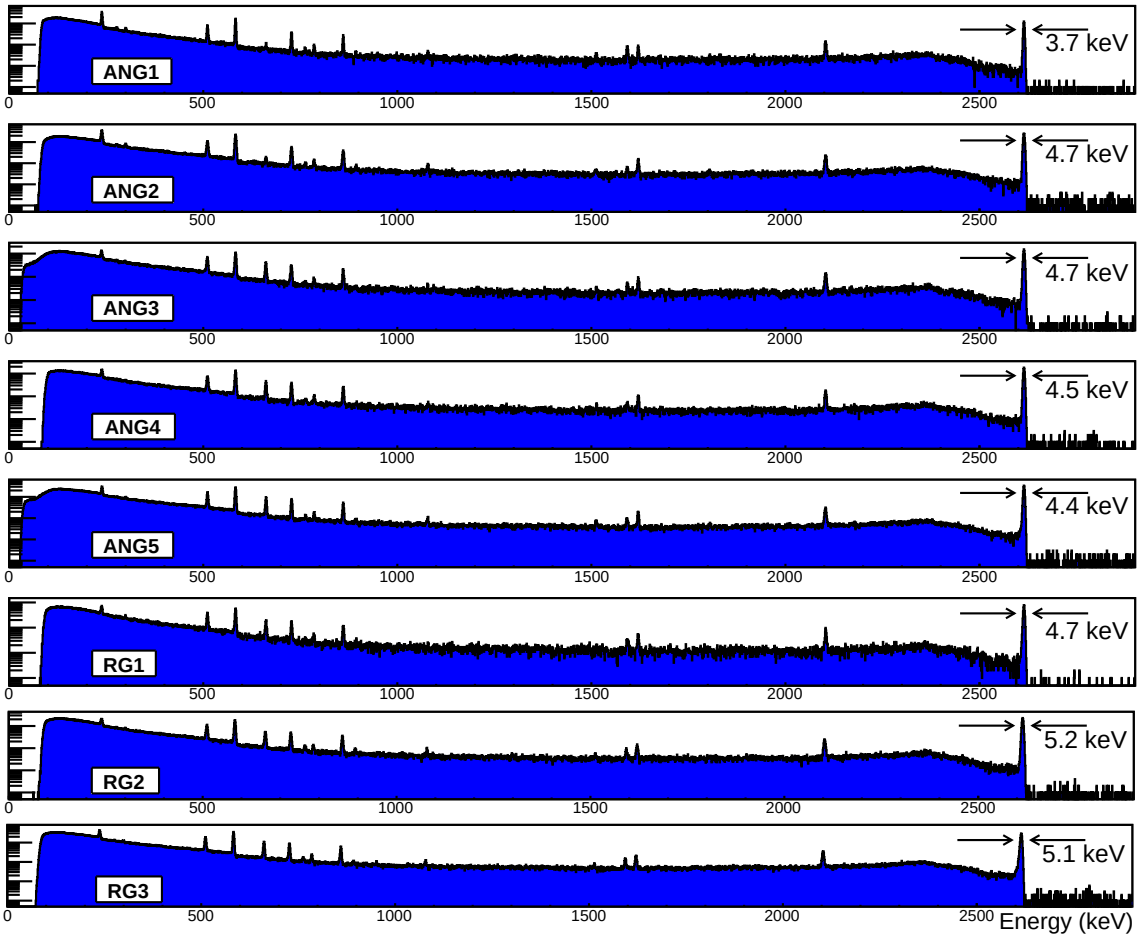

Figure 3: Spectra of the enriched detectors irradiated with a ^{228}Th calibration source. The values reported in the plot are the energy resolutions (FWHM) at the 2.6-MeV γ-line.

contamination from the natural decay chains. For the extraction of the spectral shape the location of the contamination is important. The intensity of low energy lines (583 and 609 keV) have to be measured for this determination. This is only possible with higher statistics.

In addition the β decay of ^{42}K will contribute to the background at $Q_{\beta\beta}$ and possibly also α decays at the grove or the p^+ contact of the detectors.

4 Muon Veto

During the last year, the muon Cherenkov veto was supplemented by a plastic veto on top of the clean room. Each of the plastic veto panels contains a sheet of plastic scintillator ($2000\times500\times30$ mm), a photo-multiplier and its front-end electronics. At first, feasibility tests with only seven panels were conducted underground. It was shown, that a double layer of panels in coincidence exhibits a high rate which was mostly due to γ-coincidences. Therefore, a triple layer approach was chosen for the final installation since a triple coinci-

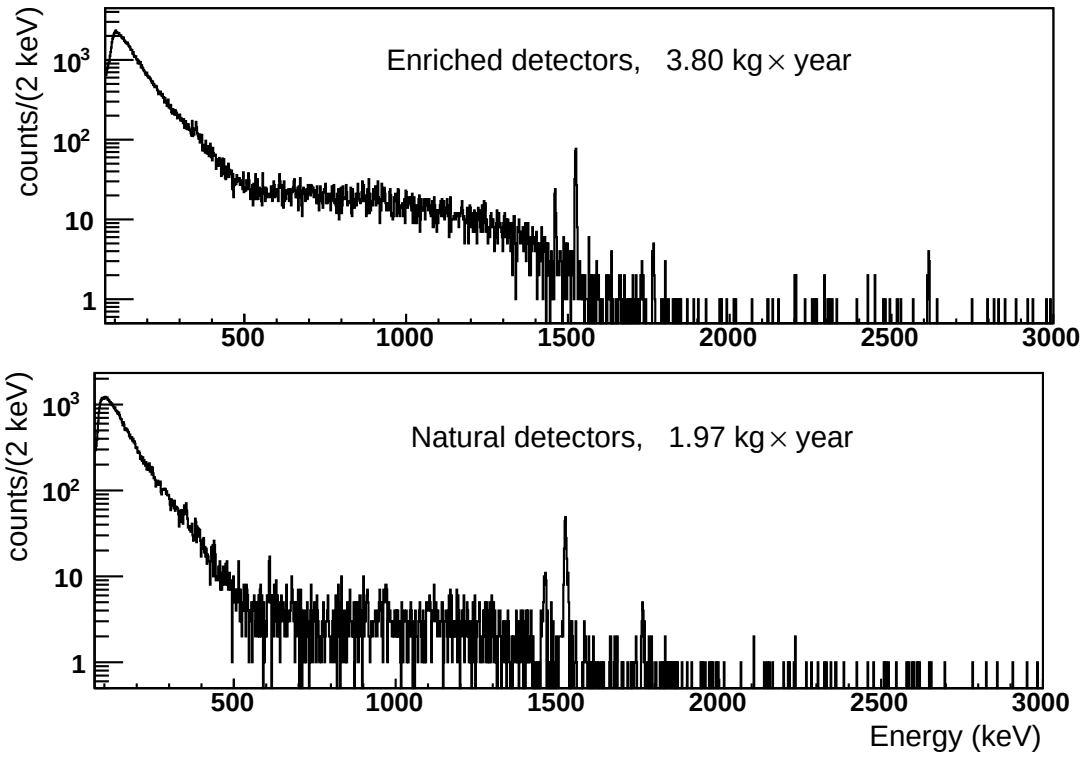

Figure 4: Background spectra for the enriched (top) and natural (bottom) detectors in the Phase I data taking. The 40-keV region around $Q_{\beta\beta}$ is empty due to data blinding.

dence shows an almost clean muon spectrum. Altogether, 36 panels were installed which cover 12 m^2 right above the neck of the cryostat (see Fig. 6). The panels reproduce the muon rates measured by MACRO and the data is particularly helpful in order to identify events in the water tank as genuine muon events and hence study their properties.

A ratio of detected photo electrons per muon per length of its track in the tank could be derived. Monte Carlo simulations were compared to the amount of detected light in both the water tank and the pillbox (volume below the cryostat) resulting in a detection of (0.9 ± 0.3) p.e./cm (see Fig. 7). Using this value and the data from the panel veto, an overall muon detection efficiency $\epsilon = (97.17 \pm 0.42)\%$ could be derived. This leads to a reduction of the background index caused by muons to 1.8×10^{-5} cts/(keV kg y), which is well below specification for Phase II of GERDA.

5 LArGe test facility

Phase I of GERDA uses liquid argon (LAr) only as a passive shield. For the next phase it is foreseen to veto background events by the detection of energy deposition in LAr, i.e. by measuring the scintillation light. This has been studied in the past with the LArGe. It is a 1 m^3 copper cryostat with 9 PMTs for light detection. The copper is lined with a wavelength shifting reflector foil. The passive shield consists of (from outside to inside)

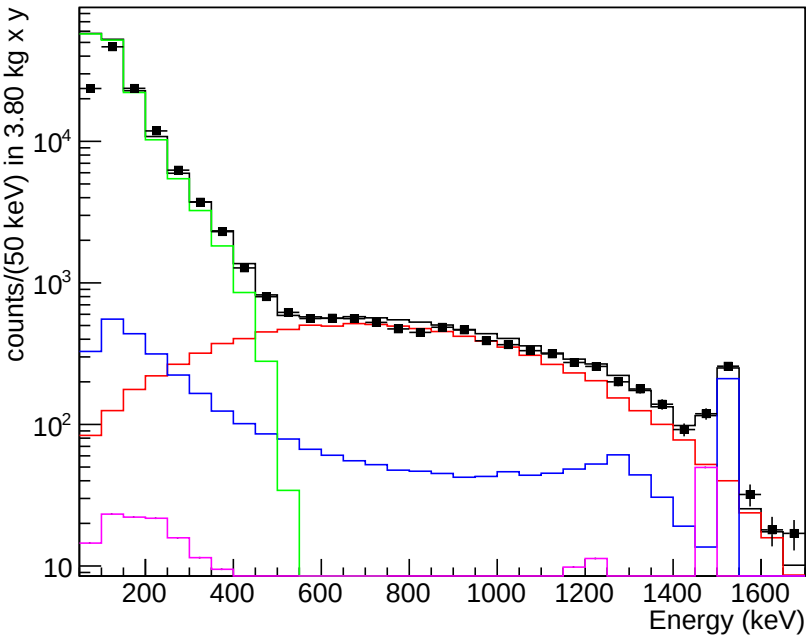

Figure 5: Spectra for the enriched detectors (square points) together with a prediction (not a fit) of the shape (black line). The prediction consists of contributions from ^{39}Ar (green), $2\nu\beta\beta$ decay of ^{76}Ge (red), the 1525 keV γ line of ^{42}K (blue) and the 1460 keV γ line from ^{40}K (magenta).

20 cm polyethylene, 23 cm steel, 10 cm lead and 15 cm copper of increasing radio-purity. Depending on the type of background and its location a reduction by a factor between 3 and 1000 could be demonstrated by the scintillation light veto. Results are discussed in last year's annual report.

Another task for LArGe emerged after the first Gerda commissioning runs which showed the need to study concentration and volume distribution of the cosmogenic isotope ^{42}Ar and its daughter ^{42}K in liquid argon. To start with a well-known activity, ^{42}Ar was produced in ^{40}Ar(^{7}Li,αp)^{42}Ar reactions at TU Munich. Two samples were prepared with activities of (5.9 ± 0.9) Bq and (5.2 ± 0.9) Bq. The second sample was transferred into the LArGe cryostat.

A GTF detector was completely encapsulated with three layers of PTFE/copper/PTFE. The copper surface could be biased such that the electric field surrounding the detector could be chosen.[3] Ions drifting in the electric field to the outer PTFE surface are stuck there since they are not neutralized. The change of the ^{42}K ion concentration close to the detector could then be studied by measuring the intensity of the 1525 keV line.

Tests included the copper surface biased from -3000 V to +3000 V. The measurements were compared to 3-D simulations of the electric field together with ion drift calculations and simulations for the detection efficiency of the 1525 keV γ-ray in the germanium

[3]Only the field from a 15 cm long unshielded part of the cable for the detector bias could not be changed.

Figure 6: The GERDA plastic veto mounted on top of the clean room. 36 panels are installed and secured with steel wires and a metal fence.

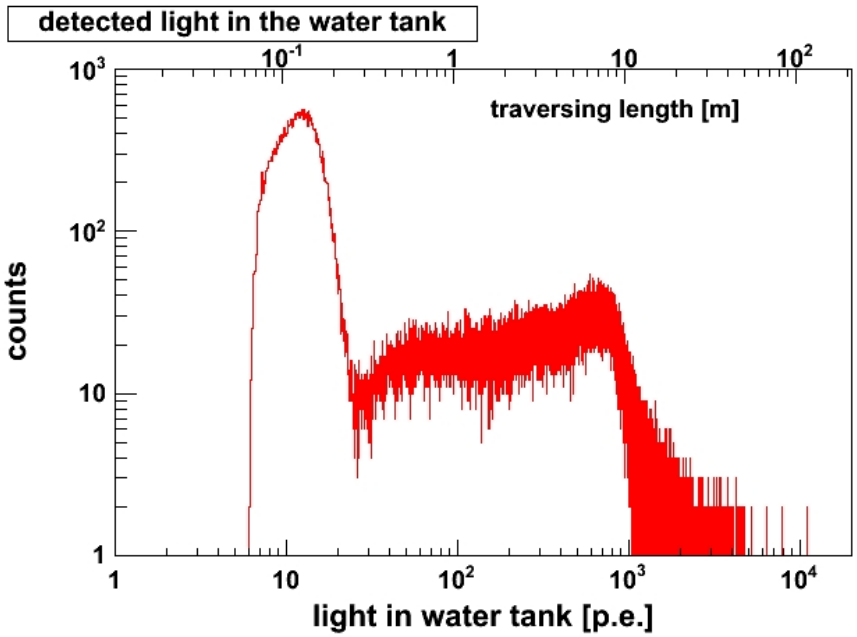

Figure 7: Cherenkov light detection in the water tank.

detector. Convection effects were not included.

The results from the measurements are

- The count rate increases with negative voltage on the encapsulation and decreases for positive voltages. This means that ^{42}K are practically all positively charged after the β decay of ^{42}Ar. Fig. 8 shows for example the 1525 keV count rate for the spiked and natural argon as a function of the applied negative voltage on the encapsulation. The trend is very similar and the count rates differ by a factor of $\approx$40.

- When the voltage was modified, the count rate changed exponentially with a time constant consistent with the half life of ^{42}K. This means that the drift time, i.e. the time until the ion is neutralized, is small compared to the half life.

- The count rate at a given voltage increases slowly with time as shown in Fig. 9. This can be explained by a "self-cleaning" due to the electric field. The concentration of electro-negative impurities reduces with time.

- During irradiation, i.e. when ions are produced, the neutralization time is reduced. The 1525 keV count rate is lower.

- For an assumed drift velocity of ^{42}K ions of $6 \cdot 10^{-4}$ cm^2/V·s [8] the observed count rates at different encapsulation voltages are still not fully explained by the model. The best approximation of the time before neutralization gives about 15 minutes. In this case only 2% of the ^{42}K atoms will be charged at a given time. A similar study for GERDA yields about 20 minutes neutralization time.

6 Phase II

In the second phase, GERDA aims at a background which is a factor of 10 lower than the one of Phase I. We plan to achieve this with two additional measures. The $0\nu\beta\beta$ events normally deposit energy only at one location inside a detector (single-site event, SSE) while the majority of backgrounds will deposit energy also in the liquid argon and/or will scatter at several locations in a diode (multi-site events, MSE). The former creates scintillation light which can be detected. The latter can be identified by an analysis of the shape of detector current pulses (pulse shape discrimination, PSD). Surface events have also normally characteristic pulse shapes and can be recognized.

Production of enriched BEGe detectors

Triggered by the PSD performance of point-contact detectors [9], GERDA has focused the detector R&D [10, 11, 12] on commercially available Broad Energy Germanium (BEGe) detectors from Canberra which exhibit similar field configurations and PSD performance. The production chain was tested earlier with material left over from the Ge enrichment.

In 2011, a contract was signed with Canberra for the production of about 25 enriched BEGe detectors with a total mass of approximately 20 kg. The process has started and

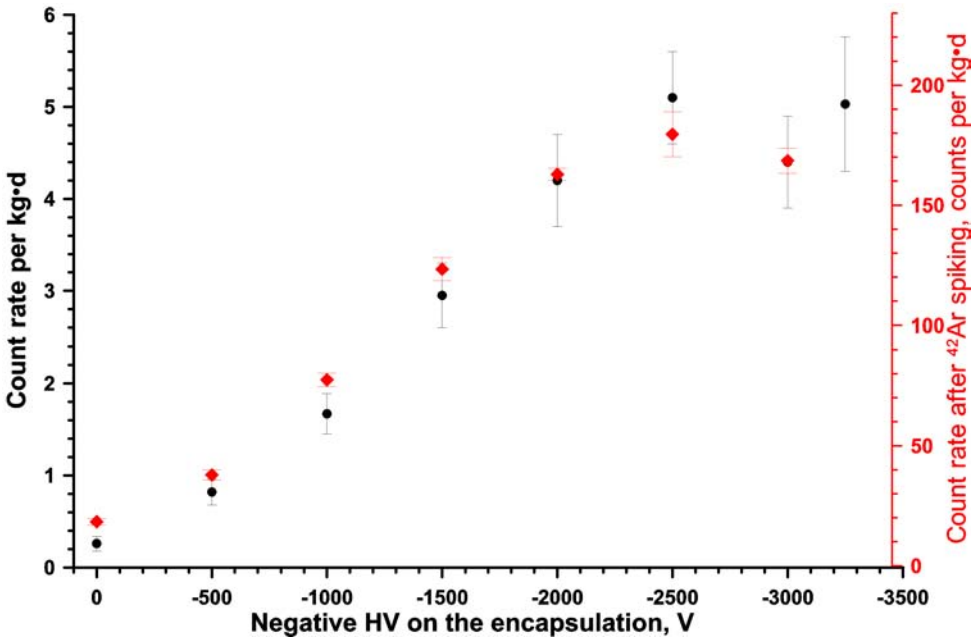

Figure 8: Count rate of the 1525 keV gamma line from ^{42}K decay for the spiked argon (red data points, right scale) and the natural argon (black points, left scale).

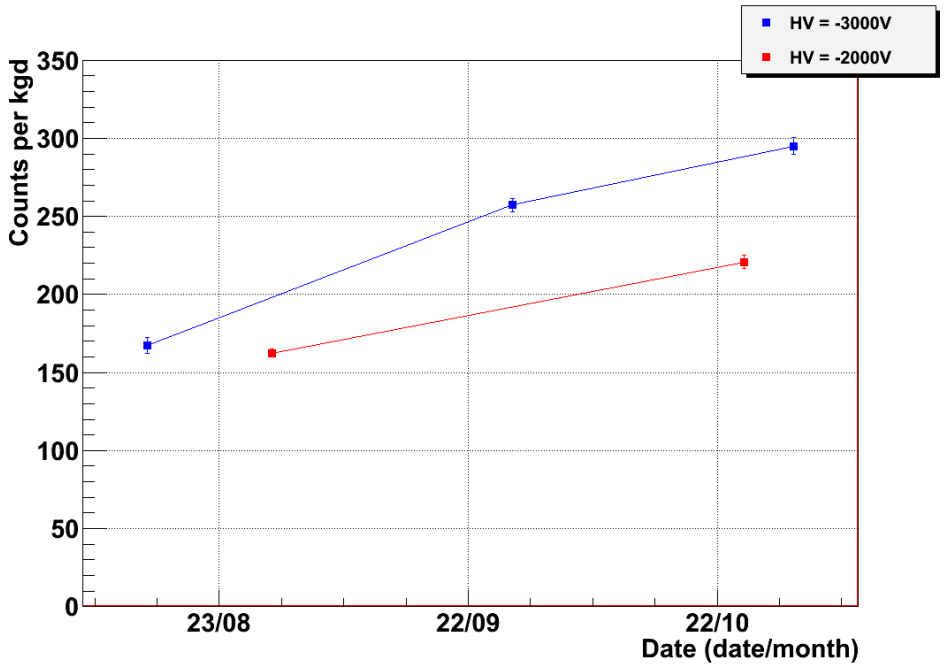

Figure 9: Rate of the 1525 keV gamma line for -2000 V (red points) and -3000 V on the encapsulation for different measurement times.

a first batch of detectors is available for characterization. The latter is done in standard vacuum cryostats with different sources (^{60}Co, ^{228}Th, ^{90}Sr, ^{133}Ba, ^{241}Am) to study energy resolution, dead layer thickness and PSD for bulk and surface events. A test stand was built to automatize this task to allow for a timely characterization. Everything is setup in the HADES underground facility, Belgium, close to Canberra. The goal is to know in detail the performance of every detector before its deployment in GERDA.

By the end of 2012 all detectors are expected to be delivered and tested.

R&D for light instrumentation

Several options are considered for the read-out of the liquid argon scintillation light. The standard method already investigated with LARGE uses PMTs. Two types have been purchased from Hamamatsu: the 3" model R11065-10 and the 8" model R5912-02. The full characterization in LAr and radio-purity measurements are ongoing.

For the PMT solution a reflective foil (VM2000) covered with a wavelength shifter (Tetra Phenyl Butadiene) defines the volume of light collection. One alternative is the use of wavelength shifting fibers instead. The fibers are sensitive to scintillation light from all sides and guide the shifted light to silicon photo-multipliers (SiPMs). Also for this option different fibers and SiPMs are available and characterization is in progress.

As a third option R&D on large area avalanche photo diodes or SiPMs without reflector or wavelength shifter has started. These devices would be mounted close to the Ge diodes.

Read-out electronics

The background goal for Phase II requires the full use of pulse shape discrimination of BEGe detectors. With the electronics used in Phase I this can only partially be achieved.

Therefore a completely different design called GeFRO is pursued [14]. At the detector, the input JFET and - in the feedback loop - a Schottky diode are mounted. Two long lines (coaxial cables or twisted pairs) connect to the rest of the amplifier which is outside of the cryostat. No other feedback components are needed close to the detector and the signal amplitude and rise time does not depend on the cable length. First tests with a coaxial detector and a BEGe detector show reasonable energy resolution but final performance numbers with an optimized setup and radiopure components are pending.

7 Summary

In fall 2011, Phase I data taking has started. The background reached is approximately $17{\cdot}10^{-3}$ cts/(keV·kg·y) which is about a factor of 10 lower than for previous experiments and close to the design goal of $10{\cdot}10^{-3}$ cts/(keV·kg·y). Currently, events in the window of ± 20 keV around $Q_{\beta\beta}$ are removed from the analysis to avoid any bias in the data selection. The sensitivity will be $1.5 \cdot 10^{25}$ years for $T^{0\nu}_{1/2}$ after one year of data taking. It is foreseen to implement some of the first produced Phase II BEGe detectors in spring 2012 and depending on their performance the sensitivity will reach $2 \cdot 10^{25}$ years beginning of 2013 which is practically the goal for Phase I [1].

In LArGe, the study of the ^{42}K background continued by spiking the liquid argon with a known activity of ^{42}Ar. The count rate of the 1525 keV gamma line increased by a factor of about 40 compared to the one for natural argon. Applying different voltages on the encapsulation of a germanium detector allowed to estimate the time before neutralization of the ^{42}K ions of 15 minutes which is small compared to the half life of 12 hours.

The production of Phase II BEGe detectors has started. A new version of the readout electronics which allows to place only radiopure components close to the detectors and to transmit the signal over a long distance has been proposed and first tests are promising. For the liquid argon instrumentation several options are under consideration. All hardware will be ready in 2013 for a timely start of Phase II.

8 List of Gerda related publications in 2011

1. M. Agostini, L. Pandola, P. Zavarise and O. Volynets, *GELATIO: a general framework for modular digital analysis of high-purity Ge detector signals*, JINST 6 (2011) P08013.

2. M. Agostini, E. Bellotti, R. Brugnera, C.M. Cattadori, A. D'Andragora, A. di Vacri, A. Garfagnini, M. Laubenstein, L. Pandola and C.A. Ur, *Characterization of a broad energy germanium detector and application to neutrinoless double beta decay search in ^{76}Ge*, JINST 6 (2011) P04005.

3. M. Agostini, C. A. Ur, D. Budjas, E. Bellotti, R. Brugnera, C. M. Cattadori, A. di Vacri, A Garfagnini, L. Pandola and S. Schönert, *Signal modeling of high-purity Ge detectors with a small readout electrode and application to neutrinoless double beta decay search in ^{76}Ge*, JINST 6 (2011) P03005.

4. I. Abt, A. Caldwell, J. Liu, B. Majorovits, O. Volynets, *Measurement of the temperature dependence of pulse lengths in an n-type germanium detector*, Eur. Phys. J. Appl. Phys. 56 (2011) 10104.

5. B. Majorovits, I. Abt, M. Laubenstein, O. Volynets, *Aluminum as a source of background in low background experiments*, Nucl.Instrum.Meth. A647 (2011) 39-45.

6. C. Cattadori, B. Gallese, A. Giachero, C. Gotti, M. Maino, G. Pessina, *A new approach to the front-end readout of cryogenic ionization detectors*, JINST 6 (2011) P05006.

References

[1] Letter of Intent, 2004, hep-ex/04040390; Proposal to the Lngs, 2004, http://www.mpi-hd.mpg.de/gerda

[2] http://www.mpi-hd.mpg.de/gerda/reportsLNGS/progress-reports.html

[3] H.V. Klapdor-Kleingrothaus et al., Nucl. Instr. Meth. A 522 (2004) 371

[4] O. Chkvorets, "Search for double beta decay with HPGe detectors at the Gran Sasso underground laboratory", Ph. D. thesis, 2008, http://www.ub.uni-heidelberg.de/archiv/8572

[5] P. Benetti et al., Nucl. Instr. Meth. A 574 (2007) 83

[6] M. Barnabé Heider, "Performance and stability tests of bare high purity germanium detectors in liquid argon for the GERDA experiment", Ph. D. thesis, 2009, http://www.ub.uni-heidelberg.de/archiv/9551

[7] C. Dörr and H.V. Klapdor-Kleingrothaus, Nucl. Instr. Meth. A 513 (2003) 596

[8] B.L. Henson, Phys. Rev. 135 (1964) A1002

[9] P.S. Barbeau et al, 2007 JCAP 0709 P009.

[10] D. Budjáš et al., JINST 4 (2009) P10007, arXiv:0909.4044.

[11] M. Barnabé Heider et al., JINST 5 (2010) P10007.

[12] M. Agostini et al., JINST 6 (2011) P03005, arXiv:1012.4300.

[13] F. Ritter, "Analysis of the Gerda muon veto - first light", PhD Thesis, Universität Tübingen, 2012.

[14] C. Cattadori et al, JINST 6 (2011) P05006.

The ICARUS Experiment

The ICARUS Collaboration

M. Antonello[a], P. Aprili[a], B. Baiboussinov[b], M. Baldo Ceolin[b,†], P. Benetti[c], E. Calligarich[c], N. Canci[a], S. Centro[b], A. Cesana[e], K. Cieślik[f], D.B. Cline[g], A.G. Cocco[d], A. Dabrowska[f], D. Dequal[b], A. Dermenev[h], R. Dolfini[c], C. Farnese[b], A. Fava[b], A. Ferrari[i], G. Fiorillo[d], D. Gibin[b], A. Gigli Berzolari[c,†], S. Gninenko[h], A. Guglielmi[b], M. Haranczyk[f], J. Holeczek[m], M. Kirsanov[h], J. Kisiel[m], I. Kochanek[m], J. Lagoda[l], S. Mania[m], G. Mannocchi[n], A. Menegolli[c], G. Meng[b], C. Montanari[c], S. Otwinowski[g], T.J. Palczewski[l], L. Periale[n], P. Picchi[n], F. Pietropaolo[b], P. Plonski[o], P. Przewłocki[l], A. Rappoldi[c], G.L. Raselli[c], M. Rossella[c], C. Rubbia[1,a,i], P. Sala[e], E. Scantamburlo[q], A. Scaramelli[e], E. Segreto[a], F. Sergiampietri[p], D. Stefan[a], J. Stepaniak[l], R. Sulej[a,l], M. Szarska[f], M. Terrani[e], F. Varanini[b], S. Ventura[b], C. Vignoli[a], H.G. Wang[g], X. Yang[g], A. Zalewska[f], K. Zaremba[o]

[a]INFN - Laboratori Nazionali del Gran Sasso, Assergi, Italy
[b]Università di Padova e INFN, Padova, Italy
[c]Università di Pavia e INFN, Pavia, Italy
[d]Università Federico II di Napoli e INFN, Napoli, Italy
[e]Politecnico di Milano e INFN, Milano, Italy
[f]H.Niewodniczański Institute of Nuclear Physics, Kraków, Poland
[g]Department of Physics, UCLA, Los Angeles, USA
[h]Institute for Nuclear Research of the Russian Academy of Sciences, Moscow, Russia
[i]CERN, Geneva, Switzerland
[l]Nuclear Center for Nuclear Research, Warszawa, Poland
[m]Institute of Physics, University of Silesia, Katowice, Poland
[n]INFN Laboratori Nazionali di Frascati, Frascati, Italy
[o]Institute for Radioelectronics, Warsaw Univ. of Technology, Warsaw, Poland
[p]Università di Pisa e INFN, Pisa, Italy
[q]Università dell'Aquila, L'Aquila, Italy

Abstract

The idea of a Liquid Argon Time Projection Chamber (LAr-TPC), proposed in 1977 by C. Rubbia [1], finally resulted in the construction of a detector of 600 tons of LAr with excellent spatial resolution and 3D imaging capabilities, allowing for an unprecedented event visualization quality combined with a good calorimetric reconstruction and the electronic event processing. The ICARUS T600 detector is smoothly running in HALL B since May 2010. The ICARUS experiment is focused on neutrino oscillation search and in particular on $\nu_\mu \rightarrow \nu_\tau$ oscillation search in

[1]Spokesman of the ICARUS Collaboration

appearance from the CNGS neutrino beam. It will also be searching for rare events up to now unobserved like the long sought for proton decay with zero background in one of its 3×10^{32} nucleons (in particular into exotic channels).

1 ICARUS T600 detector

The detector consists of a large cryostat split into two identical, adjacent half- modules with internal dimensions $3.6 \times 3.9 \times 19.6$ m^3 and filled with a total of 760 tons of ultra-pure LAr. Each half-module houses two TPCs separated by a common cathode, with a drift length of 1.5 m. Ionization electrons, produced by charged particles along their path, are drifted under uniform electric field ($E_D = 500V/cm$) towards the TPC anode made of three parallel wire planes, facing the drift volume. A total of 54000 wires are deployed, with a 3 mm pitch, oriented on each plane at different angles (0^0, $+60^0$, -60^0) with respect to the horizontal direction. The drift time of each ionization charge signal, combined with the electron drift velocity information ($v_D = 1.55mm/\mu s$), provides the position of the track along the drift coordinate. Combining the wire coordinate on each plane at a given drift time, a three-dimensional image of the ionizing event can be reconstructed with a remarkable resolution of about $1mm^3$. The absolute time of the ionizing event is provided by the prompt ultra-violet scintillation light emitted in LAr and detected through an array of 74 Photo Multiplier Tubes (PMTs), installed in LAr behind the wire planes. The detector layout is completed by a cryogenic plant made of a liquid Nitrogen cooling circuit and a system of LAr purifiers.

The commissioning in underground at LNGS of the ICARUS T600 detector has been successfully performed in the course of 2010 [3]. During 2011 the ICARUS experiment has been taking data smoothly on the CNGS neutrino beam with very high detector live-time, thanks to improvements on both cryogenics plant and DAQ systems. New electronics for PMT trigger system is under installation after exhaustive tests. Online data quality survey is active and automatic filtering procedure is applied to both CNSG and cosmic events. The CNGS neutrino spectrum, obtained from the combination of muon momentum and calorimetric energy, has been reconstructed and found in agreement with the predictions. Muons, from neutrino interactions in upstream rock, have also been measured in agreement with expectations. The analysis tools to fully reconstruct the neutrino interactions are applied, as shown in few examples, to a 2010 data sample in order to be tuned and optimized for the global data analysis.

2 Cryogenics and LAr purity

The whole T600 cryogenic plant has been operating for almost 2 years since the commissioning completion (Spring 2010) [4]. It has demonstrated to be safe, reliable and functional. In particular the cryogenic plant continuous operation and its performance guaranteed high thermal stability, high LAr thermal uniformity (within 1 K), high argon purity with no dead time at all for the detector.

The evolution of the residual impurity concentration in LAr, key issue for the detector operation, is continuously measured directly by the charge signal attenuation in Collection

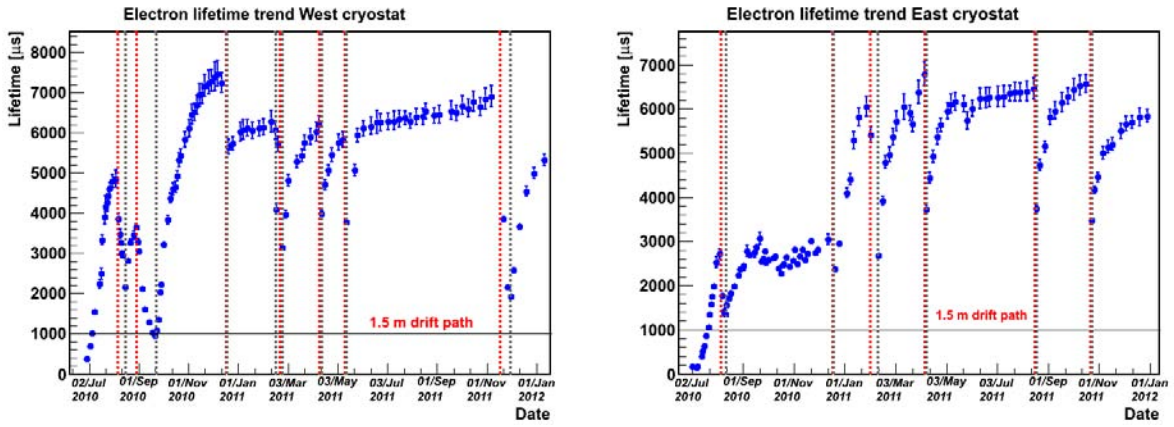

Figure 1: *Time evolution of the free electron lifetime in the West (left) and East (right) cryostats. For details see the text.*

view along through-going clean muon tracks. The electron lifetime is constantly above 6 ms in both cryostats, when the liquid recirculation system is active at a rate of $2m^3/hour$ (Figure 1). This corresponds to a maximum free electron yield attenuation of 14 %, at the maximum drift distance of 1.5 m.

During 2011 several important upgrades of the cryogenic plant and control/supervision system were implemented. The most relevant upgrade, the so called emergency cooling in termosiphon mode, was completed at the end of May 2011. It consists in the implementation of the gravity-driven nitrogen LN2 cooling circuit in order to keep cold the argon mass even during emergency situations such as total lack of power supply in the tunnel. A campaign of tests was carried on and the whole plant was tested simulating an emergency condition in order to verify the final global performance of the new development and certify all the implemented solutions and conclude the cryogenic plant upgrade phase.

A pneumatic control panel to open/close/regulate valves in case of total lack of control system (PLC system fault, total electrical power lack) was added, and tested, in order to operate cryostat termosiphon nitrogen cooling in very extreme conditions . An adequate programming logic of the PLC logic allows to run the automatic start on a predefined LN2 storage tank (the tank that is working in automatic mode) procedure of the emergency cooling in case of stop of the cooling pumps or failure of critical control nodes.

3 Trigger System

The trigger system relies on the scintillation light signals provided by the internal PMTs and on the SPS proton extraction time for the CNGS beam. The set-up is based on a controller crate, hosting a FPGA-board for signals processing, which can handle different trigger sources. It provides also the absolute time stamp for the recorded events and the opening of the CNGS proton spill gate. For each CNGS cycle an "early warning" packet is sent from CERN 80 ms before the first proton spill extraction, allowing the opening of

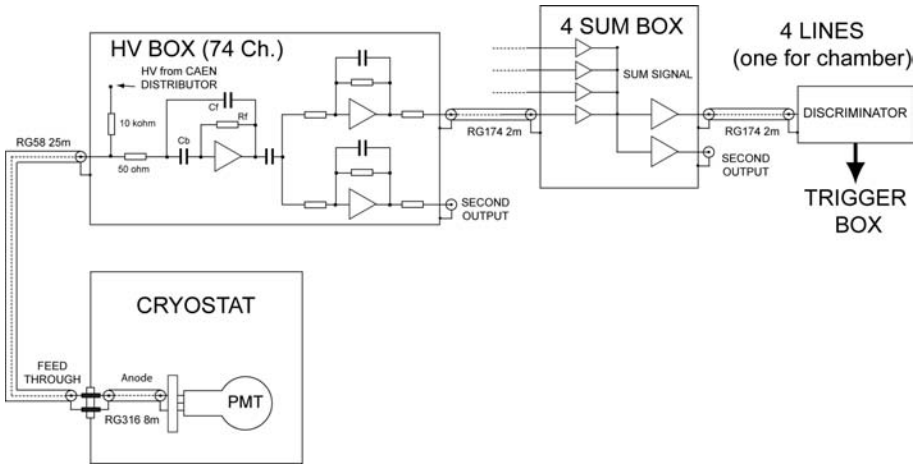

Figure 2: *The scheme of the new electronics for the PMT signal processing.*

two ~ 60 μs gates in correspondence to the predicted extraction times. The timing inside the controller is realized by a 40 MHz counter, reset every ms by a synchronization signal containing absolute time information, generated by the master clock unit of the LNGS external Laboratories (GPS unit and 10 MHz atomic clock) synchronized to CERN SPS accelerator clock. The sum signal of the PMTs behind each chamber is discriminated at ~ 85 phe to provide 4 independent trigger pulses. The CNGS-type trigger is generated when a PMT trigger pulse is present within the CNGS gate. About 80 events per day are recorded with a trigger rate of 1 mHz well distributed inside the 10.5 μs width of the two proton-spills. The trigger for cosmic events requires a low discrimination threshold to maximize the low energy event detection. An efficient reduction of the spurious signals is provided exploiting the coincidence of the PMTs sum signals of the two adjacent chambers in the same module, relying on the 50 % cathode transparency. A trigger rate of about 18 mHz per cryostat is achieved leading to about 100 cosmic events per hour collected on the full T600 (only 6 % of the events are classified as empty by a visual scanning), to be compared with the 160 events/hours predicted by Monte Carlo. In order to increase the trigger efficiency to cosmic events, the PMT HV biasing system has been re-designed (Figure 2). In each PMT channel a custom-made low-noise integrating preamplifier is adopted; this allows the PMT light integration over a time constant of at least 10 μs, thus exploiting also the slow component light signals. An external active signal adder is adopted for the signal sum. The new system has been successfully tested during the shutdown periods of the CNGS beam. The final installation has been accomplished after the CNGS beam stop. In addition to the PMT based trigger, a new algorithm (DR-slw) to detect the local Region of Interest (ROI) of each event, avoiding the full acquisition of the detector, was implemented in a new chip called SuperDaedalus [5], in order to perform a trigger based on local charge deposition. The new unit is a large piggy-back board holding a single large FPGA. Distilling the waveform signals on each wire, the DR-slw algorithm can discriminate the single hit signals which are used to perform majority logic over 16 adjacent wires in view of the ROI recognition. On each 32 wire board a Global-Trigger-Out signal (GTO) is produced if at least one of the two majority signals

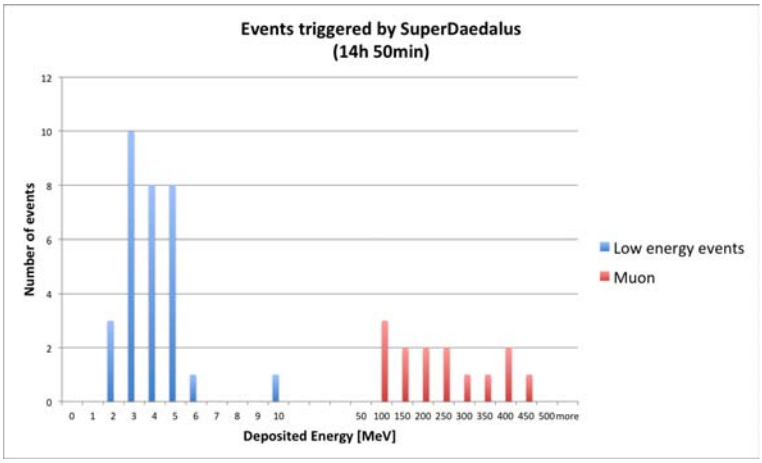

Figure 3: *Energy spectrum of recorded events triggered with the Super Daedalus chip requiring Majority = 6/16 adjacent wires signal.*

has fired. One logical board is hosted in each single crate handling the GTO signals from the 18 read-out boards (9 for Collection plus 9 for Induction view) to perform a further majority level in view of a trigger signal generation.

A preliminary test has been carried during 2011 with 18 SuperDaedalus chips, installed in adjacent boards of Collection and Induction views. The energy spectrum of the events acquired using the SuperDaedalus chip demonstrates the capability of triggering on extremely low energy events, well separated from the crossing muon tracks (Figure 3). In the meantime, the proposed DR-slw algorithm has been tested in the software version as second level trigger in order to select the CNGS events triggered only with the CNGS early warning signal. Analysis performed on the 2010 CNGS data taken with the PMTs based trigger, showed a full detection efficiency of DR-slw algorithm for both neutrinos and muons, with an empty event rejection exceeding a factor 1000, if at least 6 fired boards are required with a majority=12/16.

A direct test of this new trigger was performed in March 2011 with the CNGS beam active, triggering on the beam spill and filtering in parallel the recorded events. The online software algorithm selected only 14 events over the full sample of 5300 triggered spills, requiring 6 fired boards in Collection view, corresponding to $\sim$ 8 hours of run. A visual scan of the selected data showed 13 genuine CNGS events, i.e. 5 neutrino interactions and 8 muons from neutrino interactions in the rock, with the only empty event due to a residual cross-talk noise in the TPC chambers. Since 3^{th} May more than $1.6 \cdot 10^6$ spill events corresponding to $2.4 \cdot 10^{19}$ pot were filtered out with a real-time fake event rejection at the level of 10^4. As a result 8 events no detected by PMT (7 short m from CNGS neutrinos interactions in the rock plus a cosmic m) were find in a subsample of $4.3 \cdot 10^5$ spill.

After the successful preliminary tests, the SuperDaedalus second-level trigger was put in production at the end of April 2011 and, in December 2011, 716 ROI processors have been installed covering all the Collection boards, ready for the beam re-start.

4 DAQ System

In the present detector configuration, 91 CPUs are used for data read out: 90 for wires (one for each crate of 572 wires) and 1 for the 74 PMTs. Preliminary tests showed an event building time of about 5 s using a single building machine ($\sim$ 1 s for a single chamber).

From October 1st to October 27th the DAQ system included the multi event buffer feature, with a total of 8 buffers, in addition to a 1 s veto to avoid triggering on PMT noise. DAQ and trigger introduce an overall 7% dead time.

Since October 27th a new system, including a direct communication between the trigger management and the DAQ has been installed, tested and has been running steadily. Using this new feature the overall dead time has been reduced to a value compatible with 0.

Before the 2011 data taking, in order to improve the maximum trigger rate sustainable by the DAQ system, a splitting of the building procedure into four parallel streams has been implemented. In this way, every wire chamber data stream is collected by a different writer machine. Therefore for every event four files, one for each chamber, will be written separately. An asynchronous process running on additional writer machine is used to recombine the four different streams on a single file, after checking data quality and time stamp compatibility.

Moreover, introducing a small delay in the data collection ($\sim$ 100 ms for every 10 CPUs) avoids the congestion of the network tree, thus reducing the packet loss and improving the building speed. With these upgrades, the maximum sustainable building rate, without dead time, raised to a value of about 0.7 Hz for the whole detector, with a full-drift recording ; this value is necessary when the trigger on CNGS spill is enabled, since the average trigger rate could reach up to 0.33 Hz.

In order not to lose any CNGS related event, a multi-level veto logic has been introduced, reserving a higher priority to CNGS candidate events over cosmic rays. Among the 8 buffers available for the multi-events buffer features, the first 5 are used for all trigger types, other 2 are reserved for events triggered by the CNGS timing signal (with no PMT signal) and the last buffer is reserved for trigger of PMT in coincidence with the CNGS timing information. The dead time for the atmospheric events is $\sim$ 0.5%, the number of trigger on spill missed is $\sim$ 0.1% and up to now no trigger of PMT inside CNGS gate has been lost.

5 2011 Run data taking and filtering CNGS events

The CNGS beam restarted on March 19th 2011: the smoothly data taking operations allowed to collect an event statistics corresponding to 4.44×10^{19} pot over the 4.78×10^{19} pot delivered by CERN up to November 14th, with detector live-time of 93 % for CNGS exploitation (Figure 4).

All the CNGS events triggered by the neutrino-beam spill, whether or not in coincidence with a PMT signal, are processed offline by the DR-slw filter to separate genuine CNGS events and to identify also the few neutrino interactions/rock muons that may escape the PMT based trigger.

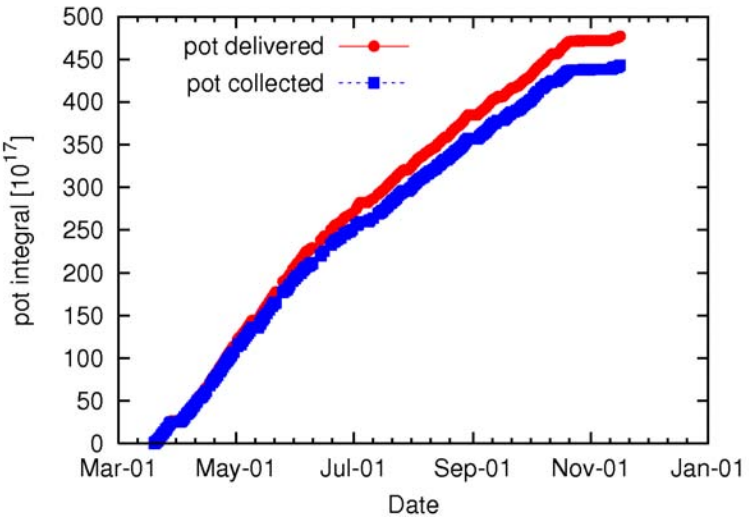

Figure 4: . *Integrated proton on target delivered to CNGS in the 2011 campaign (red), starting March 19th 2011. The beam intensity recorded by T600 is also shown (blue).*

Cosmic events, or in general events out of the CNGS spill, whose acquisition is triggered by the coincidence of PMT signals in two adjacent chambers, are also filtered in order to select physical events for further analysis from fake empty triggers. A filtering procedure validated on visually scanned data is applied offline immediately after recording. The output of the visual scan has been used to validate the automatic algorithm for event pre-selection and noise rejection, obtaining 99% efficiency with a rejection of empty events at the 10^{-3} level.

6 CNGS neutrino interactions collected in 2011

The first 1.06×10^{19} pot event sample has been filtered, visually scanned and measured resulting in 360 neutrino interactions inside the active detector volume. The fiducial target mass taken into account is 447 t, obtained from the instrumented active volume ($17.9 \times 3.1 \times 1.5 m^3$ for each TPC chamber) subtracting 5 cm upstream and 15 downstream along the longitudinal direction and 3 cm laterally from the borders. The number of CC / NC interactions foreseen per pot is $2.6 \times 10^{-17} / 0.86 \times 10^{-17}$, in the energy range up to 100 GeV. The expected number of interactions after corrections for 2% early warning packet loss and 1.57% geometrical inefficency of the detector (due to front-end electronics fault) is shown in Table 1. Thanks to the segmented detector DAQ the resulting dead time is negligible, consistent with 0. The results of the scan are in good agreement with expectations.

Event Type	Collected	Expected
νCC	247	273
νNC	71	90
νXC	37	-
Total	355	363

Table 1: *Number of collected neutrino interactions compared with predictions, in the energy range up to 100 GeV. In ν XC interaction type additional analysis is needed for the classification CC vs NC since the events were too close to the sides to identify a penetrating m.i.p. particle as a muon.*

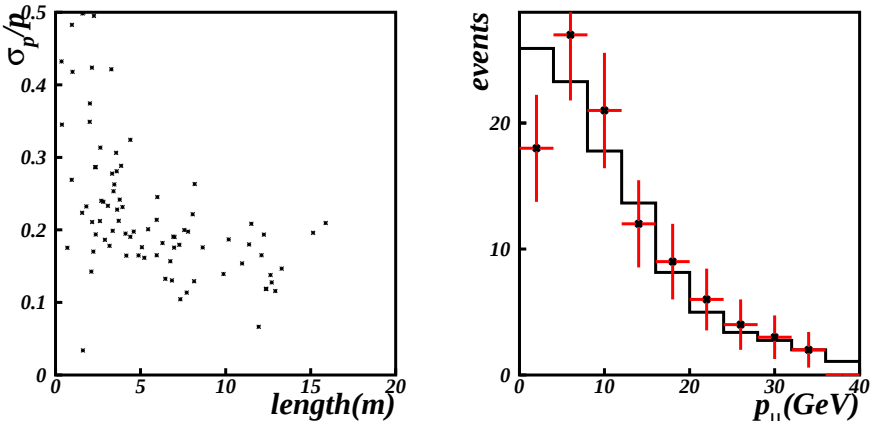

Figure 5: *Application of the multiple scattering reconstruction to CNGS events. Left: momentum resolution as a function of track length. Right: reconstructed momentum (dots with error bars) compared with the Monte Carlo expectations.*

7 Events reconstruction and analysis

During 2011 the analysis of the events collected in 2010 has been carried on. This data sample is being used as a training sample to tune the reconstruction, to check calibration and optimize the analysis tools with the aim to address in particular the main items of physics with CNGS beam, namely tau neutrino and ν_e CC identification/measurement and NC rejection performance. In the study of the Charged-Current event sample from CNGS ν_μ interactions, the momentum of muons generated in CC interactions is measured exploiting the multiple scattering along the track. The implemented algorithm is based on the Kalman filter technique. The expected momentum resolution $\Delta p/p$ depends mainly on track length: on μs from CNGS neutrinos $\Delta p/p \sim 16\%$ on average.

The application of the multiple scattering method to the 2010 data is shown in Figure 5, where the reconstructed momentum distribution is compared with the Monte Carlo predictions for CNGS ν_μ CC events. The average reconstructed momentum is $11.0 \pm 1.8 GeV/c$ in agreement with the expected value of $10.7 GeV/c$.

Besides the muon, charged particle tracks are reconstructed in two-dimensional pro-

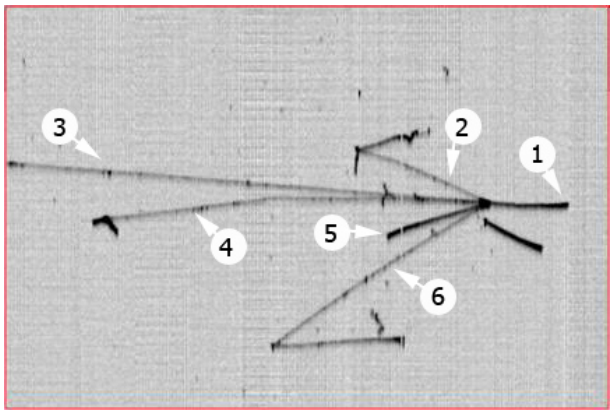

Figure 6: *Example of stopping particle identification in a CNGS ν_μ CC event. Track n. 8 is a pion, the other numbered tracks are identified as protons.*

jections with the polygonal line algorithm, and combined into 3D tracks. Corrections to recover the ionization quenching are applied to reconstruct the particle energy loss. Particle identification is performed by means of two independent measurements: a) reconstruction of dQ/dx versus track residual range; b) decay products charge deposition. Both are optimally exploited with the application of neural network based method and dedicated Bayesian optimization technique. An example of stopping particle identification is shown in Figure 6.

Identified stopping particles are also being used as check of the absolute calibration of the detector. This work is still ongoing.

The expected capabilities of the detector to distinguish between electron showers and neutral pion decays are also being tested. All the ingredients are indeed present in the observed events. The statistics is too low to produce distributions, but all the reconstructed invariant masses agree with the pion one within errors, except for a very nice example of η decay (reconstructed mass is $512 \pm 48 MeV$). Conversion distances range from few centimeters to about 80 cm, and the initial ionization is always consistent with two m.i.p.s. An example with two π^0 is shown in Figure 7.

In the 2010 analyzed sample it was possible to identify ν_e CC candidates as the one shown in Figure 8. This event has 45 GeV total energy with an e.m. shower at the vertex of about 37 GeV, with a typical longitudinal profile roughly peaking at the expected position ($\sim 88 cm$).

The full 3D reconstruction of all particles in the events allows determining the neutrino momentum and the missing transverse momentum in the interaction, as already shown in the last report. As an alternative, a calorimetric reconstruction is also possible. The calorimetric reconstruction of the energy deposited in the detector by ν_μ CC events shows a nice agreement with expectations (Figure 9[Left]).

The deposited energy in each event is corrected for quenching on average, and a further correction for non-containment and non-compensation is applied. This correction has been computed from Monte Carlo simulations and depends on the vertex position in the detector. For CC events, the energy deposited by the muon is subtracted from

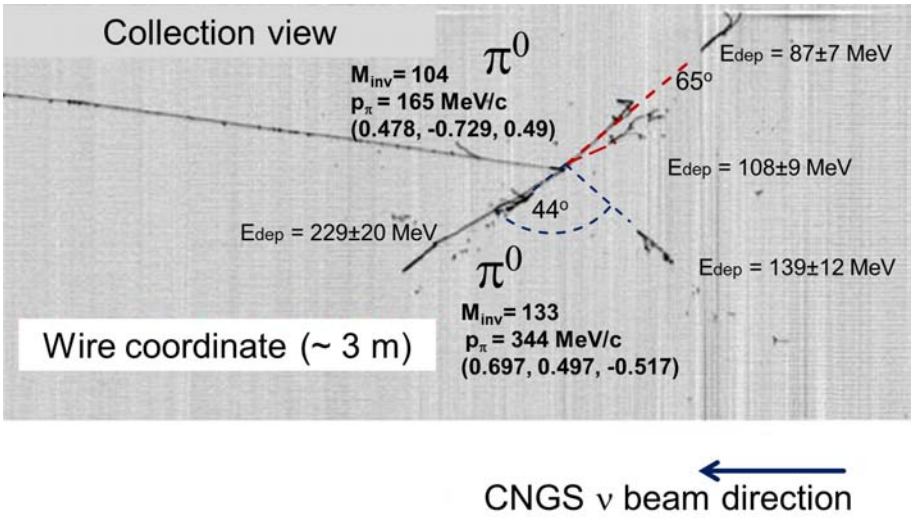

Figure 7: *Example of π^0 identification in a CNGS ν_μ CC event. The conversion distances are: 71.2 cm, 13.7 cm, 41.8 cm, 17.4 cm and the initial ionization are 5.1, 6.1, 3.1 and 4.4 MeV/cm*

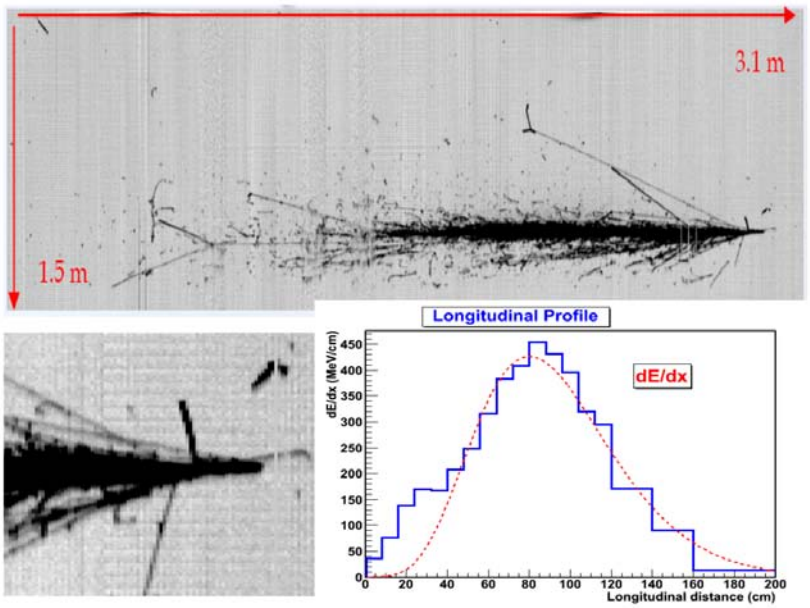

Figure 8: *A ν_e CC candidate in the analyzed 2010 sample: the collection view (top) and a close up view of the vertex (bottom left) together with the longitudinal profile of the electron candidate shower (bottom right).*

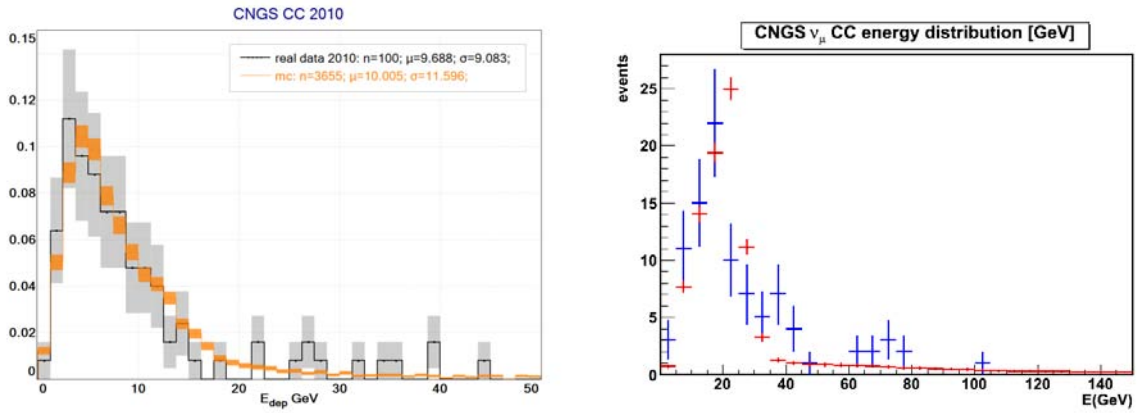

Figure 9: *CNGS ν_μ CC event sample from 2010 run. Left: Energy deposited inside the detector (calorimetric method, quenching corrected). Right: Neutrino energy spectrum reconstructed with the calorimetric method (blue), compared with MC expectations (red).*

the total, and muon momentum is anyhow reconstructed by multiple scattering. As a first check, the raw energy distribution, after the quenching correction only, has been successfully compared with the expected one.

The reconstructed neutrino spectrum, obtained from the combination of muon momentum and calorimetric energy, is shown in preliminary version in Figure 9 [Right]. The agreement with the predicted ν_μ spectrum is satisfactory.

The muons coming from CNGS beam interactions in the Gran Sasso rock can be used to extract information about the high energy tail of the CNGS beam and as a general monitoring tool. During the visual scanning of 2010 data, such "muon from the rock" events were identified and flagged. For a fraction of these events, the track direction has been reconstructed and compared with expectation.

The CNGS beam reaches the LNGS coming from below the horizon, direction upwards with a nominal inclination of 3.26^o (or 86.74^o if expressed with respect to the zenith), and is practically aligned with the LNGS hall axis in the other directions.

The angle with respect to the vertical direction of the 156 selected muons is shown in Figure 10. The reconstructed average is 86.3 ± 0.3 degrees, in fair agreement with expectation. The azimuthal direction, computed assuming $\Phi = 0$ for the tracks directed along the north-south axis of the hall, is also in Figure 10. The average measured azimuth is compatible with zero, as expected.

The deviation of muons from the original beam direction, due to the momentum transfer in the interaction and to multiple scattering in the rock, is visible in Figure 11. This plot has been obtained transforming the muon direction into the nominal CNGS reference frame. Simulated events are shown for comparison. Despite the small statistics, there is a fair agreement between data and simulation.

As previously mentioned, cosmic events have been identified by means of an automatic identification and reconstruction procedure. The region of the detector containing the events is identified (only in the Collection view at the moment) and the deposited energy is estimated taking into account the electron lifetime and quenching corrections.

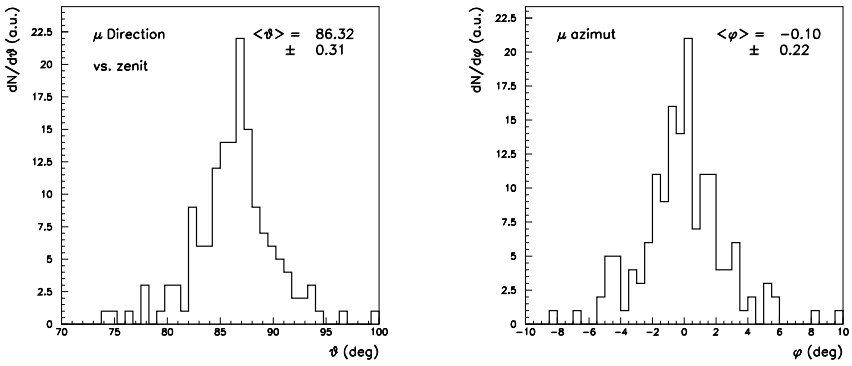

Figure 10: *Zenital and azimuthal distribution of muons from CNGS interactions in the LNGS rock.*

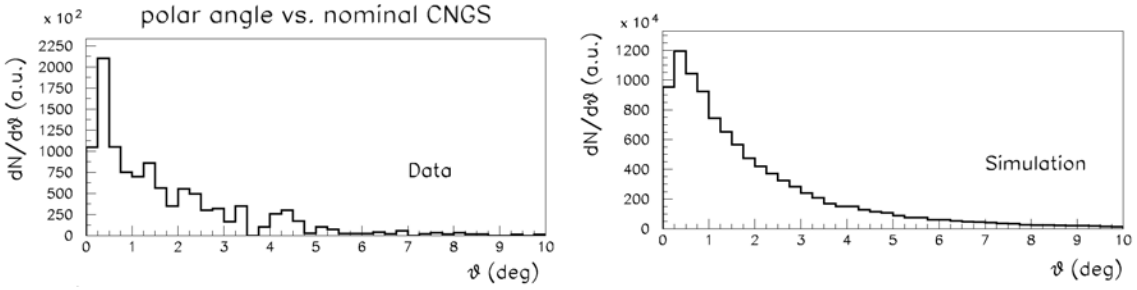

Figure 11: *Muons from CNGS interactions in the rock: angle θ between the track in the detector and the beam for collected events (left) and simulation (right).*

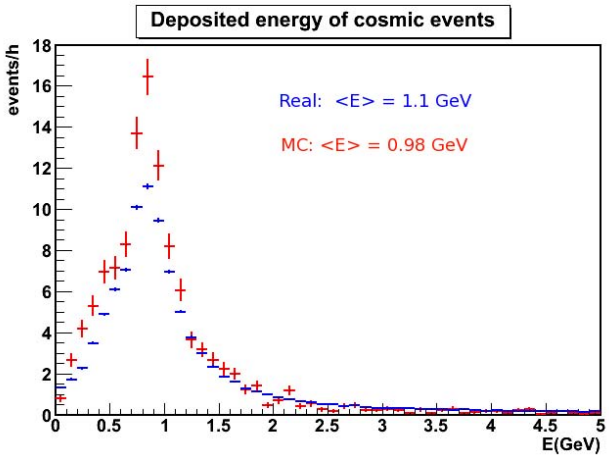

Figure 12: *Calorimetric measurement of the energy deposition by cosmic rays in the detector as determined by an automatic reconstruction (data points in blue, MC prediction in red).*

The results compare well with the Monte Carlo predictions for the spectrum of the energy deposition by cosmic muons, as shown in Figure 12. Simulations include an energy dependent correction to account for the trigger efficiency.

As shown in the previous examples the analysis tools to measure and fully reconstruct the events are working satisfactorily both for the detailed identification and measurement of all secondary particles from the neutrino interactions, for the reconstruction in the transverse plane and for a calorimetric like reconstruction.

8 Setup for the neutrino velocity measurement

In order to participate to the campaign of measurement on the neutrino time of flight, with the CNGS beam in bunched mode, the ICARUS T600 PMT readout system, used in general as primary trigger source, has been equipped with a DAQ system similar to the one of the WArP Dark Matter experiment, based on three *2-channel, 8-bit, 1-GHz AGILENT AC240* digitizer boards, with variable dynamics ranging from 50 mV to 1 V.

Similarly to the ICARUS LAr-TPC charge readout, in the new PMT-DAQ the signals are continuously read out and stored in a circular memory buffer (with a depth of 8 KB/channel corresponding to 8 μs time interval, sampling at 1 GHz). When a trigger occurs, additional data are readout and stored in second local memory buffer until the required time interval is fully readout (1400 μs in the ICARUS case corresponding to 1400 MB/channel). The content of both buffers is then send to data storage.

The signals from all PMTs behind each of the four wire chambers are summed together and integrated with four fast CANBERRA 2005 preamplifiers. The four output signals are then recorded in the PMT-DAQ together with the absolute time signal distributed by the LNGS laboratory. The trigger to the AC240 boards is provided by the ICARUS Trigger Box, and is based on the discriminated PMT signals ($\sim$ 100 phe threshold), in coincidence with a 200 μs gate opened around the CNGS neutrino arrival time as predicted by the

CERN-SPS proton extraction Early Warning Signal, sent to LNGS through the internet about 80 ms in advance.

At present, the timing signal, distributed by the LNGS laboratory, consists of a TTL positive edge sent out every ms and followed, after 200 μs, by a pulsed structure whose logical states contain the information on the absolute time related to the first edge. This signal, generated in the external laboratory and sent to the underground hall via $\sim$ 8 km fiber optics, introduces a delay which has been accurately calibrated in the last week of December 2011.

The time interval between PMT and timing signals, measurable with few ns precision, allows the determination of the absolute time of the scintillation light pulse in the T600 detector.

The propagation of the scintillation light signals along the $\sim$ 44 m from the PMT to the AC240 boards has to be included, together with the transit time within the PMTs ($\sim$ 75 ns).

Propagation of the photons from the event to the PMT's is precisely calculated through the 3D reconstruction of the associated event in the T600 LAr-TPC.

With the new PMT-DAQ, the ICARUS T600 detector will be able to tag every CNGS event with a precise time stamp, also in case of normal beam operation. However due mainly to statistics limitation, the neutrino time of flight measurement will probably be efficiently performed during the bunched beam operation. This has been demonstrated in the November 2011 bunched beam operation, when ICARUS T600 recorded 7 events (4 muons from the upstream rock, 2 CC ν_μ e 1 NC ν events), well distributed over the four bunches. The recorded event sample is compatible with the 2.2×10^{16} pot delivered to CNGS.

The overall timing accuracy of neutrino interactions, provided by the upgraded DAQ of the ICARUS detector, is foreseen to be the better than 5 ns on an event-by-event basis. With the predicted single event resolution, the neutrino time of flight accuracy should be limited by the residual systematic errors due to the CERN-LNGS time link and the geodesic localization, even for a limited statistical sample.

For the 2012 CNGS run (both normal and bunched beam), when the upgrades of the GPS/time-link systems will be operational, it is planned to record into the ICARUS PMT-DAQ also the timing signals distributed by the new systems in parallel with the existing one, for a better definition of the absolute time. It is also planned to take advantage of the Borexino set-up (with contributions in the setting-up), by sending out a tag signal generated by the ICARUS trigger box, which will be also recorded in the ICARUS PMT-DAQ. The position of the upstream wall of the T600 detector will also be measured within the LNGS reference frame to calculate neutrino flight path, in collaboration with the other experiments (Borexino, LVD).

List of Publications

1. C. Rubbia et al., Underground operation of the ICARUS T600 LAr-TPC: first results. JINST 6 (2011) P07011. e-Print: arXiv:1106.0975 [hep-ex].

2. M. Antonello et al., A Search for the analogue to Cherenkov radiation by high energy neutrinos

at superluminal speeds in ICARUS. e-Print: arXiv:1110.3763 [hep-ex].

3. M. Antonello, 23rd International Workshop on Weak Interactions and Neutrinos Conference Proceeding. Submitted for publication.

4. A. Fava, XXV Rencontres de Physique de la Vallee d'Aoste Conference Proceeding. Submitted for publication.

5. G.L. Raselli, XXIII Rencontres de Blois Conference Proceeding. Submitted for publication.

6. J. Kisiel, 2nd International Workshop towards the Giant Liquid Argon Charge Imaging Experiment Conference Proceeding. Submitted for publication.

7. N. Canci, Technology and Instrumentation in Particle Physics (TIPP) 2011 Conference Proceeding. Submitted for publication.

8. D. Dequal, Technology and Instrumentation in Particle Physics (TIPP) 2011 Conference Proceeding. Submitted for publication.

9. F. Varanini, International Europhysics Conference on High Energy Physics (EPS-HEP) 2011 Conference Proceeding. Submitted for publication.

10. D. Stefan, XIII International Workshop on Neutrino Factories, Super beams and Beta beams Conference Proceeding. Submitted for publication.

11. A. Cocco, 32nd International Cosmic Ray Conference Conference Proceeding. Submitted for publication.

12. A. Menegolli, 12th International Conference on Topics in Astroparticle and Underground Physics Conference Proceeding. Submitted for publication.

13. I. Kochanek, XXXV International Conference of Theoretical Physics Conference Proceeding. Submitted for publication.

14. A. Fava, 13th ICATPP Conference Proceeding. Submitted for publication.

References

[1] C.Rubbia, CERN-EP/77-08 (1977).

[2] S. Amerio et al., Nucl. Instr. Meth. **A527**, (2004) 329.

[3] C. Rubbia et al., JINST 6 (2011) P07011. e-Print: arXiv:1106.0975 [hep-ex].

[4] M. Antonello et al., Contribution to the "L.N.G.S. Annual Report 2010", June 2011, p. 107.

[5] B. Baibussinov et al., JINST **5**, (2010), 12006.

LUNA: Laboratory for Underground Nuclear Astrophysics

M. Aliotta[a], M. Anders[b], D. Bemmerer[b], A. Bellini[c], C. Broggini[d], A. Caciolli[d,e], P. Corvisiero[c], R. De Palo[d], A. Di Leva[f], Z. Elekes[b], A. Formicola[g], Zs. Fülöp[h], G. Gervino[i], A. Guglielmetti[j], C. Gustavino[k], Gy. Gyürky[h], G. Imbriani[f], M. Junker[g], R. Menegazzo[d], P. Prati[c], V. Roca[f], C. Rolfs[l], C. Rossi Alvarez[d], D. Scott[a], E. Somorjai[h], O. Straniero[m], F. Strieder[l], T. Szucs[h], F. Terrasi[n], H.P. Trautvetter[l], D. Trezzi[o]

Spokesperson: A. Guglielmetti

[a]University of Edinburgh, Edinburgh, United Kingdom
[b]Helmholtz-Zentrum Dresden-Rossendorf, Dresden, Germany
[c]Università degli Studi di Genova and INFN, Genova, Italy
[d]INFN, Padova, Italy
[e]Università di Siena, Siena and Centro di GeoTecnologie, San Giovanni Valdarno, Italy
[f]Università degli Studi di Napoli "Federico II", and INFN, Napoli, Italy
[g]INFN, Laboratori Nazionali del Gran Sasso (LNGS), Assergi (AQ), Italy
[h]Institute of Nuclear Research (ATOMKI), Debrecen, Hungary
[i]Università degli Studi di Torino and INFN, Torino, Italy
[j]Università degli Studi di Milano and INFN, Milano, Italy
[k]INFN, Roma, Italy
[l]Institut für Experimentalphysik III, Ruhr-Universität Bochum, Bochum, Germany
[m]Osservatorio Astronomico di Collurania, Teramo, and INFN Napoli, Italy
[n]Seconda Università di Napoli, Caserta and INFN, Napoli, Italy
[o]INFN, Milano, Italy

Abstract

Aim of the LUNA experiment is the measurement of thermonuclear fusion cross sections relevant for stellar nucleosynthesis. In the course of the year 2011, the experimental activity has been focussed on the ^{2}H(α,γ)^{6}Li and ^{17}O(p,γ)^{18}F reactions. For the former, two measurement campaingns were undertaken with an optimized setup and two different beam energies. The signal was searched for by subtracting the beam induced background. For the latter, the resonance at 193 keV as well as

the direct capture were deeply investigated both with the prompt-γ and with the activation techniques. Moreover, a round table on the LUNA-MV project was organized at LNGS and, as an outcome, a document with a list of the work packages required to underpin the realisation of the project was prepared and distributed among the interested community. In parallel, a document describing the final solutions for the shielding against neutrons of the B-node of LNGS equipped with a 3.5 MV accelerator has been prepared. This contains the results of GEANT4 Monte Carlo simulations for the expected neutron flux in several key positions.

1 Measurement of the $^2H(\alpha,\gamma)^6Li$ reaction

During 2011, the LUNA collaboration has been engaged in the study of the $^2H(\alpha,\gamma)^6Li$ reaction. This reaction is fundamental in the Big Bang Nucleosynthesis (BBN) and determines the amount of primordial ^6Li in the Universe. The measured quantity of ^6Li from the spectra of metal-poor stars has been found to be higher (two-three orders of magnitude) than expected from the present cross section estimate [1], obtained by Coulomb dissociation of $26MeV$ ^6Li projectiles at Karlsruhe [2] and recently at GSI [3]. Given that in Coulomb dissociation measurements nuclear breakup dominated the observed yield [3], the cross section obtained can be interpreted only as an upper limit. A direct measurement of the $^2H(\alpha,\gamma)^6Li$ cross section is thus strongly requested from the nuclear astrophysics community and this is possible only by using a low-background environment as LUNA. In the LUNA experiment an $\alpha-$beam produces ^6Li through collisions with deuterium gas at $0.3mbar$ pressure. The associated gammas are detected by an high purity germanium detector (HPGe).

As a consequence of the low value of the $^2H(\alpha,\gamma)^6Li$ cross section, the signal to noise ratio becomes also very low. Despite the exceptionally good LUNA environment that guarantees a reduction of the natural background, the beam induced background (BIB) is still present and dominates. The origin of this BIB was investigated by the LUNA collaboration during 2010 and can be explained as follows: alpha particles elastically scattered by deuterons produce "hot deuterons" that in turn may collide with the "cold deuterons" of the gas target producing neutrons through the $d(d,n)^3He$ reaction. These neutrons in turn may produce gammas in the energy region of interest through $(n,n'\gamma)$ reactions with the "environment" (mainly made of steel, copper, lead and germanium).

Moreover, Monte Carlo simulations showed that an ^3He beam should produce the same neutron BIB in the HPGe detector but not the $^2H(\alpha,\gamma)^6Li$ signal. In this way, it should be possible to subtract the BIB properly in future analysis. Thus, in April 2011, the LUNA accelerator was made ready to deliver an ^3He beam. However, the experiment quickly showed that the background was actually not comparable to the situation with ^4He beam, but higher, and the test was abandoned.

Another way to keep under control the neutron production is to use the "twin" reaction of the $(d,n)^3He$: the $d(d,p)t$ that produces 3.02 MeV protons. These protons are detected by a silicon detector (SD) covered by a $25\mu m$ Aluminum foil. From the theoretical point of view, the neutron rate at a given alpha energy is proportional to the proton one. So, measuring protons becomes very important in order to investigate the BIB. From a preliminary analysis of the 2011 experimental data, we can deduce that the proton rate

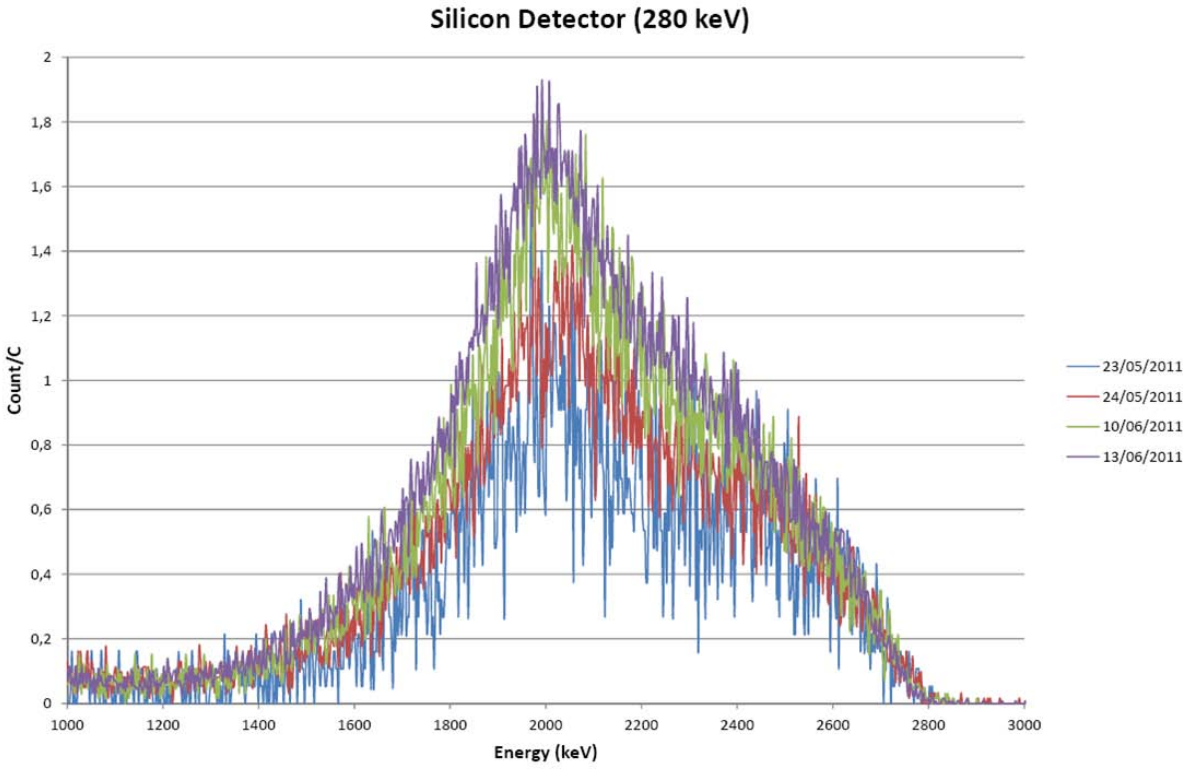

Figure 1: $d(d,p)t$ proton energy spectra as measured with the Silicon Detector for $280keV$ alphas. The proton rate increase with time maybe due to the deuterium implantation.

increases with time or more precisely with the cumulative charge in the gas target (figure 1). This process seems to be independent from the alpha beam energy and probably is due to the deuterium implantation on parts of the LUNA apparatus like the calorimeter, the SD support or collimators. A method to take into account the implantation process is being developed. Given that the BIB is connected to the proton rate thought the $d(d,n)^3He$ reaction, understanding deuterium implantation plays an important role in the overall $^2H(\alpha,\gamma)^6Li$ analysis.

Long-time measurements were scheduled for May and June, so already in April several works to improve the setup were done: an increased nitrogen flux to the anti radon box, additional air barriers and dust removal yielded a reduced natural background rate in our region of interest of about 30%. The data acquisition system was improved by solving grounding issues and by changing the Caen N1728B digitizer module from internal to external triggering.

During the two beam times dedicated to $^2H(\alpha,\gamma)^6Li$ in spring and fall, more than $1000C$ of $^4He^+$ have been applied to the deuterium gas target at a usual pressure of 0.3 mbar. The beam energy has been alternated between 400 keV and 280 keV, as GEANT4 simulations (later confirmed by the measured spectra) have shown that the beam induced background shape is similar for both beam energies. The region of interest has a width of about 30 keV due to a large Doppler shift, but reducing the beam energy by 120

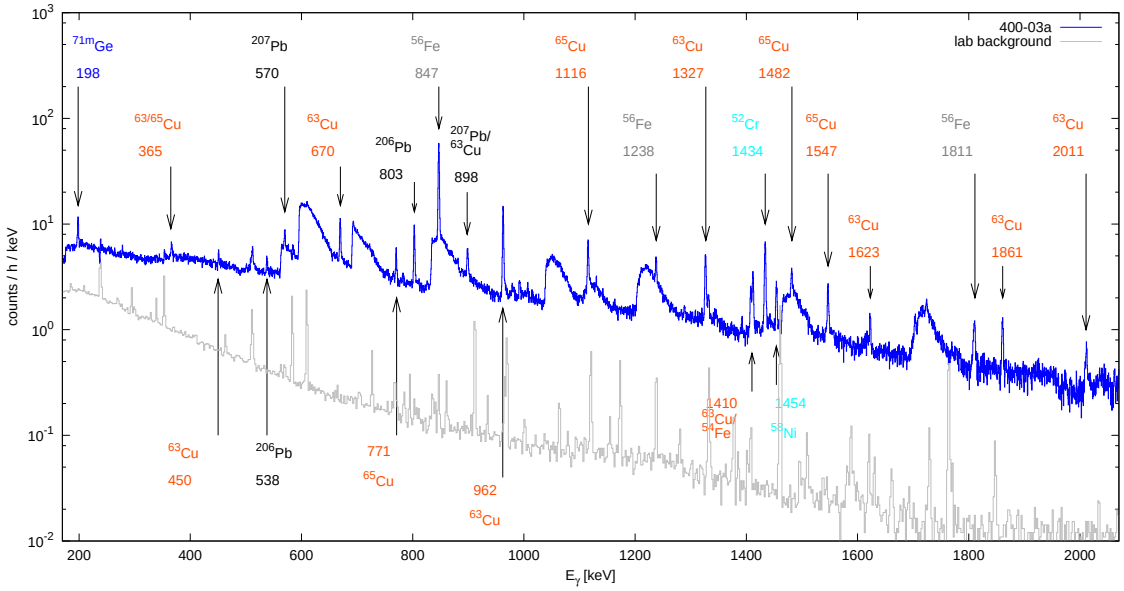

Figure 2: Acquired summed gamma spectrum at 400 keV, 0.3 mbar (blue curve) for the spring beam time with the lab background (grey curve) already subtracted. Distinct $(n, n'\gamma)$ lines are marked together with their energy.

keV moves the region of interest by 40 keV. Subtracting acquired spectra for both beam energies should therefore leave two distinct signals.

As previously underlined, the beam induced background is mainly due to neutrons produced by $d(d,n)^3He$ process. Activation of setup materials has not been observed, but the signal to noise ratio is already about 1:20, so a proper subtraction of this comparably high beam induced background is crucial for a proper $^2H(\alpha,\gamma)^6Li$ yield determination.

As already mentioned, the beam induced background shape is similar for both used beam energies. However, it is similar but not equal as the neutron energy spectra are different. Another problem which had to be solved is the question about a proper spectra normalization factor, as the applied charge is not equal for both beam energies and as the neutron rate increased noticeably with the applied charge due to deuterium implantation in the target materials. Both constraints could be addressed successfully: Along the gamma spectrum, several flat regions without distinct peaks have been chosen (see figure 2) and content ratios (for both beam energies) were calculated. In this way, data points for an energy dependent normalization function have been gained. Weighting fit functions by their reduced χ^2/DoF values yield normalization factors for every gamma energy (see figure 3), so a subtraction of the beam induced background is possible. Another approach is to choose spectra for both beam energies, finding the normalization function by subtracting channel by channel, excluding the regions of interest and using a least square method to find the optimum.

The ongoing data analysis has also shown that the shape of the beam induced background not only depends on the beam energy but also on the measurement history: As deuterium is implanted into gas target metal surfaces, additional neutron sources are cre-

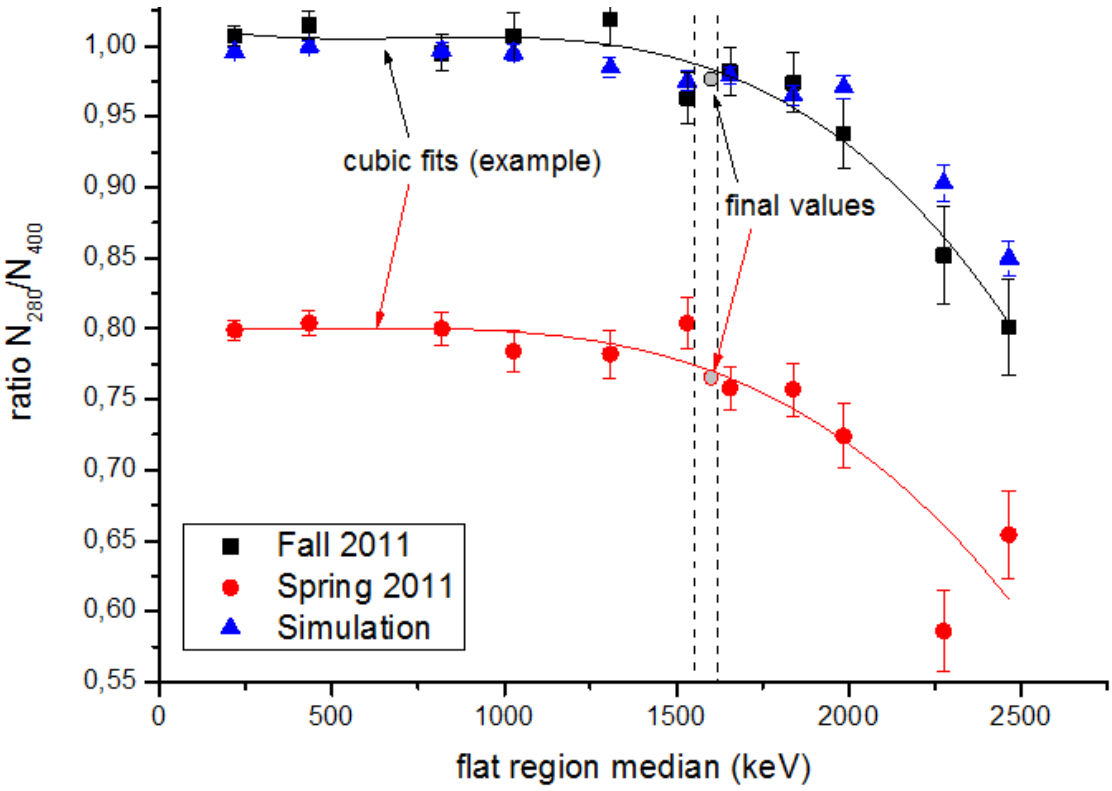

Figure 3: Ratios of flat region contents as described in the text. A cubic function has been used to fit the data points. Final values are calculated from a weighted average of several fit functions. The ratios obtained from a spectrum simulated by GEANT4 (blue) are in a good agreement.

ated, changing the neutron source geometry by applied charge, and thus also the gamma spectrum shape. A possible workaround is the frequent change of affected setup parts, but another approach is to understand their individual contributions to the beam induced background by using GEANT4 simulation results, as shown in the Fig. 4. Anyway, the data analysis already yielded promising results.

A precise measurement of the detector gamma efficiency along the beam path using not only ^{137}Cs and ^{60}Co but also a weak ^{88}Y source, a check of the gas temperature profile along the beam path and the calibration of the calorimeter in order to improve the precision of the experimental data are under way or already done. Simulations developed up to now are able to reproduce quite well the measured BIB and will be a good support for the ongoing data analysis.

2 The ^{17}O(p,γ)^{18}F reaction

The $^{17}O + p$ thermonuclear reaction rates are relevant to hydrogen burning in a variety of astrophysical sites, including red giant stars, massive stars, Asymptotic Giant Branch (AGB) stars, and classical novae. An opportunity to test nucleosynthesis models is offered

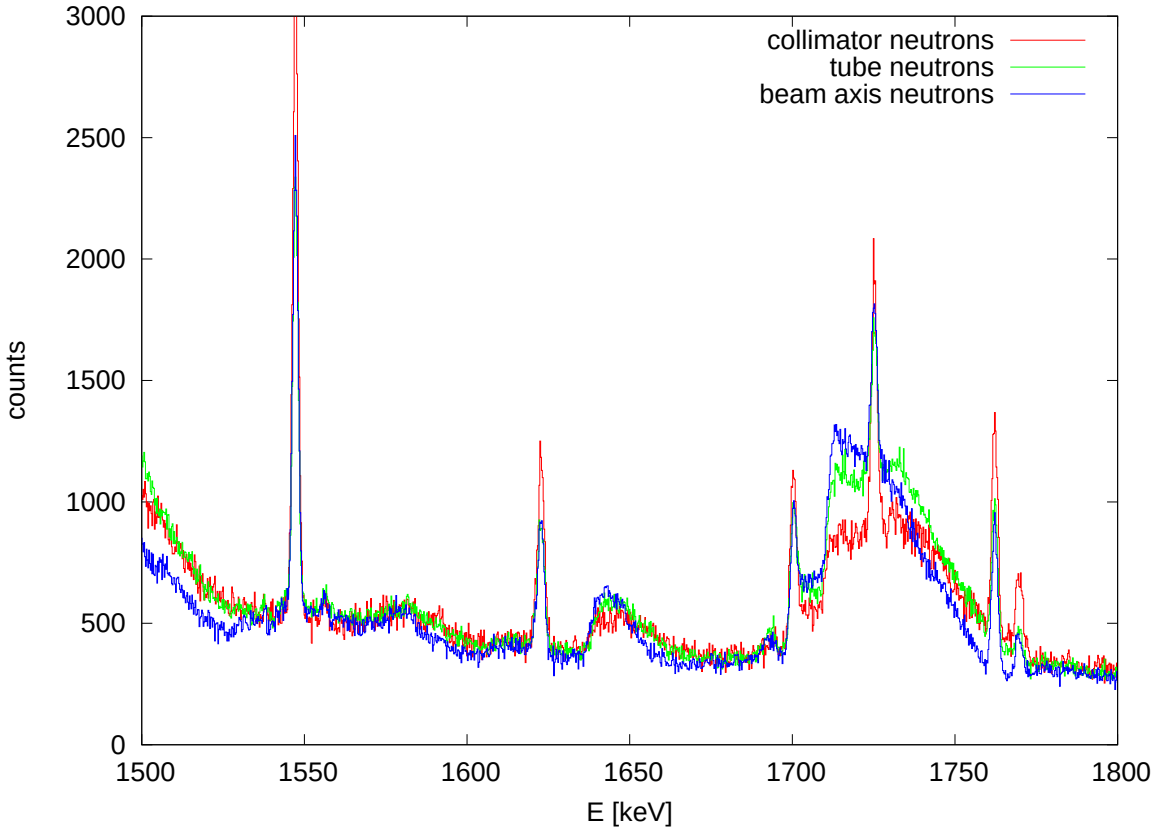

Figure 4: GEANT4 simulation of the beam induced background around the regions of interest, assuming different neutron source positions to simulate contributions to the neutron flux from implanted deuterium and from the gas target.

by classical novae through direct observations of the composition of the ejected matter and the detection of gamma rays emitted by suitably long-lived radioisotopes such as ^{18}F ($T_1/2 = 109.77 \pm 0.05$ min). Detection of such gamma rays can then put constraints on current nova models and the associated nucleosynthesis processes. The synthesis of ^{18}F crucially depends on the ^{17}O(p,γ)^{18}F reaction and its competition with the ^{17}O(p,α)^{14}N as an alternative branching route. Unfortunately, a detailed interpretation of all these observations suffers from uncertainties in the ^{17}O(p,γ)^{18}F and ^{17}O(p,α)^{14}N reaction rates at relevant stellar energies. In our study we will deeply investigate the ^{17}O(p,γ)^{18}F reaction in the novae energy region, where the importance of the strength of the resonance at $E_{R,lab}$=193keV as well the contribution of the direct capture process is evident.

The peculiarities of the 400kV facility are particulary well suited for the study of the ^{17}O(p,γ)^{18}F reaction, where reaction γ-ray lines up to $\simeq$ 5.0 MeV have to be measured with very low intensities. High beam intensities and high detection resolution have to be coupled to targets with high stability and purity. The targets are produced in the LNGS chemistry service by an anodization process of thick tantalum backings, resulting in targets with well defined stoichiometry: Ta_2O_5 [4]. A special effort was devoted to reduce the fluorine contamination from the tantalum backing before proceeding with the

anodizing process. A new technique for etching the tantalum backing was adopted: a bath in pure citric acid. The fluorine contamination, dominant in the γ spectrum, was reduced by a factor of 3 without loosing material. During the experiment, the targets were water-cooled directly on the backing. In the target chamber the target layer was shadowed by a collimator, so that a uniform beam spot was obtained within the target area by magnetic wobbling of the beam. In order to prevent build-up of impurities on the target, a LN-cooled copper cold finger was used, see fig. 5. For each run the beam current

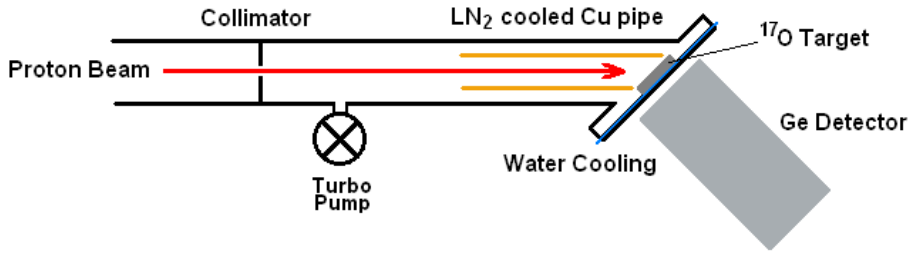

Figure 5: Schematic diagram of the experimental setup

was monitored by a digital current integrator. A Pb-shielded 120 % efficiency HPGe detector was used in close geometry at 55^o with respect to the beam direction. In order to obtain an independent determination of the resonance strength and the branching ratios to the different final states of ^{17}O(p,γ)^{18}F, a measurement of the γ-ray detection efficiency was needed. In the construction of the efficiency calibration curve the effect of target-detector distance has to be taken into account, considering that a γ-ray cascades could give a quite complex summing correction. The efficiency curve has been obtained using standard calibrated ^{137}Cs and ^{60}Co sources to fix the low energy region. The extension of the efficiency curve to higher γ-energies was achieved using the γ-ray cascade structure of the resonant state of the ^{14}N(p,γ)^{15}O reaction. The measurements were carried out at different distances between the source and the front face of the detector: 1.5, 6.5, 16.5, 21.5 cm. The distance 1.5 $\pm$0.1 cm represents the close configuration, at which all measurements of the ^{17}O(p,γ)^{18}F resonance strength have been performed. The quality of the fit of the experimental points was checked constructing a combined weighted fit, where the weighting factors included not only the statistical uncertainty but also the uncertainties on the activity of the calibrated sources for all four distances, see fig. 6. The strength of the resonance at $E_{R,lab}$=193keV has been measured with two complementary techniques: the detection of the prompt gamma-rays using a HPGe detector, and the activation method looking for ^{18}F β^+ activity ($T_{1/2}$=110min). For both approaches, the thick target yield [5] was used to determine the strength $\omega\gamma$. For a single gamma ray transition the thick target yield is given by:

$$Y_{jR}(\infty) = \frac{\lambda^2}{2}\omega\gamma \ \frac{b_j\eta_j}{\epsilon_{eff}(E_{R,lab})}\frac{M+m}{M} \qquad (1)$$

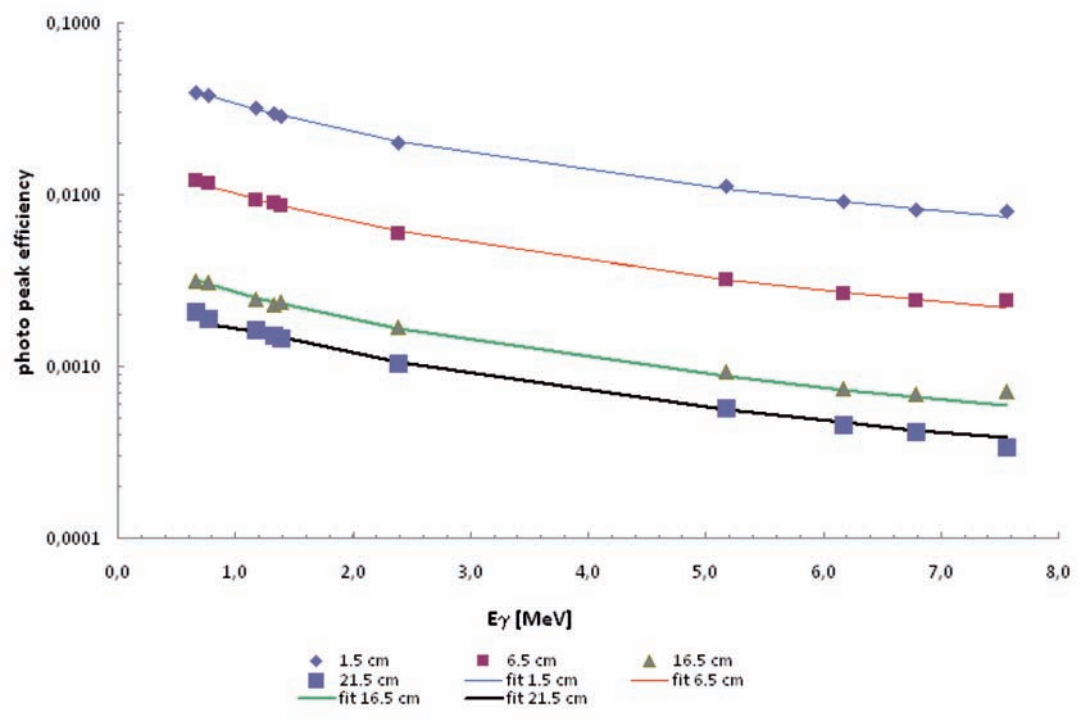

Figure 6: Full energy peak efficiency versus γ-energy for four distances d

where Y_{jR} is the yield of the j-transition, b_j and η_j are the branching-ratio and the photopeak efficiency, and $\epsilon_{eff}(E_{R,lab})$ is the effective stopping power at energy $E_{R,lab}$. The effective stopping power is related to the stopping power of active and inert atoms in the compound. Therefore, a good knowledge of the stoichiometry of the target as well as of the relative abundance of different oxygen isotopes is needed. One of the most powerful techniques to evaluate specimen stoichiometry, Rutherford Backscattering Technique (RBS), was used for our targets. This analysis was made at the Laboratori Nazionali di Legnaro using a 2.5 MV Van der Graff accelerator. For some targets, the ratio Ta/O was measured both in the target central area mostly spanned by the LUNA proton beam (beamspot) and on the target periferical area outside the beamspot (outspot). After 20C it is evident that the proton beam makes the target layer thinner, see fig.7.

A precise knowledge of target isotopic composition (^{16}O, ^{17}O and ^{18}O) and density profile is also essential. Secondary Ion Mass Spectrometry (SIMS) is widely used for analysis of trace elements in solid materials, especially thin films, and represents the proper technique, given its high sensitivity and isotope mass resolution, to determine isotopic abundances in solids with good depth and lateral resolutions. The SIMS measurements have been performed at the Department of Physics of the University of Padua (Italy) with a CAMECA IMS-4f spectrometer. Measurements performed in the beamspot region show a significantly reduced thickness, as confirmed by the RBS studies, but for target with an accumulated charge less than 20 C (around 20 h of irradiation at the LUNA accelerator) the isotopic concentration of oxygen isotopes, in the middle of the layer thickness, is stable. Each target has been measured on several different surface positions

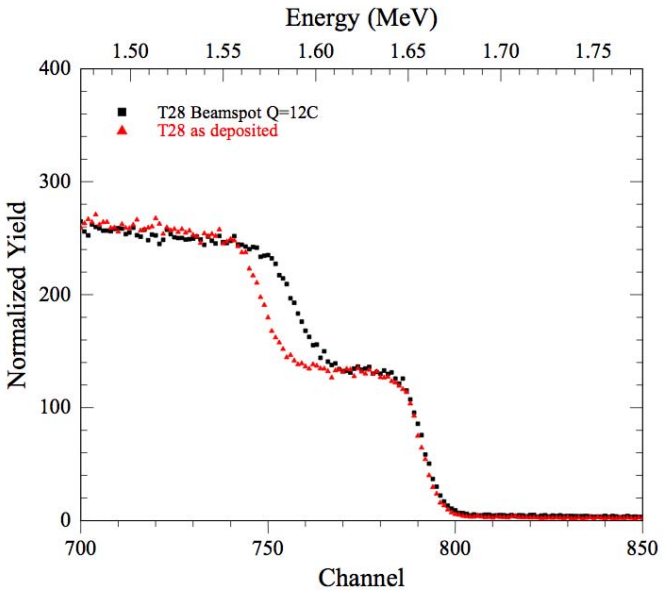

Figure 7: Comparison between RBS measurements on a target irradiated with 12 C beamspot (red triangles) and outspot (black squares). The reduction due to the high beam bombardment is evident.

of 1 μm^2 area (both beamspot and outspot) in order to evaluate the effect of the backing roughness on the oxidation process and study local variation of isotopic concentration. The overall analysis of the γ spectra is still in progress. From a preliminary comparison of the resulting strength for the resonance at $E_{R,lab}$=193keV obtained with the two methods, the discrepancy of a factor of two present in literature [6] and [7] is completly solved.

This experimental project of the LUNA collaboration is also supported by C. Salvo (INFN-Ge), M. Laubenstein (INFN-LNGS), E. Napolitani (University of Padua) and V. Rigato (INFN-LNL).

3 The LUNA-MV project

After the encouraging recommendation of the LNGS Scientific Committee, the LUNA collaboration pursued the LUNA-MV project under several aspects. Firstly, a detailed project of the preparation of the "B node" was asked to the technical division of LNGS (P. Martella and collaborators). This project includes the floor sealing, the construction of a rough experimental hall equipped with power supply and crane, the ventilation (already included in the project for the whole laboratory) and security systems. The project was prepared and constitutes the basis for discussion with local authorities like the Teramo aqueduct or ASL for obtaining the final permission to install the LUNA-MV accelerator underground. Moreover, the LUNA collaboration with the help of the LNF technical division studied how to insert the 3.5 MV single ended machine equipped with magnets, beam lines, targets and detectors inside the B-node. A key issue is here the shielding of the site against neutrons with respect to both the rest of the laboratory and the internal rock

"walls" where water uptake points of the Teramo aqueduct are present. For evaluating the neutron fluxes, a set of GEANT4 simulations were developed. Briefly, a point like and isotropically emitting neutron source with an intensity of 2000 neutrons/s and an energy of 5.6 MeV was considered. These are the maximum values for intensity and energy foreseen by the LUNA-MV project [8]. The B-NODE of the LNGS underground laboratory [9] consists of four orthogonal tunnels with a circular crossing area covered by a dome. It can be divided in five regions, as reported in Fig 8.

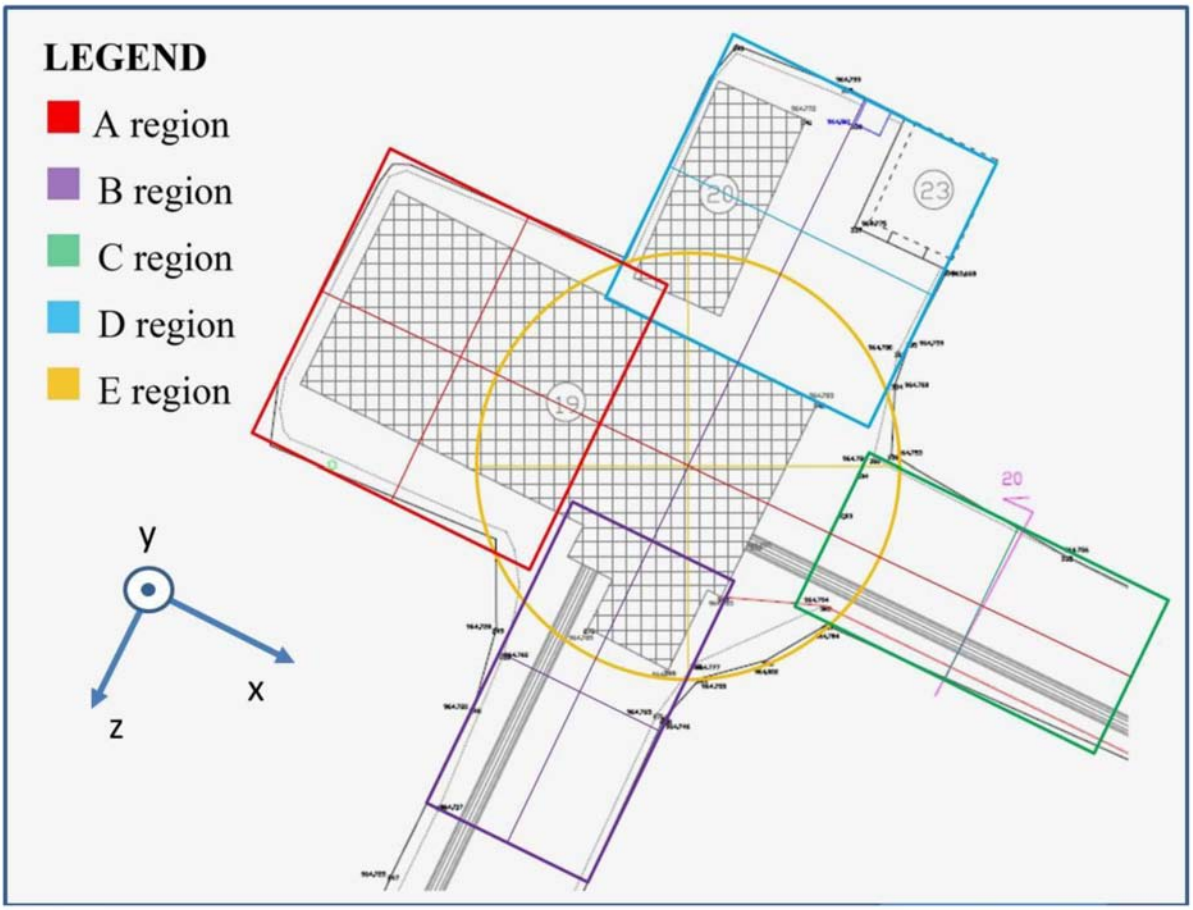

Figure 8: The B-NODE at LNGS.

The shielding against neutrons of the B-node is obtained with the solutions here described (see Fig 9). The "experimental hall" is closed by two borated concrete doors (1 meter thick) located at the end of the regions B and C (12 m from the center of the region E). Behind the doors, two borated concrete frames are present. Each one is a wall, 1 meter thick. The frames, as well as the doors, provide the accesses to the "experimental hall". The rock of the "experimental hall" is covered with 10 cm thick HDPE[5%Li] panels. In addition, a borated concrete layer, 20 cm thick, is placed on ground for the floor sealing in the whole experimental hall.

Moreover, two HDPE[5% Li] panels (10 cm thick) with dimensions 2 m x 2 m are placed on ground just behind the gas target and the solid target positions (where neutrons are

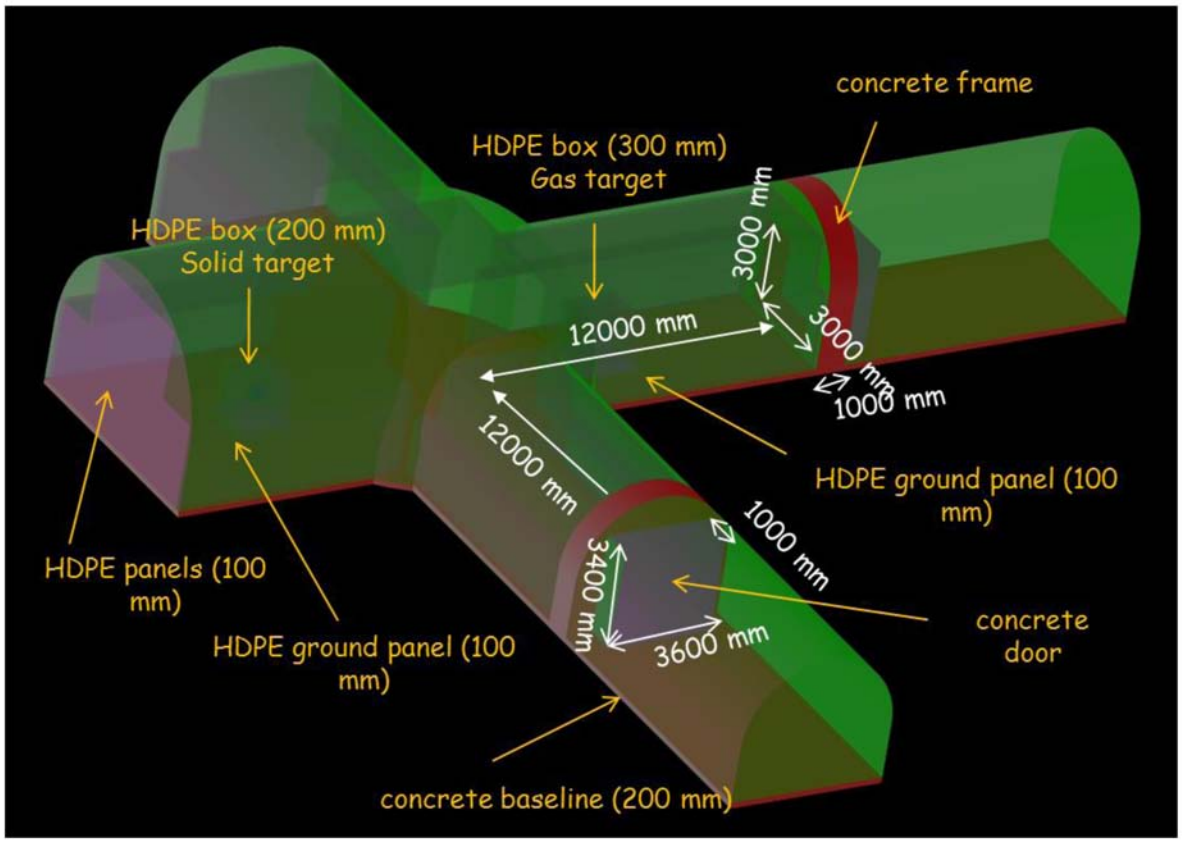

Figure 9: The experimental hall and its shielding (see text for details).

produced) and two HDPE[5% Li] boxes with half-side 60 cm and thickness 20 cm (30 cm) surround the solid (gas) target, respectively. 100 million events, 50 million with the neutron source in the gas target position and 50 million with the neutron source in the solid target position were simulated. This gives a minimum detectable flux of $\phi_{MIN} = 2.5 \cdot 10^{-10} cm^{-2} s^{-1}$. With the simulations, neutron fluxes at given points located inside and outside the regions A, B, C, D and E were obtained. As an example, for what concerns region C, which gives one of the access to the experimental hall and where the "gas target" is located, a set of 18 flux-meters located along the x-axis, 7 on the top, 7 under the floor and 7 in the lateral walls were implemented. Fig 10 shows the results for the 18 flux-meters located along the x-axis: just outside the experimental hall (at a distance of 100 cm) the neutron flux is of the order of 1% of the natural one (=3.3 $\cdot 10^{-6} cm^{-2} s^{-1}$) [10] in the case of the neutron source in the "gas target" position or well below in the case of the neutron source in the "solid target" position. For what concerns the flux-meters placed under the floor, in the lateral walls or on the top, it turns out that the average neutron flux at the surface air-rock is 2.04 $\cdot 10^{-6} cm^{-2} s^{-1}$.

Considering the whole experimental area (all 5 regions) the average neutron flux at the rock surface is 1.13 $\cdot 10^{-6} cm^{-2} s^{-1}$ reduced to 9.48 $\cdot 10^{-7} cm^{-2} s^{-1}$ at 10 cm inside the rock.

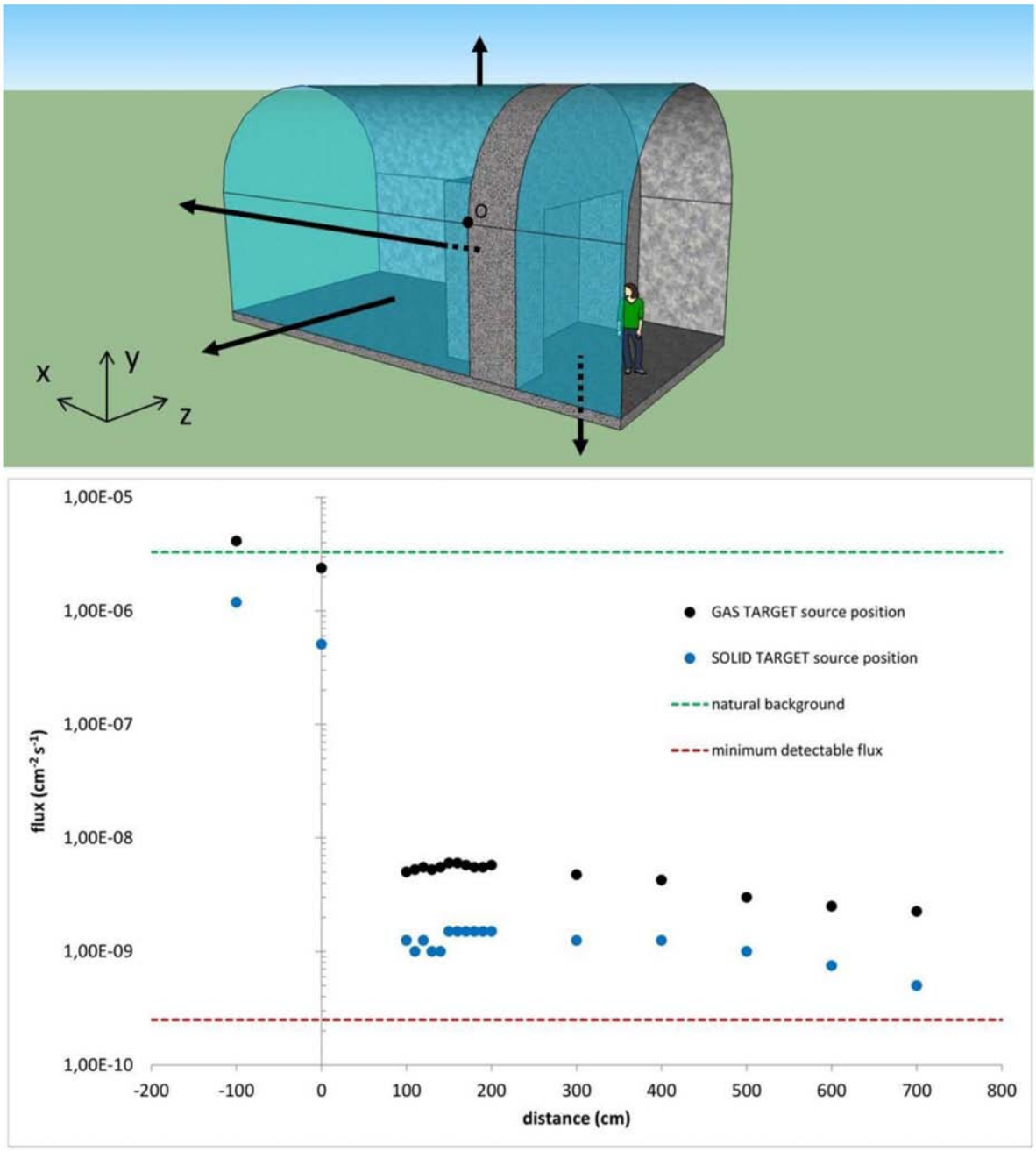

Figure 10: Simulated neutron flux for region C.

In February 2011, a two days Round Table was organized at LNGS with the aim of encouraging new groups to join the LUNA-MV project. The registered participants were 35 coming from Europe, US and Asia, 19 of which not belonging to the LUNA collaboration. The status of similar underground projects in Europe and US was reviewed, the LUNA-MV project was described both for the technical aspects (site preparation, machine, simulation,...) and for the astrophysical importance of the reactions to be mea-

sured. Open problems such as the development of detectors and the target preparation were outlined. A long discussion took place. As a result, two documents were prepared: the former contains a short summary of all the talks while the latter summarizes the situation of the project and open problems. This second document was largely circulated among the nuclear physics and astrophysics international communities. It contained a list of Work Packages to which scientists could state their interest to contribute to. To date, approximately 15 groups not belonging to the present LUNA collaboration have shown their interest and will be contacted soon.

4 List of Publications

- *"Revision of the $^{15}N(p,\gamma)^{16}O$ reaction rate and oxygen abundance in H-burning zones"*,
  A. Caciolli, C. Mazzocchi, V. Capogrosso, D. Bemmerer, C. Broggini, P. Corvisiero, H. Costantini, Z. Elekes, A. Formicola, Zs. Fulop, G. Gervino, A. Guglielmetti, C. Gustavino, Gy. Gyurky, G. Imbriani, M. Junker , A. Lemut, M. Marta. R. Menegazzo, S. Palmerini, P. Prati, V. Roca, C. Rolfs, C. Rossi Alvarez, E. Somorjai, O. Straniero, F. Strieder, F. Terrasi, H. P. Trautvetter, and A. Vomiero,
  A& A 533 (2011) A66

- *"The $^{14}N(p,\gamma)^{15}O$ reaction studied with a composite germanium detector"*,
  M. Marta, A. Formicola, D. Bemmerer, C. Broggini, A. Caciolli, P. Corvisiero, H. Costantini, Z. Elekes, Zs. Fulop, G. Gervino, A. Guglielmetti, C. Gustavino, Gy. Gyurky, G. Imbriani, M. Junker, A. Lemut, B. Limata, C. Mazzocchi, R. Menegazzo, P. Prati, V. Roca, C. Rolfs, C. Rossi Alvarez, E. Somorjai, O. Straniero, F. Strieder, F. Terrasi, H.P. Trautvetter, A. Vomiero (LUNA collaboration),
  Phys.Rev.C 83 (2011) 045804

- *"The LUNA experiment at LNGS"*,
  A. Guglielmetti,
  Proceedings of the international school of physics "Enrico Fermi", IOS Press (2011) 319

- *"Recent results on (p,γ) and (α,γ) fusion reactions at LUNA"*,
  A. Guglielmetti,
  EPJ Web of Conference, 17 (2011) 06001

5 Conference and seminar contributions

- A. Guglielmetti, "LUNA: the experimental status of the art", invited talk at International workshop on Critical Stability, Athens (Greece) 24.-25.11.2011

- A. Guglielmetti, "The LUNA experiment: direct measurement of thermonuclear cross sections of astrophysical interest", invited talk at Workshop on thermonuclear reaction rates for astrophysics applications, Erice (Italy) 09.-15.10.2011

- A. Guglielmetti, "Nuclear Astrophysics at LUNA: recent results", invited talk at The 6th European Summer School on Experimental Nuclear Astrophysics, St. Tecla (Italy) 18.-27.09.2011

- A. Guglielmetti, "Recent results on (p, γ) and (α, γ) fusion reactions at LUNA", invited talk at Fusion 11, St. Malo' (France) 02.-06.05.2011

- A. Guglielmetti, "Review of direct measurements of cross sections of thermonuclear reactions of the Hydrogen burning at LUNA", invited talk lecture at 8th Russbach workshop on nuclear astrophysics, Russbach (Austria) 13.-18.03.2011

- C. Broggini, "Origin and status of LUNA at Gran Sasso", invited talk at International Symposium on Subnuclear Physics: past, present and future, Rome (Vatican City) 30.10.-02.11.2011

- C. Broggini, "LUNA, the Sun and the other stars", invited talk at New Trends in High Energy Physics Conference, Alushta, Crimea (Russia) 03.09.2011

- D. Bemmerer, "LUNA: Underground nuclear astrophysics", invited lecture at Helmholtz International Summer School "Nuclear Theory and Astrophysical Applications", Dubna (Russia) 24.07-02.08.2011

- G. Imbriani, "Underground Measurement of the $^{17}O(p, \gamma)^{18}F$ Reaction", invited talk at VI European Summer School on Experimental Nuclear Astrophysics, Santa Tecla (Italy) 18.-27.09.2011

- A. Formicola, "Hydrogen-burning reactions at astrophysically relevant energies", invited talk at Nuclear Physics in Astrophysics V, Eilat (Israel) 03.-08.04.2011

- Zs. Fülöp, "Feasibility of low energy radiative capture experiments at the LUNA underground accelerator facility", seminar at Columbia University, Department of Physics. New York (USA) 23.01.2011

- Zs. Fülöp, "Low energy experiments at the LUNA underground accelerator facility", seminar at Uppsala Universitet, Department of Physics and Astronomy. Uppsala (Sweden) 28.04.2011

- F. Strieder, "Experimente mit Beschleunigern in Untergrundlaboren", seminar at Gelsenkirchen (Germany) 07.10.2011

- D. Trezzi, "Nuclear astrophysics deep underground: the LUNA experiment", XXXII Mazurian Lakes Conference on Physics, Piaski (Poland) 11.-18.09.2011

- M. Anders, "Study of the $^2H(\alpha, \gamma)^6Li$ reaction at LUNA", DPG-Fruehjahrstagung Muenster 2011, Muenster (Germany) 21.-25.03.2011

- M. Anders, "Direct measurement of $d(\alpha, \gamma)^6Li$ at LUNA", 8th Russbach workshop on nuclear astrophysics, Russbach (Austria) 31.-18.03.2011

- D. Scott, "Underground Measurement of the $^{17}O(p,\gamma)^{18}F$ Reaction", VI European Summer School on Experimental Nuclear Astrophysics, Santa Tecla (Italy) 18.-27.09.2011

- A. Bellini, "Direct measurement of the $^{2}H(\alpha,\gamma)^{6}Li$ cross section at energies of astrophysical interest", Societa' Italiana di Fisica - XCVII Congresso Nazionale, L'Aquila (Italy) 26.-30.09.2011

- A. Bellini, "Direct measurement of the $^{2}H(\alpha,\gamma)^{6}Li$ cross section at energies of astrophysical interest", Nuclear Physics in Astrophysics V, Eilat (Israel) 03.-08.04.2011

- M. Campeggio, "Studio della reazione $^{17}O(p,\gamma)^{18}F$ a LUNA", Societa' Italiana di Fisica - XCVII Congresso Nazionale, L'Aquila (Italy) 26.-30.09.2011

References

[1] C. Angulo et al., Nucl. Phys. A 656(1999)3

[2] J. Kiener et al., Phys. Rev. C 44(1991)2195

[3] F. Hammache et al., Phys. Rev. C 82(2010)1011.6179

[4] D. Phillips et al., Nucl.Inst.Meth A135(1976)389

[5] C.Rolfs and W.Rodney, Cauldrons in the Cosmos, The University of Chicago Press, 1988

[6] A.Chafa et al., Phys. Rev. C 75(2007)035810

[7] C. Fox et al., Phys. Rev. C 71(2005)055801

[8] A. Guglielmetti for the LUNA collaboration, Update on the LUNA MV Letter of Intent 42/07 (2010)

[9] Proceeding of the Round table "LUNA-MV at LNGS", http://luna.lngs.infn.it/luna-mv (2011)

[10] Belli et al., Il Nuovo Cimento 101A (1989), 959

2011 LVD STATUS REPORT

The LVD Collaboration

N.Yu.Agafonova[9], M.Aglietta[14], E.D.Alyea[7], P.Antonioli[1], V.V.Ashikhmin[9], G.Badino[14], G.Bari[1], M.Basile[1], V.S.Berezinsky[9], R.Bertoni[14], A. Bonardi[14], G.Bruni[1], G.Bruno[5], L.Cifarelli[1], A.Contin[1], V.L.Dadykin[9], E.A. Dobrynina[9], L.G.Dos Santos[3], R.I.Enikeev[9], W.Fulgione[14], P.Galeotti[14], M.Garbini[1], P.L.Ghia[5], P.Giusti[1], F.Gomez[14], E.Kemp[3], V.B.Korchaguin[9], M.Luvisetto[1], A.A.Machado[5], A.S.Mal'gin[9], H.Menghetti[1], N.Mengotti Silva[3], B.Miguez[3], A.Molinario[14], C.Morello[14], R.Nania[1], K.Okei[10], R.Persiani[1], I.A.Pless[8], A.Porta[14], A.Romero[14], V.G.Ryasny[9], O.G.Ryazhskaya[9], O.Saavedra[14], K.Saitoh[13], G.Sartorelli[1], I.R. Shakirianova[9], M.Selvi[1], N.Taborgna[5], N.Takahashi[12], V.P.Talochkin[9], G.C.Trinchero[14], S.Tsuji[11], A.Turtelli[3], M.Ventura[4], C.Vigorito[14], L.Votano[5], R.Weinstein[6], M.Widgoff[2], V.F.Yakushev[9], A.Zichichi[1]

[1] *University of Bologna and INFN-Bologna, Italy*
[2] *Brown University, Providence, USA*
[3] *University of Campinas, Campinas, Brazil*
[4] *INFN-LNF, Frascati, Italy*
[5] *INFN-LNGS, Assergi, Italy*
[6] *University of Houston, Houston, USA*
[7] *Indiana University, Bloomington, USA*
[8] *Massachusetts Institute of Technology, Cambridge, USA*
[9] *Institute for Nuclear Research, Russian Academy of Sciences, Moscow, Russia*
[10] *Okayama University, Okayama, Japan*
[11] *Kawasaki Medical School, Kurashiki, Japan*
[12] *Hirosaki University, Hirosaki, Japan*
[13] *Ashikaga Institute of Technology, Ashikaga, Japan*
[14] *INFN-Torino, IFSI-INAF, Torino and University of Torino, Italy*

Abstract

The Large Volume Detector (LVD) at the INFN Gran Sasso National Laboratory (LNGS), Italy, is an underground neutrino observatory mainly designed to study core-collapse supernovae. The experiment has been monitoring the Galaxy since June 1992 with increasing active mass up to the final configuration $M = 1$ kt that has been reached on January 2001. No burst candidate has been found over 6314 days of live-time, the resulting 90% c.l. upper limit to the rate of gravitational stellar collapses in the Galaxy (D $<$ 20 kpc) is 0.13 y^{-1}.

Since July 2005 LVD has taken part to the Supernovae Early Warning System (SNEWS), the network of SN neutrino observatories whose main goal is to provide the astronomical community with a prompt alert for the next galactic core-collapse supernova explosion.

Since 2006 LVD has acted as a far monitor for the Cern Neutrinos to Gran Sasso (CNGS) high energy, wide band ν_μ beam, set up at Cern and sent towards the LNGS.

LVD is continuously taking data with a live time efficiency that, in the last 10 years, has been greater than 99%. This allows to monitor time variations in the environmental conditions during long periods, the seasonal modulation of the cosmic muon flux and, through the low threshold channel dedicated to the detection of gammas from (n,p) capture, time variations in the radon concentration in the experimental hall.

1 The LVD experiment

The Large Volume Detector (LVD), located in the hall A of the INFN Gran Sasso National Laboratory, Italy, is made of 1000 tons of liquid scintillator arranged in a modular geometry. The major goal of LVD is to search for neutrinos from Gravitational Stellar Collapses (GSC) in our Galaxy [1].

The detector is a three-dimensional array of 840 scintillator counters, 1.5 m^3 each. The whole array is split into three identical parts (towers) with independent power supply, trigger and data acquisition. In turn, each tower consists of 35 cluster of 8 counters (modules). Each counter is viewed from the top by three photomultipliers (PMTs).

The main neutrino reaction in LVD[1] is $\bar{\nu}_e p \rightarrow e^+ n$, which gives two detectable signals: the prompt one, due to the e^+, followed by the signal from the (n,p) capture ($E_\gamma = 2.2$ MeV) with a mean delay of $\simeq 185$ μs.

The trigger logic is optimized for the detection of both products of the inverse beta decay and is based on the three-fold coincidence of the PMTs of a single counter. Each PMT is discriminated at two different thresholds resulting in two possible levels of coincidence between a counter's PMTs: H and L, corresponding respectively to $\mathcal{E}_H \simeq 4$ MeV and $\mathcal{E}_L \simeq 500$ keV.

[1]LVD is also sensitive to $\overset{(-)}{\nu}_i + e^- \rightarrow \overset{(-)}{\nu}_i + e^-$ scattering; $(\nu_e + \bar{\nu}_e)$ c.c. interactions and $\overset{(-)}{\nu}_i$ n.c. interactions with carbon.

The iron support structure of the detector can also act as target for neutrinos and antineutrinos. The products of the interaction can escape from iron and be detected in the liquid scintillator. The amount of neutrino-iron interactions can be as high as about 20% of the total number of interactions.
The observable signal in LVD, in different reactions and due to different kinds of neutrinos, besides providing astrophysical information on the nature of the collapse, is sensitive to intrinsic ν properties, as oscillation of massive neutrinos and can give an important contribution to define some of the neutrino oscillation properties still missing. We have studied [2] how neutrino oscillations affect the signal detected by LVD and also evaluated the impact on the signal of the astrophysical parameters of the supernova explosion mechanism, such as the total energy emitted in neutrinos, the star distance, the neutrino–sphere temperatures and the partition of the energy among the neutrino flavors.
However, being aware of the fact that the astrophysical parameters of the supernova mechanism are up to now not well defined, to compute the detector sensitivity expressed in terms of source distance or emitted neutrino flux we adopted the following conservative values for the astrophysical parameters [3], [4]: average $\bar{\nu}_e$ energy $\langle E_{\bar{\nu}_e} \rangle$=14 MeV;

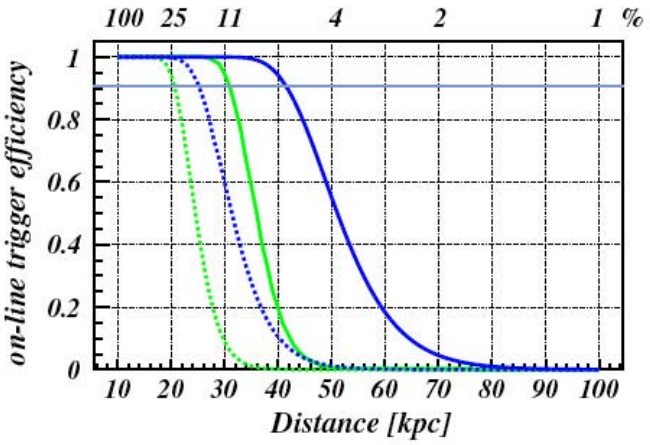

Figure 1: *On-line trigger efficiency versus distance (lower scale) and percentage of SN1987A-like signal at 10 kpc (upper scale) for E_{cut}=7-10MeV (light green and dark blue lines, respectively) and M=300t (dotted) and 1000t (continuous) for LVD stand alone.*

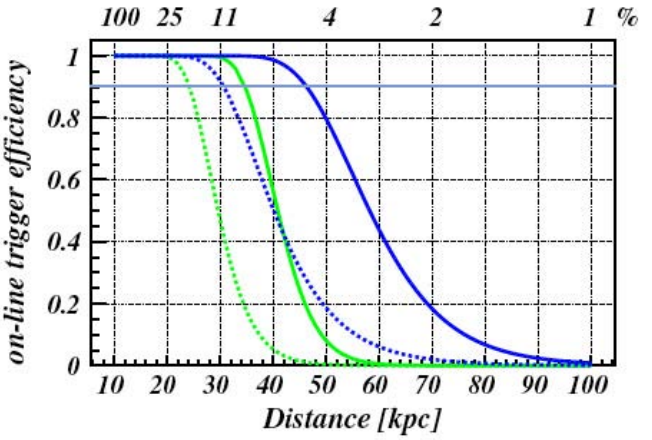

Figure 2: *Same as figure 1 for LVD in the SNEWS.*

total radiated energy $E_b = 2.4 \cdot 10^{53}$ erg and average non-electron neutrino energy 10% higher than $\bar{\nu}_e$ [5]. Concerning neutrino oscillations we conservatively assumed direct mass hierarchy. Taking into account Poisson fluctuations in the cluster multiplicity, we derived the trigger efficiency shown in figure 1 as a function of the distance (lower scale) for LVD working stand-alone (the trigger efficiency, as a function of neutrino luminosity in terms of percentage of SN1987A one is shown in the upper scale). The trigger efficiency for LVD working in the SNEWS network [6] is shown in figure 2 [7].

2 LVD: experimental activity

2.1 Supernova physics

2.1.1 Monitoring the Galaxy

LVD has been taking data since June 1992 with increasing mass configurations (sensitive mass being always greater than 300 t), enough to monitor the whole Galaxy ($D \leq 20$ kpc)[2]. In figure 3 we show sensitive mass and duty cycle of the experiment during the period 1992-2011. The LVD duty cycle, in the entire period, is greater than 92%. The search for ν burst candidates is performed by studying the temporal sequence of triggers, looking for clusters and it is widely discussed in [7].

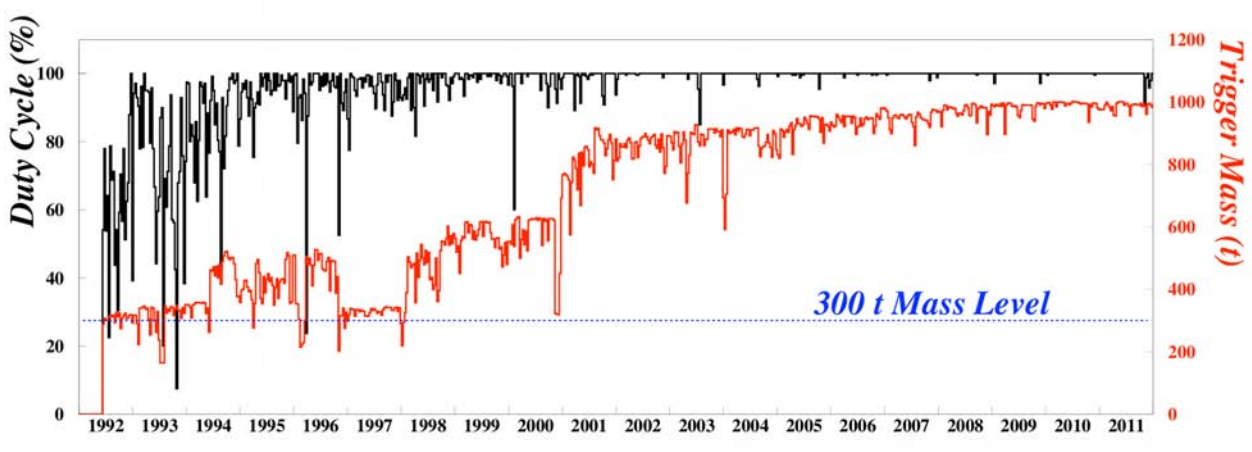

Figure 3: *LVD sensitive mass and duty cycle during 1992-2011.*

For each cluster, with multiplicity m and duration Δt, the imitation frequency F_{im} is calculated as a function of the background rate. A complete analysis of each detected cluster with $F_{im} \leq 1$ y^{-1} is performed, to test its consistency with a ν burst through the study of the topological distribution of pulses inside the detector. Additional information will come from the study of: *a)* the energy spectrum of the events in the cluster; *b)* the time distribution of the events in the cluster and *c)* the time distribution of delayed low energy pulses.

No candidates have been found since 1992, see details in table 1. Since the LVD sensitivity is higher than what is expected from GSC models (even if the source is at a distance of 20 kpc and for soft neutrino energy spectra), the resulting 90% c.l. upper limit to the rate of gravitational stellar collapses in the Galaxy ($D \leq 20$ kpc) is 0.13 y^{-1}

[2]The results of this search have been periodically updated and published in the ICRC and Neutrino Conference Proceedings, since 1993 till 2011. [8].

Table 1: LVD run.

Run	start	end	days	up (%)	mass (t)
1	6-6-1992	5-31-1993	285	60	310
2	8-4-1993	3-11-1995	397	74	390
3	3-11-1995	4-30-1997	627	90	400
4	4-30-1997	3-15-1999	685	94	415
5	3-16-1999	12-11-2000	592	95	580
6	12-12-2000	3-24-2003	821	98	842
7	3-25-2003	2-4-2005	666	> 99	881
8	2-4-2005	5-31-2007	846	> 99	936
9	5-31-2007	4-30-2009	669	> 99	967
10	5-1-2009	3-27-2011	696	> 99	981
Σ	6-6-1992	3-27-2011	6314		721

2.1.2 The Supernova On-line Monitor and SNEWS

The first, and unique, observation of ν's from gravitational stellar collapse was driven by optical observation (SN1987A), but, since the probability of such an event for a stellar collapse in our Galaxy is only of 20%, the detector capabilities of identifying a ν burst in the absence of an "external trigger" must be carefully demonstrated. In the presence of an electromagnetic counterpart, on the other hand, the prompt identification of the neutrino signal could alert the worldwide network of observatories allowing study of all aspects of the rare event from its onset.
The SNEWS (SuperNova Early Warning System) [6] project is an international collaboration including several experiments sensitive to a core-collapse supernova neutrino signal in the Galaxy and neighbourhood. The goal is to provide the astronomical community with a prompt and reliable alert of the occurrence of a Galactic supernova event, generated by the coincidence of two or more active detectors. In July 2005, after a few years of tuning, the charter members of SNEWS (i.e., LVD, Super-K and SNO[3]) together with the newly joined Amanda/IceCube, started the effective operation of the network (subscribe at *http://snews.bnl.gov* to get your own SN alert !). Since 2009 also Borexino joined the network.
Since 2001 a fast and reliable on-line ν-burst monitor has been implemented, the algorithm is based on the search for clusters of triggers within a fixed time window, Δt=20 s. The candidate is simply characterized by its multiplicity m, i.e. the number of pulses detected in Δt. All the other characteristics of the cluster are left to a subsequent independent analysis. The search for burst candidates is performed, on-line, simultaneously for two values of the energy threshold: $E_{cut} = 7$ MeV ($f_{bk} = 0.2$ Hz) and $E_{cut} = 10$ MeV ($f_{bk} = 0.03$ Hz). The chosen imitation frequencies, F_{im}, below which the detected cluster will be an on-line candidate supernova event, is 1 per 100 year working stand-alone while it is relaxed to 1 per month working in coincidence with other detectors (SNEWS), and

[3]At present the SNO experiment is decommissioned.

1 per day for monitoring task. The corresponding detection efficiency are shown in figure 1 and 2, details are discussed in [7].

2.2 CNGS beam monitor

The Cern Neutrinos to Gran Sasso (CNGS) project is a high energy, wide band ν_μ beam set up at Cern and sent towards the LNGS. Its main goal is the observation of the ν_τ appearance, through neutrino flavour oscillation. As shown in [9], due to its large area and active mass, LVD can act as a beam monitor, detecting the interaction of neutrinos inside the detector and the muons generated by the ν interaction in the rock upstream the detector. The monitor capabilities have been confirmed during CNGS runs since 2006[10].

2.2.1 MC simulation of the expected events

The CNGS events in LVD can be subdivided into two main categories:

- ν_μ charged current (CC) interactions in the rock upstream the LNGS; they produce a muon that can reach LVD and be detected,
- ν_μ CC and neutral current (NC) interactions in the material (liquid scintillator and iron of the support structure) of LVD.

A full Montecarlo simulation has been developed including the generation of the neutrino interaction products, the propagation of the muon in the Gran Sasso rock and the response of the LVD detector. The details of the simulation are described in [9]. The resulting number of expected events, at the nominal intensity 4.5 10^{19} p.o.t./y is 33400/y, equivalent to 7.422 10^{-16} events per p.o.t. (considering 200 effective days per year it corresponds to $\sim$ 165 CNGS events per day): 78% are muons from the rock, 17% are CC interactions in the detector and 5% are NC.

2.2.2 CNGS detected events

The LVD events are filtered using a very loose selection cut: we require to have at least one scintillation counter with an energy release larger that 100 MeV. The resulting rate is quite stable, with an average value of about 0.13 Hz, and it is mainly due to cosmic muon events. Among this sample the selection criteria is based on the coincidence of the LVD event time with the beam spill time written in the DB: we search for the CNGS events in the interval $[-15, +25]$ μs around the start time of the beam spill.

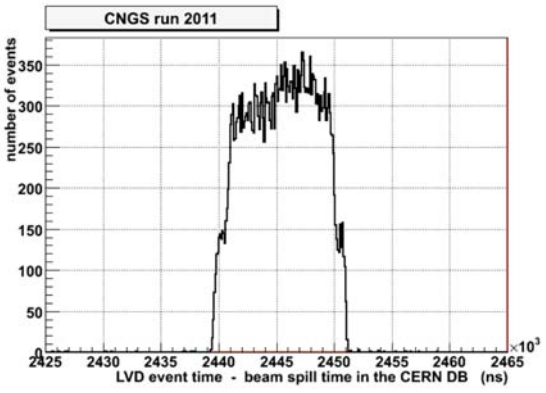

Figure 4: *Distribution of the detection time of the CNGS events, with respect to the initial time of the beam spill.*

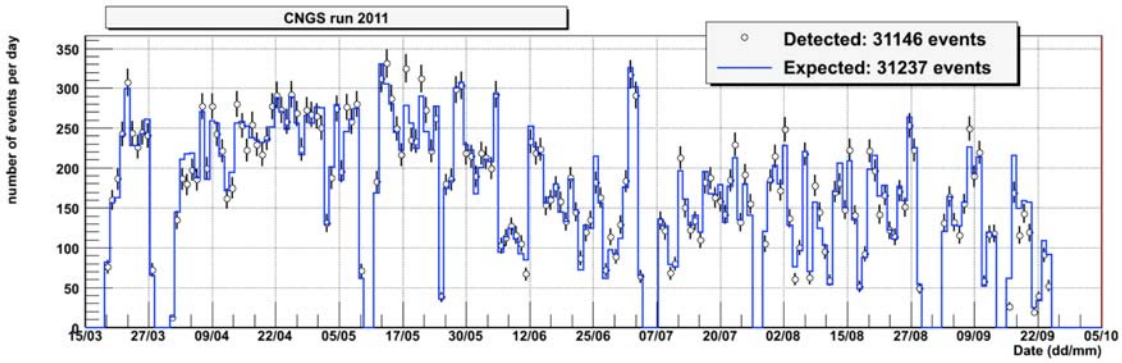

Figure 5: *Number of events per day: observed (black circles) and expected (blue line).*

An example of this distribution, corresponding to the data collected during 2011, is shown in figure 4: it reflects the 10.5 μs width of the beam spill. In figure 5 we show the comparison between the expected and detected event rate per each day of data acquisition in 2011. The background, estimated considering: the 0.13 Hz rate of events among which the CNGS events are searched for, the time window around the beam spill time, 40 μs wide, and the number of useful spills in the DB, is practically negligible.

2.3 The 2011 CNGS bunched beam

As a consequence of the neutrino time of flight measurement performed by OPERA experiment [11] unexpctedly showing evidence for superluminal propagation of ν_μ neutrinos, in the period October 21^{st} - November 7^{th} the CNGS beam was short-bunched and wide-spaced with a time structure generated by a single extraction including four bunches about 3 ns long separated by 524 ns.
The average intensity per extraction was $1.07 \cdot 10^{12}$ pot, which corresponds to a daily intensity lower of about 2 orders of magnitude with respect to the standard CNGS run.
During this short period of time LVD detected 35 events, selected with standard CNGS analysis, in agreement with expectations.
The analysis of these events, in the absence of any upgrade or tuning of the detector to increase its performance, has been useful to evaluate the capabilities of LVD to measure time flight from CERN to the LVD experiment for the next CNGS runs.
For the absolute time determination of each event, time stamps have been obtained simply using the value of the ESAT RAD-100 (SLAVE) synchronized with the external GPS receiver (MASTER) every ms, with an internal granularity given by a 10 MHz oscillator. The four bunches are very well resolved. The arrival time distribution of 33 events [4], with respect to the CERN time stamp as it appears in the data base without further corrections, defined up to an additive costant is shown in figure 6. Information coming from involved counters are used only to determine the position of the counter responsible of the trigger in order to properly correct the associated time stamp. By exploiting the information we have on the time delay of 524 ns among bunches and the fact that 33

[4]the last two events (i.e. 34 and 35) have been excluded from the analysis because cannot be unambiguously associated to one of the four bunches.

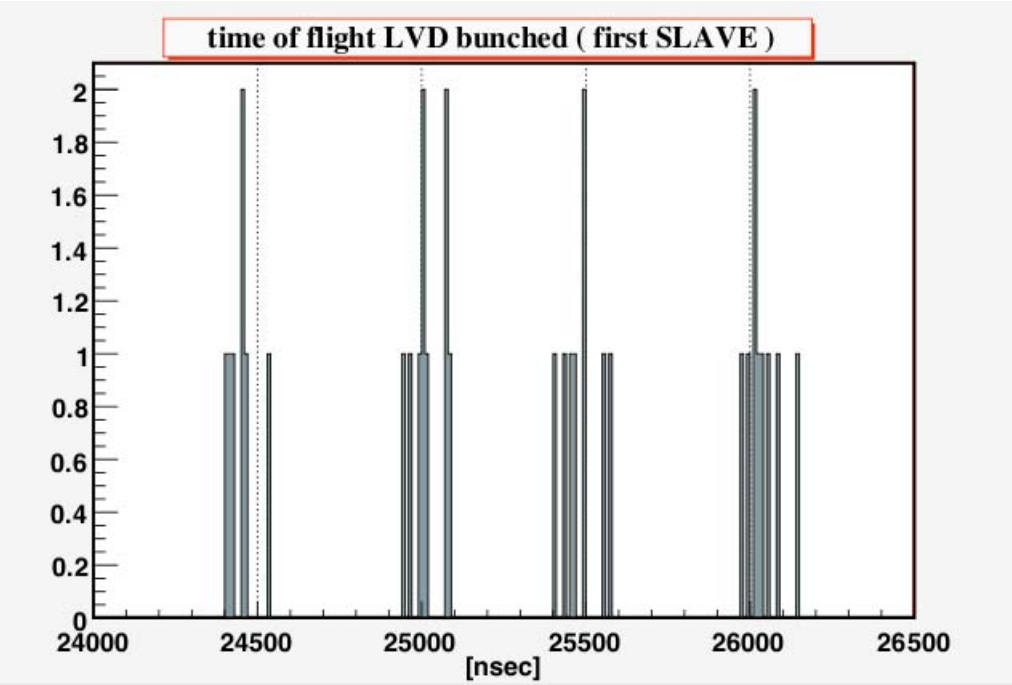

Figure 6: Arrival time distribution of the 33 LVD events of the 2011 bunched beam. The x axis is in nsec, a constant has been subtracted.

events are well identified as belonging to a specific cluster, the four clusters can be superimposed showing that all 33 events are inside a time window of about 200 ns. Result that appears to be independent from the involved tower and that can be improved introducing additional event selections.

The results obtained in the short-bunched beam during 2011 suggest that, with small improvements and a general tuning, the experiment can reach the accuracy in determining the absolute time of occurrence of CNGS neutrino events required to make a meaningful measurement of the CNGS neutrinos time of flight.

3 List of publications in 2011

- *Search for supernova neutrino bursts with the Large Volume Detector*
  W.Fulgione, A.Molinario and C.F.Vigorito On behalf of the LVD Collaboration, 32nd International Cosmic Ray Conference, Beijing 2011

References

[1] LVD Collaboration, Il Nuovo Cimento **A105** (1992) 1793

[2] N. Yu. Agafonova *et al.*, *Study of the effect of neutrino oscillations on the supernova neutrino signal in the LVD detector*, Astropart. Phys. **27**, 254-270 (2007) [arXiv: hep-ph/0609305].

[3] G. Pagliaroli, F. Vissani, M. L. Costantini, and A. Ianni, Astropart. Phys. **31**, 163 (2009)

[4] M.L. Costantini, A. Ianni and F. Vissani, Phys. Rev. D **70** (2004) 043006.

[5] M.T.Keil, G.G.Raffelt and H.T.Janka, Astrophys. J. **590** (2003) 971.

[6] P. Antonioli *et al.*, New Journal of Physics **6** (2004) 114; http://hep.bu.edu/∼snnet/

[7] N. Yu. Agafonova *et al.*, *On-line recognition of supernova neutrino bursts in the LVD detector*, Astropart. Phys. **28**, 516-522 (2008) [arXiv:0710.0259].

[8] LVD Collaboration, Proceedings of the 32nd ICRC, 2011 and reference therein.

[9] M. Aglietta et al., *CNGS beam monitor with the LVD detector*, Nuclear Instruments and Methods in Physics Research **A 516**, 96 (2004).

[10] N. Yu. Agafonova et al., *First CNGS events detected by LVD*, Eur. Phys. J. **C 52**, 849-855 (2007) [arXiv:0710.1536 hep-ex].

[11] T. Adam *et al.* [OPERA Collaboration], arXiv:1109.4897 [hep-ex].

OPERA

N. Agafonova[1], A. Aleksandrov[2], O. Altinok[3], A. Anokhina[4], S. Aoki[5], A. Ariga[6], T. Ariga[6], D. Autiero[7], A. Badertscher[8], A. Bagulya[9], A. Bendhabi[10], A. Bertolin[11,*], C. Bozza[12], T. Brugière[7], R. Brugnera[13,11], F. Brunet[14], G. Brunetti[15,16,7], S. Buontempo[2], A. Cazes[7], L. Chaussard[7], M. Chernyavskiy[9], V. Chiarella[17], A. Chukanov[18], N. D'Ambrosio[19], F. Dal Corso[11], G. De Lellis[20,2], P. del Amo Sanchez[14], Y. Déclais[7], M. De Serio[21], F. Di Capua[2], A. Di Crescenzo[20,2], D. Di Ferdinando[16], N. Di Marco[22,a], S. Dmitrievski[18], M. Dracos[23], D. Duchesneau[14], S. Dusini[11], T. Dzhatdoev[4], J. Ebert[24], O. Egorov[25], R. Enikeev[1], A. Ereditato[6], L. S. Esposito[8], J. Favier[14], T. Ferber[24], R. A. Fini[21], D. Frekers[26], T. Fukuda[27], A. Garfagnini[13,11], G. Giacomelli[15,16], M. Giorgini[15,16,b], C. Göllnitz[24], J. Goldberg[28], D. Golubkov[25], L. Goncharova[9], Y. Gornushkin[18], G. Grella[12], F. Grianti[29,17], A. M. Guler[3], C. Gustavino[19,c], C. Hagner[24], K. Hamada[27], T. Hara[5], M. Hierholzer[24], A. Hollnagel[24], K. Hoshino[27], M. Ieva[21], H. Ishida[30], K. Jakovcic[31], C. Jollet[23,*], F. Juget[6], M. Kamiscioglu[3], K. Kazuyama[27], S. H. Kim[32,d], M. Kimura[30], N. Kitagawa[27], B. Klicek[31], J. Knuesel[6], K. Kodama[33], M. Komatsu[27], U. Kose[13,11], I. Kreslo[6], H. Kubota[27], C. Lazzaro[8], J. Lenkeit[24], I. Lippi[11], A. Ljubicic[31], A. Longhin[13,11,e], P. Loverre[34], G. Lutter[6], A. Malgin[1], G. Mandrioli[16], K. Mannai[10], J. Marteau[7], T. Matsuo[30], V. Matveev[1], N. Mauri[15,16,e], E. Medinaceli[16], F. Meisel[6], A. Meregaglia[23,*], P. Migliozzi[2], S. Mikado[30], S. Miyamoto[27], P. Monacelli[22], K. Morishima[27], U. Moser[6], M. T. Muciaccia[35,21], N. Naganawa[27], T. Naka[27], M. Nakamura[27], T. Nakano[27], D. Naumov[18], V. Nikitina[4], K. Niwa[27], Y. Nonoyama[27], S. Ogawa[30], N. Okateva[9], A. Olchevski[18], M. Paniccia[17], A. Paoloni[17], B. D. Park[32,f], I. G. Park[32], A. Pastore[35,21], L. Patrizii[16], E. Pennacchio[7], H. Pessard[14], K. Pretzl[6], V. Pilipenko[26], C. Pistillo[6], N. Polukhina[9], M. Pozzato[15,16], F. Pupilli[22], R. Rescigno[12], T. Roganova[4], H. Rokujo[5], G. Romano[12], G. Rosa[34], I. Rostovtseva[25], A. Rubbia[8], A. Russo[20,2], V. Ryasny[1], O. Ryazhskaya[1], O. Sato[27], Y. Sato[36], A. Schembri[19], W. Schmidt-Parzefall[24], H. Schroeder[37], L. Scotto Lavina[20,2,g], A. Sheshukov[18], H. Shibuya[30], G. Shoziyeov[4], S. Simone[35,21], M. Sioli[15.16], C. Sirignano[12], G. Sirri[16], J. S. Song[32], M. Spinetti[17], L. Stanco[11], N. Starkov[9], M. Stipcevic[31], T. Strauss[8,h], P. Strolin[20,2], S. Takahashi[27], M. Tenti[15,16], F. Terranova[17], I. Tezuka[36], V. Tioukov[2], P. Tolun[3], A. Trabelsi[10], T. Tran[7], S. Tufanli[3,h], P. Vilain[38], M. Vladimirov[9], L. Votano[17], J. L. Vuilleumier[6], G. Wilquet[38], B. Wonsak[24] V. Yakushev[1], C. S. Yoon[32], T. Yoshioka[27], J. Yoshida[27], Y. Zaitsev[25], S. Zemskova[18], A. Zghiche[14] and R. Zimmermann[24].

1. INR-Institute for Nuclear Research of the Russian Academy of Sciences, RUS-117312 Moscow, Russia
2. INFN Sezione di Napoli, I-80125 Napoli, Italy
3. METU-Middle East Technical University, TR-06531 Ankara, Turkey

4. SINP MSU-Skobeltsyn Institute of Nuclear Physics of Moscow State University, RUS-119992 Moscow, Russia
5. Kobe University, J-657-8501 Kobe, Japan
6. Albert Einstein Center for Fundamental Physics, Laboratory for High Energy Physics (LHEP), University of Bern, CH-3012 Bern, Switzerland
7. IPNL, Université Claude Bernard Lyon 1, CNRS/IN2P3, F-69622 Villeurbanne, France
8. ETH Zurich, Institute for Particle Physics, CH-8093 Zurich, Switzerland
9. LPI-Lebedev Physical Institute of the Russian Academy of Sciences, RUS-117924 Moscow, Russia
10. Unité de Physique Nucléaire et des Hautes Energies (UPNHE), Tunis, Tunisia
11. INFN Sezione di Padova, I-35131 Padova, Italy
12. Dipartimento di Fisica dell'Università di Salerno and INFN, I-84084 Fisciano, Salerno, Italy
13. Dipartimento di Fisica dell'Università di Padova, I-35131 Padova, Italy
14. LAPP, Université de Savoie, CNRS/IN2P3, F-74941 Annecy-le-Vieux, France
15. Dipartimento di Fisica dell'Università di Bologna, I-40127 Bologna, Italy
16. INFN Sezione di Bologna, I-40127 Bologna, Italy
17. INFN - Laboratori Nazionali di Frascati dell'INFN, I-00044 Frascati (Roma), Italy
18. JINR-Joint Institute for Nuclear Research, RUS-141980 Dubna, Russia
19. INFN - Laboratori Nazionali del Gran Sasso, I-67010 Assergi (L'Aquila), Italy
20. Dipartimento di Scienze Fisiche dell'Università Federico II di Napoli, I-80125 Napoli, Italy
21. INFN Sezione di Bari, I-70126 Bari, Italy
22. Dipartimento di Fisica dell'Università dell'Aquila and INFN, I-67100 L'Aquila, Italy
23. IPHC, Université de Strasbourg, CNRS/IN2P3, F-67037 Strasbourg, France
24. Hamburg University, D-22761 Hamburg, Germany
25. ITEP-Institute for Theoretical and Experimental Physics, RUS-117259 Moscow, Russia
26. University of Münster, D-48149 Münster, Germany
27. Nagoya University, J-464-8602 Nagoya, Japan
28. Department of Physics, Technion, IL-32000 Haifa, Israel
29. Università degli Studi di Urbino "Carlo Bo", I-61029 Urbino, Italy
30. Toho University, J-274-8510 Funabashi, Japan
31. IRB-Rudjer Boskovic Institute, HR-10002 Zagreb, Croatia
32. Gyeongsang National University, ROK-900 Gazwa-dong, Jinju 660-300, Korea
33. Aichi University of Education, J-448-8542 Kariya (Aichi-Ken), Japan
34. Dipartimento di Fisica dell'Università di Roma "La Sapienza" and INFN, I-00185 Roma, Italy
35. Dipartimento di Fisica dell'Università di Bari, I-70126 Bari, Italy
36. Utsunomiya University, J-321-8505 Tochigi-Ken, Utsunomiya, Japan
37. Fachbereich Physik der Universität Rostock, D-18051 Rostock, Germany
38. IIHE, Université Libre de Bruxelles, B-1050 Brussels, Belgium
a. Now at INFN - Laboratori Nazionali del Gran Sasso, I-67010 Assergi (L'Aquila), Italy
b. Now at INAF/IASF, Sezione di Milano, I-20133 Milano, Italy
c. Now at Dipartimento di Fisica dell'Università di Roma "La Sapienza" and INFN, I-00185 Roma, Italy
d. Now at Pusan National University, Geumjeong-Gu Busan 609-735, Korea
e. Now at INFN - Laboratori Nazionali di Frascati dell'INFN, I-00044 Frascati (Roma), Italy
f. Now at Asan Medical Center, 388-1 Pungnap-2 Dong, Songpa-Gu, Seoul 138-736, Korea
g. Now at SUBATECH, CNRS/IN2P3, F-44307 Nantes, France
h. Now at Albert Einstein Center for Fundamental Physics, Laboratory for High Energy Physics (LHEP), University of Bern, CH-3012 Bern, Switzerland
*Corresponding Authors:
Email addresses: bertolin@pd.infn.it (A. Bertolin), cecile.jollet@cern.ch (C. Jollet), anselmo.meregaglia@cern.ch (A. Meregaglia)

Abstract

The OPERA neutrino detector at the underground Gran Sasso Laboratory (LNGS) was designed to perform the first detection of neutrino oscillations in ap-

pearance mode through the study of $\nu_\mu \to \nu_\tau$ oscillations. The apparatus consists of a lead/emulsion-film target complemented by electronic detectors. It is placed in the high-energy long-baseline CERN to LNGS beam (CNGS) 730 km away from the neutrino source. Runs with CNGS neutrinos were successfully conducted in 2007, 2008, 2009 and 2010 for a total luminosity of 5.9×10^{19} p.o.t. (*proton on target*). In 2011 a new CNGS run has been conducted, accumulating 4.84×10^{19} p.o.t.. After a brief description of the beam and of the experimental apparatus we report on the data and related analysis results.

1 Introduction

The solution of the long-standing solar and atmospheric neutrino puzzles has come from the hypothesis of neutrino oscillations. This implies that neutrinos have non vanishing and non-degenerate mass eigenstates, and that their flavor eigenstates involved in weak interaction processes are a superposition of the mass eigenstates.

Several experiments carried on in the last decades with solar and reactor neutrinos, as well as with atmospheric and accelerator neutrinos, contributed to build-up our present understanding of neutrino mixing. Atmospheric neutrino oscillations have been studied mainly by the Kamiokande, MACRO, Super-Kamiokande and SOUDAN2 experiments. Long baseline experiments with accelerator neutrinos (K2K and MINOS) confirmed the oscillation scenario first pointed out by the Super-Kamiokande experiment supporting the $\nu_\mu \to \nu_\tau$ oscillation channel for atmospheric neutrinos, while the CHOOZ and Palo Verde reactor experiments excluded the $\nu_\mu \to \nu_e$ channel as the dominant one.

However, the direct appearance of a different neutrino flavor is still an important open issue. This is the main goal of the OPERA experiment [1, 2] that uses the long baseline (L=730 km) CNGS neutrino beam from CERN to LNGS. The challenge of the experiment is to measure the appearance of ν_τ from ν_μ oscillations in an almost pure muon-neutrino beam. This requires the detection of the short-lived τ lepton ($c\tau = 87.11$ μm) produced in the charged-current interaction of a ν_τ. This sets two conflicting requirements: a large target mass needed to have sufficient statistics and an extremely high accuracy detector technique to observe the short-lived τ lepton.

The τ is identified by the detection of its characteristic decay topologies either in one prong (electron, muon or hadron) or in three prongs. The τ track is measured with a large-mass active target made of 1 mm thick lead plates (target mass and absorber material) inter-spaced with thin nuclear emulsion films (high-accuracy tracking devices). This detector is historically called Emulsion Cloud Chamber (ECC). Among past applications it was successfully used in the DONUT experiment for the first direct observation of the ν_τ.

The OPERA detector [2] is made of two identical Super Modules (SM) each consisting of a target section of about 625 tons made of lead/emulsion-film ECC modules (hereafter called "bricks"), of a scintillator tracker detector (TT) needed to trigger the read-out and pre-localize neutrino interactions within the target, and of a muon spectrometer (Figure 1). A single SM has longitudinal dimensions of about 10 m. The detector is equipped with an automatic machine (the Brick Manipulator System, BMS) that allows the on-line removal of bricks from the detector. Ancillary facilities exist for the handling, the

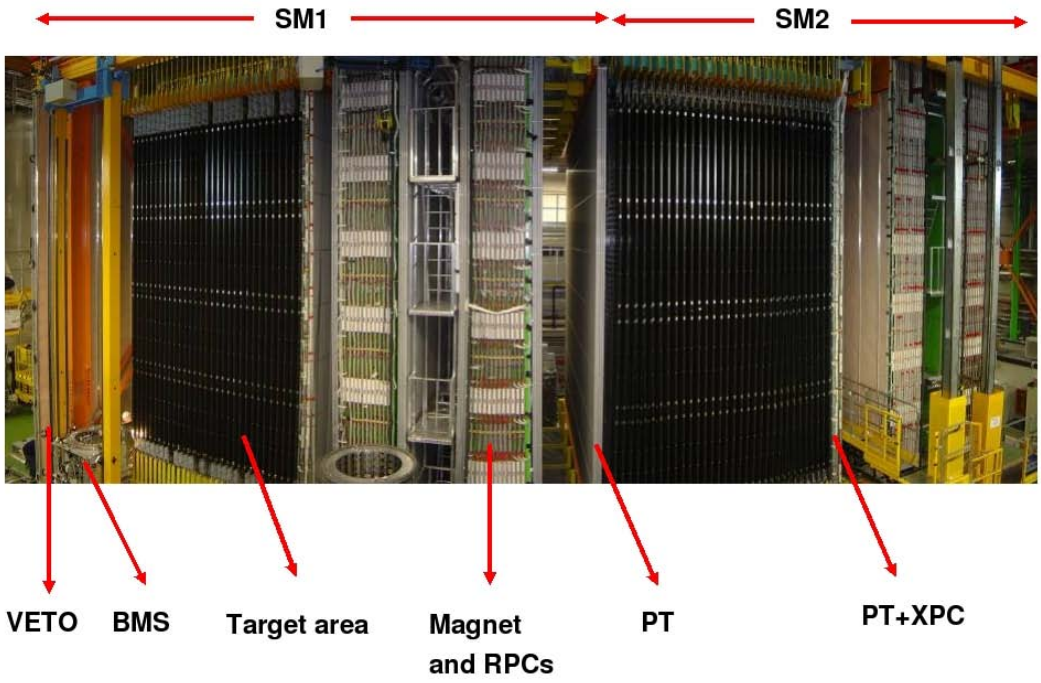

Figure 1: Fish-eye view of the OPERA detector. The upper horizontal lines indicate the position of the two identical supermodules (SM1 and SM2). The "target area" is made of walls filled with ECC bricks interleaved with planes of plastic scintillators (TT). Arrows also show the position of the VETO planes, the drift tubes (PT), the RPC with diagonal strips (XPC), the magnets and the RPC installed between the magnet iron slabs. The Brick Manipulator System (BMS) is also visible. See [2] for more details.

development and the scanning of the emulsion films. The film scanning is performed with two independent types of scanning microscopes: the European Scanning Sytem (ESS) in Europe and the S-UTS in Japan.

A target brick consists of 56 lead plates of 1 mm thickness interleaved with 57 emulsion films [4]. The plate material is a lead alloy with a small calcium content to improve its mechanical properties [5]. The transverse dimensions of a brick are 12.8 $\times$ 10.2 cm^2 and the thickness along the beam direction is 7.9 cm (about 10 radiation lengths). The construction of more than 150,000 bricks for the neutrino target has been accomplished by an automatic machine, the Brick Assembly Machine (BAM) operating underground in order to minimize the number of background tracks from cosmic-rays and environmental radiation. The BAM was delivered at LNGS in July 2006 and made operational in September 2006. The production lasted from March 2007 to June 2008 with an average rate of 650 assembled bricks/day. At the end of mass production the BAM had assembled 146621 bricks (June 2008). A few thousand more have been produced at the beginning of 2009. The bricks have been inserted in the detector target by BMS and housed in

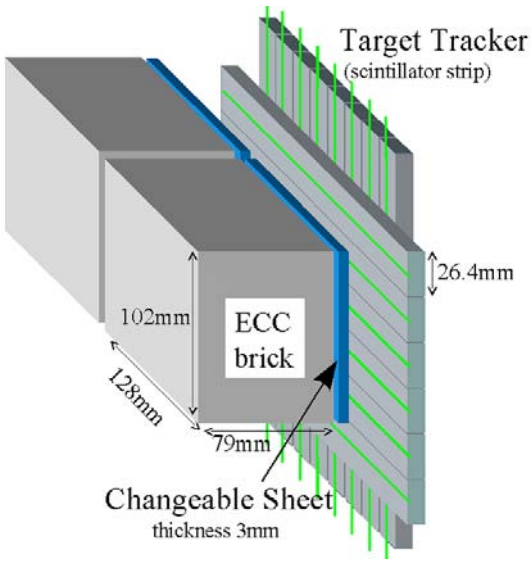

Figure 2: Schematic view of two bricks with their Changeable Sheet and target tracker planes.

a light support structure placed between consecutive TT walls. The support structure has been designed with the requirement of minimizing the material along the neutrino beam direction in order to reduce to the 0.1% level the number of interactions in regions not instrumented with emulsion films or scintillators. In order to reduce the emulsion scanning load the use of Changeable Sheets (CS) [6], successfully applied in the CHORUS experiment, was extended to OPERA. Tightly packed doublets of emulsion films are attached to the downstream face of each brick and can be removed without opening the brick. Charged particles from a neutrino interaction in the brick cross the CS and produce a trigger in the TT scintillators. Following this trigger the brick is extracted and the CS developed and analyzed in the scanning facilities at LNGS and in Nagoya. The information of the CS is used for a precise prediction of the position of the tracks in the most downstream films of the brick, hence guiding the so-called *scan-back* vertex finding procedure. The brick, CS and TT layout [6] is schematically shown in Figure 2.

2 Real time detection of CNGS Beam

The CNGS neutrino beam was designed and optimized for the study of $\nu_\mu \rightarrow \nu_\tau$ oscillations in appearance mode, by maximizing the number of charged current (CC) ν_τ interactions at the LNGS site. For a detailed description of the CNGS beam we refer to [2]. After the beam commissioning run in 2006, the CNGS run started on September 2007 at rather low intensity.

The first event inside the OPERA target was observed on October 3^{rd}.Longer runs took place in 2008, 2009, 2010 and 2011. The global CNGS performance during the 2008 to 2011 runs is summarized in table 1. The first ν_τ interaction candidate was found in 2010 [10] (Fig.4).

Figure 3: Left: Two of the six chains of the film development facility at the LNGS external laboratory. Right: The European CS Scanning Station at LNGS.

CNGS Performance in 2008-2011 Runs			
Year	POT/Year	neutrino int.	Integ.POT/proposed value
2008	1.78 10^9	1698	7.9 %
2009	3.52 10^9	3557	23.6 %
2010	4.04 10^9	3912	41.6 %
2011	4.84 10^9	4210	63.0 %

Table 1: CNGS beam performance in 2008-2011 Runs: The first column indicates the intensity of the beam integrated over each year, the second column gives the number of neutrino interactions in the OPERA target for each year, while the last column indicates the total integrated intensity divided by the proposed total luminosity

3 Overview of the OPERA activities in 2011

The total live time of the Target Tracker (which is mandatory for the prediction of where the neutrino interaction occurred) has been 99.9% during the 2011 CNGS run. The inefficiency of the spectrometer live time during the CNGS run has been 0.9%.

The two brick manipulator systems (BMS) worked for 80% of the year, 5 days/week (30% of the time during 16h/day and 70% of the time during 8h/day). So far the BMS extracted 18848 bricks.

There are blocked bricks in the detector. Each year special activities are organized to unblock as many as possible of them. As a result, the current brick extraction efficiency is 99.3%.

Taking into account the bricks reinserted in the detector, since July 2009 the total target mass has been reduced by about 7%.

The emulsion development facility is also smoothly running. The achieved average speed of the development is 55 Bricks/ Week. When needed up to about 100 bricks/week were developed.

The emulsion films quality is checked weekly and no anomalous behaviors were found up to now.

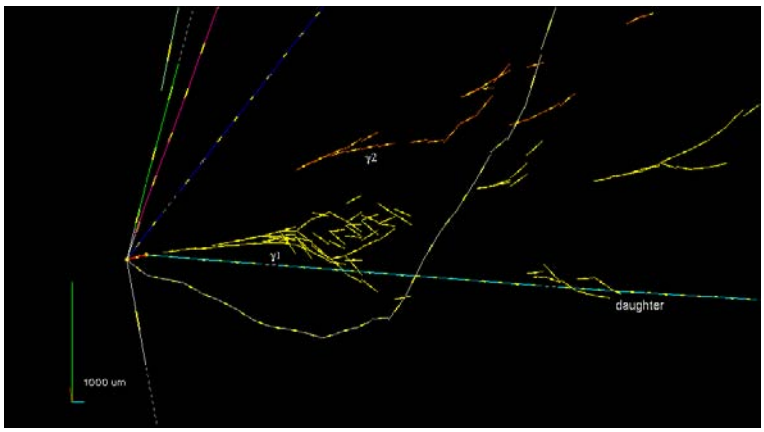

Figure 4: The first OPERA tau candidate (see [10] for details).

4 Emulsion scanning and analysis

In Figure 5, the analysis status of the neutrino interactions is shown. The black line reports the interactions expected after the normalization to the detector mass of the integrated pot, the red one the events with a brick prediction and the brown one those with at least one brick extracted. The brick extraction is the starting point of the analysis. The green lines report the scanning of changeable sheets: the upper curve shows the events with a CS scanned while the light green reports the events with a positive result after the interface emulsion film analysis. The blue line shows the number of located events in the brick. The progress in the decay search is shown in the last curve.

The two green lines have different slopes because there is the brick finding efficiency in-between. The analysis of up to 2 bricks is systematically done for all the events. Unlike it was done for the 2008 run, the extraction of a third and fourth candidate brick is done only for events predicted within 1 cm from the edge.

In autumn 2011 we have defined an optimal strategy in order to maximize the efficiency on the short term analysis, i.e. in view of the 2012 summer conferences. We have started from the following considerations: the analysis of first bricks in the probability map provides about 80% of the overall location efficiency; the increase of scanning load due to the analysis of *second* bricks is much larger than the gain in efficiency achieved; the sample of events without a muon in the final state is enriched with ν_τ, since only 18% of the τ decay into a muon; a muon momentum cut at 15 GeV does not significantly affect the efficiency while reducing of about 25% the analysis sample. The above considerations have motivated the following priorities for the 2010 and 2011 run analysis. For the 2010 run, we give priority to the analysis of all the first predicted bricks of the 0μ sample and of the 1μ sample with a momentum cut at 15 GeV. For the 2011 run we give priority to the analysis of the 0μ sample with brick probability larger than 50%. It is worth stressing that the 2008 and 2009 runs have been analyzed without any of the above cuts.

The Changeable Sheet analysis has been improved. A likelihood approach is systematically applied to events with a muon in the final state and it is selecting about 40% of the charged-current events without any visual inspection. Moreover, we are currently

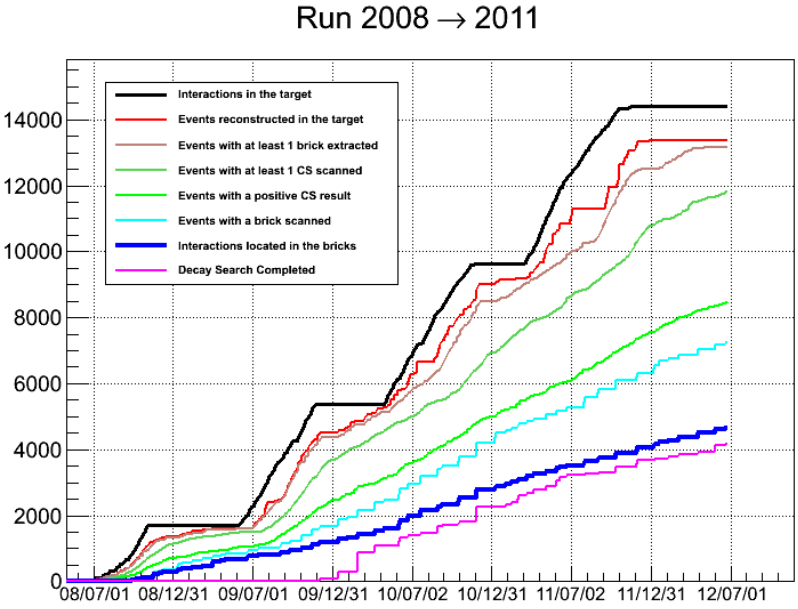

Figure 5: Run 2008 - 2011

applying an automatic selection also in the 0μ channel, i.e. for the events without any muon in the final state. Tracks validated via the likelihood approach are used as input in a vertexing algorithm. If a vertex is defined by the measured tracks, the brick is developed, thus achieving a fraction of 40% of the events without any muon in the final state validated without visual inspection.

4611 events show a vertex located within the bricks. 4126 have the decay search completed. In this analyzed sample 55 topological charm candidates and 25 electron neutrino candidates were found. A few other topologically-interesting events are under analysis. Relating to the BG studies of tau, studies of the hadron interactions are in progress using ECC bricks exposed to the test beam of 2, 4 and 10GeV/c at CERN and KEK. The features of daughter charged particle multiplicity, emitted angle, momentum, Pt and the probability of associating nuclear fragments are investigated and compared with Monte Carlo simulation.

5 ν_e search

A dedicated procedure was set up in order to make a systematic search for electron neutrinos. For the 505 events (recorded in 2008 and 2009) with the decay search completed and without any muon in the final state, all the charged tracks are considered and projected onto the changeable sheet. If a cluster of tracks is found around the projected point, the track is further checked along its trajectory to assess its possible electromagnetic nature. By this selection, 19 events were identified as ν_e, event. In parallel, BG studies for the misidentification of the electron pair conversion as a single electron is being carried out by

using electron pairs detected in CC events. The expected BG is only 0.16 events among the current sample. The event energy was estimated by using the hit information of TT. The observed number 19 is consistent with the expectation of 1.5 oscillated ν_e, plus 19.2 prompt beam ν_e,. In order to improve the S/N ratio, we set the threshold at 20 GeV, 4 events remain after this cut (E ¡ 20GeV). The observed number is again consistent with the expectation of 1.1 oscillated and 3.7 prompt beam ν_e. We have a possibility to span the region and to reach the point indicated by recent reactor experiments with full statistics and improved efficiencies and contribute to the global fit.

6 neutrino velocity measurement

The OPERA neutrino experiment at the underground Gran Sasso Laboratory has measured the velocity of neutrinos from the CERN CNGS beam over a baseline of about 730 km. The measurement is based on data taken by OPERA in the years 2009, 2010 and 2011. Dedicated upgrades of the CNGS timing system and of the OPERA detector, as well as a high precision geodesy campaign for the measurement of the neutrino baseline, allowed reaching comparable systematic and statistical accuracies. An arrival time of CNGS muon neutrinos with respect to the one computed assuming the speed of light in vacuum of (6,5+/-7,4 (stat)+8.3-8.0(sys)) ns was measured corresponding to a relative difference of the muon neutrino velocity with respect to the speed of light (v-c)/c = (2.7+/-3.1 (stat)+3.4-3.3 (sys))10^{-6}.

The above result, obtained by comparing the time distributions of neutrino interactions and of protons hitting the CNGS target in 10.5 μs long extractions, was confirmed by a test performed at the end of 2011 using a short bunched beam allowing to measure the neutrino time of flight at the single interaction level. These results were obtained by taking into account the corrections for instrumental effects discovered after the originally reported neutrino velocity anomaly. After the end of the 2011 running period, extensive tests continued in order to check all possible sources of bias in the anomalous result. In the period going from December 2011 to February 2012, two sources were identified as the origins of the anomaly, which were official announced by OPERA on the 23rd of February 2012. The main problem concerned the delay of the fiber bringing the GPS signal from the outside LNGS laboratory to the OPERA Master Clock. New measurements found a delay 73 ns larger than the value obtained with past calibrations. These measurements were repeated after one week yielding values compatible with the ones of the past calibrations. After investigation, it was realized that the fiber was not properly connected to the Master Clock during the first re-measurement taken in December 2011 and before that time. A second issue, but going in the opposite direction of overestimating the neutrino time of flight, came from the fact that the Master Clock local oscillator's frequency was found to be slightly higher than the specifications inducing a delay of 124ns/sec (up to 74 nsec in DAQ cycle of 0.6 sec).

Pictures of the fiber connector taken during last October were indicating that the first problem was at least present during the last bunched beam run (Oct.-Nov.). In order to have a clear indication when this problem occurred and of its magnitude as a function of time, correlations between OPERA and LVD using horizontal cosmic muons have been

analyzed till February 2012. These correlations showed that in 2007 and during a part of 2008 the delay of these muons to cross the two experiments was compatible with the expectations while after this period and up to December 2011 this delay increased by a value compatible to the one directly measured in the first re-measurement of December 2011, mentioned previously. The stability of the delay was investigated using the same muon events. After the correct re-connection of the fiber on the Master Clock, all successive direct measurements of the fiber delay as well as the observation of the muon delay between OPERA and LVD gave again the initial delay known since 2006. Also the stability of the local Master clock oscillator was investigated by using muons. All these measurements have been presented during a dedicated workshop at LNGS the 28th of March 2012.

References and list of publications

[1] R. Acquafredda *et al.* [OPERA Collaboration], "First events from the CNGS neutrino beam detected in the OPERA experiment,"New J. Phys. **8** (2006) 303 [arXiv:hep-ex/0611023].

[2] R. Acquafredda *et al.* [OPERA Collaboration] "The OPERA experiment in the CERN to Gran Sasso neutrino beam", JINST 4:P04018,2009.

[3] N. Agafonova *et al.* [OPERA Collaboration] "The Detection of neutrino interactions in the emulsion/lead target of the OPERA experiment", JINST 4:P06020,2009.

[4] T. Nakamura *et al.*, "The Opera Film: New Nuclear Emulsion For Large-Scale, High-Precision Experiments," Nucl. Instrum. Meth. A **556** (2006) 80.

[5] A. Anokhina *et al.* [OPERA Collaboration], "Study of the effects induced by lead on the emulsion films of the OPERA experiment," JINST **3** P07002 (2008).

[6] A. Anokhina *et al.* [OPERA Collaboration], "Emulsion sheet doublets as interface trackers for the OPERA experiment," JINST **3** (2008) P07005

[7] L. Arrabito *et al.*, "Track reconstruction in the emulsion-lead target of the OPERA experiment using the ESS microscope," JINST **2** (2007) P05004

[8] K. Kodama *et al.*, "Momentum measurement of secondary particle by multiple Coulomb scattering with emulsion cloud chamber in DONuT experiment," Nucl. Instrum. Meth. A **574** (2007) 192.

[9] M. Guler *et al.*, OPERA proposal, CERN/SPSC 2000-028, SPSC/P318, LNGS P25/2000.

[10] N. Agafonova *et al.* [OPERA Collaboration], "Observation of a first ν_τ candidate in the OPERA experiment in the CNGS beam," Phys. Lett. *B691* , 138 (2010).

[11] N. Agafonova, *et al.* [OPERA Collaboration], "Measurement of the atmospheric muon charge ratio with the OPERA detector," Eur. Phys. J. *C67* , 25 (2010).

[12] N. Agafonova *et al.* [OPERA Collaboration], "Study of neutrino interactions with the electronic detectors of the OPERA experiment." New J. Phys. *13* , 053051 (2011)

[13] N. Agafonova *et al.* [OPERA Collaboration], "Search for ν_μ -ν_τ oscillation with the OPERA experiment in the CNGS beam." New J. Phys. *14* , 033017 (2012)

[14] N. Agafonova *et al.* [OPERA Collaboration], "Momentum measurement by the Multiple Coulomb Scattering method in the OPERA lead emulsion target." New J. Phys. *14* , 013026 (2012)

THEORY GROUP

The research is organized in the five working groups: FA51, CT51, PD51, PI12, PI21, that are generically denoted as IS (from "Iniziative Specifiche"). It concerns as main areas: astroparticle physics (mainly FA51), compact stars (CT51), cosmology, large scale structures and dark matter (PD51), computer simulations of gauge theories (PI12), particle physics phenomenology (mainly PI21). There is a tradition of collaboration between the LNGS theory group and several experimental groups. In this report, we describe the activities of the theory group in 2011.

Members of the group: R. Aloisio, Z. Berezhiani, V. Berezinsky, D. Boncioli, P. Blasi, G. Di Carlo, M. Crisostomi, A. Gazizov, A.F. Grillo, E. Luzio, A. Maiezza, M. Mannarelli, M. Mitra, G. Pagliaroli, L. Pilo, N. Rossi, F. Rossi-Torres, F. Tortorici, F.L. Villante, F. Vissani.

Updated information and further info at: `http://theory.lngs.infn.it/index.html` .

Theoretical Astroparticle Physics (FA51)

The Astroparticle group of LNGS in 2011 included R. Aloisio (100%), **V. Berezinsky (0%)**, P. Blasi (70%), A. Gazizov (100%), M. Mitra (40%), F. Vissani (60%).

The group worked in close collaboration with P. Blasi (Arcetri Observatory), V. Dokuchaev (INR, Moscow), Yu. Eroshenko (INR, Moscow), S. Grigorieva (INR, Moscow), M. Kachelrieß(Trondheim Univ., Norway) G. Senjanović (ICTP, Trieste) and A. Vilenkin (Tufts University).

Scientific work

Our work covered four fields: ultra-high energy (UHE) cosmic rays, UHE neutrinos, neutrinos from supernovae and supernova remnants SN, cosmology. In UHE cosmic rays our main work was the analytic study of UHE nuclei propagation, using the homogeneous distribution of nuclei and photo-disintegration on cosmic-microwave- extra-galactic- background radiations. The "disappointing model" for explanation of the Auger data has been developed further. Cusps of superconducting cosmic strings as sources of UHE neutrinos have been investigated. UHE neutrino radiation from SNR have been discussed, and their fluxes calculated. In cosmology, the superdense clumps, and in particular, the clumps from superheavy DM particles have been studied.

Conferences, seminars and other activities

R. Aloisio, invited review "Ultra High Energy Cosmic Rays Propagation and Spectrum" at the International Symposium on the *Recent progress of ultra high energy cosmic ray observation*, Nagoya 10-12 December 2010.

V. Berezinsky, invited talk "Galactic Cosmic Rays: Progress and Problems" at Symposium *Highlights of Astroparticle Physics*, Torino, 20 September 2010.

V. Berezinsky, invited talk "Dark matter subhalos and annihilation signal" at Workshop on *Indirect Dark Matter search*, Hamburg 14 - 17 June 2011.

V. Berezinsky, introductory talk "UHE cosmic neutrinos: view from 2011" at Workshop *Looking at the neutrino sky*, Trieste 20 - 24 June 2011.

A. Gazizov, talk "Disappointing model for ultra-high energy cosmic rays" at Int. Conference *Nuclear Physics A5*, Eilat, Israel, 3-8 April, 2011.

F. Vissani, invited talk "On the detectability of HE galactic neutrino sources" at Workshop *Looking at the neutrino sky*, Trieste 20 - 24 June 2011.

F. Vissani, talk "High Energy Neutrino Astronomy: From the Hope for Surprises to Predictions," at the *National meeting of the Italian Physics Society* (SIF), Bologna, Italy, September 2010.

F. Vissani, Summary talk "PHYSUN-II: Impressions and Conclusive Remarks," at the *Second PHYSUN Workhop*, LNGS, Italy, October 2010

F. Vissani, invited talk "TeV neutrinos from SNR: How to get predictions with errorbars?" at the *Meeting on Multi-Messenger Astronomy of Cosmic Rays*, KIAA, Beijing, April 2011.

F. Vissani, Invited talk "Expectations for High-Energy Neutrinos From Galactic Sources," at *RICAP2011*, Rome 3 University, May 2011.

R. Alosio works as the secretary of the Scientific Committee of LNGS and the organizer of the LNGS seminar.

V. Berezinsky works as a member of International Advisory Board of collaboration JEM-EUSO.

F. Vissani is coordinator of the LNGS Theory group, INFN representative in the Science Advisory Commitee of ASPERA, Observer in Comm.II on behalf of Comm.IV, Referee for the INFN National Permanent Commitees II on non-accelerator physics and IV on theoretical physics. Moreover, is the LNGS representative of the Italian Physics Society (SIF) for LNGS, coordinates the local VESF group and is a member of the scientific committee INFN-ICRA.

Publications in journals, proceedings and preprints

[1] V. Berezinsky, V. Dokuchaev, Yu. Eroshenko, M. Kachelrieß, M.Aa. Solberg, *Superdense cosmological dark matter clumps,* Phys. Rev. D81 (2010) 103529

[2] V. Berezinsky, V. Dokuchaev, Yu. Eroshenko, M. Kachelriess, M.Aa. Solberg, *Annihilation of superheavy dark matter in superdense clumps,* Phys. Rev. D81 (2010) 103530

[3] R. Aloisio, V. Berezinsky, A. Gazizov,
Ultra High Energy Cosmic Rays: The disappointing model, Astroparticle Physics 34 (2011) 620

[4] V. Berezinsky, E. Sabancilar, A. Vilenkin,
Extremely High Energy Neutrinos from Cosmic Strings.
Phys. Rev. D84 (2011) 085006

[5] V. Berezinsky, V. Dokuchaev, Yu. Eroshenko,
Dense DM clumps seeded by cosmic string loops and DM annihilation.
JCAP 12 (2011) 007

[6] V. Berezinsky, A. Gazizov, M. Kachelrieß, S.Ostapchenko,
Restricting UHECRs and cosmogenic neutrinos with Fermi-LAT.
Phys. Lett. B695 (2011) 13

[7] F.Vissani, G.Pagliaroli,
The diffuse supernova neutrino background: Expectations and uncertainties derived from SN1987A,
Astronomy & Astrophysics 528 (2011) L1

[8] F. Vissani, F. Aharonian, N. Sahakyan,
On the detectability of high-energy Galactic neutrino sources,
Astroparticle Physics 34 (2011) 778

[9] F. Vissani and F. Aharonian,
Galactic Sources of High-Energy Neutrinos: Highlights,
arXiv:1112.3911 [astro-ph.HE], in press on NIM-A

[10] F.L. Villante, A. Ianni, F. Lombardi, G. Pagliaroli, F. Vissani,
A step toward CNO solar neutrinos detection in liquid scintillators.
Phys. Lett. B701 (2011) 336

[11] F. Vissani, G. Pagliaroli and M. L. Costantini,
"A parameterized model for supernova electron antineutrino emission and its applications,"
J. Phys. Conf. Ser. **309** (2011) 012025

[12] G. Pagliaroli and F. Vissani,
Supernova neutrinos and gravitational waves,
Nucl. Phys. Proc. Suppl. **217** (2011) 278

[13] F. Vissani, G. Pagliaroli and F. Rossi-Torres,
The use of supernova neutrinos to monitor the collapse, to search for gravity waves, to probe neutrino masses,
Int. J. Mod. Phys. D **20** (2011) 1873

[14] V. Tello, M. Nemevsek, F. Nesti, G. Senjanović, F. Vissani,
Left-Right Symmetry: from LHC to Neutrinoless Double Beta Decay,
Phys. Rev. Lett. 106 (2011) 151801

[15] M. Mitra, G. Senjanovic and F. Vissani,
Neutrinoless Double Beta Decay and Heavy Sterile Neutrinos,
arXiv:1108.0004 [hep-ph]

[16] V. Berezinsky,
UHE neutrinos: From standard astrophysics to new physics,
PoS HRMS2010 (2010) 027

[17] R. Aloisio, D. Boncioli,
Ultra High Energy Cosmic Rays: Anisotropies and Spectrum,
Astroparticle Physics 35 (2011) 152

[18] R. Aloisio,
Ultra High Energy Cosmic Rays Propagation and Spectrum,
arXiv:1104.0329, AIP Conf.Proc. 1367 (2011) 114

[19] R. Aloisio, V. Berezinsky, A. Gazizov,
Disappointing model for ultrahigh-energy cosmic rays,
arXiv:1105.1111, J.Phys.Conf.Ser. 337 (2012) 012042

[20] V. Berezinsky,
High Energy Neutrino Astronomy,
arXiv:1102.3591

[21] Z. Berezhiani, A. Gazizov,
Neutron Oscillations to Parallel World: Earlier End to the Cosmic Ray Spectrum?
arXiv:1105.1111

[22] R. Aloisio, V. Berezinsky, S. Grigorieva,
Analytic calculations of the spectra of ultra high energy cosmic ray nuclei. II. The general case of background radiation.
Revised and extended version of preprint arXiv:arXiv:1006.2484 v2 (2010) submitted to Phys. Rev. D

[23] V.I. Dokuchaev, V. Berezinsky, Y. .Eroshenko, M. Kachelrieß, M. A. Solberg,
Superdense dark matter clumps,
PoS IDM **2010** (2011) 047.

[24] V. Berezinsky and P. Blasi,
UHE neutrinos from Pop III stars: concept and constraints,
arXiv:1111.5461 [astro-ph.HE]

Program of work for 2011 - 2012 (Berezinsky)

As far as UHECR are concerned we will continue calculations of energy spectra. Our preliminary analysis shows that steepening of the Auger spectrum contradicts the GZK shape. We will perform the detailed calculations for proton spectra using the different models with additional assumptions about cosmological evolution of the sources, maximum energy of acceleration, local excess/deficit in the number density of sources etc. We hope to demonstrate that in spite of many free parameters the Auger spectrum contradicts the GZK shape. The observed spectrum might be fitted by nuclei composition, but realistic models with discrete source location and diffusion need complicated calculations, especially for secondary nuclei and much computer time. The preliminary estimates in the frame of "disappointing model" show that agreement might be obtained.

For the proton composition (HiRes data) we will develop further the AGN model. We will study in detail the cascade e-m spectrum, which according to our work of 2010 strongly restrict the UHE proton models. We will study the bright phase of UHE proton production, which is weaker restricted by the cascade spectrum.

UHE neutrino fluxes will be calculated in two models: bright phase and ordinary cosmic strings. Ordinary strings are the simplest Topological Defects produced at U(1) symmetry breaking in early universe. The new theoretical element we are going to use is given by interaction of the string field with ordinary particles in the cusp region. It results in radiation of these ordinary particles as the free quanta. Boosted by large Lorentz factor of a cusp, these quanta obtain very large energies, producing UHE neutrinos at decay.

We will continue analysis of UHE neutrino production by SN remnants, More generally we will continue investigations of the phenomenological and theoretical implications of neutrino oscillations as a topic of neutrino astronomy.

Concerning our Dark Matter activity we will study production and destruction of cores in small clumps, which could provide the strong enhancement of indirect signal.

Invitations

In 2012 we plan to accomplish two large projects on UHECR with participation of Dr. S. Grigorieva (Institute for Nuclear Research, Moscow).
(1) Demonstration that steepening of the spectrum found in the Auger experiment is not GZK cutoff and possible explanation of this feature by nuclei with the discrete location of the sources (R. Aloisio, V. Berezinsky, A. Gazizov and S. Grigorieva). The calculation of nuclear spectra with discrete location of sources is a complex problem, which needs very large computer time.
(2) We will continue calculation of energy spectra of extragalactic UHE nuclei in a large class of models (R. Aloisio, V. Berezinsky, and S. Grigorieva).
Dr. S. Grigorieva is an active collaborator of LNGS Astroparticle group. The recent works include: V. Berezinsky, A. Gazizov and S. Grigorieva, *On astrophysical solution to ultrahigh energy cosmic rays,* Phys. Rev. D 74 (2006) 043005 (242 citations). R. Aloisio, V. Berezinsky, S. Grigorieva, *Analytic calculations of the spectra of ultra-high energy cosmic ray nuclei*, arXiv:1006.2484.
Financial request: 30 days visit in beginning of 2012, 1500 euro local expenses, and 450

euro travel expenses. The short CV is given below:

Svetlana Grigorieva Born 1944. Institute for Nuclear Research of Russian Academy of Sciences, Moscow, senior research associate, PhD from P.N. Lebedev Institute of Physics 1984, over 70 publications in the Russian and International journals, including Sov. Journal of Nucl. Phys., JETP Letters, Phys. Rev. D, Phys. Letters and others. She is known by classical works in UHECR, in particular, Astron. Astrophys. 199, 1, 1988 (217 citations) and Phys. Rev. D 74, 043005, 2006 (242 citations). Field of expertise: elementary particle physics and astroparticle physics, UHECR and UHE cosmic neutrinos.

The second invitation is planned for the work on small Dark Matter clumps (subhalos) with participation of Dr. Yu. Eroshenko. We are going to investigate the problem of the core. The core, i.e., flattening of the density profile, must exist due to convergence of annihilation signal for the steep density profiles seen in analytic solutions and numerical simulations. A small core provides large enhancement of annihilation signal. We are going to investigate several mechanisms of clump production using the Liouville theorem for limiting the core size. Dr. Eroshenko is an active collaborator of LNGS group. The list of recent works includes: V. Berezinsky, V. Dokuchaev, Yu. Eroshenko, *Remnants of dark matter clumps,* Phys. Rev. D 77 (2008) 083519 and *Superdense cosmological dark matter clumps,* Phys. Rev. D 81 (2010) 103529.
Financial request: 30 days visit in middle of 2012, 1500 euro local expenses, and 450 euro travel expenses. The short CV is given below:

Yurii Eroshenko Born 1973. Institute for Nuclear Research of Russian Academy of Sciences, Moscow, Russia, PHD (2000), junior scientist, 33 publications in Russian and International journals, including Phys. Rev. Lett., Phys. Rev. D, JETP, Astron. Lett. and others. Field of expertise: cosmology, black holes, galaxy formation and GRBs.

1 Particle Physics Phenomenology (PI21)

Members: **Z. Berezhiani**, A. Maiezza, P. Panci, L. Pilo and F. Villante, worked in collaboration with A. Gazizov (DESY, Germany), D. Comelli (INFN Ferrara), A. Dolgov (Univ. Ferrara), F. Nesti (ICTP, Triest and Univ. L'Aquila), Y. Kamyshkov (Univ. Tennessee, USA), M. Cirelli (CEA, Saclay) and N. Fornengo (Univ. Torino)

Scientific work

In ref. [1] ingredients and recipes were provided for computing signals of TeV-scale Dark Matter annihilations and decays in the Galaxy and beyond. For each DM channel, the energy spectra of electrons and positrons, antiprotons, antideuterons, gamma rays, neutrinos and antineutrinos production were presented, computed by high-statistics simulations. The Monte Carlo simulations were used by comparing the results yielded by the

Pythia and Herwig event generators. The propagation functions for charged particles in the Galaxy, for several DM distribution profiles and sets of propagation parameters were provided. Propagation of electrons and positrons is performed with an improved semi-analytic method that takes into account position-dependent energy losses in the Milky Way. Using such propagation functions, the energy spectra of electrons and positrons, antiprotons and antideuterons were computed at the location of the Earth. Then gamma ray fluxes, both from prompt emission and from Inverse Compton scattering in the galactic halo, were presented, and finally, the spectra of extragalactic gamma rays we provided. All results are available in numerical form and ready to be consumed.

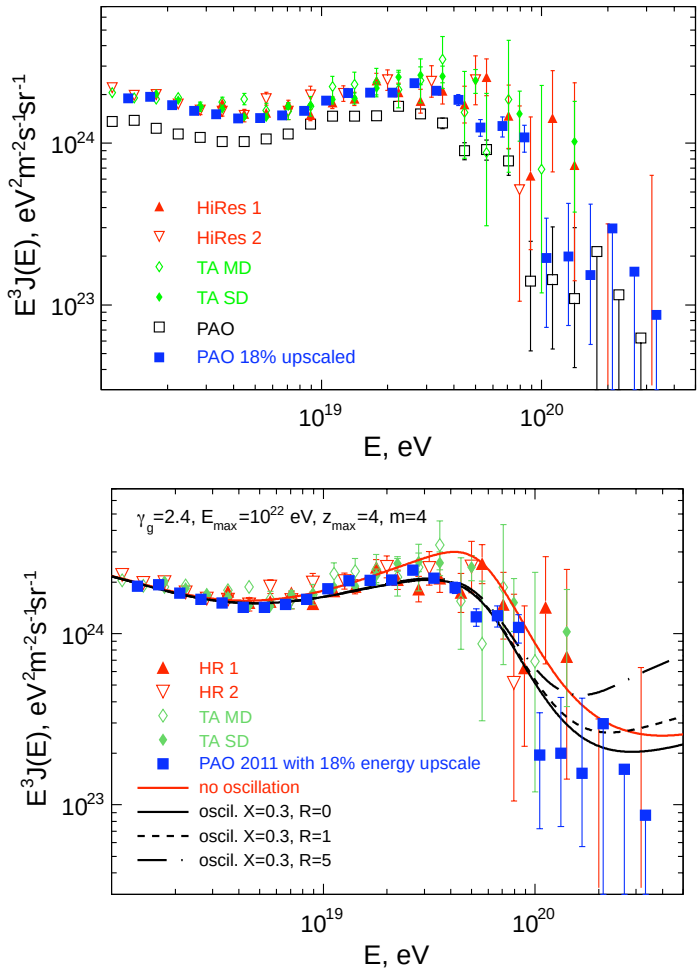

Figure 1: *Upper panel:* Original PAO spectrum disagrees with the HiRes 1, HiRes 2, Telescope Array MD and SD spectra. However, we see that if the PAO spectrum is upscaled in energies by 18%, it becomes consistent with the other data within the experimental uncertainties. *Lower panel:* The PAO spectrum even 18% upscaled, is inconsistent with the cosmic proton spectrum in the region of the GZK cutoff. However spectrum predicted in the presence of $n - n'$ oscillation is in agreement with the PAO spedtrum. Here we show modified spectra by $n - n'$ oscillation for $\gamma_g = 2.4$ and different values of the mirror sources: $R = Q'/Q = 0,\ 1,\ 5$ (lower (black) curves). The upper (red) solid curve represents the standard GZK prediction without n-n' oscillation.

In ref. [8] the baryon number violation in the propagation of the ultra-high energy cosmic rays we investigated. Present experimental data do not exclude fast oscillation

of the neutron n to its degenerate twin from a hypothetical parallel sector, the so called mirror neutron n'. It was shown that this effect brings to a remarkable modifications of the ultrahigh-energy cosmic ray spectrum testable by the present Pierre Auger Observatory (PAO) and Telescope Array (TA) detector, and the future JEM-EUSO experiment. In particular, the baryon non-conservation during UHECR propagation at large cosmological distances shifts the beginning of the GZK cutoff to lower energies, while in presence of mirror sources it may enhance the spectrum at $E > 100$ EeV. As a consequence, a significant reduction of the expected diffuse cosmogenic neutrino flux is predicted.

Conferences, seminars and other activities

Int. Workshop "Beyond Three Family Neutrino Oscillations", LNGS, Assergi (AQ), Italy, May 2011 (talk of F.L. Villante).

Int. Workshop on "The origin of elements: A modern perspective", ECT*, Trento, Italy, May 2011 (talk of F.L. Villante).

15th Int. School on "Particles and Cosmology 2011", Troitsk, Russia, May-June 2011 (invited lecture of Z. Berezhiani)

Int. Institute CETUP* on "Experimental and Theoretical Underground Physics", Black Hills, S. Dakota, USA, June 2011 (two seminar talks of Z. Berezhiani)

Int. conf. on "Astrophysics, Clocks and Fundamental Constants" ACFC 2011, Bad Honeff, Germany, July (invited lecture of Z. Berezhiani)

Int. EuroPhysics Conference on High Energy Physics, Grenoble, France, July 2011 (talk by L. Pilo).

III Int. Workshop on "Baryon and Lepton Violation" BLV 2011, Gatlinburg, USA, Sept. 2011 (invited talk of Z. Berezhiani)

Int. Workshop on Infrared Modification of Gravity, ICTP, Triest, Italy, Sept. 2011 (talk by L. Pilo).
International Workshop on *Topics in Astroparticle and Underground Physics (TAUP2011)*, Munich, Germany, September 2011 (talk of F.L. Villante).

Int. Conf. on "Recent Advances in Quantum Field and String Theory", Tbilisi, Georgia, Sept. 2011 (invited talk of Z. Berezhiani)

Int. Workshop "Low dimensional physics and gauge principles", S. Matinyan Fest, Tbilisi, Georgia, Sept. 2011 (invited talk of Z. Berezhiani)

F.L. Villante gave a seminar in Milan (October 2011)

L. Pilo gave a seminar in Ferrara (July 2011)

Z. Berezhiani gave seminars at the Theoretical Physics Institute, Univ. Minnessota, USA (June 2011), at the JINR, Dubna, Russia (August 2011), at the Univ. of Tennessee, Knoxville, USA (Sept. 2011), at the Tbilisi State Univ., Georgia (Nov. 2011) and at the Scuola Normale Superiore, Pisa (Nov. 2011).

Publications in journals, proceedings and preprints

[1] M. Cirelli, G. Corcella, A. Hektor, G. Hutsi, M. Kadastik, P. Panci, *et al.*,
PPPC 4 DM ID: A Poor Particle Physicist Cookbook for Dark Matter Indirect Detection,
JCAP **1103** (2011) 051.

[2] N. Fornengo, P. Panci and M. Regis,
Long-Range Forces in Direct Dark Matter Searches,
Phys. Rev. D **84** (2011) 115002.

[3] D. Comelli, F. Nesti and L. Pilo,
Stars and (Furry) Black Holes in Lorentz Breaking Massive Gravity,
Phys. Rev. D **83**, 084042 (2011).

[4] D. Comelli, M. Crisostomi, F. Nesti and L. Pilo,
Finite energy for a gravitational potential falling slower than $1/r$*,*
Phys. Rev. D **84**, 104026 (2011).

[5] D. Comelli, M. Crisostomi, F. Nesti and L. Pilo,
Spherically Symmetric Solutions in Ghost-Free Massive Gravity,
Phys. Rev. D **85**, 024044 (2012) [arXiv:1110.4967 [hep-th]].

[6] F. L. Villante, A. Ianni, F. Lombardi, G. Pagliaroli and F. Vissani,
A Step toward CNO solar neutrinos detection in liquid scintillators,
Phys. Lett. B **701**, 336 (2011).

[7] F. L. Villante,
Observational constraints on the solar opacity profile,
Nucl. Phys. Proc. Suppl. **217**, 115 (2011).

[8] M. Mannarelli, M. Mitra, F. L. Villante and F. Vissani,
Non-Standard Neutrino Propagation and Pion Decay,
JHEP **1201**, 136 (2012) [arXiv:1112.0169 [hep-ph]].

[9] Z. Berezhiani and A. Gazizov,
Neutron Oscillations to Parallel World: Earlier End to the Cosmic Ray Spectrum?,
arXiv:1109.3725 [astro-ph.HE], Phys. Rev. D – in press

2 Cosmology and Dark Matter (PD51)

Members: Z. Berezhiani, M. Crisostomi, E. Luzio, M. Mitra, L. Pilo, F. Tortorici and **F.L. Villante**. They worked in collaboration with L. Canton and C. Broggini (INFN-Padova), A. Serenelli (UAM-Barcellona), D. Comelli and F. Nesti (INFN-Ferrara), A. Riotto (CERN and INFN-Padova), A. Drago (University of Ferrara), D. Blas (IPT, Lausanne).

Scientific work

The research activity has been focused on the following topics:

i) Modifications of gravity. We have studied modification of gravity at large distances. We focused our activity on both the internal consistency of such models and on their phenomenological implications. In particular, the Stuckelberg formulation that requires an additional non dynamical, god given metric is compared with an alternative approach where the extra metric is dynamical. The physically important cases of spherically symmetric solutions and cosmological Friedman Robertson Walker solutions are discussed. The bottom line is that the formulation of massive gravity with two dynamical metrics works better than the Stuckelberg one. However, compared with general relativity, massive gravity is less predictive at the scale of the solar system due to strong coupling.

ii) Big Bang Nucleosynthesis. The primordial abundance of ^{7}Li as predicted by Big Bang Nucleosynthesis (BBN) is more than a factor 2 larger than what observed in metal poor halo stars. We analyzed the possibility that this discrepancy originates from incorrect assumptions about the nuclear reaction cross sections relevant for BBN. In order to do this, we introduced an efficient method to calculate the response of the ^{7}Li primordial abundance to an arbitrary modification of the nuclear reaction rates. We applied our approach to the various possible ^{7}Be destruction channels: See Fig.2. We improved with respect to previous analysis by introducing a better description of the nuclear processes. As a results of this, the parameter space for a nuclear physics solution of the ^{7}Li puzzle is considerably reduced.

iii) Neutrino phenomenology. Motivated by the initial findings of the OPERA experiment, we discussed the hypothesis that neutrino propagation does not obey Einstein special relativity. Under a minimal set of modifications of the standard model Lagrangian, we considered the implications of non standard neutrino propagation on the description of neutrino interactions and, specifically, on the pion decay process. We have shown that all the different dispersion relations which were proposed to explain the (probably erroneous) OPERA results, imply huge departures from the standard expectations. The decay channel $\pi^+ \to e^+\nu_e$ becomes significantly larger than in the standard scenario, and may even dominate over $\pi^+ \to \mu^+\nu_\mu$. Moreover, the spectral distribution of neutrinos produced in the decay processes and the probability that a pion decays in flight in neutrinos show large deviations from the standard results.

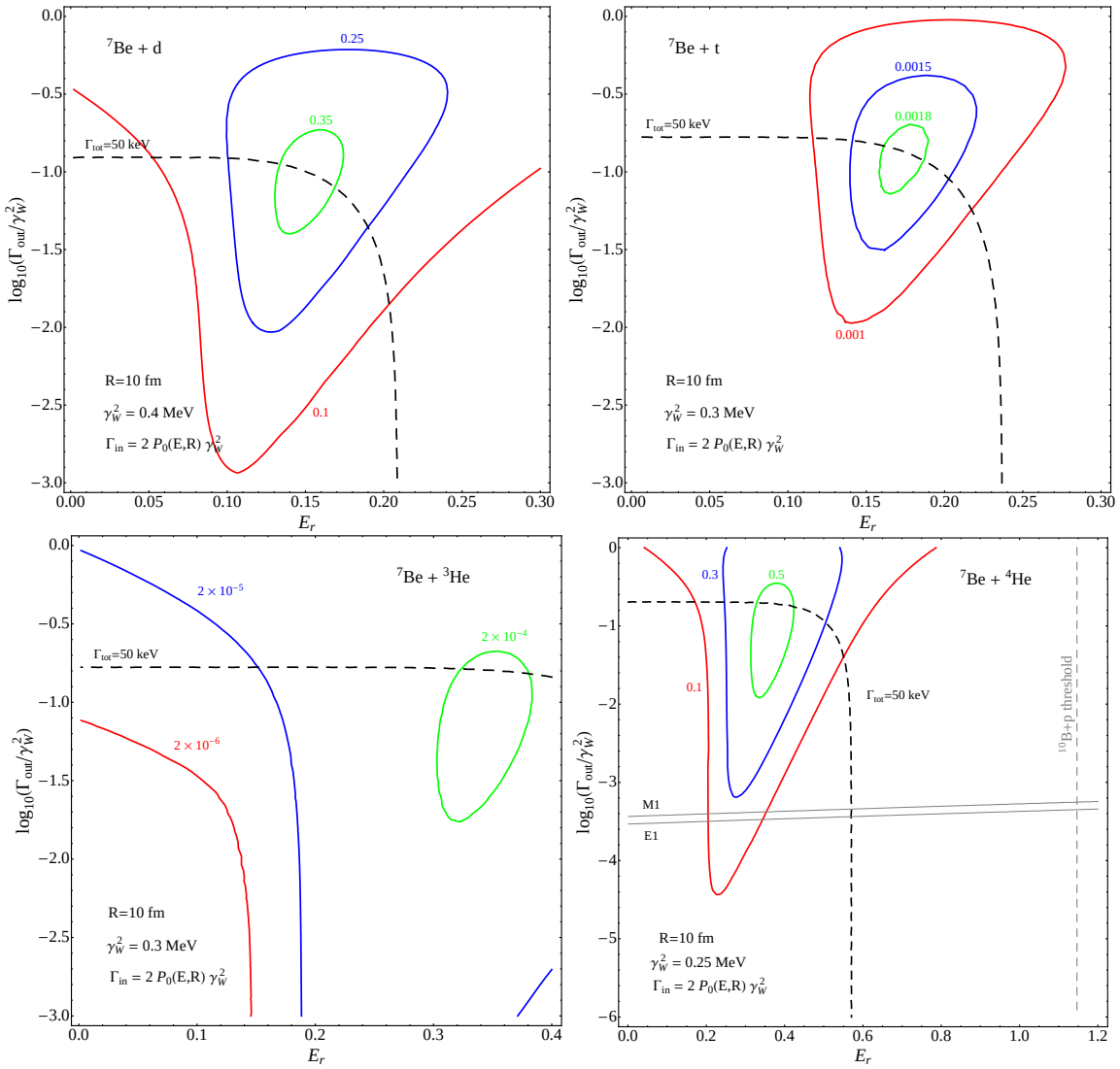

Figure 2: The coloured lines show the fractional reduction of the primordial ^{7}Li abundance that can be achieved by a resonance in the $^7\mathrm{Be} + a$ reaction. The various panels correspond to $a = d$, t, ^{3}He and ^{4}He, respectively, starting from the upper-left corner. The black dashed lines correspond to the condition $\Gamma_{\mathrm{tot}}(E_r, R) = 50\,\mathrm{keV}$, which is the limit for narrow resonance. The gray solid lines in the lower-right panel correspond to the upper limits for Γ_{out} when we assume E1 and M1 electromagnetic transitions to ^{11}C ground state.

Conferences, seminars and other activities

International EuroPhysics Conference on High Energy Physics, Grenoble, France July 2011 (talk by L. Pilo).

International Workshop on Infrared Modification of Gravity, ICTP, Trieste Italy, September 2011 (talk by L. Pilo).

International Workshop on *Beyond Three Family Neutrino Oscillations*, LNGS, Assergi (AQ), Italy, May 2011 (invited talk of F.L. Villante).

International Workshop on *The origin of elements: A modern perspective*, ECT*, Trento, Italy, May 2011 (invited talk of F.L. Villante).

International Workshop on *Topics in Astroparticle and Underground Physics (TAUP2011)*, Munich, Germany, September 2011 (talk of F.L. Villante).

15th Int. School on "Particles and Cosmology 2011", Troitsk, Russia, May-June 2011 (invited lecture of Z. Berezhiani)

Int. Institute CETUP* on "Experimental and Theoretical Underground Physics", Black Hills, S. Dakota, USA, June 2011 (two seminar talks of Z. Berezhiani)

Int. Conf. on "Astrophysics, Clocks and Fundamental Constants"; ACFC 2011, Bad Honeff, Germany, July (invited lecture of Z. Berezhiani)

Int. Conf. on "Recent Advances in Quantum Field and String Theory", Tbilisi, Georgia, Sept. 2011 (invited talk of Z. Berezhiani)

Int. Workshop "Low dimensional physics and gauge principles", S. Matinyan Fest, Tbilisi, Georgia, Sept. 2011 (invited talk of Z. Berezhiani)

F.L. Villante gave a seminar in Milan (October 2011). L. Pilo gave a seminar in Ferrara (July 2011). Z. Berezhiani gave seminars at the Theoretical Physics Institute, Univ. Minnessota, USA (June 2011), at the JINR, Dubna, Russia (August 2011), at the Univ. of Tennessee, Knoxville, USA (Sept. 2011), at the Tbilisi State Univ., Georgia (Nov. 2011) and at the Scuola Normale Superiore, Pisa (Nov. 2011).

2D–IDAPP Meeting, APC Paris, France, 20-22 June (talk of M. Crisostomi).

Publications in journals, proceedings and preprints

[1] F. L. Villante, A. Ianni, F. Lombardi, G. Pagliaroli and F. Vissani,
A Step toward CNO solar neutrinos detection in liquid scintillators,
Phys. Lett. B **701** (2011) 336

[2] F. L. Villante,
Observational constraints on the solar opacity profile,
Nucl. Phys. Proc. Suppl. **217** (2011) 115

[3] M. Mannarelli, M. Mitra, F. L. Villante and F. Vissani,
Non-Standard Neutrino Propagation and Pion Decay,
arXiv:1112.0169 [hep-ph], JHEP **1201** (2012) 136

[4] D. Comelli, F. Nesti and L. Pilo,
Stars and (Furry) Black Holes in Lorentz Breaking Massive Gravity,
Phys. Rev. D **83** (2011) 084042

[5] D. Comelli, M. Crisostomi, F. Nesti and L. Pilo,
Finite energy for a gravitational potential falling slower than $1/r$*,*
Phys. Rev. D **84** (2011) 104026

[6] D. Comelli, M. Crisostomi, F. Nesti and L. Pilo,
Spherically Symmetric Solutions in Ghost-Free Massive Gravity,
arXiv:1110.4967 [hep-th], Phys. Rev. D **85** (2012) 024044

[7] D. Comelli, M. Crisostomi, F. Nesti and L. Pilo,
FRW Cosmology in Ghost Free Massive Gravity,
arXiv:1111.1983 [hep-th]

[8] Z. Berezhiani and A. Gazizov,
Neutron Oscillations to Parallel World: Earlier End to the Cosmic Ray Spectrum?,
arXiv:1109.3725 [astro-ph.HE]

Astrophysics and high energy physics (CT51)

Members: G. Pagliaroli (30%), **M. Mannarelli (100%)** and F. Vissani (40%). In 2011, the group worked in collaboration with ML. Costantini, V. Tello, M. Nemevsek, F. Nesti, G. Senjanovic, F. Rossi-Torres, F. L. Villante, A. Ianni, F. Lombardi, C. Manuel, J. Soto, M. Escobedo, R. Anglani, M. Ruggieri, G. Colucci.

Scientific work

The scientific achievements concern several aspects of gravitational waves interferometers, neutrino physics and compact stars in the framework of high energy physics. The gravitational wave search, within the VIRGO and LIGO scientific collaborations, regarded several astronomical sources, including emitters of continuous signals as binary black holes and deformed neutron stars, as well as sources of bursts of gravitational waves, as magnetars. Collective modes associated with gravitational wave instabilities of compact stars were also studied. Of particular interest have been the results of the S5 scientific

run of LIGO [16], which allowed, among various things, to constrain the parameter space for maximally deformed compact sources. The investigation of the properties of neutrinos was pursued aiming at various goals in connection with neutrinoless double beta decays as well as employing them as a probe for supernovae collapse and the CNO solar cycle. Quite remarkable was the result in [9], where it has been shown that the Large Hadron Collider has the potential to probe the scale of left-right symmetry restoration. Finally, the binding of bound states in a thermal medium relevant for the quark epoch of the Universe was studied in [18], shedding light on the dissociation mechanism for various values of the relative velocity between the bound state and the thermal medium.

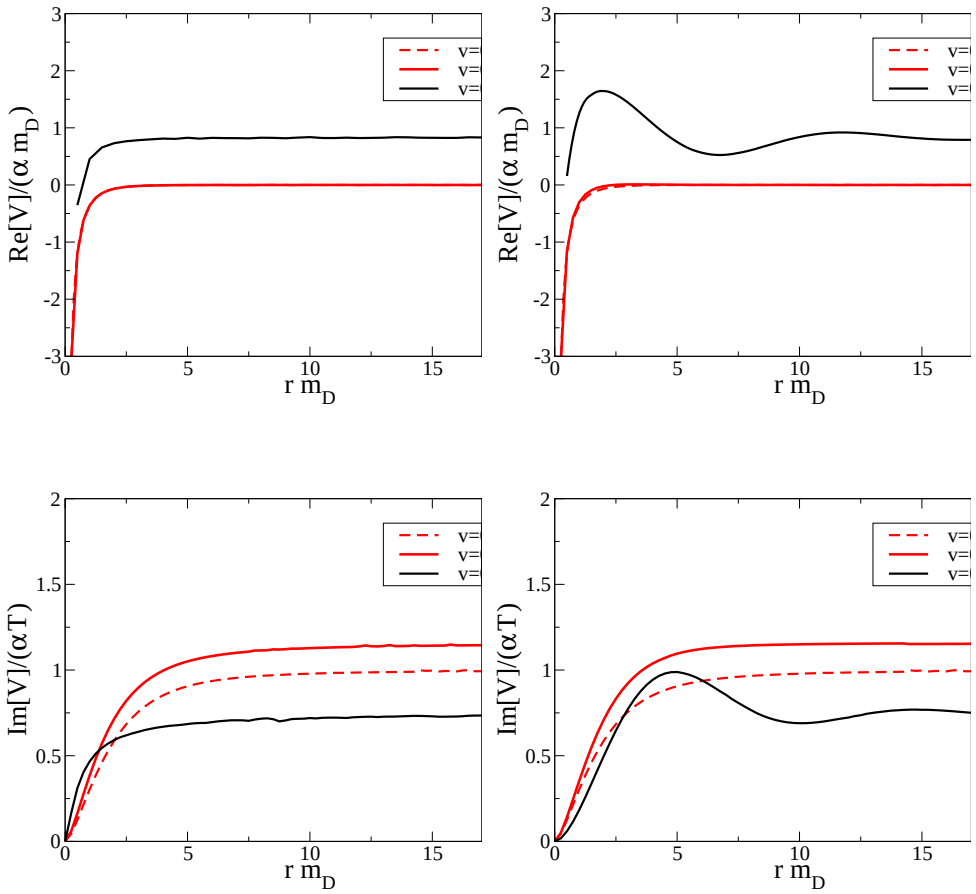

Figure 3: Real (upper panels) and imaginary (lower panels) parts of the potential between a quark and an antiquark moving with velocities $v = 0$, 0.55, 0.99 with respect to the thermal bath. Right (left) panels correspond to the direction parallel (perpendicular) to the velocity of the thermal medium. From Ref. [18].

Conferences, seminars and other activities

Talks by F. Vissani:
Apr.: *Multi-Messenger Astronomy of Cosmic Rays* at KIAA, Beijing: talk on TeV neutrinos from SNR: How to get predictions with error-bars?
May: *RICAP 2011*, talk on Expectations for High-Energy Neutrinos from Galactic Sources
June: Lectures on neutrino physics at the PhD course of Milano University
June: Workshop *Looking at the neutrino sky* at ICTP, Trieste, talk On the detectability of HE galactic neutrino sources.
July: *1st CAPPA Summer School on High Energy Astrophysics*, Dublin, Ireland; lecture on Progresses in Neutrino Astronomy
July: *International Neutrino Summer School 2011*, Geneva, Switzerland; lecture on The Standard Model and the current physics scene at the beginning of LHC
September: *SIF XCVII Congresso Nazionale*, talk on High Energy Neutrino Astronomy: From the Hope for Surprises to Predictions
October: *Frontiers in Neutrino Physics*, Paris, France: talk on SN1987A, was it what we expected?
October: *Second PHYSUN Workhop*, LNGS, Italy, summary talk on PHYSUN-II: Impressions and Conclusive Remarks
Other commitments of F. Vissani:
Coordinator of the LNGS theory group; Co-organizer of the LNGS seminar series; SIF referent person at LNGS; Member of the scientific committee for the ICRANet-INFN agreement. INFN representative in the Science Advisory Committee (SAC) of ApPEC/ASPERA. Member of the scientific council of the Groupement de Recherche Neutrino (CEA and IN2P3)

Talks by M. Mannarelli:
April: Seminar given at the University of Florence on superfluid quark matter
May: *Compstar 2011 Workshop*, Catania, Italy, talk on Superfluid compact stars
September: *The Network Workshop TORIC*, Heraklion, Crete, Greece 2011, talk on Non-relativistic bound states across a thermal medium.
December: *Xmas workshop*, Bari, Italy, talk on Pion decay and superluminal neutrinos

Other commitments of M. Mannarelli:
Scientific secretary of the LNGS; Co-organizer of the LNGS seminar series.

Publications in journals and proceedings

[1] T. Accadia *et al.* ,
The seismic Superattenuators of the Virgo gravitational waves interferometer,
Journ. of Low Freq. Noise and Act. Contr. **30** (2011) 63

[2] T. Accadia *et al.*,
Automatic alignment system during the second science run of the Virgo interferom-

eter,
Astropart. Phys. **34** (2011) 327

[3] T. Accadia *et al.*,
Calibration and sensitivity of the Virgo detector during its second science run,
Class. Quant. Grav. **28** (2011) 025005 [Erratum-ibid. **28** (2011) 079501] [arXiv:1009.5190 [gr-qc]].

[4] T. Accadia *et al.*,
A state observer for the Virgo inverted pendulum,
Rev. Sci. Instr. **82** (2011) 094502

[5] T. Accadia *et al.*,
Performance of the Virgo interferometer longitudinal control system during the second science run,
Astropart. Phys. **34** (2011) 521

[6] F. Vissani and G. Pagliaroli,
The diffuse supernova neutrino background: Expectations and uncertainties derived from SN1987A,
Astron. Astrophys. **528** (2011) L1

[7] G. Pagliaroli and F. Vissani,
Supernova neutrinos and gravitational waves,
Nucl. Phys. Proc. Suppl. **217** (2011) 278

[8] F. Vissani, G. Pagliaroli and M. L. Costantini,
A parameterized model for supernova electron antineutrino emission and its applications,
J. Phys. Conf. Ser. **309** (2011) 012025

[9] V. Tello, M. Nemevsek, F. Nesti, G. Senjanovic and F. Vissani,
Left-Right Symmetry: from LHC to Neutrinoless Double Beta Decay,
Phys. Rev. Lett. **106** (2011) 151801

[10] F. Vissani, G. Pagliaroli and F. Rossi-Torres,
The use of supernova neutrinos to monitor the collapse, to search for gravity waves, to probe neutrino masses,
Int. J. Mod. Phys. D **20** (2011) 1873

[11] T. Accadia *et al.*,
Status of the Virgo project,
Class. Quant. Grav. **28** (2011)114002

[12] J. Abadie *et al.*,
Search for Gravitational Wave Bursts from Six Magnetars,
Astrophys. J. **734** (2011) L35

[13] F. L. Villante, A. Ianni, F. Lombardi, G. Pagliaroli and F. Vissani,
A Step toward CNO solar neutrinos detection in liquid scintillators,
Phys. Lett. B **701** (2011) 336

[14] J. Abadie *et al.* ,
Beating the spin-down limit on gravitational wave emission from the Vela pulsar,
Astrophys. J. **737** (2011) 93

[15] T. Accadia *et al.* ,
The Virgo interferometer for gravitational wave detection,
Int. J. Mod. Phys. D **20** (2011) 2075

[16] J. Abadie *et al.*,
Directional limits on persistent gravitational waves using LIGO S5 science data,
Phys. Rev. Lett. **107** (2011) 271102

[17] J. Abadie *et al.*,
Search for gravitational waves from binary black hole inspiral, merger and ringdown,
Phys. Rev. D **83** (2011) 122005

[18] M. A. Escobedo, J. Soto and M. Mannarelli,
Non-relativistic bound states in a moving thermal bath,
Phys. Rev. D **84** (2011) 016008

[19] R. Anglani, M. Mannarelli and M. Ruggieri,
Collective modes in the color flavor locked phase,
New J. Phys. **13** (2011) 055002

[20] M. Mannarelli, G. Colucci and C. Manuel,
Dissipative processes in superfluid neutron stars,
AIP Conf. Proc. **1343** (2011) 577

Lattice QCD (PI12)

Sign problem and topology in lattice field theories: non-zero baryonic density QCD, Aoki phases and models with theta term. Member: **Giuseppe Di Carlo (100%)** in collaboration with V. Azcoiti, E. Follana, M. Giordano, A. Vaquero Universidad de Zaragoza (Spain).

We are running extensive simulations of QCD in the Aoki phase with Wilson fermions in order to clarify the actual situation about the possible existence of other phases in this region of parameter space and the related issues about the symmetries of the spectral density of the Hermitian Wilson operator.

We are finalizing the study of the analogous of the hermitian-Wilson spectral flow for staggered fermions, in order to have a mathematical well founded definition of topological

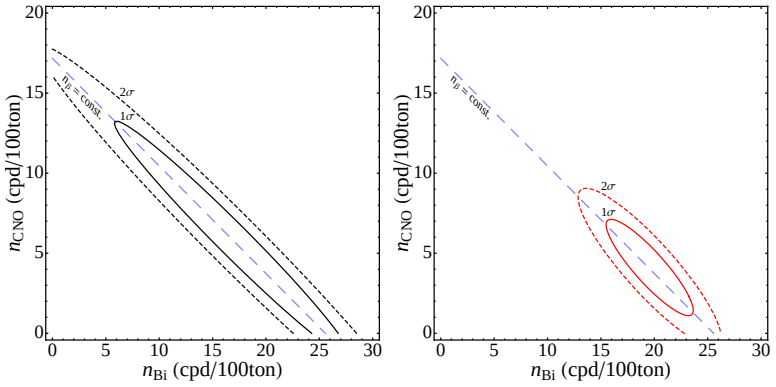

Figure 4: *1σ and 2σ allowed regions in the plane $(n_{\rm Bi}, n_{\rm CNO})$ obtained by a fit to simulated data, assuming a detector mass $M = 100\,$ton, an observation period $\Delta t = 1\,$yr and an initial $\alpha-$decay rate of Po-210 equal to $n_{\rm Po,0} = 2000\,$cpd/100ton. Left panel: using only the energy distribution of the events. Right panel: when the information from the time evolution of Po-210 decay rate is included, the error in the reconstructed CNO neutrino signal is considerably reduced.*

charge in theories with staggered fermions; a comparision with the corresponding operator for Wilson fermions, in terms of numerical complexity and efficiency, has been performed. Preliminary results have been presented to the annual Lattice conference.

We are studying the issue on universality in the presence of a theta term using numerical methods we developed in the past years; the behaviour of the topological order parameter as a function of theta has been used to characterize the critical behaviour of the $\theta = \pi$ theory in three different lattice realizations of O(3)-CP(1) model, relevant for the testing of the Haldane conjecture.

Publications in journals and proceedings

[1] V. Azcoiti, G. Di Carlo, E. Follana, A. Vaquero,
Spectral Flow and Index Theorem for Staggered Fermions,
arXiv:1111.3502, to appear in PoS (Lattice 2011).

Theory Group and LNGS

There are several direct connections between the research at the LNGS Theory Group and the INFN experiments on astroparticle physics: this applies to cosmic rays, high and low energy neutrinos, search for dark matter, gravity, etc. Here, certain results obtained in 2011 that have a rather direct connection with the existing experimental activities hosted at the LNGS are highlighted. They regard the search for solar neutrinos from the CNO cycle, the mechanism for neutrinoless double beta decay, and the implications of superluminal neutrinos in longbaseline neutrino experiments. In the following, we present briefly the above mentioned results, illustrating them by mean of some figures.

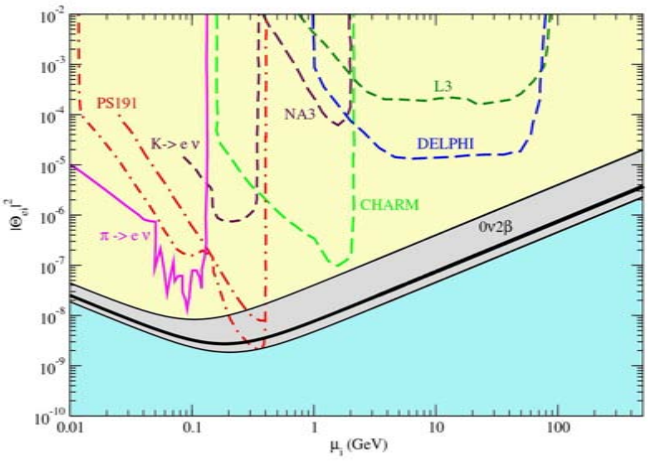

Figure 5: *Bounds on the mixing between the electron neutrino and a heavy neutrino. The upper thin black line corresponds to old nuclear matrix elements for the neutrinoless double beta decay; the thick black the revised ones; the lower thin black line is a conservative assessment on the residual uncertainty. For comparison, we show other experimental constraints, as compiled in Atre, Han & Pascoli 2009.*

- Fig. 4, from Villante et al., Phys.Lett. B701 (2011) 336, illustrates that the Bi-210 background $n_{\rm Bi}$ that provides the major limitation for the extraction of the CNO solar neutrino signal $n_{\rm CNO}$ in ultrapure liquid scintillators can be determined by looking at the time evolution of $\alpha-$decay rate ($n_{\rm Po}$) of Po-210 nuclei.

- Fig. 5, from Mitra et al., Nucl.Phys. B856 (2012) 26, depicts the constraints on the masses and mixing angles of heavy sterile (right-handed) neutrinos, showing the very important (and possibly dominant) role played for the neutrinonoless double beta decay in this range of masses.

- Fig. 6, from Mannarelli et al., JHEP 1201 (2012) 136, argues that superluminal neutrinos with velocities larger than 2 parts in 100,000, compatible with the 2011 analysis of OPERA collaboration (unpublished), would not be compatible with a proper functioning of the pion decay tunnel.

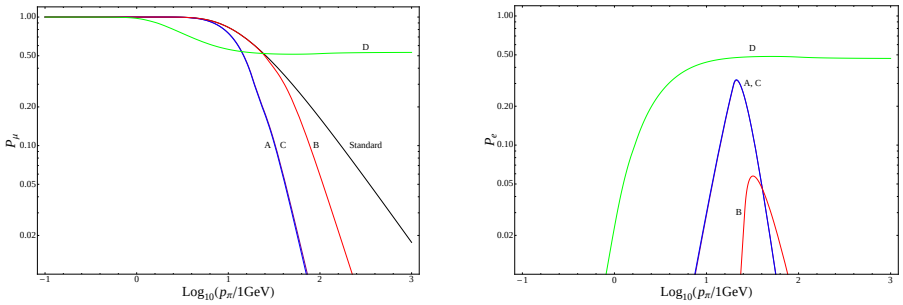

Figure 6: *Left Panel: Probability that a pion produces a muon neutrino in a tunnel of length* $L = 1\,\mathrm{km}$ *as function of the pion momentum. Right Panel: Probability that a pion produces an electron neutrino in a tunnel of length* $L = 1\,\mathrm{km}$ *as function of the pion momentum. The labels A, B, C and D refer to various scenarios for superluminal neutrinos considered in the literature.*

Finally, a special mention is due to Giuseppe Di Carlo, who offered his collaboration to Servizio Calcolo to understand the origin of the OPERA anomaly (2011) and realized an interesting experiment in collaboration with Bellotti, Broggini, Laubenstein and Menegazzo. This experiment is illustrated by mean of Fig. 7, taken from Bellotti et al., Phys.Lett. B710 (2012) 114 and briefly described below.

Starting from June 2011, the activity of a ^{137}Cs source has been measured by means of a HPGe detector installed deep underground in the Gran Sasso Laboratory. In total about 5100 energy spectra, one hour measuring time each, have been collected. These data allowed the search for time variations of the decay constant with periods from a few hours to 1 year. No signal with amplitude larger than $9.6 \cdot 10^{-5}$ at 95% C.L. has been detected. These limits are more than one order of magnitude lower than the values on the oscillation amplitude reported in literature.

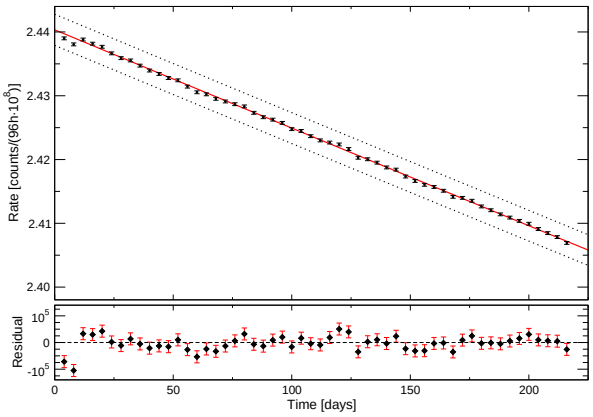

Figure 7: *Detected activity of the ^{137}Cs source. Dead-time corrected data are summed over 96 hours. The first two points correspond to the beginning of data taking, when the set-up was stabilizing, and they are not considered in the analysis. Dotted lines represent a 0.1% deviation from the exponential trend. Residuals (lower panel) of the measured activity to the exponential fit. Error bars include statistical uncertainties and fluctuations in the measured dead time.*

The XENON100 Dark Matter Experiment

E. Aprile[a *], M. Aglietta[b], M. Alfonsi[c], K. Arisaka[d], F. Arneodo[e], A. Askin[f], C. Balan[g], L. Baudis[f], B. Bauermeister[h], A. Behrens [f], P. Beltrame [d], K. Bokeloh[i], A. Breskin[j], A. Brown[k], E. Brown [i], F. Bruenner [l], G. Bruno[e], R. Budnik[a], A. Cahill[d], J. Cardoso[g], W.T. Chen[m], B. Choi[a], D. Cline[d], A.P. Colijn[c], H .A. Contreras[a], J.-P. Cussonneau[m], P. Decowski[c], E. Duchovni[j], S. Duval[m], S. Fattori[n], A. Ferella[f], W. Fulgione[b], F. Gao[o], M. Garbini[p], C. Ghag[d], K.L. Giboni[o], L. Goetzke, [a], C. Grignon[h], E. Gross[j], W. Hampel[l], V. Hannen[i], J. Hasell[n], F. Kaether[l], G. Kessler[f], A. Kish[f], C. W. Lam[d], J. Lamblin[m], H. Landsman[j], R.F. Lang[k], M. Le Calloch[m], D. Lellouch[j], L. Levinson[j], C. Levy[i], K.E. Lim[a], Q. Lin[o], F. Linde[c], S. Lindemann[l], M. Lindner[l], J.A.M. Lopes[g], K. Lung[d], T. Marrodan-Undagoitia[f], Y. Mei[h], F.V. Massoli[p], A.J. Melgarejo[a], Y. Meng[d], M. Messina[a], A. Molinario[b], E. Nativ[j], K. Ni[o], U. Oberlack[n], S.E.A. Orrigo[g], E. Pantic[d], V. Patricio[g], R. Persiani[p], G. Plante[a], N. Priel[j], R. Santorelli[f], L. Scotto Lavina[m], A. Rizzo[a], S. Rosendahl[i], G. Sartorelli[p], J. M. F. dos Santos[g], J. Schreiner[l], P. Scovell[d], M. Schumann[f] , M. Selvi[p], P. Shagin[h], H. Simgen[l], A. Teymourian[d], D. Thers[m], O. Vitells[j], H. Wang[d], M. Weber[l], C. Weinheimer[i]

[a] Department of Physics, Columbia University, New York, NY 10027, USA
[b] INFN Torino, Italy
[c] Nikhef, the Netherlands
[d] University of California, Los Angeles
[e] INFN, Laboratori Nazionali del Gran Sasso, Assergi, 67100, Italy
[f] Physics Department, University of Zurich, Switzerland
[g] Department of Physics, University of Coimbra, R. Larga, 3004-516, Coimbra, Portugal
[h] Department of Physics and Astronomy, Rice University, Houston, TX 77251, USA
[i] Institut für Kernphysik, Wilhelms Universität, 48149 Münster, Germany
[j] Weizmann Institute, Israel
[k] Purdue University, USA
[l] Max-Planck-Institut für Kernphysik, Saupfercheckweg 1, 69117 Heidelberg, Germany
[m] Subatech Laboratory, University of Nantes, 44307 Nantes, France
[n] Institut für Physik, Johannes Gutenberg Universität Mainz, 55099 Mainz, Germany
[o] Shanghai Jiao Tong University, Shanghai, China
[p] University of Bologna and INFN-Bologna, Bologna, Italy

[*] Spokesperson

Abstract

This report summarizes the current status of the XENON100 experiment and the XENON1T project. XENON100 data from a $\mathcal{O}(100)$ -day-search for dark matter have been published, excluding fractions of expected dark matter parameter space. Inelastic dark matter scattering off iodine as an explanation for the DAMA/LIBRA annual modulation signature has now been excluded as well. Data taking with XENON100 continues under improved conditions to push the sensitivity further. In parallel, the XENON1T project is making progress. An area in Hall B has been assigned to XENON1T and the detailed design of the detector parts and infrastructures is ongoing.

XENON100

Published Data

We published the results from 100.9 live days of data, acquired between January and June 2010. No evidence for dark matter was found. This leads to the most stringent limit on

dark matter interactions today, excluding spin-independent elastic WIMP-nucleon scattering cross sections above $7.0 \times 10^{-45}\,\mathrm{cm}^2$ for a WIMP mass of $50\,\mathrm{GeV/c}^2$ at 90% confidence level [1]. The paper has received more than 100 citations on SPIRES. Inelastic Dark Matter scattering off iodine as an explanation for the DAMA modulation signature is excluded by this data [2]. To accompany these major data releases, we have published an extensive report on the design and performance of the detector [3]. We also point out, incidentally, that our 2008 paper [4] is in the SPIRES Topcites +500 list.

Status of XENON100

The XENON100 detector is operating continuously since the maintenance works and ^{85}Kr purification campaign of 2010. The amount of electronegative contaminants has been constantly decreasing and a value of the electron lifetime (survival probability of electrons during its drifting through the LXe) of $\sim 580\,\mu$s or more than 1 m drift has been achieved. Figure 1 shows the data taken since early 2011.

In this present run, we are collecting much more calibration data than for the previous data set, both quantitatively, as well as qualitatively using additional sources, such as a Th-232 source for azimuthally symmetric electronic recoil band calibration. In addition, extended calibration data from activated xenon lines following the neutron calibration earlier this year was taken. Additional dedicated calibration data addressing detailed questions have also been taken. This allows to refine our analysis and algorithms further. In addition, the lower background in the present run due to the processing of the xenon through the krypton column, together with a lowered S2 trigger threshold due to improved electronics, allows dark matter data taking with increased sensitivity. The dark matter data taken under these improved conditions already exceed the previously published livetime, is blinded in the region of interest, and under thorough analysis.

Outlook for XENON100

The improved running conditions of XENON100 allow to further push the sensitivity of XENON100 to remain the world-leading experiment to search for Weakly Interacting Massive Particles. We plan to continue data taking to further increase the sensitivity of the experiment to elastic spin-independent and spin-dependent WIMP interactions but also to look for an annual modulation which would correspond to the signal claimed by the DAMA/LIBRA experiment. In March 2012 we will have completed a full year of dark matter search, but we will keep taking data until the next cryogenics maintenance is needed. We propose to continue the XENON100 Dark Matter experiment at the Laboratori Nazionali del Gran Sasso.

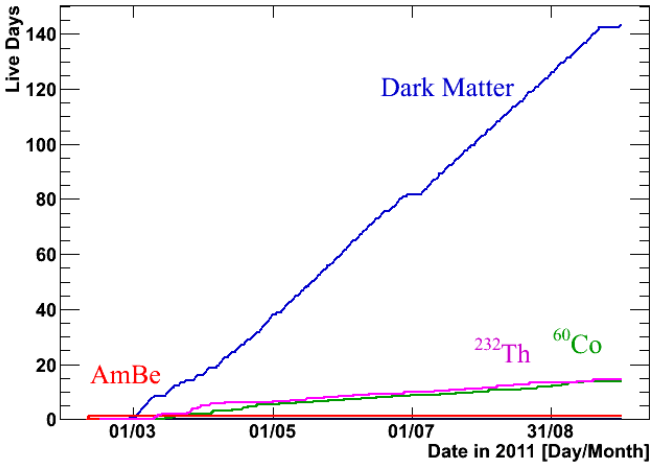

Figure 1: Data taken in the present run. The newly taken dark matter data exceeds the previously published livetime, and the amount of calibration data exceeds that available in previous runs.

XENON1T

Status of XENON1T

Good progress has been made since the last meeting of the scientific committee. INFN has approved XENON1T to be located in hall B at LNGS. A XENON memorandum of understanding (MoU) has been written and it is meanwhile signed by all involved parties. A common fund has been installed. It will be used for some of the XENON100 operating costs. The common fund in 2012 will also be used to cover some common infrastructure items of XENON1T. A large fraction of the required construction funds for XENON1T are already approved (i.e. in place) and significant investments have already been made or will be made very soon (xenon inventory, analytics, PMTs, ...). Some remaining grant applications will be submitted and decided rather soon. The over-all funding situation of XENON1T is thus already very good.

The layout of XENON1T is shown in Figure 2. The collaboration is aware of the fact that some space must be left free to allow removal of ICARUS T600 components, but we would like to emphasize that the available space for the water tank (shielding) is a critical issue for XENON1T and its scalability. The original design had an 11 m diameter water tank, a reasonable compromise appears to be a diameter of 9.60 meters.

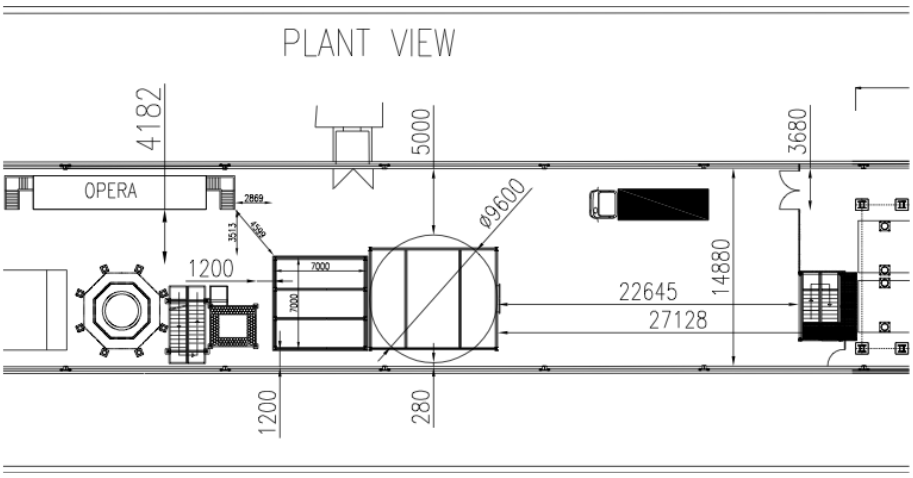

Figure 2: The layout of XENON1T in hall B.

Developments towards XENON1T

Progress has been made on various topics and components of XENON1T. We will highlight below the work which is ongoing towards the most challenging requirements for XENON1T: a) reduce the Kr concentration in Xe below 1 ppt and develop the required analytical tools to establish the level; b) develop the tools to reduce and measure Rn related background; c) demonstrate the ability to operate a LXe TPC with a nominal field of 1 kV/cm over 1 meter drift and e) demonstrate the ability to purify the LXe to sub-ppb level required for the long drift using continuously circulation through a hot getter at a gas flow rate of about 100 liters/minute.

In addition, we have recently finalized the choice of photosensor for XENON1T. The commercially available, 3 inch diameter, Hamamatsu R11410-MOD PMT will be used. Although QUPIDs remain an extremely promising technology, the remaining developmental issues precluding their immediate use in liquid noble gas detectors may not be addressed on a timescale compatible with the XENON1T experiment. Furthermore, it would be premature to adopt QUPIDs for XENON1T without significant testing and validation.

XENON1T distillation column: The XENON100 experiment uses a dedicated distillation column (owned and run by Columbia University) to purify xenon from traces of krypton in order to reduce the man-made beta-decay isotope ^{85}Kr . XENON1T requires a factor 100 lower krypton concentration than XENON100 to achieve a low enough background required to reach a 10^{-47} cm^2 sensitivity on the WIMP cross section. In addition to a significantly stronger Kr depletion a much higher throughput of the

column is required: During the commissioning and the operation of XENON100 several distillation runs were necessary to purify the Xenon. Therefore a distillation duration of about one month for the whole XENON1T inventory is necessary to be able to react on malfunctions of XENON1T.

Since a new and improved distillation column with the above specifications is not easily available on the market, the XENON1T collaboration has decided to develop – based on the knowledge and the experience with the present column of Columbia University – a new column, which fulfills the XENON1T requirements. This task is assigned to University of Münster. Two key features of the new column will be included in this development: Rigorous application of ultraclean materials and outbakeabilty as well as ultrasensitive detection of Kr in xenon to characterize and optimize the operation of the distillation column. The first goal can be achieved by using the very successful technologies developed for XENON100, KATRIN and GERDA. The second aim will be pursued by applying new kinds of trace analyses, such as a dedicated single atom trap at Columbia University, an ultra-sensitive rare-gas mass spectrometer following gas chromatography at Max Planck-Institute Heidelberg and the development of a novel tracer method using the short-lived isomer ^{83m}Kr from a ^{83}Rb source [5] at Unversity of Münster.

The University of Münster has hired a process engineer on a permanent position to do the development, the construction, the building and the maintaining of a new and dedicated distillation column for the XENON1T experiment at LNGS. The first design steps of the column have been pursued: the design of mass flow and the depletion of the column following the McCabe-Thiele-Method, a preliminary heat and mass flow design, a preliminary flow diagram with all components as well as the construction of the insulation vacuum tank. The packages, at which the krypton-xenon-separation takes place, have been selected to be Sulzer Laboratory Packing Ex with a diameter of 45 mm. This design yields a 4.5 m high destillation column with an effective column height of 3 m. The total weight will be less than 1 ton. The design parameters result in a purification rate of 3 kg/h at a depletion factor of 10000.

After a successful funding application by University of Münster the major components for building the distillation column have been purchased: the packages, two cold heads with He-compressors, the insulation vacuum tank, vacuum tubes, valves and pressure sensors, etc. A new 5-m-high xenon laboratory equipped with overhead cranes has been put into operation at Münster. The laboratory has a xenon handling and purification system as well as a small two-phase xenon TPC for purification measurements. This system is also a prototype for the input part of the distillation column and xenon liquifidation and recuperation has been successfully demonstrated. To measure larger krypton concentrations in xenon a system consisting of a quadrupole mass spectrometer following a LN2 cold trap (following the idea of D.S. Leonard et al., Nucl. Instr. Meth. A621 (2010)

678) has been successfully commissioned and about 100 ppt sensitivity demonstrated. The first successful steps of the mass spectrometer at Heidelberg towards ppt-sensitivity have been done after installation of the necessary equipment and instruments (see below). At Columbia University the atom trap experiment is trapping and detecting successfully noble gas atoms.

A design review by the external distillation expert Dr. Ion Cristescu/KIT has been performed in early 2012. Dr. Cristescu will collaborate with the Mnster group in finishing the design and doing experiments with a smaller test column to be built in 2012 to test new design ideas and operation parameters. **Radon Control and Monitoring:** XENON1T requires to reduce and control Rn-related backgrounds to unprecedented levels. The ^{222}Rn emanation technique described in the last XENON1T progress report was applied at Max-Planck-Institut für Kernphysik in Heidelberg to measure a getter purifier type PS4-MT50-R-2 from SAES which is intended to be used for XENON1T. At room temperature its ^{222}Rn emanation rate was found to be (0.60 ± 0.04) mBq (saturation activity). At operation temperature ($\sim$ 400°C) the rate increases to (1.42 ± 0.10) mBq. Since the purifier is part of the recirculation loop this ^{222}Rn will be transported to the TPC and will be a potential source of background. Thus, we plan to remove ^{222}Rn online from the circulating xenon by means of cryo-adsorption on activated carbon. We recently have build and commissioned a test-stand to measure the adsorption equilibrium for radon and have successfully investigated a first carbon sample.

Our main focus was on the screening of various xenon samples for krypton and electronegative impurities. For the latter we will use an atmospheric pressure ionisation mass spectrometer (APIMS) which has 10 ppt - 100 ppt sensitivity. However, xenon cannot be injected directly to the APIMS, thus the impurities must first be separated from the xenon by means of a gas chromatograph (GC). In the last months we have successfully finished the commissioning of the GC and it was recently connected to the APIMS. In the near future first tests of the fully assembled system will start. The krypton in xenon measurements are performed with a rare gas mass spectrometer and a highly customized ultrahigh purity GC setup. The system is fully operational and the background is so low that ppt-sensitivity is achievable. A first sample of one of the isotopically depleted xenon batches foreseen for XENON1T (from Iceblick) was tested and a Kr concentration of (9.7 ± 0.4) ppb was found (see Fig. 3). This is in agreement with the supplier's specification (< 300 ppb). Next, we will investigate xenon from the running XENON100 experiment whose Kr concentration can be measured independently from the XENON100 data.

XENON1T Demonstrator: to address the technical challenges associated with the operation of a LXe TPC for XENON1T, a new gas purification with continuous circulation and an apparatus called the XENON1T Demonstrator system was designed and

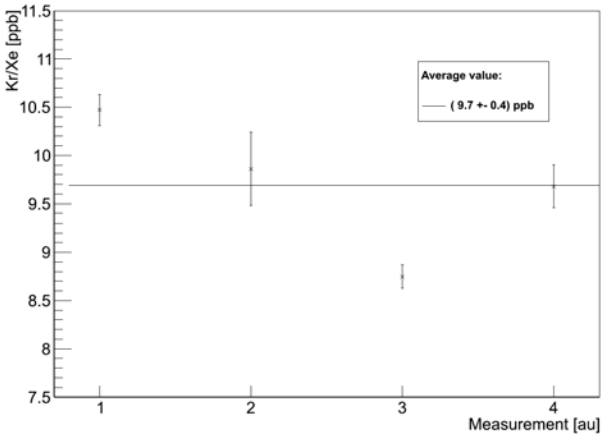

Figure 3: Preliminary results of four measurements of the krypton concentration in depleted xenon from Iceblick.

constructed at Columbia University. The demonstrator is being tested to demonstrate electron drift in liquid Xenon over distances of ∼1 m, 3 times longer than in XENON100, which requires the ability to safely and reliably apply HV at the 100 kV level and the ability to remove with high speed circulation through a hot getter the impurities introduced by materials in contact with the liquid.

The XENON1T demonstrator consists of three large vessels that contain the detector, the cooling tower, and the heat exchanger, connected through a gas system made of 1/2 stainless steel pipes, a recirculation pump and hot getter. Figure 4 shows the experimental setup operating at the Columbia Nevis Laboratory and a computer model of the cryogenic and detector vessels. For the cooling system we use an Iwatani PC-150 pulse tube refrigerator (PTR) with a 6.5 KW water-cooled He compressor with 200 W of cooling power at 165K. This PTR is the same as the one used on XENON100, connected to the inside of the chamber through a copper cold finger at the top of the cooling tower. The entire system is vacuum insulated. Xenon gas is purified by continuous circulation through a hot getter. The liquid is taken from the detector through the heat exchanger where the latent heat is transferred to the returning xenon gas stream with a very high efficiency. The use of a commercial parallel-plate heat exchanger was recently demonstrated by the Columbia group [6] to pre-cool recirculated xenon gas with an efficiency larger than 96%. A new gas system, built with 1/2 pipes and including a large capacity SAES getter and a large capacity KNF diaphragm pump, was built for the Demonstrator set-up. With this system

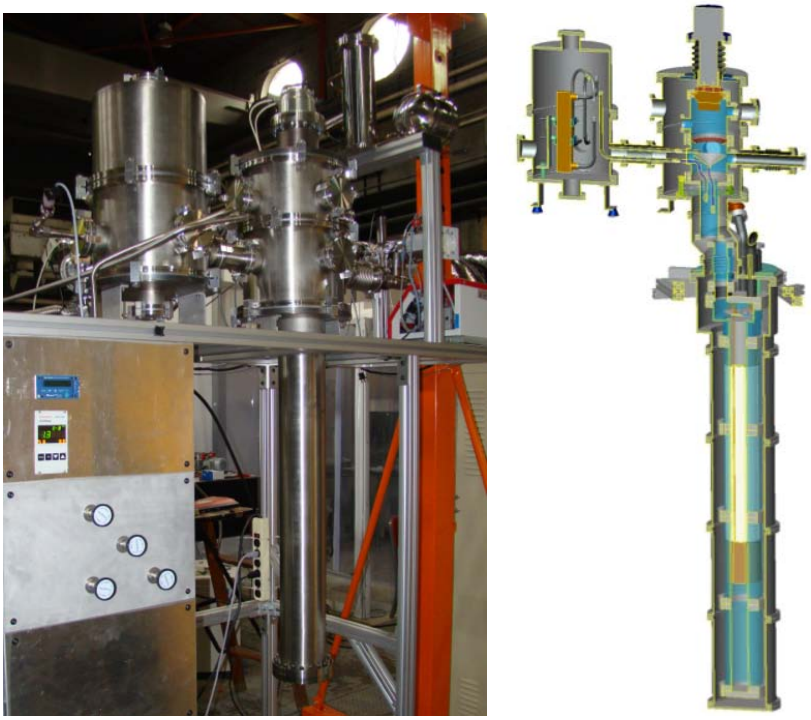

Figure 4: (Left): The XENON1T demonstrator setup at Columbia Nevis Laboratory. (Right): The computer model design of the XENON1T demonstrator.

and a larger heat exchanger than that used in [6], we have already achieved stable Xe gas flow up to 100 slpm (see Figure 5). The estimation of the heat exchange efficiency also includes the radiative heating of the heat exchanger, which was only vacuum insulated in these first tests. The inferred efficiency of the heat exchange is close to 90% at flows up to 80 slpm.

This system will allow to demonstrate the purification and HV required for XENON1T. It will also be used to test surfaces, introduce controlled impurities and verify the HV components and photosensors to be used in XENON1T.

A custom-made high voltage feedthrough, made of PTFE and a stainless steel rod, based on the original XENON100 design developed by the Columbia group, has been built and tested up to 60 kV in liquid xenon, along with a cathode mesh immersed in the liquid. The voltage was limited by the power supply. Larger size feedthroughs will be tested using a 100 kV supply in the near future. The HV system will be tested in the XENON1T Demonstrator.

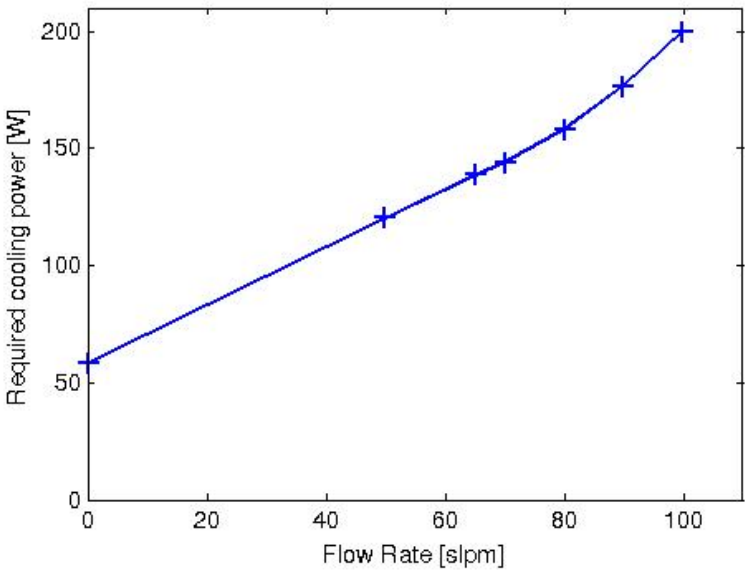

Figure 5: Cooling power required for circulation at different flow rates.

Summary

XENON100 has accumulated already another 200 days of data which are currently being analyzed. The fact that the background is lower than in previous analyses should lead to a significantly improved sensitivity covering even more of the expected WIMP parameter space. We propose to continue to run and analyze data to fully exploit the unique potential of XENON100.

Significant progress has been made in the XENON1T project. The experiment has been approved by INFN for hall B at LNGS, the MoU has been drafted and signed and a common fund is being installed. The current report describes some of the most important achievements during the last months. The space for XENON1T has been allocated and the Collaboration is working on the final design.

List of publications during 2011

- New measurement of the scintillation efficiency of low-energy nuclear recoils in liquid xenon Author(s): Plante G.; Aprile E.; Budnik R.; et al. PHYSICAL REVIEW C Volume: 84 Issue: 4 Article Number: 045805 DOI: 10.1103/PhysRevC.84.045805

Published: OCT 17 2011

- Dark Matter Results from 100 Live Days of XENON100 Data Author(s): Aprile E.; Arisaka K.; Arneodo F.; et al. Group Author(s): XENON100 Collaboration PHYSICAL REVIEW LETTERS Volume: 107 Issue: 13 Article Number: 131302 DOI: 10.1103/PhysRevLett.107.131302 Published: SEP 19 2011

- Likelihood approach to the first dark matter results from XENON100 Author(s): Aprile E.; Arisaka K.; Arneodo F.; et al. PHYSICAL REVIEW D Volume: 84 Issue: 5 Article Number: 052003 DOI: 10.1103/PhysRevD.84.052003 Published: SEP 7 2011

- Implications on inelastic dark matter from 100 live days of XENON100 data Author(s): Aprile E.; Arisaka K.; Arneodo F.; et al. PHYSICAL REVIEW D Volume: 84 Issue: 6 Article Number: 061101 DOI: 10.1103/PhysRevD.84.061101 Published: SEP 6 2011

- Material screening and selection for XENON100 Author(s): Aprile E.; Arisaka K.; Arneodo F.; et al. ASTROPARTICLE PHYSICS Volume: 35 Issue: 2 Pages: 43-49 DOI: 10.1016/j.astropartphys.2011.06.001 Published: SEP 2011

- Gator: a low-background counting facility at the Gran Sasso Underground Laboratory Author(s): Baudis L.; Ferella A. D.; Askin A.; et al. JOURNAL OF INSTRUMENTATION Volume: 6 Article Number: P08010 DOI: 10.1088/1748-0221/6/08/P08010 Published: AUG 2011

- Search for Light Dark Matter in XENON10 Data Author(s): Angle J.; Aprile E.; Arneodo F.; et al. Group Author(s): XENON10 Collaboration PHYSICAL REVIEW LETTERS Volume: 107 Issue: 5 Article Number: 051301 DOI: 10.1103/PhysRevLett.107.051301 Published: JUL 27 2011

- Study of the electromagnetic background in the XENON100 experiment Author(s): Aprile E.; Arisaka K.; Arneodo F.; et al. Group Author(s): XENON100 Collaboration PHYSICAL REVIEW D Volume: 83 Issue: 8 Article Number: 082001 DOI: 10.1103/PhysRevD.83.082001 Published: APR 19 2011

- Design and performance of the XENON10 dark matter experiment Author(s): Aprile E.; Angle J.; Arneodo F.; et al. ASTROPARTICLE PHYSICS Volume: 34 Issue: 9 Pages: 679-698 DOI: 10.1016/j.astropartphys.2011.01.006 Published: APR 2011

- Limits on the release of Rb isotopes from a zeolite based 83mKr calibration source for the XENON project
  V Hannen et al 2011 JINST 6 P10013 doi:10.1088/1748-0221/6/10/P10013

References

[1] **XENON100** Collaboration, E. Aprile *et. al.*, *Dark Matter Results from 100 Live Days of XENON100 Data*, *Phys.Rev.Lett.* (2011) [arXiv:1104.2549].

[2] **XENON100** Collaboration, E. Aprile *et. al.*, *Implications on Inelastic Dark Matter from 100 Live Days of XENON100 Data*, *Phys. Rev.* **D84** (2011) 061101, [arXiv:1104.3121].

[3] **XENON100** Collaboration, E. Aprile *et. al.*, *The XENON100 Dark Matter Experiment*, arXiv:1107.2155.

[4] **XENON** Collaboration, J. Angle *et. al.*, *First Results from the XENON10 Dark Matter Experiment at the Gran Sasso National Laboratory*, *Phys. Rev. Lett.* **100** (2008) 021303, [arXiv:0706.0039].

[5] V. Hannen, E. Aprile, F. Arneodo, L. Baudis, M. Beck, K. Bokeloh, A. Ferella, K. Giboni, R. Lang, O. Lebeda, H.-W. Ortjohann, M. Schumann, A. Spalek, D. Venos, and C. Weinheimer, *Limits on the release of Rb isotopes from a zeolite based ^{83m}Kr calibration source for the XENON project*, *JINST* (2011) [arXiv:1109.4270]. JINST 6 (2011) P10013.

[6] K. Giboni, E. Aprile, B. Choi, T. Haruyama, R. Lang, K. Lim, A. Melgarejo, and G. Plante *JINST* **6, 3002** (2011).

THE PIERRE AUGER EXPERIMENT

D. Boncioli*, A.F. Grillo[b], S. Petrera[a], V. Rizi[a], F. Salamida[a,+]
for the Auger Collaboration

[a] INFN and Dipartimento di Fisica, Università dell'Aquila - Italy
[b] LNGS-INFN - Italy
* INFN and Dipartimento di Fisica, Università di Roma Tor Vergata - Italy
+Institut de Physique Nucléaire d'Orsay (IPNO), Université Paris 11, CNRS-IN2P3, Orsay,France

Abstract

The Pierre Auger Project is an international Collaboration involving over 400 scientists from 17 countries, with the objective of studying the highest energy cosmic rays. Recent results from the Collaboration as well as further developments in the detector are presented in this report.

1 Introduction

Ultra-high energy cosmic rays are of intrinsic interest as their origin and nature are unknown. It is quite unclear where and how particles as energetic as $\simeq 10^{20}$ eV are accelerated. Over 40 years ago it was pointed out that if the highest energy particles are protons then a fall in the flux above an energy of about $\times\ 10^{19}$ eV is expected because of energy losses by the protons as they propagate from distant sources through the CMB radiation. At the highest energies the key process is photo-pion production in which the proton loses part of its energy in each creation of a Δ resonance. This is the Greisen-Zatsepin-Kuzmin (GZK) effect. It follows that at 10^{20} eV any proton observed must have come from within about 50 Mpc and on this distance scale the deflections by intervening magnetic fields in the galaxy and intergalactic space are expected to be so small that point sources should be observed. Despite immense efforts in the period since the prediction, the experimental situation remains unclear. The main problem in examining whether or not the spectrum steepens is the low rate of events which, above 10^{20} eV, is less than 1 per km^2 per century so that the particles are only detectable through the giant air showers that they create.

These showers have particle footprints on the ground of $\simeq 20$ km^2 and suitably distributed detectors can be used to observe them. Also the showers excite molecules of atmospheric nitrogen and the resulting faint fluorescence radiation, which is emitted isotropically, can be detected from distances of several tens of kilometers.

The Pierre Auger Observatory has been developed by a team of over 400 scientists from 17 countries. The Observatory comprises about 1600 10 $m^2 \times$ 1.2 m water-Cherenkov detectors deployed over 3000 km^2 on a 1500 m hexagonal grid. This part of the Observatory (the surface detector, SD) is over-looked by 24 fluorescence telescopes in 4 clusters located on four hills around the SD area which is extremely flat. The surface detectors contain 12 tonnes of clear water viewed by 3 × 9" hemispherical photomultipliers. The fluorescence detectors (FD) are designed to record the faint ultra-violet light emitted as the shower traverses the atmosphere. Each telescope images a portion of the sky of 30° in azimuth and 1°-30° in elevation using a spherical mirror of 3 m^2 effective area to focus light on to a camera of 440 × 18 cm^2 hexagonal pixels, made of photomultipliers complemented with light collectors, each with a field of view of 1.5° diameter.

An important feature of the design of the Observatory was the introduction of the hybrid technique as a new tool to study airshowers. It is used here for the first time. The hybrid technique is the term chosen to describe the method of recording fluorescence data coincident with the timing information from at least one surface detector. Employing these two complementary observation methods provides the Auger Observatory with high quality information about angular reconstruction, determination of the core position of the shower and of the types of particles in the primary cosmic rays. Comparing results from the different types of detectors also helps scientists reconcile the two sets of data and produce the most accurate results about the energy of primary cosmic rays.

2 Recent results from the Pierre Auger Cosmic Ray Observatory

2.1 The Energy Spectrum

The energy spectrum of ultra-high energy cosmic rays at energies greater than 2.5×10^{18} eV has been derived using data from the surface detector array of the Pierre Auger Observatory [1]. This measurement provided evidence for the suppression of the flux above 4×10^{19} eV and is updated here. In 2009 we extended the previous measurements to lower energies by analysing air showers measured with the fluorescence detector that also triggered at least one of the stations of the surface detector array. Despite the limited event statistics due to the fluorescence detector on-time of about 13 %, the lower energy threshold and the good energy resolution of these *hybrid* events allow us to measure the flux of cosmic rays in the region of the ankle.

The energy spectrum of hybrid events is determined from data taken between November 2005 and September 2010 [2]. Using selection criteria that are set out below, the exposure accumulated during this period was computed and the flux of cosmic rays above 10^{18} eV determined. The spectrum obtained with the surface detector array, updated using data until the end of December 2010, is combined with the hybrid one to obtain a spectrum measurement over a wide energy range with the highest statistics available [2].

The combined energy spectrum scaled with E^3 is shown in Fig. 1. The dominant systematic uncertainty of the spectrum stems from that of the overall energy scale, which is estimated to be 22%.

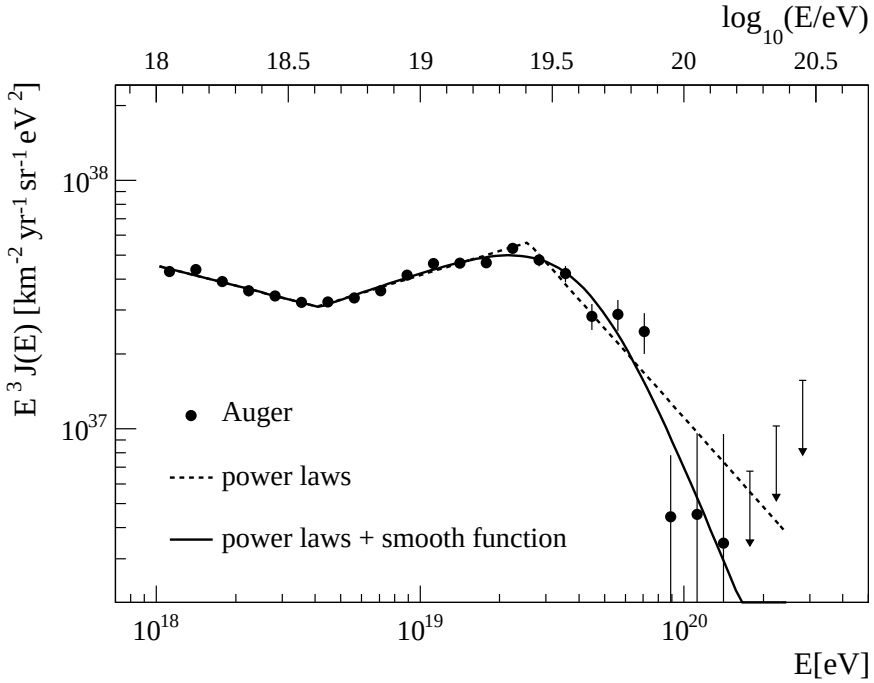

Figure 1: The combined energy spectrum [2] is fitted with two functions (see text). The systematic uncertainty of the flux scaled by E^3 due to the uncertainty of the energy scale of 22% is indicated by arrows.

The position of the ankle at $\log_{10}(E_{\rm ankle}/{\rm eV}) = 18.61 \pm 0.01$ has been determined by fitting the flux with a broken power law $E^{-\gamma}$. An index of $\gamma = 3.27 \pm 0.02$ is found below the ankle. Above the ankle the spectrum follows a power law with index 2.68 ± 0.01. In comparison to the power law extrapolation, the spectrum is suppressed by a factor two at $\log_{10}(E_{1/2}/{\rm eV}) = 19.63 \pm 0.02$. The significance of the suppression is larger than $20\,\sigma$. The suppression is similar to what is expected from the GZK effect for protons or nuclei as heavy as iron, but could in part also be related to a change of the shape of the average injection spectrum at the sources.

2.2 The Mass Composition

The atmospheric depth, X_{max} , at which the longitudinal development of a shower reaches its maximum in terms of the number of secondary particles is correlated with the mass of the incident cosmic ray particle. With the generalization of Heitler's model of electron-photon cascades to hadron-induced showers and the superposition assumption for nuclear primaries of mass A, the average depth of the shower maximum, Xmax , at a given energy E is expected to follow [3]

$$\langle X_{max} \rangle = \alpha(\ln E - \ln\langle A \rangle) + \beta \qquad (1)$$

where $\ln\langle A \rangle$ is the average of the logarithm of the primary masses. The coefficients α and β depend on the nature of hadronic interactions, most notably on the multiplicity, elasticity and cross-section in ultra-high energy collisions of hadrons with air, see e.g. [4].

At ultra high energies, the shower maximum can be observed directly with fluorescence detectors. Previously published X_{max} measurements [5], [6] as a function of energy had only limited statistics above 10^{19} eV.

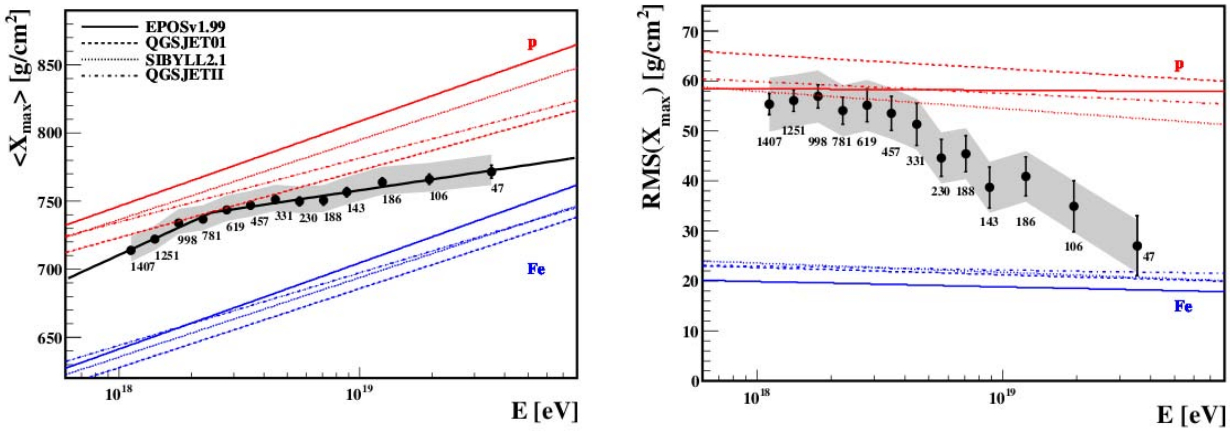

Figure 2: Measurements of X_{max} (left) and its RMS (right) as a function of energy [7].

A recent analysis [7] based on high quality and high statistics hybrid data collected with the southern site of the Pierre Auger Observatory has been addressed to the $\langle X_{max} \rangle$ measurement and its energy dependence.

The results of such measurements are presented in Fig. 2 together with predictions for proton and Fe primaries using different hadronic interaction models [7]. These models need to extrapolate the features of hadronic interactions well beyond the cms-energies accessible at man-made accelerators. Their uncertainties are correspondingly large and the wide distribution of predictions in the figure demonstrates that the systematic uncertainties in this analysis can be significant. With this caveat kept in mind, a transition from a light composition up to the ankle approaching the expectations for heavier nuclei up to 40 EeV is inferred from both the Xmax values and from its RMS values.

2.3 The Cosmic Ray Anisotropy

Between January 2004 and December 2009 the Pierre Auger Observatory has detected 69 cosmic rays events with energy in excess of 55 EeV. Their arrival directions are reported in [8] This data set is more than twice as large as the one analyzed in [9], which provided evidence of anisotropy in CR arrival directions at the 99% confidence level. The anisotropy was tested with a priori parameters through the correlation between the arrival directions of CRs and the positions of nearby active galaxies from the 12th edition of the Veron-Cetty Veron catalog of quasars and active galactic nuclei. The degree of that observed correlation has decreased from $(69^{+11}_{-13})\%$ to $(38^{+7}_{-6})\%$, to be compared with the 21% expected to occur by chance if the flux were isotropic. More data are needed to determine this correlating fraction accurately. The evidence for anisotropy has not strengthened since the analysis reported in [9].

The correlation of recent data with objects in the VCV catalog is not as strong as that observed in 2007. If the evidence for anisotropy is substantiated by future data, then

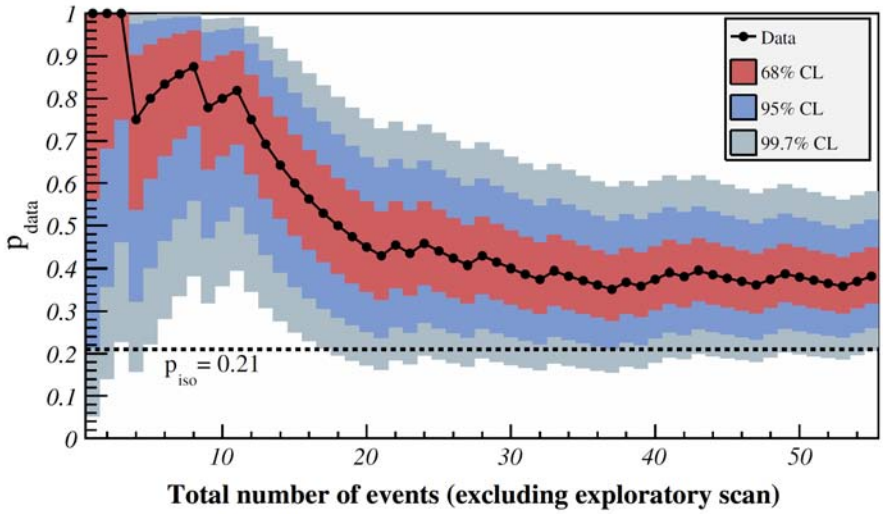

Figure 3: The most likely value of the degree of correlation p_{data} = k/N is plotted with black circles as a function of the total number of time-ordered events (excluding those in period I). The 68%, 95% and 99.7% confidence level intervals around the most likely value are shaded. The horizontal dashed line shows the isotropic value $p_{iso} = 0.21$.

it should also become possible to discriminate between different astrophysical scenarios using techniques of the type that have been presented here to explore the compatibility of different models with the present set of arrival directions.

The time sequence of the correlations between events with energy exceeding 55 EeV and AGN in the VCV catalog is shown in Fig.3. Period I is the exploratory period [9] from 1 January, 2004 through 26 May, 2006. The data collected during this period was scanned to establish the parameters which maximize the correlation. Period II is from 27 May, 2006 through 31 August, 2007 when the correlation paper [9] was published and period III includes data collected after, from 1 September, 2007 through 31 December, 2009. The time sequence is shown in terms of p_{data}, the degree of correlation with objects in the VCV catalog as a function of the total number of time-ordered events after the exploratory period.

We have also compared the distribution of arrival directions with the positions of different populations of nearby extragalactic objects: galaxies in the 2MRS survey and AGNs detected in X-rays by Swift-BAT. These studies are a posteriori and do not constitute further quantitative evidence for anisotropy.

We have analyzed the region of the sky close to the location of the radiogalaxy Cen A, since this corresponds to the largest observed excess with respect to isotropic expectations. The region of Cen A is densely populated with different types of nearby extragalactic objects. From all the arrival directions of CRs with E 55 EeV, 18.8% lie within 18° of Cen A, while 4.7% is the isotropic expectation. There are two arrival directions very close to the position of the Cen A nucleus. Aside from those two events, the excess is distributed rather broadly.

A knowledge of CR composition is important for deciding which of several source scenar- ios is more likely. The trajectories of highly charged nuclei are expected to un-

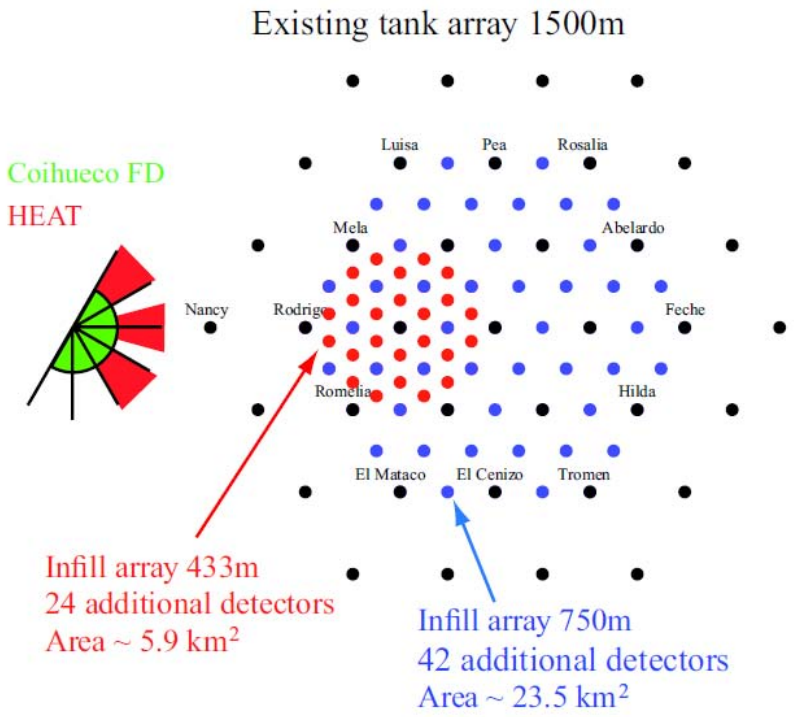

Figure 4: Layout of the enhancements AMIGA and HEAT for the soutern site of the Pierre Auger Observatory.

dergo large deflections due to the Galaxy's magnetic fields. While a correlation of arrival directions with nearby matter on small angular scales is plausible for protons above 55 EeV, it is puzzling if the CR are heavy nuclei. If the particles responsible for the measured excesses for example around Centaurus A at E >55 EeV are heavy nuclei with charge Z, the proton component of the sources should lead to excesses in the same regions at energies E/Z. In [10] the lack of anisotropies in the directions of the excesses at energies above E_{th}/Z is reported, setting constraints on the allowed proton fraction at the lower energies.

3 Enhancements of the Southern Observatory

After having completed the southern observatory, there are several enhancements under construction to improve the sensitivity of the observatory at low energy. Many of these activities are motivated by the interest in understanding the transition between galactic and extragalactic cosmic rays [11].

The extension of the surface detector is called AMIGA ("Auger Muons and Infill for the Ground Array"). It is itself a hybrid system containing an array of water Cherenkov detectors, called infill, each accompanied by a muon counter. Due to the higher flux for low energy cosmic rays, it is sufficient to only extend the surface detector in a small part of the whole ground array. This area is located close to the site of the HEAT extension to allow combined hybrid measurements. The infill part contains 66 new detector stations

which will be deployed inside the 1.5 km grid to achieve a dense array with 61 stations on a 750 m grid and 24 stations on a 433 m grid (see Fig. 4). The design of these additional stations is the same as for the standard stations. Additionally, there are scintillators buried next to each of the infill stations at a depth of about 3 m. These muon counters allow for a precise measurement of the showers electron to muon ratio at ground level, which is a direct indicator of the composition. The counter is sub-divided into three scintillator modules. Preliminary results of the first muon counter modules installed are reported in [12].

Moreover three new telescopes, called HEAT [13] ("High Elevation Auger Telescope"), have been built and are taking data on a regular basis since September 2009. They have the same field of view as the current telescopes, but are mounted inside a tiltable housing, which can be inclined by 30°. The location of the telescopes is in the direct vicinity of the existing telescope station Coihueco. This allows two interesting ways of measuring: if the building is not tilted, which is the only position a person can enter the building for maintenance work, the field of view of HEAT and Coihueco is overlapped and the measurements can be used for cross calibrations; In the tilted position, which is intended to be the usual data taking position, HEAT and Coihueco see different parts of the same shower and a combined reconstruction could be done to gain a higher precision. Apart from the new housing, the basic design of the telescopes is the same as in the current ones. However, a few changes have been done in the DAQ electronics to use state-of-the-art technique with increased readout speed.

An intense activity is also going on searching for signals of UHECRs using radio detection methods, both at the VHF (AERA,EASIER) frequencies and microwave (AMBER, MIDAS, FDWave,EASIER).

4 Activity of the L'Aquila - Gran Sasso Group

The activity of the group has followed two main lines:

- Developement of a Monte Carlo code (*SimProp*) for the propagation of UHECR Nuclei in extragalactic space, and its use for the study of physical observables
- Developement and test of the Raman Lidar system for an enhanced atmospheric test beam within the Observatory.

Concerning the first item, the work has been the subject of the PhD thesis of D. Boncioli (PhD obtained in December 2011). The code has been developed also in collaboration with F.Salamida (now at Paris-Orsay) and R. Aloisio (LNGS).

Using *SimProp*, several physical analyses are in progress, concerning mainly the mass composition of UHECRs detected in the Observatory.

D. Boncioli has presented her work at the Italian Physical Society (SIF) held in L'Aquila, receiving a special mention for the presentation [14].

Concerning the second reserch argument, the Raman Lidar system has been run in coincidence with a lateral scattering facility in Lamar (Colorado). The whole system will be moved this year to Malargue, to form part of the so-called Super Beam System [15].

5 List of Publications

1. P. Abreu *et al.* [Pierre Auger Collaboration], "The effect of the geomagnetic field on cosmic ray energy estimates and large scale anisotropy searches on data from the Pierre Auger Observatory," JCAP **1111**, 022 (2011) [arXiv:1111.7122 [astro-ph.IM]].

2. P. Abreu *et al.* [The Pierre Auger Collaboration], "Search for signatures of magnetically-induced alignment in the arrival directions measured by the Pierre Auger Observatory," Astropart. Phys. **35**, 354 (2012) [arXiv:1111.2472 [astro-ph]].

3. P. Abreu *et al.* [Pierre Auger Observatory Collaboration], "A Search for Ultra-High Energy Neutrinos in Highly Inclined Events at the Pierre Auger Observatory," Phys. Rev. D **84**, 122005 (2011) [Phys. Rev. D **85**, 029902 (2012)] [arXiv:1202.1493 [astro-ph.HE]].

4. P. Abreu *et al.* [Pierre Auger Collaboration], "The Lateral Trigger Probability function for the ultra-high energy cosmic ray showers detected by the Pierre Auger Observatory," Astropart. Phys. **35**, 266 (2011) [arXiv:1111.6645 [astro-ph.HE]].

5. P. Abreu *et al.* [The Pierre Auger Collaboration], "Anisotropy and chemical composition of ultra-high energy cosmic rays using arrival directions measured by the Pierre Auger Observatory," JCAP **1106**, 022 (2011) [arXiv:1106.3048 [astro-ph.HE]].

6. P. Abreu *et al.* [The Pierre Auger Collaboration], "Search for First Harmonic Modulation in the Right Ascension Distribution of Cosmic Rays Detected at the Pierre Auger Observatory," Astropart. Phys. **34**, 627 (2011) [arXiv:1103.2721 [astro-ph.HE]].

7. P. Abreu *et al.* [Pierre Auger Collaboration], "The Pierre Auger Observatory scaler mode for the study of solar activity modulation of galactic cosmic rays," JINST **6**, P01003 (2011).

8. P. Abreu *et al.* [AUGER Collaboration], "Advanced functionality for radio analysis in the Offline software framework of the Pierre Auger Observatory," Nucl. Instrum. Meth. A **635**, 92 (2011) [arXiv:1101.4473 [astro-ph.IM]].

9. P. Abreu *et al.* [Pierre Auger Observatory Collaboration], "The exposure of the hybrid detector of the Pierre Auger Observatory," Astropart. Phys. **34**, 368 (2011) [arXiv:1010.6162 [astro-ph.HE]].

References

[1] J.Abraham *et al.* [The Pierre Auger Collaboration], Phys. Lett. **B685**, 239-246 (2010).
(arXiv:1002.1975 [astro-ph.HE]).

[2] F. Salamida for the Pierre Auger Collaboration, Proc. 32th ICRC (Beijing, China) 2011, arXiv:1107.4809.

[3] W. Heitler, Oxford University Press, 1954;
J. Matthews, Astropart. Phys. **22** (2005), 387

[4] T. Wibig, Phys. Rev. D **79**, 094008;
R. Ulrich *et al.* for the Pierre Auger Collaboration, Proc. 32th ICRC (Beijing, China) 2011

[5] D.J. Bird, *et al.* [Fly's Eye Coll.], Phys. Rev. Lett. **71** (1993), 3401.

[6] R. U. Abbasi *et al.* [HiRes Coll.] Astrophys. J. **622** (2005),910.

[7] P. Facal San Luis *et al.* for the Pierre Auger Collaboration, Proc. 32th ICRC (Beijing, China) 2011

[8] P.Abreu *et al.* [The Pierre Auger Collaboration], Astropart. Phys. **34**, 314-326 (2010). ([arXiv:1009.1855])

[9] Pierre Auger Collaboration [J. Abraham et al.], Science 318 (2007) 938.
Astropart. Phys. 29 (2008) 188.

[10] Pierre Auger Collaboration [J. Abraham et al.], JCAP 1106 (2011) 022 and arXiv:1106.3048 [astro-ph.HE].

[11] G. Medina-Tanco et al. for the Pierre Auger Collab., Proc. of 30th Int. Cosmic Ray Conf., Merida 5 (2007) 1101.

[12] B. Wundheiler for the Pierre Auger Collaboration, Proc. 32nd ICRC, Beijing, China, 2011

[13] T. Hermann-Josef Mathes for the Pierre Auger Collaboration, Proc. 32nd ICRC, Beijing, China, 2011

[14] D.Boncioli for the Pierre Auger Collaboration, to appear in Nuovo Cimento C - Colloquia and Communication in Physics.

[15] L. Wiencke for the Pierre Auger Collaboration, Proc. 32nd ICRC, Beijing, China, 2011

The Pierre Auger Collaboration
P. Abreu[65], M. Aglietta[53], M. Ahlers[95], E.J. Ahn[83], I.F.M. Albuquerque[16], D. Allard[30], I. Allekotte[1], J. Allen[87], P. Allison[89], A. Almela[11, 7], J. Alvarez Castillo[58], J. Alvarez-Muñiz[75], R. Alves Batista[17], M. Ambrosio[47], A. Aminaei[59], L. Anchordoqui[96], S. Andringa[65], T. Antiči'c[24], C. Aramo[47], E. Arganda[4, 72], F. Arqueros[72], H. Asorey[1], P. Assis[65], J. Aublin[32], M. Ave[38], M. Avenier[33], G. Avila[10], T. Bäcker[42], A.M. Badescu[68], M. Balzer[37], K.B. Barber[12], A.F. Barbosa[14] , R. Bardenet[31], S.L.C. Barroso[19], B. Baughman[89] [f], J. Bäuml[36], C. Baus[38], J.J. Beatty[89], K.H. Becker[35], A. Bellétoile[34], J.A. Bellido[12], S. BenZvi[95], C. Berat[33], X. Bertou[1], P.L. Biermann[39], P. Billoir[32], F. Blanco[72], M. Blanco[32, 73], C. Bleve[35], H. Blümer[38, 36], M. Boháčová[26], D. Boncioli[48], C. Bonifazi[22, 32], R. Bonino[53], N. Borodai[63], J. Brack[81], I. Brancus[66], P. Brogueira[65], W.C. Brown[82], R. Bruijn[77] [i], P. Buchholz[42], A. Bueno[74], R.E. Burton[79], K.S. Caballero-Mora[90], B. Caccianiga[45], L. Caramete[39], R. Caruso[49], A. Castellina[53], O. Catalano[52], G. Cataldi[46], L. Cazon[65], R. Cester[50], J. Chauvin[33], S.H. Cheng[90], A. Chiavassa[53], J.A. Chinellato[17], J. Chirinos Diaz[86], J. Chudoba[26], M. Cilmo[47], R.W. Clay[12], M.R. Coluccia[46], R. Conceição[65], F. Contreras[9], H. Cook[77], M.J. Cooper[12], J. Coppens[59, 61], A. Cordier[31], S. Coutu[90], C.E. Covault[79], A. Creusot[30], A. Criss[90], J. Cronin[92], A. Curutiu[39], S. Dagoret-Campagne[31], R. Dallier[34], B. Daniel[17], S. Dasso[5, 3], K. Daumiller[36], B.R. Dawson[12], R.M. de Almeida[23], M. De Domenico[49], C. De Donato[58], S.J. de Jong[59, 61], G. De La Vega[8], W.J.M. de Mello Junior[17], J.R.T. de Mello Neto[22], I. De Mitri[46], V. de Souza[15], K.D. de Vries[60], L. del Peral[73], M. del Río[48, 9], O. Deligny[29], H. Dembinski[38], N. Dhital[86], C. Di Giulio[48, 44], M.L. Díaz Castro[14], P.N. Diep[97], F. Diogo[65], C. Dobrigkeit [17], W. Docters[60], J.C. D'Olivo[58], P.N. Dong[97, 29], A. Dorofeev[81], J.C. dos Anjos[14], M.T. Dova[4], D. D'Urso[47], I. Dutan[39], J. Ebr[26], R. Engel[36], M. Erdmann[40], C.O. Escobar[83, 17], J. Espadanal[65], A. Etchegoyen[7, 11], P. Facal San Luis[92], H. Falcke[59, 62], G. Farrar[87], A.C. Fauth[17], N. Fazzini[83], A.P. Ferguson[79], B. Fick[86], A. Filevich[7], A. Filipčič[69, 70], S. Fliescher[40], C.E. Fracchiolla[81], E.D. Fraenkel[60], O. Fratu[68], U. Fröhlich[42], B. Fuchs[38], R. Gaior[32], R.F. Gamarra[7], S. Gambetta[43], B. García[8], S.T. Garcia Roca[75], D. Garcia-Gamez[31], D. Garcia-Pinto[72], A. Gascon Bravo[74], H. Gemmeke[37], P.L. Ghia[32], M. Giller[64], J. Gitto[8], H. Glass[83], M.S. Gold[94], G. Golup[1], F. Gomez Albarracin[4], M. Gómez Berisso[1], P.F. Gómez Vitale[10], P. Gonçalves[65], J.G. Gonzalez[36], B. Gookin[81], A. Gorgi[53], P. Gouffon[16], E. Grashorn[89], S. Grebe[59, 61], N. Griffith[89], M. Grigat[40], A.F. Grillo[54], Y. Guardincerri[3], F. Guarino[47], G.P. Guedes[18], P. Hansen[4], D. Harari[1], T.A. Harrison[12], J.L. Harton[81], A. Haungs[36], T. Hebbeker[40], D. Heck[36], A.E. Herve[12], C. Hojvat[83], N. Hollon[92], V.C. Holmes[12], P. Homola[63], J.R. Hörandel[59], P. Horvath[27], M. Hrabovský[27, 26], D. Huber[38], T. Huege[36], A. Insolia[49], F. Ionita[92], A. Italiano[49], C. Jarne[4], S. Jiraskova[59], M. Josebachuili[7], K. Kadija[24], K.H. Kampert[35], P. Karhan[25], P. Kasper[83], I. Katkov[38], B. Kégl[31], B. Keilhauer[36], A. Keivani[85], J.L. Kelley[59], E. Kemp[17], R.M. Kieckhafer[86], H.O. Klages[36], M. Kleifges[37], J. Kleinfeller[9, 36], J. Knapp[77], D.-H. Koang[33], K. Kotera[92], N. Krohm[35], O. Krömer[37], D. Kruppke-Hansen[35], D. Kuempel[40, 42], J.K. Kulbartz[41], N. Kunka[37], G. La Rosa[52], C. Lachaud[30], D. LaHurd[79], L. Latronico[53], R. Lauer[94], P. Lautridou[34], S. Le Coz[33], M.S.A.B. Leão[21], D. Lebrun[33], P. Lebrun[83], M.A. Leigui de Oliveira[21], A. Letessier-Selvon[32], I. Lhenry-Yvon[29], K. Link[38], R. López[55], A. Lopez Agüera[75], K. Louedec[33, 31], J. Lozano Bahilo[74], L. Lu[77], A. Lucero[7], M. Ludwig[38], H. Lyberis[22, 29], M.C. Maccarone[52], C. Macolino[32], S. Maldera[53], D. Mandat[26], P. Mantsch[83], A.G. Mariazzi[4], J. Marin[9, 53], V. Marin[34], I.C. Maris[32], H.R. Marquez Falcon[57], G. Marsella[51], D. Martello[46], L. Martin[34], H. Martinez[56], O. Martínez Bravo[55],

H.J. Mathes[36], J. Matthews[85, 91], J.A.J. Matthews[94], G. Matthiae[48], D. Maurel[36], D. Maurizio[14, 50], P.O. Mazur[83], G. Medina-Tanco[58], M. Melissas[38], D. Melo[7], E. Menichetti[50], A. Menshikov[37], P. Mertsch[76], C. Meurer[40], S. Mi'canovi'c[24], M.I. Micheletti[6], I.A. Minaya[72], L. Miramonti[45], L. Molina-Bueno[74], S. Mollerach[1], M. Monasor[92], D. Monnier Ragaigne[31], F. Montanet[33], B. Morales[58], C. Morello[53], E. Moreno[55], J.C. Moreno[4], M. Mostafá[81], C.A. Moura[21], M.A. Muller[17], G. Müller[40], M. Münchmeyer[32], R. Mussa[50], G. Navarra[53] , J.L. Navarro[74], S. Navas[74], P. Necesal[26], L. Nellen[58], A. Nelles[59, 61], J. Neuser[35], P.T. Nhung[97], M. Niechciol[42], L. Niemietz[35], N. Nierstenhoefer[35], D. Nitz[86], D. Nosek[25], L. Nožka[26], J. Oehlschläger[36], A. Olinto[92], M. Ortiz[72], N. Pacheco[73], D. Pakk Selmi-Dei[17], M. Palatka[26], J. Pallotta[2], N. Palmieri[38], G. Parente[75], E. Parizot[30], A. Parra[75], S. Pastor[71], T. Paul[88], M. Pech[26], J. Pękala[63], R. Pelayo[55, 75], I.M. Pepe[20], L. Perrone[51], R. Pesce[43], E. Petermann[93], S. Petrera[44], A. Petrolini[43], Y. Petrov[81], C. Pfendner[95], R. Piegaia[3], T. Pierog[36], P. Pieroni[3], M. Pimenta[65], V. Pirronello[49], M. Platino[7], M. Plum[40], V.H. Ponce[1], M. Pontz[42], A. Porcelli[36], P. Privitera[92], M. Prouza[26], E.J. Quel[2], S. Querchfeld[35], J. Rautenberg[35], O. Ravel[34], D. Ravignani[7], B. Revenu[34], J. Ridky[26], S. Riggi[75], M. Risse[42], P. Ristori[2], H. Rivera[45], V. Rizi[44], J. Roberts[87], W. Rodrigues de Carvalho[75], G. Rodriguez[75], I. Rodriguez Cabo[75], J. Rodriguez Martino[9], J. Rodriguez Rojo[9], M.D. Rodríguez-Frías[73], G. Ros[73], J. Rosado[72], T. Rossler[27], M. Roth[36], B. Rouillé-d'Orfeuil[92], E. Roulet[1], A.C. Rovero[5], C. Rühle[37], A. Saftoiu[66], F. Salamida[29], H. Salazar[55], F. Salesa Greus[81], G. Salina[48], F. Sánchez[7], C.E. Santo[65], E. Santos[65], E.M. Santos[22], F. Sarazin[80], B. Sarkar[35], S. Sarkar[76], R. Sato[9], N. Scharf[40], V. Scherini[45], H. Schieler[36], P. Schiffer[41, 40], A. Schmidt[37], O. Scholten[60], H. Schoorlemmer[59, 61], J. Schovancova[26], P. Schovánek[26], F. Schröder[36], S. Schulte[40], D. Schuster[80], S.J. Sciutto[4], M. Scuderi[49], A. Segreto[52], M. Settimo[42], A. Shadkam[85], R.C. Shellard[14], I. Sidelnik[7], G. Sigl[41], H.H. Silva Lopez[58], O. Sima[67], A. 'Smiałkowski[64], R. Šmída[36], G.R. Snow[93], P. Sommers[90], J. Sorokin[12], H. Spinka[78, 83], R. Squartini[9], Y.N. Srivastava[88], S. Stanic[70], J. Stapleton[89], J. Stasielak[63], M. Stephan[40], A. Stutz[33], F. Suarez[7], T. Suomijärvi[29], A.D. Supanitsky[5], T. Šuša[24], M.S. Sutherland[85], J. Swain[88], Z. Szadkowski[64], M. Szuba[36], A. Tapia[7], M. Tartare[33], O. Taşcău[35], R. Tcaciuc[42], N.T. Thao[97], D. Thomas[81], J. Tiffenberg[3], C. Timmermans[61, 59], W. Tkaczyk[64] , C.J. Todero Peixoto[15], G. Toma[66], L. Tomankova[26], B. Tomé[65], A. Tonachini[50], P. Travnicek[26], D.B. Tridapalli[16], G. Tristram[30], E. Trovato[49], M. Tueros[75], R. Ulrich[36], M. Unger[36], M. Urban[31], J.F. Valdés Galicia[58], I. Valiño[75], L. Valore[47], A.M. van den Berg[60], A. van Vliet[41], E. Varela[55], B. Vargas Cárdenas[58], J.R. Vázquez[72], R.A. Vázquez[75], D. Veberič[70, 69], V. Verzi[48], J. Vicha[26], M. Videla[8], L. Villaseñor[57], H. Wahlberg[4], P. Wahrlich[12], O. Wainberg[7, 11], D. Walz[40], A.A. Watson[77], M. Weber[37], K. Weidenhaupt[40], A. Weindl[36], F. Werner[36], S. Westerhoff[95], B.J. Whelan[90, 12], A. Widom[88], G. Wieczorek[64], L. Wiencke[80], B. Wilczyńska[63], H. Wilczyński[63], M. Will[36], C. Williams[92], T. Winchen[40], M. Wommer[36], B. Wundheiler[7], T. Yamamoto[92 a], T. Yapici[86], P. Younk[42, 84], G. Yuan[85], A. Yushkov[75], B. Zamorano Garcia[74], E. Zas[75], D. Zavrtanik[70, 69], M. Zavrtanik[69, 70], I. Zaw[87 h], A. Zepeda[56 b], J. Zhou[92], Y. Zhu[37], M. Zimbres Silva[35, 17], M. Ziolkowski[42]

[1] Centro Atómico Bariloche and Instituto Balseiro (CNEA-UNCuyo-CONICET), San Carlos de Bariloche, Argentina

[2] Centro de Investigaciones en Láseres y Aplicaciones, CITEDEF and CONICET, Argentina

[3] Departamento de Física, FCEyN, Universidad de Buenos Aires y CONICET, Argentina

[4] IFLP, Universidad Nacional de La Plata and CONICET, La Plata, Argentina
[5] Instituto de Astronomía y Física del Espacio (CONICET-UBA), Buenos Aires, Argentina
[6] Instituto de Física de Rosario (IFIR) - CONICET/U.N.R. and Facultad de Ciencias Bioquímicas y Farmacéuticas U.N.R., Rosario, Argentina
[7] Instituto de Tecnologías en Detección y Astropartículas (CNEA, CONICET, UNSAM), Buenos Aires, Argentina
[8] National Technological University, Faculty Mendoza (CONICET/CNEA), Mendoza, Argentina
[9] Observatorio Pierre Auger, Malargüe, Argentina [10] Observatorio Pierre Auger and Comisión Nacional de Energía Atómica, Malargüe, Argentina
[11] Universidad Tecnológica Nacional - Facultad Regional Buenos Aires, Buenos Aires, Argentina
[12] University of Adelaide, Adelaide, S.A., Australia
[14] Centro Brasileiro de Pesquisas Fisicas, Rio de Janeiro, RJ, Brazil
[15] Universidade de São Paulo, Instituto de Física, São Carlos, SP, Brazil
[16] Universidade de São Paulo, Instituto de Física, São Paulo, SP, Brazil
[17] Universidade Estadual de Campinas, IFGW, Campinas, SP, Brazil
[18] Universidade Estadual de Feira de Santana, Brazil
[19] Universidade Estadual do Sudoeste da Bahia, Vitoria da Conquista, BA, Brazil
[20] Universidade Federal da Bahia, Salvador, BA, Brazil
[21] Universidade Federal do ABC, Santo André, SP, Brazil
[22] Universidade Federal do Rio de Janeiro, Instituto de Física, Rio de Janeiro, RJ, Brazil
[23] Universidade Federal Fluminense, EEIMVR, Volta Redonda, RJ, Brazil
[24] Rudjer Boškovi'c Institute, 10000 Zagreb, [25] Charles University, Faculty of Mathematics and Physics, Institute of Particle and Nuclear Physics, Prague, Czech Republic
[26] Institute of Physics of the Academy of Sciences of the Czech Republic, Prague, Czech
[27] Palacky University, RCPTM, Olomouc, Czech Republic
[29] Institut de Physique Nucléaire d'Orsay (IPNO), Université Paris 11, CNRS-IN2P3, Orsay, France
[30] Laboratoire AstroParticule et Cosmologie (APC), Université Paris 7, CNRS-IN2P3, Paris, France
[31] Laboratoire de l'Accélérateur Linéaire (LAL), Université Paris 11, CNRS-IN2P3, Orsay, France
[32] Laboratoire de Physique Nucléaire et de Hautes Energies (LPNHE), Universités Paris 6 et Paris 7, CNRS-IN2P3, Paris, France
[33] Laboratoire de Physique Subatomique et de Cosmologie (LPSC), Université Joseph Fourier, INPG, CNRS-IN2P3, Grenoble, France
[34] SUBATECH, École des Mines de Nantes, CNRS- IN2P3, Université de Nantes, Nantes, France
[35] Bergische Universität Wuppertal, Wuppertal, Germany
[36] Karlsruhe Institute of Technology - Campus North - Institut für Kernphysik, Karlsruhe, Germany
[37] Karlsruhe Institute of Technology - Campus North - Institut für Prozessdatenverarbeitung und Elektronik, Karlsruhe, Germany

[38] Karlsruhe Institute of Technology - Campus South - Institut für Experimentelle Kernphysik (IEKP), Karlsruhe, Germany
[39] Max-Planck-Institut für Radioastronomie, Bonn, Germany
[40] RWTH Aachen University, III. Physikalisches Institut A, Aachen, Germany
[41] Universität Hamburg, Hamburg, Germany
[42] Universität Siegen, Siegen, Germany
[43] Dipartimento di Fisica dell'Università and INFN, Genova, Italy
[44] Università dell'Aquila and INFN, L'Aquila, [45] Università di Milano and Sezione INFN, Milan, Italy
[46] Dipartimento di Fisica dell'Università del Salento and Sezione INFN, Lecce, Italy
[47] Università di Napoli "Federico II" and Sezione INFN, Napoli, Italy
[48] Università di Roma II "Tor Vergata" and Sezione INFN, Roma, Italy
[49] Università di Catania and Sezione INFN, Catania, Italy
[50] Università di Torino and Sezione INFN, Torino, Italy
[51] Dipartimento di Ingegneria dell'Innovazione dell'Università del Salento and Sezione INFN, Lecce, Italy
[52] Istituto di Astrofisica Spaziale e Fisica Cosmica di Palermo (INAF), Palermo, Italy
[53] Istituto di Fisica dello Spazio Interplanetario (INAF), Università di Torino and Sezione INFN, Torino, Italy
[54] INFN, Laboratori Nazionali del Gran Sasso, Assergi (L'Aquila), Italy
[55] Benemérita Universidad Autónoma de Puebla, Puebla, Mexico
[56] Centro de Investigación y de Estudios Avanzados del IPN (CINVESTAV), México, D.F., Mexico
[57] Universidad Michoacana de San Nicolas de Hidalgo, Morelia, Michoacan, Mexico
[58] Universidad Nacional Autonoma de Mexico, Mexico, D.F., Mexico
[59] IMAPP, Radboud University Nijmegen, [60] Kernfysisch Versneller Instituut, University of Groningen, Groningen, Netherlands
[61] Nikhef, Science Park, Amsterdam, Netherlands [62] ASTRON, Dwingeloo, Netherlands
[63] Institute of Nuclear Physics PAN, Krakow, [64] University of Łódź, Łódź, Poland
[65] LIP and Instituto Superior Técnico, Technical University of Lisbon, Portugal
[66] 'Horia Hulubei' National Institute for Physics and Nuclear Engineering, Bucharest-Magurele, [67] University of Bucharest, Physics Department, Romania
[68] University Politehnica of Bucharest, Romania [69] J. Stefan Institute, Ljubljana, Slovenia
[70] Laboratory for Astroparticle Physics, University of Nova Gorica, Slovenia
[71] Instituto de Física Corpuscular, CSIC- Universitat de València, Valencia, Spain
[72] Universidad Complutense de Madrid, Madrid, [73] Universidad de Alcalá, Alcalá de Henares (Madrid), Spain
[74] Universidad de Granada & C.A.F.P.E., Granada, Spain
[75] Universidad de Santiago de Compostela, Spain [76] Rudolf Peierls Centre for Theoretical Physics, University of Oxford, Oxford, United Kingdom [77] School of Physics and Astronomy, University of Leeds, United Kingdom
[78] Argonne National Laboratory, Argonne, IL, USA [79] Case Western Reserve University, Cleveland, OH, USA
[80] Colorado School of Mines, Golden, CO, USA
[81] Colorado State University, Fort Collins, CO, [82] Colorado State University, Pueblo, CO,

USA
[83] Fermilab, Batavia, IL, USA
[84] Los Alamos National Laboratory, Los Alamos, NM, USA
[85] Louisiana State University, Baton Rouge, LA, [86] Michigan Technological University, Houghton, MI, USA
[87] New York University, New York, NY, USA
[88] Northeastern University, Boston, MA, USA
[89] Ohio State University, Columbus, OH, USA
[90] Pennsylvania State University, University Park, PA, USA
[91] Southern University, Baton Rouge, LA, USA
[92] University of Chicago, Enrico Fermi Institute, Chicago, IL, USA
[93] University of Nebraska, Lincoln, NE, USA
[94] University of New Mexico, Albuquerque, NM, [95] University of Wisconsin, Madison, WI, USA
[96] University of Wisconsin, Milwaukee, WI, USA
[97] Institute for Nuclear Science and Technology (INST), Hanoi, Vietnam

() Deceased
(a) at Konan University, Kobe, Japan
(b) now at the Universidad Autonoma de Chiapas on leave of absence from Cinvestav
(f) now at University of Maryland
(h) now at NYU Abu Dhabi
(i) now at Université de Lausanne

GIGS. The Interferometric Station at LNGS

Antonella Amoruso[a,b], Luca Crescentini[a,b,c], Verdiana Botta[a]

[a] Dip.to di Fisica Univ. di Salerno, Salerno - Italy
[b] INFN - Gruppo collegato di Salerno, Salerno - Italy
[c] Spokeperson

Abstract

During 2011 the activity has been devoted to:

1) the completion of tidal analysis of about 8-years of strain data in order to evidence the fluid core resonance (FCR) effect in the diurnal tidal band and study the resonance function;

2) the investigation of the Gran Sasso carbonate aquifer, and the relation between aquifer dynamics and ground deformation recorded by the interferometers;

3) the installation of two geodetic interferometers, similar in design to the Gran Sasso ones, close to the Canfranc Underground Laboratory (LSC), Spain.

1 Introduction

Since several years two geodetic extensometers are working at LNGS. Both instruments are unequal-arm Michelson interferometers, using a 90-m long measurement arm and an about 20-cm long reference arm, and sharing the same stabilized HeNe laser source. Nominal sensitivity is better than 10^{-12} and, in the present configuration, recording rate is 600Hz. The two interferometers are monitoring extension along two orthogonal directions, striking N66E (BC interferometer) and N24W (BA interferometer).

Few years ago, we performed ([1]) preliminary studies of the Free Core Nutation (FCN), a rotational eigenmode which appears in addition to the well-known Chandler period ($\approx$ 435 days). This mode is due to the pressure coupling between the liquid core and the solid mantle which acts as a restoring force. The FCN causes a resonance on the Earth response to tidal forcing whose period T_{FCR} (situated in the diurnal tidal band) and quality factor Q depend on the core-mantle boundary (CMB) ellipticity, the Earth's inelasticity, and the viscomagnetic coupling of the CMB. Most of the experimental studies of the FCR are based on the analysis of tidal gravity data and Very Long Baseline Interferometry (VLBI) data. Although tidal signal-to-noise (S/N) ratio for strain is usually lower than for gravity, the analysis of strain data is promising, since relative perturbations in strain tides are about ten times larger than in gravity tides. The unusual depth of the

Gran Sasso station largely reduces contamination caused by environmental effects in the diurnal band of recorded tides. From our preliminary analyses we obtained values of the FCR period consistent with but slightly lower than those published by others, and a more realistic quality factor than coeval estimates. During 2011 we have completed the tidal analysis of about 8-years of strain data, after an accurate correction of measured strain for local distortion of the regional strain field and ocean loading.

As regards the Gran Sasso carbonate aquifer, we have already proposed ([2]) a conceptual model of the consequences of the April 6^{th}, 2009, L'Aquila earthquake. The model excluded the contribution of seasonal recharge, and the short-term hydrologic effects, registered immediately after the mainshock, were determined to have been caused by a pore pressure increase related to aquifer deformation. Mid-term effects observed in the months following the mainshock suggested that there was a change in groundwater hydrodynamics. Supplementary groundwater that flows towards aquifer boundaries and springs in discharge areas reflected a possible increase in hydraulic conductivity in the recharge area, nearby the earthquake fault zone. This increase can be attributed to fracture clearing and/or dilatancy. Simulations by numerical modeling, related to pore pressure and permeability changes with time, showed results in accordance with observed field data, supporting the conceptual model and confirming the processes that influenced the answer of the Gran Sasso aquifer to the L'Aquila earthquake. During 2011 we have tried to identify the effective aquifer features that mostly affect the spring discharges of the Gran Sasso area, and started modeling the recharge/discharge cycle at regional scale considering as input data infiltration and effective permeability distribution. We have also continued to investigate the relationship between the strain time series and seasonal recharge/discharge regime of groundwater flow in the tunnels.

Moreover, during 2011 two laser strainmeters, similar in design to the Gran Sasso ones, have been installed close to the Canfranc Underground Laboratory (LSC), Spain.

2 The FCR and the diurnal strain tides

Each diurnal strain tide harmonic (extension positive) in a given azimuthal direction η can be expressed as [6]

$$\varepsilon(\eta) = F(\theta)\left\{\left[h - 2l\left(1+\cos^2\eta\right)\right]\cos\left(2\pi ft+\varphi-\phi\right) - l\frac{\sin 2\eta}{\cos\theta}\sin\left(2\pi ft+\varphi-\phi\right)\right\} \quad (1)$$

where f is frequency, $F(\theta)$ is a function depending on the location of the station and proportional to the amplitude of the tidal potential harmonic, θ and ϕ are the co-latitude and longitude of the instrument, φ is a phase depending on the harmonic and time origin, h and l are the Love and Shida numbers respectively. Because the solid Earth tides are affected by the FCR, h and l depend on f:

$$h = h_0 + h_1\frac{f-f_0}{f_{FCR}-f} \qquad l = l_0 + l_1\frac{f-f_0}{f_{FCR}-f} \quad (2)$$

where f_0 is the frequency of O1 and f_{FCR} is the FCR frequency. Because of the anelasticity of the Earth, h_0, h_1, l_0, l_1, and f_{FCR} are complex. In particular, f_{FCR} can be expressed

as

$$f_{FCR} = f_1 \left(1 + j\frac{1}{2Q}\right) \tag{3}$$

We can re-write Eq. 1 as

$$\varepsilon(\eta) = \{C(f)\,\cos(2\pi ft + \varphi - \phi) + D(f)\,\sin(2\pi ft + \varphi - \phi)\}\,F(\theta) \tag{4}$$

where

$$C(f) \equiv a_0 + f_2 \left\{a_1 (f_1 - f) + b_1 \frac{f_1}{2Q}\right\} \tag{5}$$

$$D(f) \equiv b_0 + f_2 \left\{b_1 (f_1 - f) - a_1 \frac{f_1}{2Q}\right\} \tag{6}$$

$$f_2 \equiv (f - f_0) \,/\, \left\{(f_1 - f)^2 + (f_1/2Q)^2\right\} \tag{7}$$

The coefficients a_0, a_1, b_0, and b_1 can be expressed in a compact form as

$$a_k \equiv \mathrm{Re}\left\{h_k - 2l_k\left(1 + \cos^2\eta\right)\right\} + \mathrm{Im}\left\{l_k \sin 2\eta / \cos\theta\right\} \tag{8}$$

$$b_k \equiv \mathrm{Im}\left\{h_k - 2l_k\left(1 + \cos^2\eta\right)\right\} - \mathrm{Re}\left\{l_k \sin 2\eta / \cos\theta\right\} \tag{9}$$

where k is 0 or 1.

Strain processing of records from BA and BC interferometers aimed to investigate the FCN parameters includes correction for ocean tidal loading and local strain distortion. Ocean loading tidal strain at Gran Sasso is due to the Mediterranean Sea by about 50% and consists essentially in a small rotation of phasors whose amount and sign depend on the tidal component and the interferometer. After correcting tidal amplitudes and phases for ocean loading, the residual discrepancies between experimental and predicted values far from the FCR frequency are attributable to the local distortion of the strain field. We determine the three strain cross-coupling coefficients for each interferometer by comparing observed tides and reference Earth tide strains (solid Earth and ocean loading) for Q_1, O_1, N_2, M_2, and K_2. For estimating the FCR parameters we used eight diurnal tidal constituents (Q_1, O_1, P_1, K_1, Ψ_1, Φ_1, J_1, OO_1) and compared measurements (corrected for ocean loading) and model predictions (corrected for the local strain distortion) through a joint fit on the BA and BC tidal parameters, minimizing the L_1-norm misfit function. We tested different Earth models. When we use the more reliable Earth model between those tested and leave all the inversion parameters free, we [3] estimate T_{FCN} values (about 428 sidereal days) comparable to those from gravity tides, obtained from the joint inversion of data from several stations. Q is not well constrained because of the large uncertainties on the Ψ_1 phase, however our results are consistent with recently published values (≈ 20000). The agreement between observations and predictions looks better than in any previous work that makes use of strain tides (see e. g., Fig. 8 in [6]). Our inversions provide also an independent estimate of $\mathrm{Re}(h_1 - 3l_1)$, which is the dominating term in the resonance strength expression, in agreement with IERS Conventions (2003).

In the near future, we plan to perform a joint inversion of strain data from the Gran Sasso and Baksan ([5]) interferometers, and, as soon as a sufficiently long record is available, from the two interferometers recently installed close to the underground Canfranc Laboratory (Spain).

3 Strain-hydrology analyses

Numerical simulations have been applied to validate a conceptual model of the recharge / discharge cycle at regional scale in the carbonate fractured aquifer of the Gran Sasso. To identify the effective aquifer features that mostly affect the spring discharges, simple parsimonious models, based on few key parameters whose effective values are well-constrained by previous hydrological/geological studies, have been used. Input data are represented by infiltration, calculated through the Thornthwaite-Mather method and considering rainfall, snowmelt and runoff in endorheic basins, and effective permeability distribution, estimated by geological, tectonic and hydrogeological setting of the aquifer. Discharges of tapped springs and tunnel drainages for the 1999-2009 period have been simulated, after estimating the recharge area of each monitored spring by the hydrogeological setting and checking them by mean isotope elevation values. Discharge monitoring has been compared with the simulations, obtaining a good agreement both at seasonal and yearly time basis [4]. Moreover, the relationship between deformation and groundwater flow is allowing to analyze in detail the mechanism of recharge close to the LNGS, which is developing along preferential direction of fractures. More analyses, including a deep insight on hydrochemical and isotope data and fracture network, are required before drawing definitive conclusions. These studies are carried out in co-operation with R. Adinolfi Falcone, A. Falgiani, M. Petitta, and M. Tallini.

4 The Canfranc (Spain) interferometers

The installation of two interferometers, several tens of meters long but much smaller in size with respect to the Gran Sasso ones (see following Figures), started at the end of last August, and the first preliminary data acquisition began on October 24^{st}, 2011. They have been funded by Spanish governmental Institutions, and their technical characteristics are quite similar to those of the Gran Sasso instruments. The interferometers are located close to the Canfranc Underground Laboratory (LSC), namely in the Bypass 16 and the Laboratory 780.

The comparison between typical noise Power Spectral Density at Gran Sasso and Canfranc is in Figure 4.

The estimated Power Spectral Density for the Canfranc instruments for frequencies below 10^{-4} Hz is not robust, because of the insufficient length of the analysed records. The peaks in the frequency range $0.1 \div 0.4$ Hz are obviously higher at Canfranc, since they are caused by ocean microseisms. Noise level of the Canfranc instruments is lower than the Gran Sasso ones in the frequency range 10^{-4} a few 10^{-2} Hz, up to one order of magnitude for the noise of the instrument installed in the Laboratory 780. This latter frequency region includes several interesting geophysical phenomena, e.g. slow earthquakes, long-period seismic waves and Earth free oscillations. With reference to the last two mentioned phenomena, the joint analysis of the data recorded at Canfranc and Gran Sasso would allow a deeper insight in Earth's global behaviour.

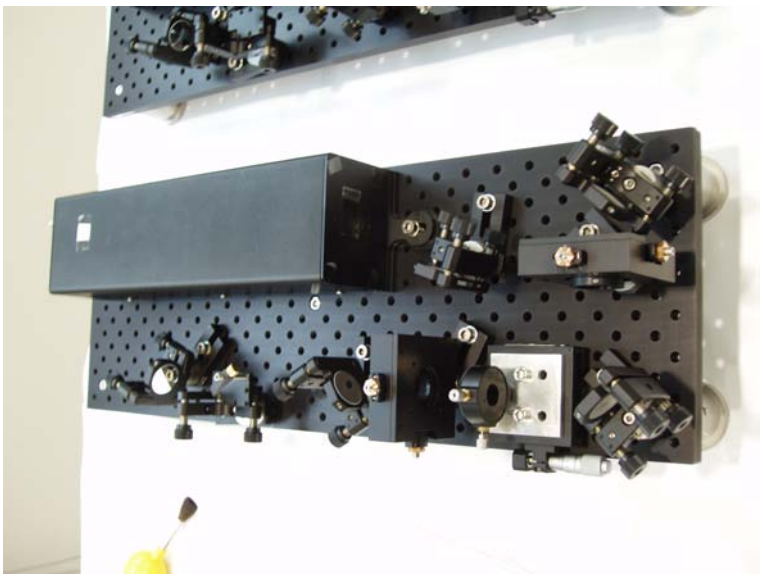

Figure 1: Laser head and optical set-up for the laser beam conditioning. This system is placed out of the main chamber of each interferometer.

Figure 2: Main plinth in Bypass 16.

Figure 3: Main plinth in Laboratory 780.

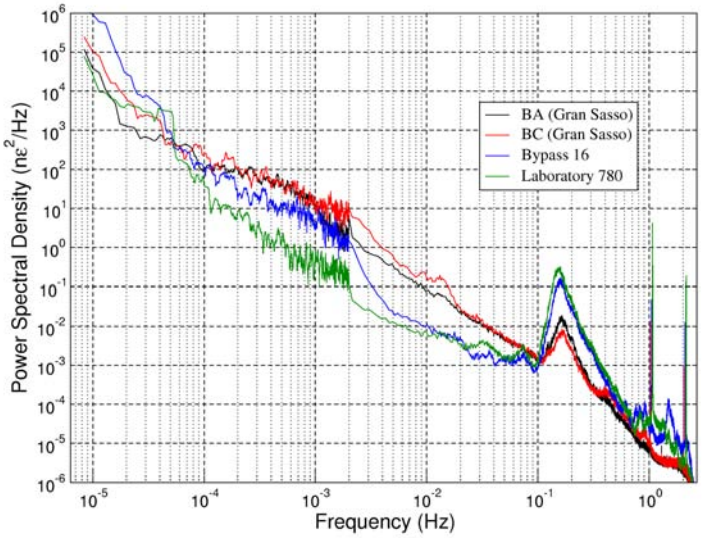

Figure 4: Power Spectral Density: BA and BC interferometers (Gran Sasso), Bypass 16 and Laboratory 780 (Canfranc).

5 List of Publications

1. Amoruso A., L. Crescentini, M. Petitta, S. Rusi, and M. Tallini, *Hydrol. Process.*, doi:10.1002/hyp.7933, 2011.

2. Amoruso A., and L. Crescentini, Boll. Geofis. Teor. Appl., doi:10.4430/bgta0039, 2011.

References

[1] Amoruso A., and L. Crescentini, AGU Fall Meeting, S. Francisco, 2008.

[2] Amoruso A., L. Crescentini, M. Petitta, S. Rusi, and M. Tallini, *Hydrol. Process.*, doi:10.1002/hyp.7933, 2011.

[3] Amoruso A., V. Botta, and L. Crescentini, *Geophys. J. Int.*, under revision.

[4] Amoruso A., L. Crescentini, M. Petitta, and M. Tallini, submitted.

[5] Milyukov, V. K., B. S. Klyachko, A. V. Myasnikov, P. S. Striganov, and A. F. Yanin, *Instruments and Experimental Techniques*, **48**, 780-795, 2005.

[6] Mukai, A., S. Takemoto, and T. Yamamoto, *Geophys. J. Int.*, **156**, 22-28, 2004.

PLAXA experiment

A plasma-laser source based on yttrium and mylar targets employed in the realization of an X-ray microbeam at 2.48 nm wavelength

L. Palladino[a,b], R. G. De Lorenzo[a,b], M. Di Paolo Emilio[a,b] and T. Limongi[a,c]

[a] Physics Department - L'Aquila University - Italy
[b] Gran Sasso National Laboratory of INFN, Assergi (Aq) - Italy
[c] Italian institute of technology(IIT), Via Morego 30, 16163 Genova, Italy

Abstract

In this report, the 2011 PLAXA experiment activities are presented. They have had as main purpose the study (1) of the X-ray beam generated from a plasma produced by focusing a Nd-Yag/glass laser beam on mylar or yttrium target and (2) of a monochromatic soft X-ray microbeam set-up at 2.48 nm wavelength. The monochromatic radiation was collected by multilayer spherical mirrors reflecting at an incidence angle close to the normal of the surface [1]. For each target material, the conversion efficiencies of the soft X-ray emission in two different energy ranges, (i) 300-510 eV (almost coincident with the Water Window), (ii) 450-850 eV were measured. The experimental results of the conversion efficiencies will be utilized for the realization of an intense monochromatic X-ray microbeam to be used in radiobiological [2] and in transmission X-ray microscopy [3, 4] applications. The geometry of the optical system, the preliminary measures of the monochromatic beam intensity and the measures of the conversion efficiency were described.

1 Experimental apparatus

The laser-plasma source, at the PLASMA-X laboratory of L'Aquila University, consists of a Nd YAG/glass laser that generates a pulse of 6 ns long and with an energy which depends on three operating configurations: about 300 mJ, about 1.5 and about 4 J and an interaction chamber at 10^{-3} mbar internal pressure. The focal spot size was 65 ($\pm$ 2) μm, corresponding to a power density between 10^{12} and 10^{13} W/cm^2. The X-rays were detected using a PIN-diode (100-PIN-125, with SiO_2 0.3 μm as entrance window, dead layer, and Si 125 μm as intrinsic zone, by Emerge Corporation). The detector was placed at a 30 degree angle to the direction of the laser beam, with a sensitive area 7 mm in diameter. A second detector measured the intensity of X-rays to control the better conditions of the focus on the target. This detector had on entrance window an aluminum

micro-foil 3 μm thick and was placed at 60 degrees respect the direction of the laser beam. To make our measures of x-ray conversion efficiency of mylar and yttrium, we placed the PIN diode at a distance of 84.5 cm from plasma. We have filtered the radiation by putting in front of the entrance window of the detector or a vanadium micro-foil 1 μm thick or a nickel micro-foil 1 μm thick or an aluminum micro-foil 7.5 μm thick. In Figure 1 the experimental set-up was represented; in figure were indicated the geometrical parameters and the characteristics of the micro-foil used as X-ray filters. The 2.48 nm monochromatic microbeam is obtained using a multilayer spherical mirror which selects the wavelength of X-rays at an incident angle of 8 degrees from the normal to the surface of the mirror. The mirror has a useful diameter D = 30 mm and a curvature radius R = 265 mm. A 50 nm thick silicon nitride membrane was used to protect the mirror from the debris produced during the plasma generation.

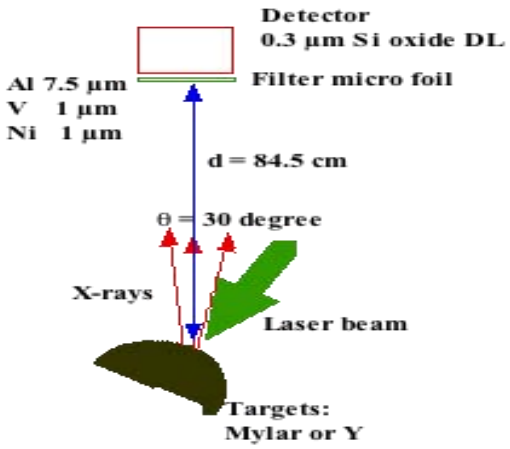

Figure 1: Schematic description of the experimental arrangement for the conversion efficiency measurement. The geometrical parameters of the measure are shown in the figure.

In the pictures of Figure 2 it is represented the inside of the interaction chamber, in particular the layout of the spherical mirror respect to the target, with their positioning systems remote controlled by computer. The sensitivity of the movement is 1 μm.

This mechanical configuration will be used in future to realize monochromatic microbeams with different optical configurations and for various X-ray energies.

2 Experimental results

2.1 Measurements of conversion efficiencies

To measure the conversion efficiency in the range of about 300 eV - 510 eV and between about 450 eV - 800 eV, an 1 μm thick vanadium micro-foil and an 1 μm thick nickel micro-foil were placed in front of entrance window of the detector. For the measurement of the radiation component of more than 800 eV, we used an 7.5 μm thick aluminum micro-foil. In Figure 3 the transmission curves for the three micro-foils used were reported. The

vanadium micro-foil 1 μm thick had a transmission range between 300 and 510 eV with a tail to higher energy of 800 eV. The nickel micro-foil 1 μm thick had a transmission between 500 and 800 eV with a tail to higher energy of 800 eV, but less important than that of vanadium. Instead, the aluminum micro-foil of 7.5 microns thick had a significant transmission for energies greater than 800 eV [5]. To obtain the conversion efficiency from the experimental data for the intervals between about 300 and 510 eV (V) and between 450 and 850 eV (Ni) was necessary to subtract the contribution of photons with energy greater than 800 eV from the total signal of the detector filtered with the V and Ni. This contribution was derived from the detector signals filtered with 7.5 μm of aluminum, which as shown in Figure 3 has a transmission ($> 10^{-4}$) for photon energy greater than 800 eV.

Since the data collected with the three filters (V, Ni and Al) were taken under the same conditions of laser pulse energy and power density on the target, the distribution of intensity of X-ray emission from plasma was considered as a function of energy, S (E_x), similar in all three situations. So for each targets:

$$Q_V^{tot} \sim \int S(E_x) \times T_{DL}(E_x) \times T_V^{t=1\mu m}(E_x) dE_x \tag{1}$$

$$Q_{Ni}^{tot} \sim \int S(E_x) \times T_{DL}(E_x) \times T_{Ni}^{t=1\mu m}(E_x) dE_x \tag{2}$$

$$Q_{Al}^{tot} \sim \int S(E_x) \times T_{DL}(E_x) \times T_{Al}^{t=7.5\mu m}(E_x) dE_x \tag{3}$$

where Q_V^{tot}, Q_{Ni}^{tot} and Q_{Al}^{tot} are the charges obtained from the time integrated signal of the filtered detector by V, Ni and Al, respectively. $T_{DL}(E_x)$, $T_V^{t=1\mu m}(E_x)$, $T_{Ni}^{t=1\mu m}(E_x)$ and $T_{Al}^{t=7.5\mu m}(E_x)$ are the transmissions, versus X-ray energy, Ex, of the dead layer detector and the V, Ni and Al micro-foils respectively.

The proportionality factors in the relations 1, 2 and 3, were considered constant, because the geometrical and physical conditions of the measures remain unchanged, as shown in Figure 1. From these relations wrote:

$$\frac{Q_V^{E_x>800eV}}{Q_{Al}^{tot}} = \frac{\int_{800eV} S(E_x) \times T_{DL}(E_x) \times T_V^{t=1\mu m}(E_x) dE_x}{\int S(E_x) \times T_{DL}(E_x) \times T_{Al}^{t=7.5\mu m}(E_x) dE_x} = \frac{\int_{800eV} T_V^{t=1\mu m}(E_x) dE_x}{\int T_{Al}^{t=7.5\mu m}(E_x) dE_x} \tag{4}$$

$$\frac{Q_{Ni}^{E_x>850eV}}{Q_{Al}^{tot}} = \frac{\int_{850eV} S(E_x) \times T_{DL}(E_x) \times T_{Ni}^{t=1\mu m}(E_x) dE_x}{\int S(E_x) \times T_{DL}(E_x) \times T_{Al}^{t=7.5\mu m}(E_x) dE_x} = \frac{\int_{850eV} T_{Ni}^{t=1\mu m}(E_x) dE_x}{\int T_{Al}^{t=7.5\mu m}(E_x) dE_x} \tag{5}$$

where $Q_V^{E_x>800eV}$ and $Q_{Ni}^{E_x>850eV}$ are the charges of the integrated detector signals filtered with the V and Ni for x-ray energy greater than 800 eV and 850 eV, respectively. From previous assumptions, the signal component for energies greater than 800 eV was given by:

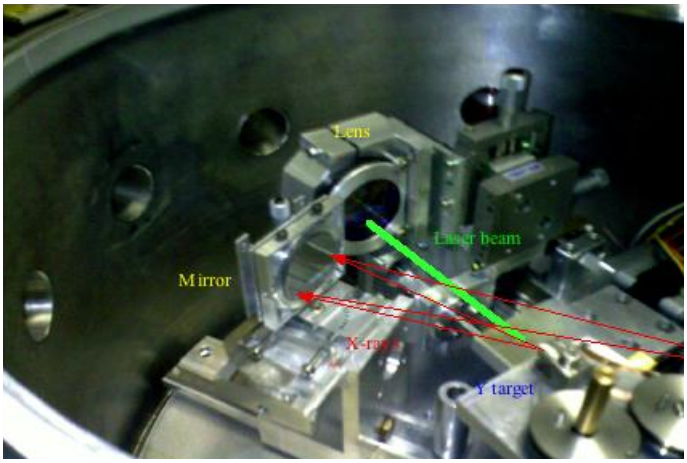

Figure 2: Photo of the interaction chamber. Photons with a wavelength of 2.48 nm are selected and focused by multilayer spherical mirror of curvature radius of 265 mm.

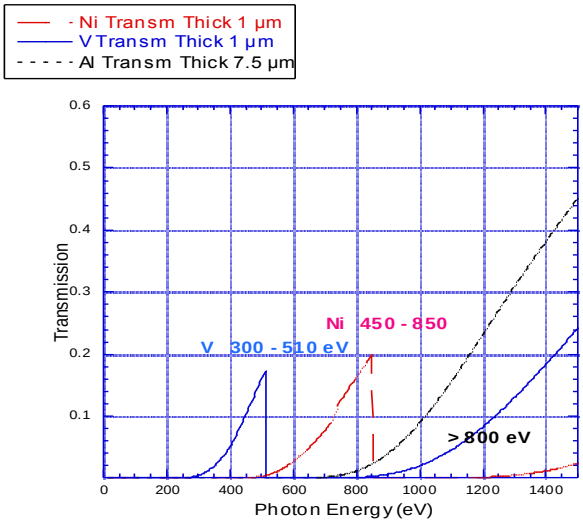

Figure 3: Transmission curves for the three microfoils used. The vanadium microfoil, 1 μm thick, has a average transmission $\sim$ 10% between 300 and 510 eV and a tail to higher energy of 800 eV. The nickel microfoil, 1 μm thick, has a average transmission $\sim$ 12% between 500 and 800 eV and a small tail to higher energy of 800 eV. The aluminum microfoil, 7.5 μm thick, has a significant transmission for energies greater than 800 eV.

$$Q_V^{E_x>800eV} = Q_{Al}^{tot} \times \frac{\int_{800eV} T_V^{t=1\mu m}(E_x)dE_x}{\int T_{Al}^{t=7.5\mu m}(E_x)dE_x} \tag{6}$$

$$Q_{Ni}^{E_x>850eV} = Q_{Al}^{tot} \times \frac{\int_{850eV} T_{Ni}^{t=1\mu m}(E_x)dE_x}{\int T_{Al}^{t=7.5\mu m}(E_x)dE_x} \tag{7}$$

Subtracting 1 from 6 and 2 from 7, the X-ray signals from the windows of the V (300-510 eV) and Ni (450-850 eV) was obtained by the following relations:

$$Q_V^{300\div510eV} = Q_V^{tot} - Q_V^{E_x>800eV} \tag{8}$$

$$Q_V^{450\div850eV} = Q_{Ni}^{tot} - Q_{Ni}^{E_x>850eV} \tag{9}$$

Using the 8 and 9 equations in the experimental data analysis for the yttrium and mylar were shown in Table 1, Table 2 and Table 3 for the three configurations of the laser energy. The energy of the laser beam were indicated in each tables. In these tables for each target material, the power density on the target and the X-ray energy produced by the plasma with the conversion efficiencies for the three different energy ranges were reported.

2.2 Measurement of microbeam

One of the aims of the presented work is to realize a monochromatic microbeam at 2.48 nm wavelength, which is within the water window energy region. To reflect and select photons with a wavelength of 2.48 nm, a multilayer spherical mirror [1] with a resolution $\lambda/\Delta\lambda \sim 200$ and a reflectivity $\sim 1\%$ was used. The photons were selected with a reflection angle of 8 degrees to the mirror surface normal. In Figure 4 the reflection curve of the mirror with geometric parameters was shown. The component to 2.48 nm had been focused in the geometry shown in Figure 5.

The distance mirror plasma was 201.5 mm and the image point of the plasma is formed at a distance of 400.2 mm from the mirror. The X-ray detector was placed in the proximity of the focus point of the monochromatic beam. To separate the ultraviolet and visible ranges a 1 micron thick vanadium micro-foil was placed before the input of the detector. The soft X-rays were generated from an yttrium target with a laser beam energy of 3.6 J. The charge collected by the detector was 4 nC corresponding to approximately 3×10^9 photons of energy of 500 eV and focused reflection in the mirror. Considering a double magnification of the image of the source it was estimated that the focus of microbeam had a density of photons equal to 2×10^5 photons/mum^2.

Tables

Target **MYLAR** - E_{laser} = 321 mJ +- 7 mJ

W (W/cm^2)	Filter	Energy Interval (eV)	E_X (mJ in 2π sr)	η% (in 2π sr)
1.4×10^{12}	V 1 μm tick	300 - 510	3.93	1.2
1.4×10^{12}	Ni 1 μm tick	450 - 850	1.34	0.4
1.4×10^{12}	Al 7.5 μm tick	> 800 eV	2 μJ in 2 π sr	6×10^{-4}

Target **Y** E_{laser} = 308 mJ +- 9 mJ

W (W/cm^2)	Filter	Energy Interval (eV)	E_X (mJ in 2π sr)	η% (in 2π sr)
1.3×10^{12}	V 1 μm tick	300 - 510	10.2	3.3
1.3×10^{12}	Ni 1 μm tick	450 - 850	1.4	0.5
1.3×10^{12}	Al 7.5 μm tick	> 800 eV	9.8 μJ in 2 π sr	3×10^{-3}

Table 1 – Analysis of the intensity measurements of X-rays and conversion efficiencies (on 2π sr) of ittrium and mylar for the three energy intervals indicated in the table for $E_{laser} \approx 300$ mJ.

Target **MYLAR** - E_{laser} = 1.6 J +- 0.1 J

W (W/cm^2)	Filter	Energy Interval (eV)	E_X (mJ in 2π sr)	η% (in 2π sr)
6.9×10^{12}	V 1 μm tick	300 - 510	59.1	3.7
6.9×10^{12}	Ni 1 μm tick	450 - 850	22.9	1.4
6.9×10^{12}	Al 7.5 μm tick	> 800 eV	0.3	2×10^{-2}

Target **Y** - E_{laser} = 1.63 J +- 0.06 J

W (W/cm^2)	Filter	Energy Interval (eV)	E_X (mJ in 2π sr)	η% (in 2π sr)
7×10^{12}	V 1 μm tick	300 - 510	136.8	8.4
7×10^{12}	Ni 1 μm tick	450 - 850	22.4	1.4
7×10^{12}	Al 7.5 μm tick	> 800 eV	0.35	2×10^{-2}

Table 2 – Analysis of the intensity measurements of X-rays and conversion efficiencies (on 2π sr) of ittrium and mylar for the three energy intervals indicated in the table for $E_{laser} \approx 1.6$ J.

Target **MYLAR** - E_{laser} = 3.7 J +- 0.2 J

W (W/cm^2)	Filter	Energy Interval (eV)	E_X (mJ in 2π sr)	η% (in 2π sr)
1.6×10^{13}	V 1 μm tick	300 - 510	146.6	4.0
1.6×10^{13}	Ni 1 μm tick	450 - 850	83.6	2.3
1.6×10^{13}	Al 7.5 μm tick	> 800 eV	1.2	3×10^{-2}

Target **Y** - E_{laser} = 3.7 J +- 0.2 J

W (W/cm^2)	Filter	Energy Interval (eV)	E_X (mJ in 2π sr)	η% (in 2π sr)
1.6×10^{13}	V 1 μm tick	300 - 510	413.4	11.2
1.6×10^{13}	Ni 1 μm tick	500 - 850	67.2	1.8
1.6×10^{13}	Al 7.5 μm tick	> 800 eV	1.6	4×10^{-2}

Table 3 – Analysis of the intensity measurements of X-rays and conversion efficiencies (on 2π sr) of ittrium and mylar for the three energy intervals indicated in the table for $E_{laser} \approx 3.7$ J.

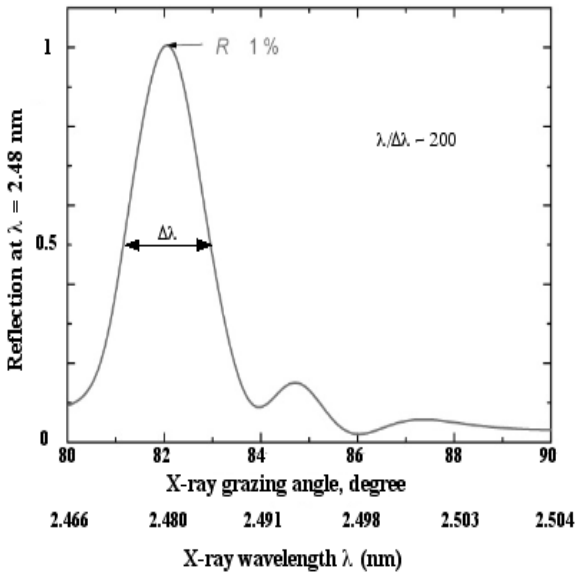

Figure 4: Curve of the reflectivity of the multilayer deposited on the substrate of the spherical mirror. It has a reflectivity of about 1% for Bragg angle of 82 degree which corresponds to a photon energy of 500 eV.

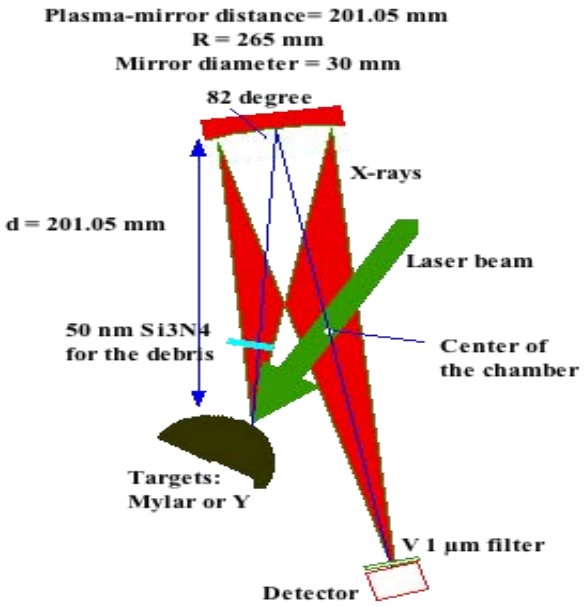

Figure 5: Schematic description of the experimental microbeam arrangement for the measurement of the energy of the X-ray beam reflected from the spherical mirror. The figure shows the optical configuration of the microbeam.

3 Conclusion and discussion

From the experimental data resulted that the conversion efficiency in the vanadium energy window, which almost coincides with the water window, yttrium was systematically 2 or 3 times larger than the conversion efficiency of the mylar. While for the nickel energy window the conversion efficiencies were essentially identical for the two different materials. This was confirmed at every power density.

The difference in vanadium energy window was due to the type of spectrum emitted by the two materials. In yttrium resulted a quasi-continuous emission due to the excited threshold M and then a uniform spectrum around 400 eV was obtained. In mylar a line spectrum of the carbon K threshold (280 eV) was generated. The conversion efficiencies were similar for the two materials in the energy region of the nickel window, because they mainly emitted bremsstrahlung radiation. Then in the Water Window, the yttrium had a good X-ray emitter and so it will be suitable for X-ray microscopy application where it is necessary to obtain an image of a biological sample with a single X-ray shot.

From the microbeam measures, approximately 3×10^9 photons of 500 eV energy were obtained, wich correspond to a photon density of 2×10^5 photons/μm^2. If a cubic micron of water was considered in the focal of microbeam, it released the dose of 200 Gy and this conclusions were of considerable interest for biological applications. An optimization of optical parameters and an improvement of the X-ray emissions using other materials such as rhenium have been just programmed.

4 Acknowledgment

We would like to thank Dott. L. Votano Director of Gran Sasso National Laboratories of INFN and Prof. S. Santucci Director of The Physics Department of L'Aquila University for supporting us. This work is financially supported by INFN, PLAXA experiment.

References

[1] Artyukov, I., Bugayev, Y., Devizenko, O., Gullikson, E., Kondratenko, V., Vinogradov, A. -ray Schwarzschild objective for the carbon window (lambda approximately 4.5 nm). Opt. Lett. 34, 2930-2932, (2009)

[2] Prise, K. M., Schettino, G., Vojnovic, B., Belyakov, O. Shao, C. Microbeam Studies of the Bystander Response. Journal of Radiation Research 50, A1-A6, doi:10.1269/jrr.09012S (2009).

[3] Kobayashi, Y. et al. Microbeam irradiation facilities for radiobiology in Japan and China. J Radiat Res (Tokyo) 50 Suppl A, A29-A47 (2009).

[4] Gerardi, S. Ionizing Radiation Microbeam Facilities for Radiobiological Studies in Europe. Journal of Radiation Research 50, A13-A20, doi:10.1269/jrr.08133S (2009).

[5] X-Ray Data Booklet, Center for X-ray Optics and Advanced Light Source-Lawrence Berkeley National Laboratory. *http* : *//henke.lbl.gov/optical_constants/*

PULEX experiment

Hamster cells show reduced resistance to genotoxic agents when cultured under low environmental radiation conditions.

G. Simone [a], M. C. Carbone [b,e], M. A. Tabocchini [a], E. Sorrentino [a], M. Pinto [a,e], O. Sapora [a], L. Conti Devirgiliis [b], M. Balata [c], M. Belli [d], L. Satta [d]

[a] Istituto Superiore di Sanit (ISS) and INFN Roma1 Gr, coll. Sanit, Rome, Italy
[b] Department of Basic and Applied Biology, LAquila University, LAquila, Italy
[c]Service of Chemistry and Chemical Plants, Gran Sasso National Laboratory, INFN, Assergi, Italy
[d] Frascati National Laboratory, Istituto Nazionale di Fisica Nucleare (INFN), Frascati, Italy
[e] Museo Storico della Fisica e Centro Studi e Ricerche Enrico Fermi, Rome, Italy

Abstract

Several experiments have been performed in the last few years aimed at understanding if environmental radiation has a permanent influence on the biochemistry of living matter. The experiment described in the following was preceded by a similar experiment which was subject to the criticism that for a large number of generations a random selection of a radiosensitive mutant with the observed properties cannot be excluded.

The present experiment, named PULEX, lasting 10 months, represents a substantial improvement given that the number of independent cultures was doubled and the random selection of mutants with the same characteristics was highly unlikely. Again we obtained results compatible with those of the previous experiment for the following end-points: (i) mutation frequency at the *hprt* genetic locus after a challenging dose of X-rays and (ii) antioxidant enzymes activity.

1 Introduction

Living organisms have incorporated in their normal biology and functioning a daily stimulus of ultra-low dose radiation due to the presence of environmental ionizing radiation. Life has evolved on Earth for 3.6 billion years in such environmental conditions. It is, therefore, legitimate to ask whether the biochemical behaviour of living organisms would differ in the absence of radiation. A possible experimental design to answer this question consist in the twin set-up of a cell culture in a laboratory where environmental radiation is reduced as low as possible (LRE, low radiation environment), and in a reference laboratory at reference environmental level (RRE, reference radiation environment). Using

a number of experimental assays, the experimenter would look for the appearance of any differential response in the biological model across the two laboratories.

To achieve a condition of reduced environmental radiation, a suitable location is the underground laboratory of the Italian National Institute for Nuclear Physics at Gran Sasso (LNGS/INFN), located in central Italy alongside a highway tunnel between the cities of LAquila and Teramo, underneath at least 1400m of limestone rock. Our first experiment, performed with a yeast cell line, suggested that cells grown in reduced environmental radiation conditions manifested an altered response to genotoxic agents such as methyl-methan-sulphonate (MMS) [1].

Markers of such deviations included recombination and aberrations frequencies. The second one, performed with an Hamster cell line, also manifested an altered response to genotoxic agents such as acute doses of ionizing radiations. The deviations were observed in gene mutations and activity of enzymes involved in the management of oxidative stress [2]. Specifically, cells grown in reduced environmental radiation conditions were less capable of facing the damage induced by genotoxic agents, relative to cultures maintained in reference environmental conditions (at Istituto Superiore di Sanit, ISS, in Rome).

From these data we inferred a possible role of environmental radiation in determining the different response to genotoxic agents. However, one could not exclude that, after many generations (9 months, the duration of the experiment, correspond to roughly 540 cell duplications for the Hamster cell line), radiosensitive mutant clones with the observed characteristics had been selected by chance among the cells cultured at LNGS. Therefore, we decided to perform a new experiment (PULEX) with a number of improvements with respect to the previous one. To face the problem of possible random mutations, the number of cultures was doubled: two independent cultures were set up in the LRE and, in parallel, two cultures were set up in the RRE. Furthermore, to assure a uniform treatment of all four cultures, the RRE laboratory was installed in the Chemistry department building of the LNGS - INFN, outside the Gran Sasso mountain. In this way the operators in charge of the maintenance of all four cell cultures were the same, so as to eliminate a possible source of experimental variability. To the same end, with the exception of environmental radiation, all other controllable conditions, such as culture medium, serum, buffers, plastics, etc., have been kept identical (i.e., prepared in the same way or ordered from the same batch) for all four cultures.

In the following we describe and discuss the results obtained by studying the two pair of chinese hamster V79 cultures for 10 continuous months. We here report on a number of biological end points, including: (i) cell growth, (ii) micronuclei induction, (iii) mutations at the genetic locus hprt induced by X-rays, and (iv) alterations in anti-oxidant enzymatic activities.

2 Materials and methods

2.1 Dosimetry and irradiation

Background radiation dosimetry was discussed thoroughly in reference [3]. Briefly, sources of background radiation were divided in ^{222}Rn decay, cosmic, and terrestrial γ-rays components. The radiation dose associated to the gamma component was measured directly

using TLD detectors, whereas the ^{222}Rn component was determined using a combination of direct ^{222}Rn concentration measurements and a mathematical model to convert concentration levels to cellular radiation doses. When needed, challenging dose was delivered using X-rays from the 6 MV medical linear accelerator of the Radiotherapy Unit, San Salvatore Hospital, Coppito, L'Aquila, at a dose rate of 2.0 Gy min^{-1}.

2.2 Culture conditions

Chinese hamster V79 fibroblasts were grown as monolayer in Eagle's minimal essential medium supplemented with 10% foetal calf serum (FCS), 1 mmol dm^{-3} glutamine, 50 U dm^{-3} of penicillin and streptomycin. They were sub-cultured 3 times a week in order to maintain them in exponential phase of growth. All reagents used throughout the entire experiment were from Gibco, presently Invitrogen, and from the same batches. Duplicate and independent cultures, all starting from the same frozen batch, were grown up to 10 months in parallel at the RRE laboratory (cultures A and B) and at the LRE laboratory (cultures C and D).

2.3 Cell growth

To measure cell growth, $\simeq 5\times10^4$ cells/dish were seeded in 6 cm diameter Petri dishes and cultured for 8 days. Twice daily, cells from two dishes were trypsinized, suspended in fresh medium, and counted using a Beckman Coulter Counter.

2.4 Micronuclei induction

Some DNA damage events can lead to morphological changes in the nuclear DNA that may be readily visualized using conventional fluorescence microscopy techniques. When a damaged DNA fragment, detached from a chromosome is produced, it may be lost when a cell attempts to undergo mitotic division. The micronucleus assay allows the visualization of these events by blocking cell division before such fragments go lost. At the microscope, the detached DNA fragment will appear as a fluorescent spot, similar to a cell nucleus, but about 1/10 its size, positioned nearby two regular nuclei which the cell was attempting to segregate into two daughter cells. The frequency of micronucleated events will serve as a quantitative indicator of failed repair of damage to DNA caused by ionizing radiation.

2.5 Mutation induction

For mutation experiments, about 7×10^6 cells per dose point were irradiated as monolayer with 2, 4, and 6 Gy X-rays. After irradiation, cells were washed, trypsinized, counted, diluted, and plated at a density of 1.5×10^6/175 cm^2 flask for a total of about 6.0×10^6 cells per dose point. The cells were sub-cultured every 48 hours at the same density to allow the phenotypic expression of mutation at the hypoxanthine-guanine phosphoribosyl transferase (*hprt*) locus. Mutation frequency was evaluated on days 8 and 10 after irradiation. Petri dishes of 90 mm diameter (ten for each dose point) were seeded with 3×10^5 cells/dish in the presence of 6-thioguanine (0.5 μg/ml) (Sigma) and 5 % FCS. At

the same time, 200 cells/dish were plated in each of 4 Petri dishes of 60 mm diameter to determine the cloning efficiency. For each experiment, the number of mutants per viable cell was determined by averaging the results obtained on the 8th and the 10^{th} day after irradiation.

2.6 Cell extracts preparation and enzymatic activity assays

Cells were harvested and suspended at the concentration of 10^7 cells/mL in 10 mM phosphate buffer, pH 7.0, containing 10 mM dithiotreitol (DTT) (Sigma) (for glutathione peroxidase enzyme) or Triton X-100 (Sigma) (for catalase and total SOD enzymatic assay). All chemicals were purchased from Sigma unless otherwise specified. Cell suspensions were thawedfrozen three times in liquid N_2, homogenized and centrifuged at 13,000 rpm for 30 min at 4. The resulting cell extracts were used for spectrophotometrical measurement of enzymatic activity and protein content.

Total superoxide dismutase (SOD, EC 1.15.1.1) activity in cell extracts was assayed at 480 nm and 30 by its ability to inhibit the epinephrine autoxidation. The reaction was carried out in 50 mmol/L sodium carbonate buffer, pH 10.2, and was initiated by the addition of 0.1 mmol/L adrenaline. A standard curve, with a purified Cu-Zn bovine SOD, was obtained by plotting the inverse values of the amount of enzyme used and the percentage inhibition observed. This standard curve was used to determine the amount of extract necessary for a 50 % inhibition. One unit of SOD was defined as the amount of the enzyme required to halve the rate of epinephrine autoxidation.

Catalase (CAT, EC 1.11.1.6) activity was measured at 240 nm and 25 by following the rate of reduction of hydrogen peroxide. The reaction mixture contained 100 mmol/L potassium phosphate buffer pH 6.8 and 10 mmol/L H_2O_2. One unit of CAT is defined as 1 μmol of H_2O_2 reduced/min. Selenium-dependent glutathione peroxidase (SeGPX, EC 1.11.1.9) activity was assayed with a solution containing 50 mM monobasic potassium phosphate, pH 7.0, 1 mM EDTA, 1.5 mM sodium azide, 0.4 U glutathione reductase, 0.45 mM GSH, 0.2 mM NADPH and 0.25 mM H_2O_2 as substrate. The oxidation of NADPH was followed at 340 nm and 25. One unit of SeGPX was defined as 1 μmol of NADPH oxidized/min. Protein concentration was determined by Protein Assay Kit (Bio-rad), using bovine serum albumine (BSA) as standard.

2.7 Data analysis and statistical tests

Data on mutation induction as a function of radiation dose were fitted against a linear quadratic model and comparison of regressions were made using an F-test, implemented in a custom-made electronic worksheet. Statistical differences on enzymatic activities were analyzed using the StudentNewmanKeuls test (SigmaStat software; Jandel ScientiWc Software Corporation, San Rafael, CA, USA).

3 Results

3.1 Cell growth (PULEX)

Growth curves were measured immediately after the cultures were set up (t_0) and several times during the 10 months of continuous culture in LRE and RRE laboratories. No differences were observed in growth rate independently of culture time and of radiation environmental conditions (data not shown). This result is in agreement with our previous finding [2]. In the present study, no differences were observed in the plateau level that was constantly reached at around 5×10^6 cells/dish.

3.2 Micronuclei induction (PULEX)

The frequency of micronuclei was determined for all the cultures maintained for ten months under reduced and reference environmental radiation, as well as for the cell culture that was used to generate the previous two when the experiment was first set up (denominated t_0). To determine the frequency of micronuclei events, an estimate of mis-repair of chromosomal damage, cells were exposed to an acute dose of 1 Gy of ionizing radiation, large enough to produce extensive DNA damage. The results are reported in figure 1. Measurement indicate a modest increase of the micronuclei frequency with time in both reference and low environmental laboratories, compared to the initial level (t_0 value, fig. 1). Overall, there is not a significative difference between micronuclei induction in V79 cells, neither with time, nor with environmental radiation exposure.

3.3 Mutation induction

To study the mutagenic sensitivity to ionising radiation, V79 cells were exposed to increasing doses of X-rays at the beginning of the cell cultures (t_0) and after 10 months of continuous culture either at the RRE (cultures A and B) or at the LRE underground laboratory (cultures C and D).

Data obtained for mutations induction at the *hprt* genetic locus are shown in figure 2, together with the t_0 measurement. Data collected at t_0 are fitted by a linear regression analysis rather than by the usual linear quadratic equation, while data obtained after 10 months of continuous cultures are well fitted by the linear quadratic curve; for the B culture a negative slope was obtained. C culture shows a spontaneous mutation background of 2×10^{-5}, subtracted in the fit shown.

After 10 months of continuous growth, independent measurements on the two cultures maintained in RRE conditions yielded results significantly different from those obtained on the two cultures maintained in LRE conditions. This result is particularly evident at the highest dose used, 6 Gy. The measured mutation frequencies are reported in table 3.3.

3.4 Antioxidant enzymatic activity

The biochemical activities of superoxide dismutase (SOD), catalase (CAT) and selenium-dependent glutathione peroxidase (Se-GPx) were assayed in V79 cells at zero time and

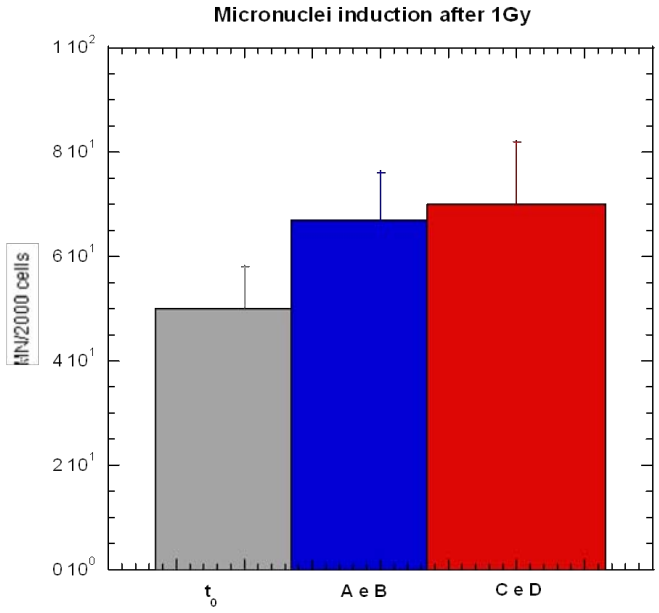

Figure 1: Micronuclei induction in averaged A and B (blue bar) = RRE cultures, and C and D (red bar) = LRE cultures after 1 Gy irradiation. The results obtained at t0 is also shown (grey bar).

V79 culture	PULEX (10 months)
t_0	2.94 ± 0.2
A	5.27 ± 0.29
B	2.47 ± 0.28
C	7.67 ± 0.51
D	7.18 ± 0.39

after 10 months of continuous culture. The biochemical activities measured in the A and B (RRE) cultures, as well as in the C and D (LRE) cultures were often pooled together, when they were not statistically different ($P > 0.05$) based on a StudentNewmanKeuls test. Therefore, when applicable, data are presented as average values for each pair of cultures.

Figure 3 shows the SOD, CAT and Se-GPx enzymatic activity at t0, after 10 months (PULEX), in both environmental conditions.

One should note that cell sensitivity to a ROS attack depends on the relationship between CAT or GPx and SOD rather than on the absolute amount of individual antioxidant enzymes. The ratios CAT/SOD and Se-GPx/SOD are indicators of the scavenging efficiency of cells against ROS. A decrease in one of these ratios indicates a poor ROS scavenging efficiency (Somani et al 1996), while an increase of one or both ratios indicates an increased ROS scavenging efficiency.

Figure 4 shows the ratio Se-GPx/SOD as a function of time. It can be seen that

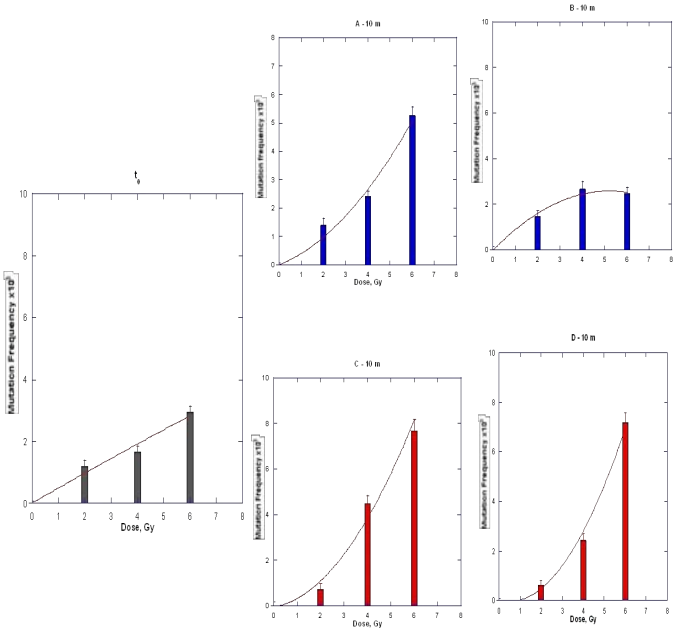

Figure 2: Mutation frequency as a function of X-ray dose and after 10 months of continuous culture. A and B (blue bar) = RRE cultures, and C and D (red bar) = LRE cultures. The response at zero time (gray bar) is also reported. Each data point is the mean ? SE of 2 different determination performed on day 8 and 10 after irradiation.

after 10 months of culture the Se-GPx/SOD ratio exhibits a significant decrease for LRE cultures (P=0.018) as well as a significant increase for the RRE cultures (P=0.017).

The ratio CAT/SOD is sown in figure 5. Contrary to Se-GPx/SOD, there is essentially no variation, neither as a function of time, nor as a function of culture site (LRE or RRE). Consequently we cannot deduce anything about its contribution to the ROS scavenging efficiency of cells.

4 Discussion

4.1 PULEX

The present measurement, carried out with a continuous culture of V79 cells during 10 months, confirms our previous results suggesting a possible role of environmental radiation in determining an adaptive response in V79 Chinese hamster cells, which is lost after many generations spent in a low radiation environment. However, in the previous experiments we could not exclude that mutant radiosensitive clones carrying the sought for characteristics had been selected by chance. The use of the same batches of medium, serum, and other reagents as in the previous studies, and by testing independent pairs of cultures for each cell culture condition (RRE or LRE), the present experiment made the occurrence of such a selection during the continuous culture very unlikely. This is due to

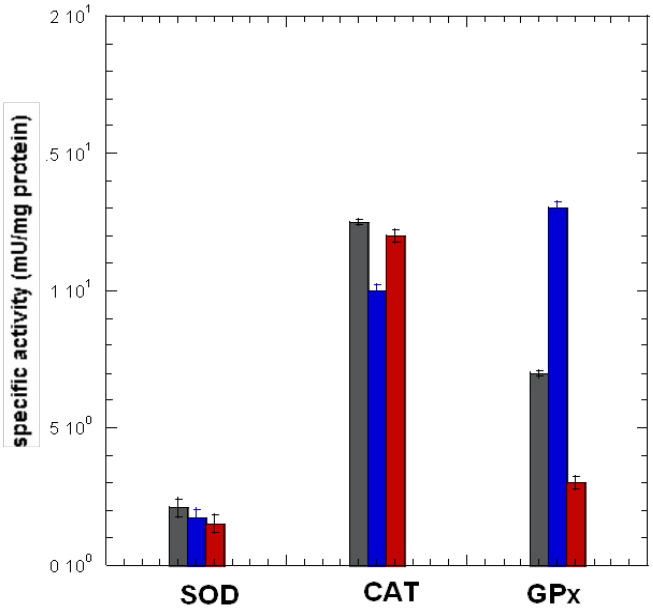

Figure 3: Antioxidant enzymatic specific activities at zero time (gray bars, t0) and at the end of PULEX (grid line) and CODA (hatched line) experiments. Blue bars: A and B cultures, always in RRE; red bars: C and D cultures, 10 months in LRE followed by 6 months in RRE. Data are the mean ± SE of 3 independent experiments.

the scarce probability to select the same phenotype in two parallel cultures growing in the same environmental radiation conditions.

In fact, the two pairs of cultures gave similar results, i.e., the differences observed between cultures A and B, or cultures C and D, were not statistically significant for all end points studied. In general, the overall results for all the assays performed after 10 months of continuous culture, described in the previous sections, suggest a possible adaptive response induced by the reference radiation environment.

As a matter of fact, even if our results after 10 months of continuous culture do not provide absolute indications of higher resistance induced by the RRE (see, for instance the micronuclei result), we never found opposite results, i.e. we could never measure cells cultured under the Gran Sasso tunnel becoming more resistant then cells grown in the external laboratory.

A clear cut result is that based on measurements of mutation induced by X-rays after 10 months of culture. The data show that V79 cells cultured in LRE became more sensitive compared to cells grown in RRE, in agreement with the adaptive response hypothesis.

In fact, as mentioned before, the experimental design that we used (two pairs of cultures for each environmental radiation condition) makes it very unlikely that these observations are due to a random selection of mutants. If such random selection occurred, in fact, it should happen in both sister cultures. However, if one assumes that the mutation frequency in V79 cell cultures is of the order of $10^{-4} \div 10^{-5}$ for a given genetic locus, and

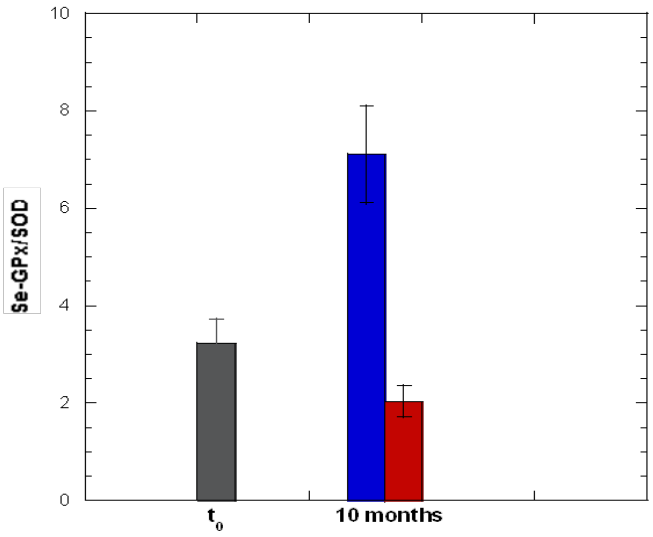

Figure 4: Se-GPx/SOD ratio.

if one makes the simplistic assumption that one mutated locus is sufficient to determine the features that were observed here, the probability of obtaining by chance the same mutant in two independent cultures is very low, in the order of $10^{-8} \div 10^{-10}$.

Measurements of anti-oxidant enzyme activity, after 10 months of continuous culture, showed that it is reduced in cells cultured in LRE compared to cultures maintained in RRE. Our results after 10 months of continuous culture revealed a significant reduction of the Se-GPx/SOD ratio in the LRE cultures either with respect to the RRE cultures ($P=0.02$) or with respect to the t0 culture ($P<0.05$). This indicates that cells growing in LRE are less protected against ROS, compared to the parallel external cultures, a finding that may explain the higher proneness in hprt mutation of LRE cultures.

Overall, our results are apparently consistent with the possibility that background radiation induces an adaptive response in living cells. After ten months of continuous culture, V79 cells grown in LRE experienced a total γ-ray dose of 25.9 μGy, while cells grown in RRE experienced a dose of 460.8 μGy. The peculiarity of our study is that it refers to ranges of dose and dose rate given by the standard environment, by investigating the reduction of this standard, so as to give new insight on the role of natural environmental radiation.

5 Conclusions

We now have 4 experiments with different biological models (one with yeast, two with Chinese hamster, one with human lymphoblastoid cell line, this last one not discussed in

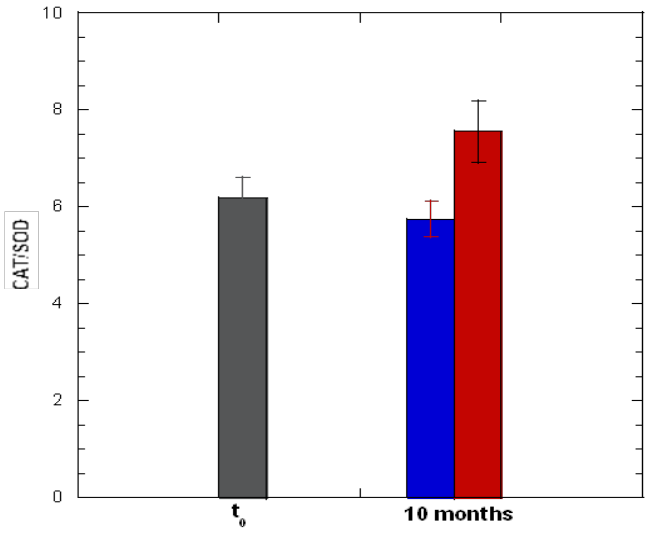

Figure 5: CAT/SOD ratio.

the text) all confirming one another. Even if on the basis of a limited number of biological end points it appears certain that living matter somehow do understand when and if it is deprived of the natural radiation environment, and reacts by reducing its defence capacity. The reason of such a behaviour is far from being clear. A possible explanation is that of the role of the environmental radiation as conditioning agent, i.e. functioning as a physiological stimulus that contributes to the activation of the internal defense of cells.

It is also to be stressed that the measurement on the micronuclei do not indicate any significant difference in the damage to DNA for cells grown in the RRE or the LRE. In formulating hypotheses, since data offer different independent indications, one should take into account the entire state of affairs. For instance, one should try to understand why cells, grown in the LRE in nearly absence of environmental radiation, manifest permanent alterations in their biochemistry. It seems and probably is a difficult task, but the Gran Sasso Laboratory offers still unequaled possibilities for the exploration of the interaction of living matter with radiation at very low dose and dose rate.

6 Acknowledgements

The authors are grateful to Prof. V. Tombolini and to the technical staff at the Radiotherapy Unit - Ospedale San Salvatore, Coppito, L'Aquila, for allowing irradiations of biological samples at the 6 MV medical linear accelerator. Thanks are also due to F. Antonelli, Ph.D. (ISS) for her help with cell culture, and to Mr. Marco Sabatini (ISS), Mr. Stefano Nisi and Mr. Luca Ioannucci (LNGS) for their technical assistance.

Background radiation component	LRE (nGy/h)	RRE (nGy/h)
Cosmic rays [(a)]	negligible	30
All γ-rays[(b)]	3.6	34
^{222}Rn and daughters[(c)]	0.17	0.17
Total dose rate	3.77	65.7

Table 1: [(a)] based on UNSCEAR 2000 Report, Sources, Annex E; [(b)] TLD measurements; [(c)] based on the application of the model by Jostes et. al. (44)

References

[1] L. Satta, G. Augusti-Tocco, R. Ceccarelli, A. Esposito, M. Fiore, P. Paggi, I. Poggesi, R. Ricordy, G. Scarsella and E. Cundari, Low environmental radiation background impairs biological defence of the yeast Saccharomyces cerevisiae to chemical radiomimetic agents. Mutat Res 347, 129-133 (1995).

[2] L. Satta, F. Antonelli, M. Belli, O. Sapora, G. Simone, E. Sorrentino, M. A. Tabocchini, F. Amicarelli, C. Ara, et al., Influence of a low background radiation environment on biochemical and biological responses in V79 cells. Radiat Environ Biophys 41, 217-224 (2002).

[3] M. C. Carbone, M. Pinto, F. Antonelli, F. Amicarelli, M. Balata, M. Belli, L. Conti Devirgiliis, L. Ioannucci, S. Nisi, et al. M. C. Carbone, M. Pinto, F. Antonelli, F. Amicarelli, M. Balata, M. Belli, L. Conti Devirgiliis, L. Ioannucci, S. Nisi, et al., Radiat Environ Biophys 48, 189-196 (2009).

[4] M. C. Carbone, M. Pinto, F. Antonelli, F. Amicarelli, M. Balata, M. Belli, L. Conti Devirgiliis, L. Ioannucci, S. Nisi, et al. M. C. Carbone, M. Pinto, F. Antonelli, F. Amicarelli, M. Balata, M. Belli, L. Conti Devirgiliis, L. Ioannucci, S. Nisi, et al.,NCB 125,422(2010)

TELLUS Experiment. A Multi-instrument Payload for the investigation of the Topside Ionosphere

V. Sgrigna[a], L. Conti[b], D. Zilpimiani[c]

[a] Dipartimento di Fisica and Sezione INFN, Università Roma Tre, Rome, Italy.
[b] Facoltà di Ingegneria, Università Telematica Internazionale UNINETTUNO and INFN, Rome, Italy.
[c] Institute of Geophysics, Georgian Academy of Sciences, Tbilisi, Georgia.

Abstract

A new space project, which summarizes previous ones reported in several LNGS Annual Reports, has been proposed by the TELLUS team for the investigation of ionospheric and magnetospheric phenomena within the Earth-near-Earth space couplings. The project includes the study of natural disasters taking place in the Earth surface (as earthquakes) and their possible deterministic prediction on the basis of precursory phenomena to be reconciled with perturbations occurring in the topside ionosphere. After an introductory section on the subject, technical, scientific, and methodological details are given on the project.

1 Introduction

The deterministic prediction of the time occurrence, hypocentral (or epicentral) location and magnitude of an impending earthquake, is an open scientific problem. The reason is that such predictions are based on the detection of the so-called earthquake precursors (i.e. seismic and non seismic phenomena accompanying the rock deformation during the earthquake preparation time in the focal zone), and the physical interpretation of these pre-earthquake phenomena is a very complicated matter. Up to now there have been systematic observations of mechanical intermediate-term and electromagnetic (EM) short-term precursors, which have been shown to be more suitable for the above mentioned future applications. Of relevant importance appear to be EM emissions from approximately DC to a few tens of MHz radiated from the Earth's surface and produced as a consequence of earthquake preparation and occurrence (the so-called precursory SEME-waves). They demonstrated to cause ionospheric perturbations that are detectable by

	Scientific Objective	*Expected Results*	International collaborations
Geomagnetic field mapping	Main field and secular variation will be the principal goals.	Contribution to the IGRF. A better knowledge of the Earth's core dynamics, secular variation, field inversions and crustal anomalies. 3D reconstruction of the mantle conductivity.	Synergy with SWARM mission, INGV ground network & SEGMA-ULF geomagnetic networks.
Monitoring of ionosphere and plasmasphere	Simultaneous measurements of local changes in the topside ionosphere and space and time variability of plasmasphere.	Contributions to the IRI model , ionospheric tomography, study of space weather events by in situ measurements and plasmaspheric TEC investigations.	Collaboration with NASA missions C/NOFS and STPSAT1. Use of CITRIS-like detector to collect signals from CERTO satellite & DORIS radio beacons terrestrial network. Comparisons with INGV & DIAS ionosonde data.
Detection of transient phenomena associated with thunderstorms	Detection of tropospheric transient luminous emissions (TLE), lightnings, terrestrial gamma ray flashes (TGF) & related energy transfer (~0,25-1GW) from troposphere to iono-magnetosphere.	Understanding of TLE e TGF effects in the framework of the ionosphere-magnetosphere couplings.	Complementary observation campaigns of TLE e TGF phenomena to be carried out with the TARANIS satellite.
Study of iono-magnetospheric perturbations due to EM emissions of terrestrial origin	Study of the possible effects produced in the near-Earth space by EM emissions of seismic and volcanic origin.	The AUSONIA team can take profit from the expertise of the previous ESPERIA project (see the 2007 IUGG resolution N.5, www.iugg.org/resolutions)	The AUSONIA team is guest investigator of the DEMETER mission to study whistlers and radiation belt particles.
Investigation of Van Allen particle fluxes & tropospheric X / γ rays	Study of temporal stability of the Van Allen radiation belts, detection of particle precipitation and tropospheric & cosmic X/γ emissions.		A few key persons of the AGILE mission are also members of the AUSONIA team.

Table 1: Science and methods of the AUSONIA space project.

Low-Earth-Orbit (LEO) satellites. In spite of the difficulty in the understanding of the physical mechanisms underlying the earthquake preparation and occurrence, research with this aim continues with a critical view, new ideas and thorough investigations and the results seem to be promising. Within this framework a few projects and experiments have been carried out on the subject by our team and accompanied by specific theoretical interpretations to corroborate the observations. In the last ten years several contributions has been given by the TELLUS team on the subject. The ESPERIA space project was a first approach for investigating earthquake precursors from the near-Earth and a few ESPERIA space instruments (the LAZIO-EGLE magnetometer and the ARINA particle detector), have been already designed, constructed, and tested in space. They have been reported in previous LNGS annual reports [1,2] and in literature [3-5]. Theoretical modeling (fault creep episodes in crustal block modeling, SEME-waves propagation in the lithosphere and atmosphere) and analysis of data (intermediate-term deformations, PBs, TLE and TGF phenomena) have accompanied the experiments mentioned above [2,6-13]. Also an original signal waveform reconstruction board was proposed [14].

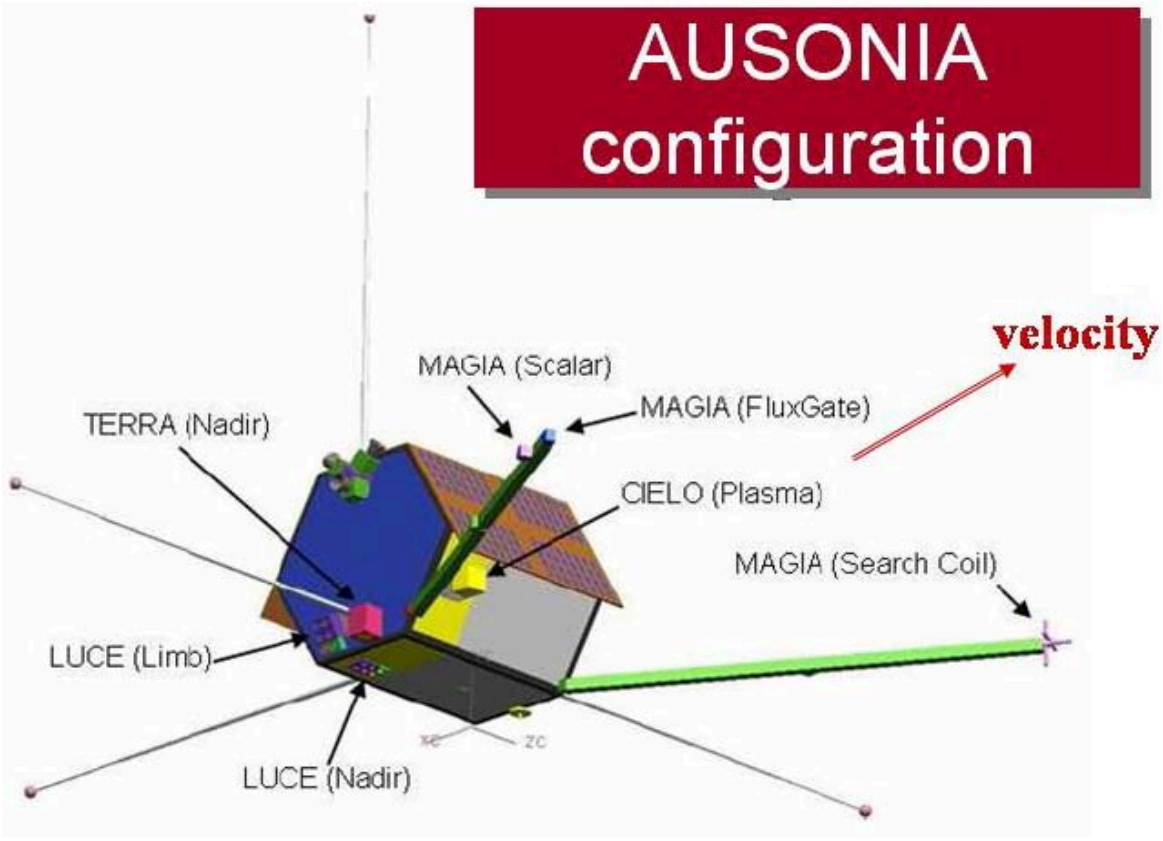

Figure 1: Schematic representation of the AUSONIA satellite project.

2 The experiment

Aim of the proposed space project is to design and construct a small space platform planned with a multi-instrument payload and a LEO mini-satellite mainly concerned with the monitoring and mapping of the ionosphere-magnetosphere transition region.

The scientific program is based on coordinated, continuous and simultaneous space and ground-based observations, and on mutual data comparison with other missions of similar quality. On the basis of the experimental and theoretical results mentioned in the Introduction section, it has been clarified that a more complete space project is necessary to investigate the ionosphere-magnetosphere transition zone. A specific AUSONIA project was proposed after the IUGG resolution in support of ESPERIA (2007 IUGG resolution N.5) (http://www.iugg.org/resolutions/), which welcomes the planning of several nations to launch ionospheric monitoring satellite missions. AUSONIA includes both the study of perturbative phenomena in the topside ionosphere and the field mapping of the same region to give a contribution in defining the IGRF and IRI models. This will also allow to separate SEME signals from tropospheric, cosmic rays, and solar effects. The field mapping of the topside ionosphere will also allow the monitoring of TLE and TGF tropospheric phenomena that have recently assumed a relevant importance [10]. Optical-UV instruments (videocameras and photometers) have been proposed to study TLE and

	Experiment	Module/Code	Probe/Instrument	Positioning / Pointing mode
Geomagnetic measurements	**MAGIA** (MAGnetic Instrument Array)	MAGIA_Scalar	Scalar Magnetometer	Boom_M_Right
		MAGIA_Flux-Gate	Flux-gate Magnetometer	Boom_M_Right
		MAGIA_Search-Coil	Search-coil Magnetometer	Boom_M_Left
Electromagnetic measurements	**ELECTRA** (ELECTRic field Analyser)	ELECTRA_Zenith	Electric Probe	Boom_E_Zenit
		ELECTRA_Tan	Electric Probe	Boom_E_Tan
		ELECTRA_DX	Electric Probe	Boom_E_DX
		ELECTRA_SX	Electric Probe	Boom_E_SX
Ultraviolet & Optical measurements	**LUCE** (transient LUminous emissions Combined Experiment)	LUCE_Nadir_VID1	Video-Camera Sprite	Nadir
		LUCE_Nadir_VID2	Video-Camera Lightning	
		LUCE_Nadir_PH1,2,3,4	Photometer 1,2,3,4	
		LUCE_Limb_VID1	Video-Camera Sprite	Limb
		LUCE_Limb_VID2	Video-Camera Lightning	
		LUCE_Limb_PH1,2,3,4	Photometer 1,2,3,4	
Plasma measurements	**CIELO** (Combined Ionospheric Experiment in Low Earth Orbit)	CIELO_GPS	GPS	Zenith
		CIELO_PLASMA	LP, RPA, Plasma Driftmeter	Along the same direction of the satellite velocity
High-energy particles & X-Gamma rays measurements	**TERRA** (circumTerrestrial high-Energy paRticle and X-gamma Ray Analyser)	TERRA_Nadir	High-energy particles & X-Gamma rays detector	Nadir
		TERRA_Tan	High-energy particles & X-Gamma rays detector	In the opposite direction to the satellite velocity

Table 2: AUSONIA experiments and their positioning on board the satellite.

lightnings, as well as X/gamma rays and particle detectors have been designed to investigate TGF phenomena [13]. Scientific and methodological aspects of the AUSONIA space project are reported in Table 1.

3 The instruments

Five (MAGIA, ELECTRA, LUCE, CIELO and TERRA) space experiments have been planned on the AUSONIA satellite (see figure 1). They are devoted to monitor geomagnetic field, plasma and particle environment in the ionosphere-magnetosphere transition zone as well as to study optical/ UV and X/gamma emissions induced by tropospheric activity. The MAGIA (MAGnetic Instrument Array) experiment is constituted by a scalar, a fluxgate, and a 3-axes search-coil magnetometers to detect stationary, lower-frequency and higher-frequency magnetic field. The magnetometers are installed on the tips of two deployable booms (Boom_M_Right and Left, each one 5 meters long from the satellite spacecraft) to reduce the electromagnetic interference from the satellite equipments. The ELECTRA (ELECTRic field Analyser) experiment consists of 4 electric preamplified probes, each one installed on the tips of 4 meters deployable booms (4 meters long, called ELECTRA_Zenith, TAN, Right, and Left) to allow to measure the 3 electric field components in the frequency range from about DC up to about 10 MHz). The MA-

GIA and ELECTRA sensors can highlight the correlation between iono-magnetospheric disturbances and lightnings occurrence and reconstruct the dynamics of the atmosphere-ionosphere electromagnetic interaction. These measurements are also essential to study the LEP (Lightning-Induced Electron Precipitation) and the particle disturbances of the Van Allen belt-induced induced by tropospheric and geomagnetic storms. In the AUSONIA project are also included optical and UV detectors devoted to the observation of TLEs with high spatial and temporal resolution in specific frequency bands. Measurements are taken with video cameras and photometers to reconcile the need for high capture rate with the high resolution images. The optical-UV devices for these observations are concentrated in the experiment LUCE in two separate blocks oriented to nadir and to limb, respectively. Each block consists of 2 cameras with filters optimized for the shooting of red sprites (VID1) and lightning (VID2), respectively, and 4 photometers (PH1, 2,3,4) for UV-visible measurements. The precipitation of particles of the Van Allen belts was observed by several satellite missions, but many questions need an answer about the temporal and spatial stability of the Van Allen belts and the dynamics of interaction disturbances associated with magnetic storms, the electromagnetic emissions of tropospheric origin, the EM emissions of anthropogenic origin, etc. Other themes of topical scientific interest are the X and gamma emissions from the troposphere (TGF). They represent a background for satellite missions such as AGILE designed to explore gamma bursts from the sky. To study these phenomena, the TERRA detector is designed to be install on board the AUSONIA satellite. The experiment consists of two identical modules: TERRA_Nadir and TERRA_Tan oriented to Nadir and in the opposite to the speed of the satellite, respectively. X and gamma ray detectors will be constantly active during the optical and EM measurements to allow to investigate the characteristics and origin of the TGF and their correlation with TLE. TERRA aims at revealing X-and gamma-ray bursts (TGF) from the Earth's troposphere. AUSONIA has been designed to map TGF phenomena, to observe the precipitation of particles from the Van Allen belts induced by magnetic storms, tropospheric phenomena, seismo-electromagnetic emissions and emissions from anthropogenic EM, to measure range, direction and temporal variation of the flow of precipitating charged particle, to reveal the runaway electrons, to study the interactions between whistler waves and trapped particles, to gather information on the length, height, changes in TGF, and to acquire a statistically significant amount of TGF events as a function of local time, geomagnetic conditions, etc. Figure 1 illustrates the general satellite layout.

Planned experiments and instruments and their positioning on board the AURONIA satellite are reported in Table 2.

4 Mission Project Characteristics

At this preliminary step the final parameters of the AUSONIA project have not yet been completely defined. In Table 3 values are given for a MITA platform solution and a sun-synchronous orbit. The satellite orbit altitude has be chosen to optimise observations at the sunrise-sunset local time for a better identification of seismo-induced ionospheric disturbances. In fact, as reported by Molchanov and Hayakawa [15] and Chuo et al. [16],

Orbit	Sun-synchronous circular orbit 98° Inclination.
	Altitude between 600 to 800 km (TBD). See also notes after Table 3 in sub-section 3.3.
	Revisit time: ≤ 24 h
Budgets	Power Satellite total: ~ 270 W (Payload total: 120W; Platform total: 150W) (TBD)
	P/L Data: ~ 306 kbps (36,5Gbit of daily data, margin included) (TBD)
	Payload Mass: ~ 120 kg (TBD)
Attitude orbit control system	Attitude determination : 0.001° (TBD)
	Attitude Accuracy (3 axes) : 0.1° (TBD)
	3 reaction wheels, 3 magnetic coils, 2 star trackers, 3 gyroscopes, GPS receivers, three-axis magnetometer, 10 sun sensors
Spacecraft	Platform MITA or other platform of similar quality (TBD)
	Nadir pointing
	Thrusters applied to the platform (constant altitude and/or possible orbit changes) (TBC)
Mission duration	3 years

Table 3: AUSONIA satellite mission characteristics.

an increase in the sporadic E-layer critical frequency at the terminator time (sunrise and sunset) is observed within 5 days before the earthquake that determines a corresponding increase in the D-layer electron density and a variation of the VLF propagation at the terminator time. Should AUSONIA be installed on board of another spacecraft, budgets, volume, orbit inclination and altitude will be changed accordingly.

5 Conclusions.

A space project has been proposed for investigating lithosphere-atmosphere-ionosphere-magnetosphere couplings through the monitoring of the topside ionosphere with a multi-instrument payload installed on board of a LEO satellite. The study of perturbative phenomena in the topside ionosphere and the field mapping of the same region is a primary goal of the project. This will give a contribution in defining the IGRF and IRI models, in studying tropospheric (TLE and TGF), solar, and cosmic rays effects as well as in detecting perturbations provoked by SEME-waves of terrestrial origin and generated before the occurrence of earthquakes.

References

1. Sgrigna, V., Buzzi, A., Conti, L., Stagni C., Zilpimiani, D., 2006. TELLUS. Ground deformations and their effects in the near-Earth space, Laboratori Nazionali del Gran sasso, INFN, Annual Report 2005, LNGS/EXP-03/06, July 2006, pp.185-194.

2. Sgrigna, V., Buzzi, A., Conti, L., M. Parrot, J.L. Pincon, Stagni,C, Zilpimiani, D., 2007. TELLUS. Ground deformations and their effects in the near-Earth space, Laboratori Nazionali del Gran Sasso, INFN, Annual Report 2006, LNGS/EXP-02/07, July 2007, pp. 217-228.

3. Sgrigna, V., A. Buzzi, L. Conti, P. Picozza, C. Stagni, D. Zilpimiani, 2008. The ESPERIA satellite project for detecting seismic-associated effects in the topside ionosphere. First instrumental tests in space, Earth Planets and Space, 60, 463-475.

4. Sgrigna, V., Altamura, F., Ascani, S., Battiston, R., Bencardino, R., Blasko, S., Buzzi, A., Casolino, M., Conti, L., Lucidi, S., Minori, M., Papi, A., Picozza, P., Rossi, S., Stagni, C., Zilpimiani, 2007. First data from the EGLE space experiment onboard the ISS, Microgravity and Sci. Technology, XIX-2, 45-49.

5. Sgrigna, V., 2004. Description and Testing of ESPERIA Instruments (ARINA and LAZIO- SIRAD) in Space, EOS Trans., AGU, vol. 85, T53C-03, n.47, F1795, 2004 (Invited).

6. Sgrigna, V., And V. Malvezzi, 2003. Preseismic creep strains revealed by ground tilt measurements in central Italy on the occasion of the 1997 Umbria-Marche Apennines earthquake sequence, Pure and Appl. Geophys.(PAGEOPH), 160, 1493-1515.

7. Sgrigna, V., Buzzi, A., Conti, L., Picozza, P., Stagni, C., Zilpimiani, D., 2007. Seismo- induced Effects in the Near-Earth Space: Combined Ground and Space Investigations as a contribution to Earthquake Prediction, Tectonophysics, 431, 153-171.

8. Sgrigna, V., D'ambrosio, C., Yanovskaya, T.B., 2002. Numerical modeling of pre-seismic slow movements of crustal blocks caused by quasi-horizontal tectonic forces, Phys Earth. Planet. Int., 129, 313-324.

9. Sgrigna, V., Carota, L., Conti, L., Corsi, M., Galper, A., Koldashov, S.V., Murashov, A.M., Picozza, P., Scrimaglio, R., Stagni, L., 2005. Correlations between earthquakes and anomalous particle bursts from SAMPEX/PET satellite observations, J. Atm. Solar-Terrestrial Phys., 67, 1448-1462.

10. Buzzi, A., Conti, L., Galper, A. M., Koldashov, S.V., Malvezzi, V., Murashov, A.M., Picozza, P., Scrimaglio, R., Sgrigna, V., Stagni, L., 2006. Sismo-electromagnetic emissions, Proc. NATO Adv. Study Institute on "Sprites, Elves and Intense Lightning Discharges", Edited by M. Fullekrug, E.A. Mareev and M.J. Rycroft, Published by Springer, vol. 225, pp. 388-389, 2006. (NATO Science Series II: Mathematics, Physics and Chemistry- vol.225. ISBN-10 1-4020-4628-6 (PB)).

11. Sgrigna, V., Conti, L., Malvezzi, V., 2003. TELLUS. Ground deformations and their effects in the near-Earth space, Laboratori Nazionali del Gran sasso, INFN, Annual Report 2002, July 2003, pp.217-232.

12. Sgrigna, V., Buzzi, A., Cirella, A., Conti, L., Malvezzi, V., 2004. TELLUS. Ground deformations and their effects in the near-Earth space, Laboratori Nazionali del Gran sasso, INFN, Annual Report 2003, July 2004, pp. 221-228.

13. Sgrigna, V., Conti, Zilpimiani, D., 2010. TELLUS Experiment. Detection of transient phenomena associated with thunderstorms, Laboratori Nazionali del Gran Sasso, INFN, Annual Report 2009, LNGS/EXP-01/10, May 2010, pp.199-204.

14. Sgrigna, V., Conti, Zilpimiani, D., 2011. TELLUS Experiment. Signal waveform reconstruction by multichannel selection and variable feed-back differential amplification, Laboratori Nazionali del Gran Sasso, INFN, Annual Report 2010, LNGS/EXP-01/11, May 2011, pp 211-213.

15. Molchanov, O. A., and M. Hayakawa, 1998. Subionospheric VLF signal perturbations possibly related to earthquakes. J. Geophys. Res., 103, 17489-17504.

16. Chuo, Y. J., Liu, J. Y., Pulinets, S. A., and Chen, Y. I.: The ionospheric perturbations prior to the Chi-Chi and Chia Yi earthquakes, J. Geodyn., 33, 509-517, 2002.

ERMES
Estimation of Radioactive Release from the Fukushima Dai-ichi Nuclear Power Plant Accident

W. Plastino[a b],M. Schöppner[a b], P.P. Povinec[c], G. Wotawa[d],
F. Bella[a], A. Budano[b], M. De Vincenzi[a b], F. Ruggieri[b]

[a] Dept. of Physics, Univ. of Roma Tre, I-00146 Rome, Italy
[b] INFN, Section of Roma Tre, I-00146 Rome, Italy
[c] Comenius Univ., Dept. of Nuclear Physics and Biophysics, SK-84248 Bratislava, Slovakia
[d] Central Institute for Meteorology and Geodynamics, A-1190 Vienna, Austria

Abstract

As a consequence of the accident at the Fukushima Dai-ichi nuclear power plant on March 2011, it is important to characterize radioactivity release into the environment. Several isotopes, amongst others caesium-137 and iodine-131, are monitored at multiple stations throughout the world by the International Monitoring System of the Comprehensive Nuclear Test Ban Treaty Organization (CTBTO). The sensitivity between source and receptor was determined using the Atmospheric Transport Modeling (ATM), running on the GRID computing facility of the Italian National Institute of Nuclear Physics (INFN) - Roma Tre.

1 Introduction

The isotopes caesium-137 and iodine-131 play a significant role here, since both are solely anthropogenic and usually only produced during nuclear weapon tests and nuclear accidents. The Comprehensive Nuclear Test Ban Treaty Organization (CTBTO) has built up an International Monitoring System (IMS), including 80 stations to measure the atmospheric radioactivity. From these daily sampling activities the radioactive concentration (Bq/m^3) of caesium-137 and iodine-131 at the monitoring stations can be determined. Compared with other stations in the IMS network the station JPP38 in the city of Gunma, Japan, has continuously measured the highest concentration of both isotopes. As a second station for comparison USP79 on Hawaii, USA, has been selected. Then Atmospheric Transport Modeling (ATM) can be used to estimate the radioactive source term at the

Fukushima Dai-ichi NPP (37.42 N, 141.03 E) that is supposed to be mainly responsible for the signal received at the stations JPP38 in Gunma (36.31 N, 139.00 E) and USP79 (21.52 N, 157.99 W). The station JPP38 is in the southwest of Fukushima and with a distance of about 250 km it is also the closest IMS station to the assumed source, and therefore the majority of the atmospheric transport can be assumed to be over land. The second station, USP79, on the other hand, has a distance of 6,200 km to the assumed source, while the transport is mainly over the sea.

2 Results and Discussion

Atmospheric Transport Modeling has been proven to be a valid tool for determining Source-Receptor Sensitivity (SRS) matrices. The calculations in this work have been accomplished by using the Lagrangian type model. Both, source and receptor locations, are known in the case of the Fukushima Dai-ichi accident in March 2011 and the IMS measurements at the stations JPP38 and USP79. Forward modeling is usually more efficient when the number of known sources is limited and the receptors are undefined. Backward modeling is usually more efficient when the number of receptors is limited and the sources are unknown. However, both possibilities can be used in this case to determine the sensitivity between source and receptor. In the frame of the presented results the Lagrangian type model has been used in the backward mode. The worst case estimation of the source term is used as input data. The presented simulations assume the whole NPP as one single source, which releases radioactive particles in form of caesium-137 and iodine-131 as follows:

- From 12 March 2011 - the day of the first explosion in a reactor building, a continuous emission of 10^{19} Bq/day per isotope has been assumed. This is a simplifying assumption that does not take into account the temporal variation caused by the fact that the number of damaged nuclear facilities increased during the first week. Three units and possibly a fuel storage pool have been damaged with different delays [1]. However, this estimated release is probably higher than a real situation at NPP.

- Before 12 March 2011 - it has been estimated that no radioactive release took place. This assumption is significant, since releases prior to the first measurement could contribute through longer atmospheric trajectories to the measurement signal. The sensitivities between the source and the receptor are calculated, including overlapping contributions from different time intervals. For the meteorological data a resolution of $1\,^{\circ} \times 1\,^{\circ}$ in terms of longitude and latitude has been used. The simulation includes radioactive decay for both isotopes, i.e. a half-life of 30.17 years for caesium-137, and 8.02 days for iodine-131. It does not include any isotope-specific wet deposition in the atmosphere. Finally the results are summed up for each day and compared to the IMS signal.

Nevertheless, the concentrations time series is highly dependent not only from the source term, but also from the atmospheric conditions, e.g. wind direction, rain, vertical

movement of air masses etc. [2]. Therefore, similar characteristics of both signals, i.e. local maxima and minima, can be explained with corresponding meteorological effects; whereas, differences in the characteristics are rather caused by a time dependent source term. A scaling factor is introduced for both isotopes expressing the ratio of the signal measurement to the signal simulation. A value of one would mean that the signal has been estimated correctly, a value smaller (higher) than one would signify that the simulation has produced a higher (smaller) signal. However, this factor cannot be used as the correction factor for thesource term, i.e. it is not equal to the ratio of the real source term to the estimated source term. This is not the case due to the possibility of atmospheric trajectories from different source times can reach the detector at the same day, and vice versa. For the JPP38 station the scaling factor of iodine-131 is generally higher than of caesium-137; up to two orders of magnitude are observed, while the calculated point-to-point average suggests the factor two for the iodine-131 source term over the caesium-137. For the USP79 station caesium-137 has a generally higher scaling factor, which would lead to an estimation of a stronger caesium-137 source term [3]. However, the time series of both scaling factors indicates a source term smaller than the estimation of a worst case scenario: from the JPP38 comparison an iodine-131 source term of $10^{15} \div 10^{18}$ Bq/day (factor 0.5 for caesium source term) is suggested. The scaling factors of the USP79 station are suggesting a much weaker iodine source term of $10^{12} \div 10^{15}$ Bq/day (factor 5 for caesium source term).

3 Conclusions

This straight-forward approach shows that through the usage of ATM the actual source term can be approximated. Based on the estimation of a worst case scenario with continuous release and the measurement at the JPP38 station, the estimation of the iodine source term can be narrowed down to $10^{15} \div 10^{18}$ Bq/day (factor 0.5 for caesium) [3]. It is noticeable that an estimation of the source term based on the USP79 station would lead to an iodine source term that is smaller by three orders of magnitude. However, the presented analysis involves only a time independent source term, which continuously emits particles. Future work will include an estimation of the source term correction factor, i.e. the adjustment of the source term in a way that the produced signal at the coordinates of JPP38 and USP79 is similar to actual measurements. In order to accomplish a time dependent source term, a recursive usage of ATM will be necessary for step-by-step approximation. Furthermore, the inclusion of the wet deposition effect for each isotope will be added, and more IMS stations will be included in the analysis [4].

References

[1] International Atomic Energy Agency, Fukushima Nuclear Accident Update Log, http://iaea.org/newscenter/news/tsunamiupdate01.html, April 2011.

[2] W. Plastino, R. Plenteda, G. Azzari, A. Becker, P.R.J. Saey, and G. Wotawa, Radioxenon Time Series and Meteorological Pattern Analysis for CTBT Event Categorisation, Pure Appl. Geophys., vol. 167, pp. 559-573, 2010.

[3] W. Plastino, M. Schppner, P. P. Povinec, G. Wotawa, F. Bella, A. Budano, M. De Vincenzi, F. Ruggieri, Atmospheric transport modeling based estimation of radioactive release from the Fukushima Dai-ichi nuclear power plant accident, 4, IEEE, 2027-2030, 2011.

[4] M. Schppner, W. Plastino, P. P. Povinec, G. Wotawa, F. Bella, A. Budano, M. De Vincenzi, F. Ruggieri, Estimation of the time-dependent radioactive source-term from the Fukushima nuclear power plant accident using atmospheric transport modelling, Journal of Environmental Radioactivity, http://dx.doi.org/10.1016/j.jenvrad.2011.11.008.